UNIVERSITÉ DU QUÉBEC À MONTRÉAL

TRACAGES ISOTOPIQUES DE L'ORIGINE ET DE L'ÉVOLUTION DES MAGMAS EN MILIEU CONTINENTAL : CONTRIBUTIONS RELATIVES DES SOURCES MANTELLIQUES ET DE LA CROÛTE CONTINENTALE

THÉSE PRESENTÉE À L'UNIVERSITÉ DU QUÉBEC À CHICOUTIMI
COMME EXIGENCE PARTIELLE DU
DOCTORAT EN RESSOURCES MINÉRALES
OFFERT À L'UNIVERSITÉ DU QUÉBEC À MONTRÉAL
EN VERTU D'UN PROTOCOLE D'ENTENTE
AVEC
L'UNIVERSITÉ DU QUÉBEC À CHICOUTIMI

PAR
ÉMILIE ROULLEAU

NOVEMBRE 2010

UNIVERSITÉ DU QUÉBEC À MONTRÉAL

ISOTOPIC TRACING OF ORIGIN AND EVOLUTION OF MAGMAS IN THE CONTINENTAL CONTEXT: RELATIVE CONTRIBUTIONS OF MANTLE SOURCES AND CONTINENTAL CRUST

THESIS PRESENTED TO UNIVERSITÉ DU QUÉBEC À CHICOUTIMI AS A PARTIAL REQUIREMENT Of THE DOCTORAT EN RESSOURCES MINÉRALES AT THE UNIVERSITÉ DU QUÉBEC À MONTRÉAL ACCORDING TO THE AGREEMENT WITH THE UNIVERSITÉ DU QUÉBEC À CHICOUTIMI

PAR
ÉMILIE ROULLEAU

NOVEMBER 2010

REMERCIEMENTS

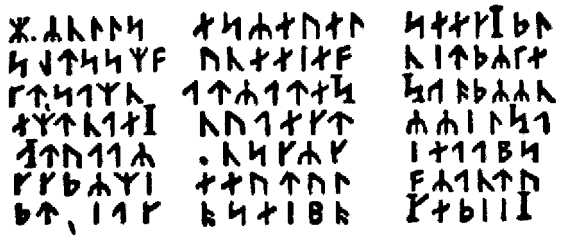

Cryptogramme rédigé en caractère runique,

signifiant :

« Descends dans le cratère du Yocul de
Sneffels que l'ombre du Scartaris vient
caresser avant les calendes de Juillet,
voyageur audacieux, et tu parviendras
au centre de la terre. Ce que j'ai fait.
Arne Saknussemm. »

Extrait de *Voyage au centre de la Terre*

Jules Verne

Tout d'abord, je tiens particulièrement à remercier mon directeur Ross Stevenson pour m'avoir fait confiance dans ce projet et m'avoir fait découvrir le monde obscur des isotopes radiogéniques. Je tiens également à lui exprimer toute ma reconnaissance pour sa patience et ses conseils afin que ce projet aboutisse, sans pour autant m'imposer ses idées.

Je voudrais également remercier mon co-directeur Daniele Pinti pour m'avoir initié au monde des gaz rares (aussi obscur que les isotopes radiogéniques) et m'avoir permis de me diversifier dans mon travail de thèse. Il a toujours su m'aider dans les moments les plus importants. Je souhaiterais le remercier pour m'avoir permis de participer au Programme JSPS à l'été 2009. Ce voyage au Japon a été une vraie chance pour moi, par le fait de travailler dans un laboratoire étranger d'une part, et pour la magnifique expérience personnelle et humaine d'autre part.

Je souhaiterais remercier Jean David pour ses discussions scientifiques très enrichissantes, son enseignement de la chimie du plomb, et pour m'avoir soutenu quand le moral était au plus bas.

J'aimerais remercier Yuji Sano, ORI, Tokyo, ainsi que toute son équipe pour m'avoir accueilli pendant 3 mois dans son laboratoire et m'avoir permis de travailler avec lui. « *Arigato Gozaimasu.* »

Un gros merci à Raynald Lapointe pour son aide précieuse pour tous les problèmes au TIMS. Et il y en a eu.

Je ne peux oublier ici toutes les personnes du GEOTOP qui m'ont accompagnées tout au long de ma thèse et principalement : Jenny, Jean Baptiste, Quentin, Olivia, Olivier, Laurence, Christelle, Benoit, Chantal, Josée, Brice et tous les autres. Encore un merci à mon « office-mate » de fin de thèse, Quentin, pour m'avoir supporté à la fin, même quand le téléphone sonnait toutes les 2 minutes..

J'ai une pensée particulière pour la « PS DREAM TEAM » que j'ai rencontrée sur les pentes du Vésuve durant l'été 2003, et avec qui j'ai partagé ma passion pour les volcans en gravissant autant que possible les volcans italiens. Merci pour avoir supporté mes joies et mes peines durant ces 4 années. Un merci particulier à Mika qui m'a rejoint dans ce grand pays du pôle nord et que je porte dans mon cœur ; ainsi qu'à Snef pour nos éternelles conversations à distance.

Je ne veux surtout pas oublier ma famille pour leur soutien continuel même à distance. Merci aussi à mes amies Nadège et Céline, ainsi que Coralie et Céline qui, même de l'autre coté de l'Atlantique, ont su me rassurer.

Et le meilleur pour la fin!!!! Un énorme merci à Nicolas pour sa patience, son soutien perpétuel et sa sagesse même lorsque j'étais devenue un petit démon.

TABLE DES MATIÈRES

LISTE DES FIGURES

INTRODUCTION

CHAPITRE 1

CHAPITRE 2

CHAPITRE 3

LISTE DES TABLEAUX

CHAPITRE 1

CHAPITRE 2

CHAPITRE 3

RÉSUMÉ

Les roches volcaniques et plutoniques représentent une excellente fenêtre d'observation sur le manteau terrestre. Les études isotopiques sur le volcanisme océanique suggèrent un manteau actuel hétérogène, composé de pôles appauvris (DM, PREMA) et enrichis (EM1 et EM2) par rapport à la valeur initiale chondritique. En contexte continental, la contamination par la croûte participe largement à compliquer l'identification des réservoirs mantelliques dans la genèse d'une suite magmatique continentale.

Cette thèse présente les résultats de deux études sur roches volcaniques/plutoniques appartenant respectivement à des dépôts volcaniques distaux jeunes (téphras) retrouvés dans une séquence de varves carbonatées des Alpes italiennes (Formation de Piànico, Alpes du Sud, Italie) et à une province ignée continentale ancienne (les Collines Montérégiennes, Québec, Canada). Le but commun à ces deux études est d'identifier et quantifier la contribution des sources magmatiques dans des situations « ambiguës » et difficiles d'interprétation, en utilisant le couplage des isotopes (isotopes radiogéniques et gaz rares) et des éléments majeurs et traces. Dans le premier cas (téphras de Piànico), l'ambiguïté dans la détermination des sources volcaniques est liée à la distance entre les dépôts (Alpes italiennes) et les sources présumées (Massif Central, France ; Province Magmatique Romaine, Italie). Dans le deuxième cas (Collines Montérégiennes), la contamination crustale des magmas a masqué ou modifié sensiblement la signature isotopique originale de la source mantellique, rendant ambiguë sa détermination (manteau inférieur versus manteau supérieur).

La thèse est composée de trois chapitres, chacun étant un article scientifique publié ou soumis dans une revue internationale avec comité de révision. Le premier article (publié en 2009 dans *Quaternary International*) traite d'une étude géochimique et isotopique (Nd–Sr) sur deux téphras jeunes, T21d et T32, retrouvés dans la séquence interglaciaire de Piànico (Italie). Le téphra rhyolitique T21d, précédemment daté par la méthode K-Ar à 779 ± 13 ka, semble provenir du complexe Mont Dore-Sancy dans le Massif Central français. Le téphra T32 représente les produits de la Province Magmatique Romaine, et plus particulièrement d'une éruption de l'un des centres éruptifs des Monts Sabatini, daté entre 802 ± 74 ka et 783 ± 77 ka. L'utilisation des systèmes isotopiques du Sr et Nd a permis d'établir un âge relatif des dépôts d'environ 780 ka pour les deux téphras, cohérent avec la datation K-Ar de T21d ainsi qu'avec de récentes études paléomagnétiques sur la formation de Piànico qui ont montré une inversion de polarité assignée à la période Matuyama-Brunhes correspondant à la période interglaciaire MIS 19 du Pléistocène Moyen.

Le deuxième article (en révision pour soumission dans la revue *Lithos*) fait l'objet d'une étude géochimique et isotopique sur des intrusions alcalines formant les Collines Montérégiennes. Le couplage des isotopes de Nd, Sr, Hf et Pb ainsi que l'étude géochimique des éléments majeurs et traces a permis de montrer pour la première fois l'implication du manteau lithosphérique sub-continental (SCLM) dans la formation de ces magmas. Les données des isotopes du Pb ($^{207}Pb/^{204}Pb$ et $^{208}Pb/^{204}Pb$) montrent clairement l'implication d'une composante qui pourrait être celle d'un manteau lithosphérique Archéen. Cette étude a permis de s'interroger sur les deux grandes hypothèses fournies dans les années 80 sur la formation des magmas des Montérégiennes : 1) un point chaud (impliquant des magmas issus d'un manteau inférieur) et 2) un rift continental (impliquant des magmas issus d'un manteau supérieur). L'hypothèse du point chaud est fortement ébranlée par les conclusions présentées

dans l'article 2. On suggère que la formation des Montérégiennes soit le résultat de la réactivation du rift Ottawa-Bonnechère successive à l'ouverture de l'Océan Atlantique Nord.

Le troisième article (en révision pour soumission dans la revue *Chemical Geology*) présente une étude sur les isotopes des gaz rares (^{4}He et ^{36,38,} ^{40}Ar) et les isotopes de l'azote ($\delta^{15}N$) analysés dans des clinopyroxènes et amphiboles séparés des roches mafiques des Montérégiennes. Les signatures isotopiques de l'Ar, He et N ont permis de mettre en évidence une source mantellique similaire à celle d'un manteau supérieur de type MORB ou bien de type SCLM, et d'exclure l'hypothèse d'une source mantellique profonde de type OIB (point chaud). On a en particulier mis en évidence pour la première fois une corrélation entre les isotopes de l'azote, les isotopes du plomb ($^{208}Pb/^{204}Pb$ et $^{207}Pb/^{204}Pb$) et certains rapports d'éléments traces (La/Nb et Ba/Nb), permettant ainsi de confirmer une source dominante de type SCLM.

Mots-Clés : Province des Montérégiennes (Québec), Rb-Sr, Sm-Nd, Lu-Hf, Pb commun, gaz rares (He-Ar), azote, manteau lithosphérique, Tépho-chronostatigraphie, Formation de Pianico (Italie), complexe Sancy - Mont-Dore, Province Magmatique Romaine.

ABSTRACT

Volcanic and plutonic rocks can represent an open window in the earth mantle. Isotopic studies of oceanic volcanism suggest that the mantle is currently heterogeneous, and composed of depleted (DM, PREMA) and enriched (EM1, EM2) end-members against the initial chondritic value. In continental context, contamination by the crust participates to complicate the identification of the mantle reservoirs that are involved in the genesis of the continental magmatic province.

This thesis presents the results of two studies on volcanic/plutonic rocks that belong to 1) young distal volcanic deposits (tephras) from a carbonate varve sequence from the Italian Alps (Piànico formation, South Alps, Italy), and 2) an old continental igneous province (Monteregian Hills, Québec, Canada). The common aim of these two studies is to identify and quantify the contribution of different magma sources, particularly in ambiguous cases; this is done by integration of isotope and major and trace element data. The ambiguity in the determination of the volcanic source of Piànico tephras is due to the distance between the distal deposits (Italian Alps) and the presumed source (Massif Central, France; Roman Magmatic Province, Italy). The ambiguity related to the mantle source (lower mantle vs. upper mantle) of the Monteregian Hills is that crustal contamination of magma modified the original isotopic signature.

This thesis is composed of three chapters; each is a scientific article published or submitted in peer-reviewed international journal. The first article (published in Quaternary International, August 2009) is a geochemical and isotopic study of two young tephras, T21d and T32, found in the lacustre interglacial sequence of Piànico (Italy). The rhyolitic tephra, T21d, dated at 779 ± 13 ka (K-Ar), seems to originate from Mont Dore-Sancy complex (Massif Central, France). The phonolitic tephra, T32, represents the Roman Magmatic Province deposits, and originates from Mount Sabatini events that were dated from 802 ± 74 ka to 783 ± 77 ka. Use of the Nd and Sr isotopic systems permitted to assume a relative age of deposits of the two tephras at about 780 ka. This is coherent with the K-Ar datation of T21d, as well as the recent paleomagnetic studies of the Piànico formation, which showed a reverse polarity assigned to the interglacial sequence of MIS 19, Matuyama-Brunhes period.

The second article (in revision for submission in Lithos) is a geochemical and isotopic study of the alkaline intrusions forming the Monteregian Hills. The combination of Nd, Sr, Hf and Pb isotopes, as well as major and trace elements, permitted to show for the first time the implication of the subcontinental lithospheric mantle (SCLM) in the formation of the Monteregian magmas. The Pb isotopic data ($^{207}Pb/^{204}Pb$ and $^{208}Pb/^{204}Pb$) clearly show the influence of one component that may correspond to the archean lithospheric mantle. This study deals with the two major hypotheses of the 80's about the formation of the Monteregian magmas: 1) the hot spot model, which implies magmas derived from the lower mantle; and 2) the continual rift model, which implies magmas derived from the upper mantle. The conclusions of this second article are not consistent with the hot spot model. Instead, I suggest that the Monteregian Hills formed by the reactivation of the Ottawa-Bonechere rift during the opening of the North Altantic Ocean.

The third article (in revision for submission in Chemical Geology) is a study of noble gas (^{4}He and $^{36,38,40}Ar$) and nitrogen ($\delta^{15}N$) isotopes that were analyzed in clinopyroxene and amphibole separates from mafic rocks of the Monteregian Hills. The isotopic signatures of Ar, He and N permit to evidence an upper mantle source, which is similar to MORB or SCLM. Thus, I exclude the hypothesis of a deep mantle source, such as OIB (i.e. directly related to the hot spot model). I highlight for the first time the correlation between N and Pb ($^{208}Pb/^{204}Pb$ and $^{207}Pb/^{204}Pb$) isotopes, and N and trace element ratios (La/Nb and Ba/Nb); these correlations are consistent with the SCLM source.

Key words: Monteregian Hills (Québec), Rb-Sr, Sm-Nd, Lu-Hf, Pb common, noble gases (He-Ar), nitrogen, lithospheric mantle, tepho-chronostatigraphy, formation of Piànico (Italy), Sancy - Mont-Dore complex, Roman Magmatic Province.

INTRODUCTION

Problématique

L'évolution du manteau au cours de l'histoire géologique de la Terre reste mal connue. Le manteau n'étant pas accessible à des observations *in situ*, il existe différentes approches pour l'étudier : (1) l'analyse des données sismiques ; (2) l'étude d'échantillons du manteau supérieur ramenés à la surface par le volcanisme ou la tectonique (xénolites, massifs ophiolitiques, diamants, etc.); et (3) l'étude des magmas émis en surface et subsurface. Les roches volcaniques et plutoniques étant largement répandues à la surface de la Terre aussi bien en domaine continental qu'en domaine océanique, elles représentent une excellente fenêtre pour observer l'évolution du manteau supérieur et profond au cours du temps.

Les études géochimiques et isotopiques sur le volcanisme océanique récent de type OIB (Oceanic Island Basalt) et MORB (Mid-Ocean Ridge Basalt) suggèrent que le manteau actuel est hétérogène et constitué de composants appauvris et enrichis en éléments lithophiles (De Paolo and Wasserburg, 1976; Hart, 1988; Hofmann and White, 1982) par rapport à la composition initiale de la Terre, celle chondritique. Ces composants mantelliques ont été identifiés à travers les réservoirs isotopiques suivants (Hart, 1988; White, 1985; Zindler and Hart, 1986; Fig. 1) :

- DMM (*Depleted Mantle*), réservoir appauvri en éléments lithophiles ;
- PREMA (*Prevalent Mantle*), réservoir hybride globalement appauvri, à l'exception de l'enrichissement en $^{143}Nd/^{144}Nd$;
- HIMU (*High-μ*), réservoir mantellique enrichi en $^{206}Pb/^{204}Pb$ et $^{208}Pb/^{204}Pb$, lié au recyclage de croûte océanique ;
- EMI (*Enriched Mantle 1*), réservoir modérément enrichi en $^{87}Sr/^{86}Sr$ et $^{206}Pb/^{204}Pb$, représentatif d'une ancienne lithosphère océanique fortement appauvrie et d'anciens sédiments recyclés dans le manteau profond ;
- EMII (*Enriched Mantle 2*), de rapport élevé en $^{87}Sr/^{86}Sr$, modéré en $^{206}Pb/^{204}Pb$ et faible en $^{143}Nd/^{144}Nd$, donc représentatif de la signature isotopique d'une croûte continentale ou de sédiments océaniques modernes ;

- FOZO (*Focus Zone*), réservoir peu connu, dont la source est généralement attribuée à la couche limite D'' ou bien au recyclage progressif d'une croûte océanique dans le manteau (Hart et al., 1992; Stracke et al., 2005).

En contexte continental, la contribution enrichie de la croûte continentale et du manteau lithosphérique (SCLM : *Sub-Continental Lithospheric Mantle*) peut venir compliquer l'identification de ces réservoirs mantelliques. Le magmatisme du Rift Est Africain est un exemple actuel d'une province magmatique continentale où les différentes contributions mantelliques sont difficiles à discriminer. Cette province magmatique s'est formée par l'ouverture d'un rift continental associée à la fusion du manteau lithosphérique sous-jacent (SCLM), mais également par l'apport en magma d'un ou plusieurs points chauds, tels que les points chauds de l'Afar et du Kenya (Fig. 2 et Fig. 3; Furman, 2007; Furman and Graham, 1999; Pik, 1999; Pik et al., 2006). À ces différentes signatures mantelliques s'ajoutent une composante crustale que l'on observe dans les laves associées au *Main Ethiopian Rift* et liée à la contamination du magma durant son ascension vers la surface (Fig. 2).

La problématique principale de cette thèse est de contraindre la contribution relative de la croûte et des différents réservoirs enrichis et appauvris du manteau dans la genèse d'une suite magmatique continentale. Cette question est examinée à travers deux études de magmatisme continental d'âges différents à travers des couplages isotopiques classiques (Nd_Sr; Chapitre 1 et 2) ou novateurs (N-Pb; Chapitre 3).

Tout d'abord, nous allons démontrer comment les contributions relatives des sources mantelliques et de la croûte continentale peuvent être utilisées pour discriminer différentes sources volcaniques des dépôts distaux jeunes (téphras) retrouvés à l'intérieur des séquences sédimentaires (téphro-chronostratigraphie). En effet, les téphras volcaniques sont à la fois de très bons marqueurs stratigraphiques et de bons marqueurs temporels (Izett, 1981; Sarna-Wojcicki and Davies, 1991; Self and Sparks, 1981; Thorarinsson, 1944; Wilcox, 1965).

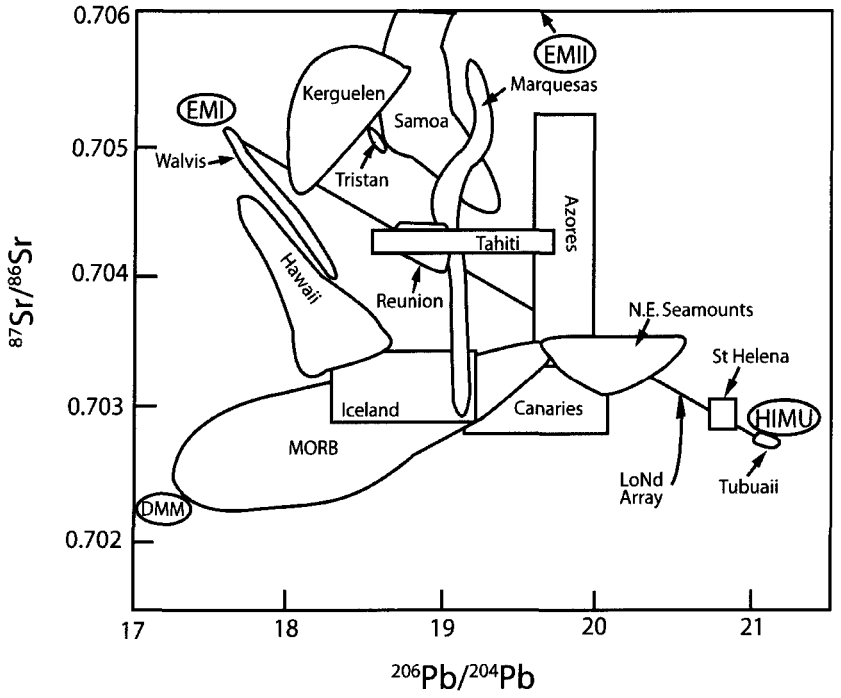

Figure 1 : Les rapports isotopiques du Sr et Pb montrent les signatures typiques des OIBs et des MORBs. La ligne nommée "LoNd array" connecte le pôle HIMU au pôle EMI, principaux réservoirs des OIBs (Modifié à partir de Hart, 1988).

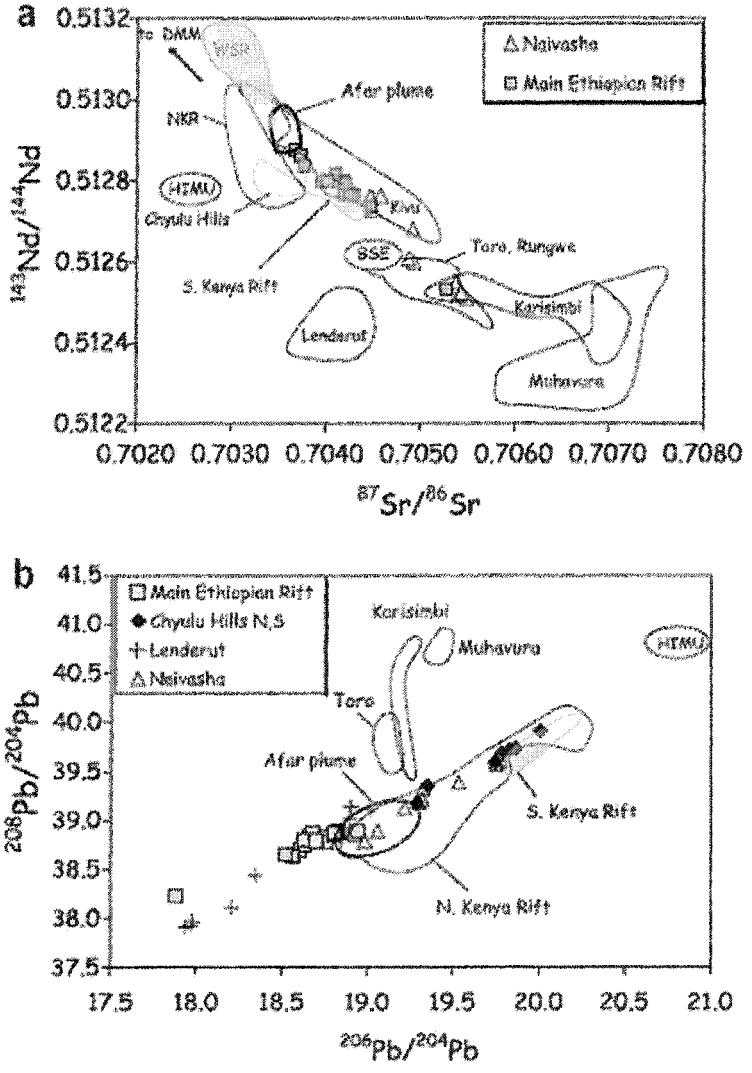

Figure 2 : Variations des isotopes radiogéniques dans les laves du Rift Africain. a) Corrélation $^{143}Nd/^{144}Nd$ vs. $^{87}Sr/^{86}Sr$. b) Variation $^{208}Pb/^{204}Pb$ vs. $^{206}Pb/^{204}Pb$ (Furman, 2007)

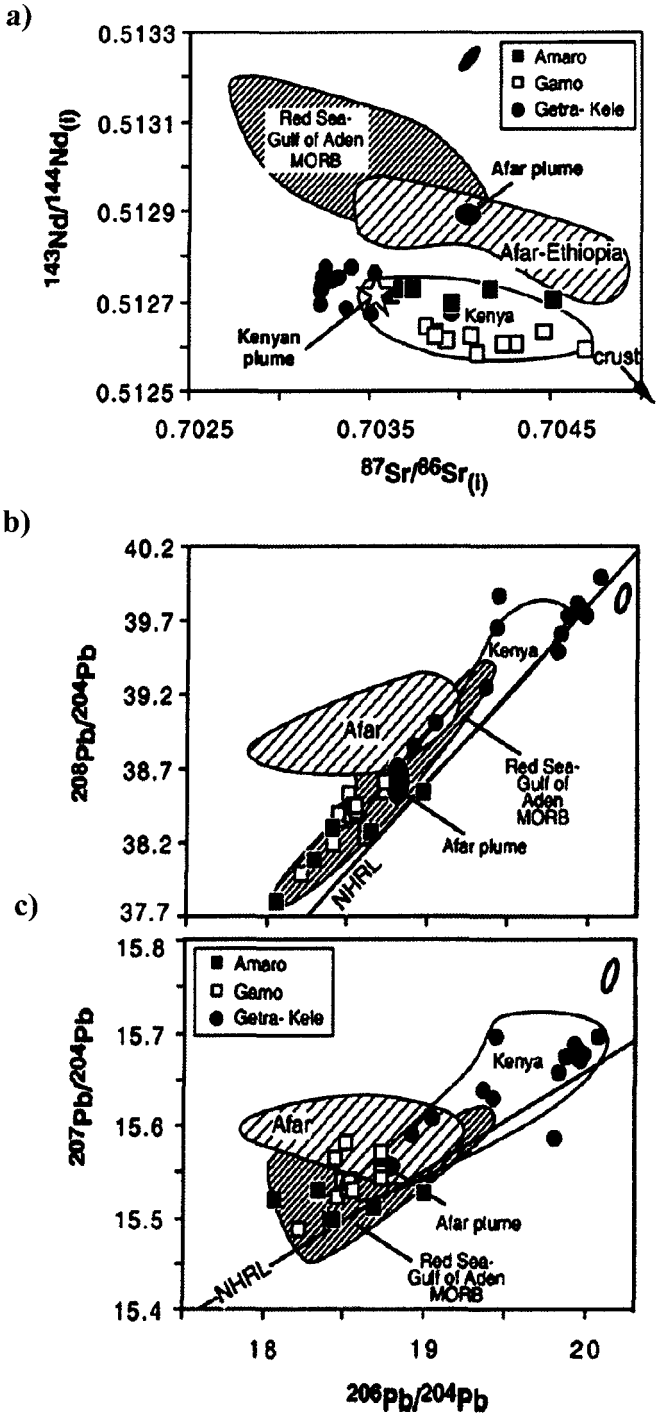

Figure 3 : a) $^{143}Nd/^{144}Nd_{(i)}$ vs. $^{87}Sr/^{86}Sr_{(i)}$, b) $^{208}Pb/^{204}Pb$ vs. $^{206}Pb/^{204}Pb$ et c) $^{207}Pb/^{204}Pb$ vs. $^{206}Pb/^{204}Pb$ des laves du sud de l'Éthiopie comparées aux MORBs de la Mer Rouge, aux points chauds de l'Afar et du Kenya (George and Rogers, 2002).

Depuis plus de 50 ans, la téphro-chronologie s'est beaucoup développée et s'avère être un outil idéal pour étudier la stratigraphie et la tectonique régionale, dans la calibration et l'évaluation des autres méthodes chronologiques, ainsi que pour la corrélation des stades isotopiques et polliniques (Izett, 1981; Sarna-Wojcicki et al., 1991). Malheureusement, les téphras sont souvent trop altérés et ne peuvent pas être datés. Par conséquent, ils ne peuvent pas être utilisés directement comme marqueurs stratigraphiques absolus. Une solution au problème est de caractériser le contenu géochimique du téphra et de le relier à celui des sources volcaniques probables. Les rapports entre éléments majeurs et plus rarement les éléments traces sont utilisés dans ce but. Cependant, les éléments majeurs et traces ne sont pas toujours de bons indices pour discriminer la source, et d'autres outils géochimiques, comme les isotopes radiogéniques, doivent impérativement être utilisés.

Ainsi, les isotopes radiogéniques (Sr et Nd) peuvent être utilisés pour identifier les édifices volcaniques à l'origine de téphras jeunes retrouvés dans la formation de Piànico (Italie; Fig. 4). Cette étude est basée sur deux téphras, T21d et T32, de la séquence de varves carbonatées de Piànico (Fig. 5). La séquence varvée (17 700 varves) constitue l'interglaciaire le plus long et le mieux préservé de toutes les Alpes (Moscariello et al., 2000). Depuis une dizaine d'années les scientifiques essayent de dater et décrire cette séquence dans le but de la soumettre à la Commission de Stratigraphie comme un strato-type du Quaternaire. Brauer (2007) a montré des similarités chimiques entre T21d et le téphra « Rivaux » lié au volcanisme du complexe du Puy de Sancy et daté à 320±30 ka. Cependant, Pinti (2001) a daté par la méthode K-Ar le téphra T21d à 779±13 ka. L'âge du téphra T32 a été obtenu par une méthode relative, puisque les leucites de cet échantillon sont trop altérées et donc difficilement datable par une méthode classique de datation. Brauer (2007) a montré que la composition en éléments majeurs du téphra T32 était similaire à celle du dépôt BLT (*Brown Leucitic Tuff*) de Roccamonfina et daté à 393±12 ka. Ces deux téphras ont par conséquent 300 ka de différence, ce qui pose problème. Dans la séquence de varves, aucun hiatus entre les deux téphras n'a été enregistré ; une des datations semble donc incorrecte. Grâce aux isotopes du Nd et Sr et à leurs relations avec certains éléments traces (Ta/Nb et Th/Nb), nous avons mis en évidence que la source du tephra T32 n'était pas le volcan Roccamonfina, mais plutôt l'un des paléocentres éruptifs des monts Sabatini dans la Province Magmatique Romaine et daté entre 805±2 ka et 783±7 ka (Karner, 2001).

Un des intérêts majeurs dans l'étude de la séquence de Piànico est d'approfondir nos connaissances sur les périodes interglaciaires et la néotectonique alpine. Penck and Bruckner (1909) ont attribué la formation de Piànico à la période interglaciaire de l'Eemien correspondant au Pléistocène Supérieur (130 ka). Il s'agit également du stade OIS 5^{éme} de la chronologie marine, d'après l'identification des restes du *Rhinoceros merckii Jaeg* et des mollusques du genre *Tanousia Servain*, caractéristiques du Pléistocene Supérieur-Moyen (Esu and Gianolla, 2009). Cependant, de récentes études paléomagnétiques sur les varves carbonatées de Piànico ont montré une inversion de polarité assignée à la période Matuyama-Brunhes indiquant que la formation Piànico appartient à la période interglaciaire MIS 19, correspondant au Pléistocéne Moyen. Ceci est cohérent avec l'âge de 779 ± 13 ka du téphra T21d (Esu and Gianolla, 2009; Pinti, 2001; Scardia and Muttoni, 2009). Dans ce contexte controversé de l'origine de cette séquence carbonatée, il nous parait important de mieux comprendre la signature géochimique et isotopique de ces deux téphras afin de caractériser la source mantellique, d'identifier l'évent volcanique à l'origine de ces téphras et ainsi de contraindre l'âge de cette séquence interglaciaire.

Le second but de cette thèse est d'identifier les sources mantelliques d'une ancienne province magmatique continentale telle que la Province des Collines Montérégiennes au Québec, Canada. Les Collines Montérégiennes sont une série de neuf intrusions alcalines initialement datées à 118-136 Ma ± 10 Ma (Eby, 1984; Cox, 2006). D'autres datations donnent un âge moyen de 124 Ma ± 1.5 Ma (Eby, 2006; Foland et al., 1986). Ces intrusions sont alignées le long du paléo-rift Ottawa-Bonnechère, à la jonction avec le graben du St-Laurent (Fig. 6). Elles présentent une grande variété de roches, de composition sous-saturée à sur-saturée. Cette province magmatique a longtemps été interprétée comme l'expression en surface d'un point chaud. Cette hypothèse reposait sur la distribution spatiale des intrusions, leur caractère alcalin et la signature isotopique (Sr-Pb) de type OIB des roches qui les constituent (Eby, 1985; Foland et al., 1988). Cependant, certains auteurs ont proposé que ce magmatisme soit associé à la réactivation d'anciennes failles du paleo-rift Ottawa-Bonnechère durant l'ouverture de l'Océan Atlantique Nord (Faure et al., 1996; McHone, 1996).

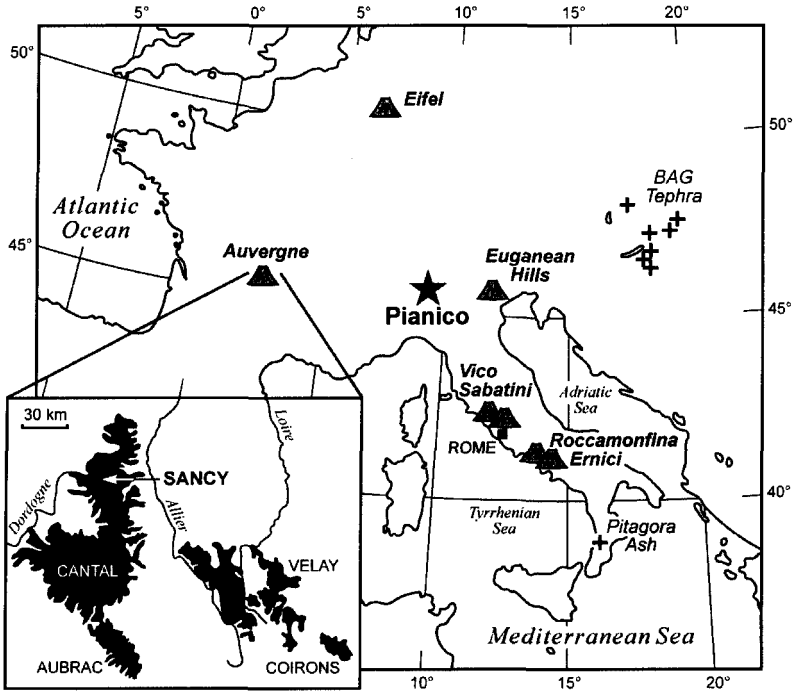

Figure 4 : Carte simplifiée de l'Europe et de la péninsule italienne avec la localisation de Piànico et des volcans italiens. En encart, la carte de localisation des volcans du Massif Central, le Complexe Sancy - Mont Dore (modifié à partir de Brauer, 2007).

Figure 5 : Photo illustrant la séquence des varves de Piànico, Italie.

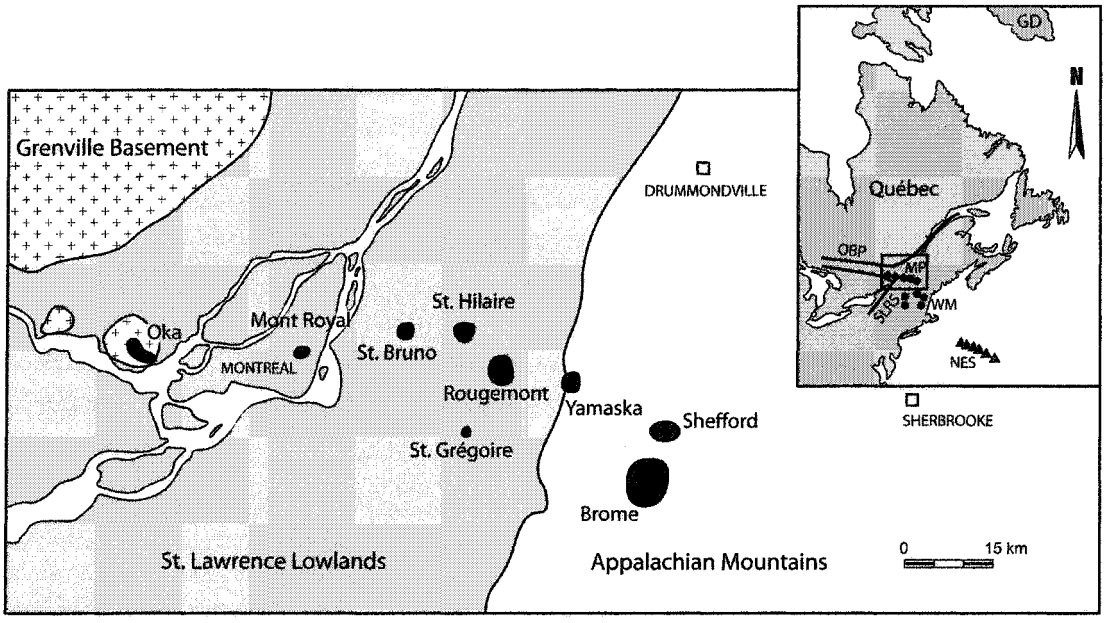

Figure 6 : Carte de la Province Magmatique des Montérégiennes montrant la distribution des intrusions crétacées, accompagnée d'une carte simplifiée de l'Est de l'Amérique du Nord avec la localisation de la Province des Montérégiennes. GD : Groenland ; NES : New England Seamounts ; WM : White Mountains ; SLRS : St Lawrence Rift System ; OBP : Paleo-rift Ottawa-Bonnechere ; MP : Province des Montérégiennes.

Définir la composition isotopique du manteau source est un moyen efficace de mieux comprendre le contexte géodynamique régional durant le Crétacé, âge de mise en place des magmas des Montérégiennes. Les principaux objectifs de cette thèse sont donc les suivants :

- Démontrer concrètement le rôle du manteau supérieur dans la genèse des collines Montérégiennes, grâce aux isotopes du Sr, Nd, Hf et Pb ;
- Déterminer l'influence de la contamination crustale dans la mise en place des magmas des Montérégiennes ;
- Démontrer l'efficacité de l'utilisation des isotopes des gaz rares (He, Ar) et des isotopes stables (N) dans la détermination de source mantellique.

Rappel sommaire sur les systèmes isotopiques utilisés dans cette étude

Les roches terrestres possèdent certains éléments, appelés éléments fils, qui proviennent de la désintégration radioactive d'autres éléments instables, appelés éléments pères. Les processus de désintégration ont deux applications importantes en Sciences de la Terre : (i) la détermination des âges d'échantillons géologiques; et (ii) l'étude de la pétrogenèse des roches terrestres. Cette dernière application concerne principalement les systèmes (père-fils) ^{87}Rb-^{87}Sr, ^{147}Sm-^{143}Nd, ^{238}U-^{206}Pb, ^{235}U-^{207}Pb, ^{232}Th-^{208}Pb et ^{176}Lu-^{176}Hf. L'utilisation de ces systèmes en pétrogenèse des roches est permise par les répartitions différentes des éléments pères et des éléments fils dans les différents réservoirs terrestres. En effet, durant l'individualisation des divers ensembles géologiques de la Terre solide (le noyau, le manteau et la croûte continentale), les éléments radioactifs n'ont pas été distribués en proportions équivalentes à leurs éléments fils, du fait de leur comportement géochimique différent. Ces distributions hétérogènes des éléments pères et fils ont engendré au cours du temps la variation des compositions isotopiques pour les éléments radiogéniques dans les différents ensembles géologiques de la Terre. Ces traceurs isotopiques permettent de comparer les signatures isotopiques à l'échelle régionale et globale du manteau terrestre. Ce principe d'utilisation des rapports isotopiques d'éléments traces afin de déterminer la source de matériaux est mis en application dans cette thèse.

Le système Rb-Sr est basé sur la désintégration radioactive de l'isotope 87 du rubidium en isotope 87 du strontium par rayonnement β ($T_{1/2}$ = 50 Ga, λ= 1.42 x 10^{-11} an^{-1}).

Le rubidium est plus incompatible que le strontium, ainsi le rapport $^{87}Sr/^{86}Sr$ tend à être plus élevé dans la croûte que dans le manteau. Par contre, le rubidium et le strontium étant facilement mobilisés par les fluides, le système Rb/Sr est sensible à l'altération.

Le système Sm-Nd est basé sur la désintégration radioactive de l'isotope 147 du samarium en isotope 143 du néodyme par radioactivité α ($T_{1/2}$ = 106 Ga, λ= 6.54 x 10^{-12} an^{-1}). Le samarium et le néodyme sont deux terres rares qui ont un comportement chimique voisin. Cependant, le samarium présente une compatibilité plus importante que le néodyme, ce qui permet l'utilisation de la méthode Sm-Nd en domaine magmatique. Le rapport $^{143}Nd/^{144}Nd$ est donc plus élevé dans le manteau que dans la croûte. Le samarium et le néodyme sont peu sensibles aux processus d'altération et au métamorphisme.

Le système U-Th-Pb est complexe car trois isotopes du plomb sont radiogéniques :

- $^{238}U \rightarrow {}^{206}Pb$ avec une constante λ de 1.55 x 10^{-10} an^{-1} ($T_{1/2}$ = 4.47 Ga)
- $^{235}U \rightarrow {}^{207}Pb$ avec une constante λ' de 9.85 x 10^{-10} an^{-1} ($T_{1/2}$ = 0.704 Ga)
- $^{232}Th \rightarrow {}^{208}Pb$ avec une constante λ'' de 4.95 x 10^{-11} an^{-1} ($T_{1/2}$ = 14.0 Ga)

Il s'agit en fait de chaînes de désintégration radioactives, dont le maillon le plus lent correspond à la constante donnée ci-dessus. Les périodes sont relativement courtes par rapport aux systèmes Sm-Nd et Rb-Sr. L'uranium, le thorium et le plomb sont trois éléments lourds de la famille des actinides, et sont largement fractionnés dans les processus magmatiques. Cependant, les systèmes U-Pb sont sensibles à l'altération et au métamorphisme car le plomb est facilement mobilisable par les fluides. Dans le système U/Pb, l'élément père est plus incompatible que l'élément fils, ainsi les rapports $^{206}Pb/^{204}Pb$, $^{207}Pb/^{204}Pb$ et $^{208}Pb/^{204}Pb$ sont plus élevés dans la croûte que dans le manteau.

Le système Lu-Hf est basé sur la désintégration radioactive de l'isotope 176 du lutétium en isotope 176 de l'hafnium par radioactivité β ($T_{1/2}$ = 35.9 Ga, λ= 1,93 x 10^{-11} an^{-1} ou 1.87 x 10^{-11} an^{-1} [(1)]) (Blichert-Toft and Albarede, 1997; Sguigna et al., 1982; Soderlund et al., 2004). Lors des processus de fusion partielle des matériaux terrestres, le lutétium et l'hafnium sont fractionnés deux fois plus que le néodyme et le samarium (Blichert-Toft,

[1] La calibration expérimentale sur des échantillons extraterrestres (météorites) donne une constante λ pour le lutécium de 1.93 x 10^{-11} an^{-1}. La calibration expérimentale sur des échantillons terrestres (roches ignées mafiques) donne une constante λ de 1.87 x 10^{-11} an^{-1}.

1997; Hofmann, 1988; Patchett et al., 1981). Ainsi les rapports $^{176}Hf/^{177}Hf$ dans le manteau sont plus élevés que dans la croûte.

Nous avons également utilisé les isotopes de l'argon, de l'hélium et de l'azote comme traceurs du manteau-source des Collines Montérégiennes. L'argon possède trois isotopes stables correspondant aux masses 40, 38 et 36. Le potassium ^{40}K ($T_{1/2}$ = 1,250 Ga) contenu dans les roches se désintègre par radioactivité β en ^{40}Ar. Il s'est accumulé majoritairement dans la croûte terrestre (son père, le K, étant un élément incompatible) depuis son accrétion. Les deux autres isotopes de l'argon (^{36}Ar et ^{38}Ar) représentent la composante primordiale de l'argon qui a été incorporée à la Terre pendant son accrétion. Le rapport $^{38}Ar/^{36}Ar$ dans l'atmosphère (0.1880; Ozima and Podosek, 1983) devrait être constant depuis 4.5 milliards d'années. En revanche, le rapport $^{40}Ar/^{36}Ar$ atmosphérique a augmenté depuis sa valeur initiale de 10^{-4} à la valeur actuelle de 295.5 par accumulation de ^{40}Ar produit par la décroissance du K. Le rapport $^{40}Ar/^{36}Ar$ peut être utilisé pour différencier une composante manteau inférieur (ca. 8000; Trieloff et al., 2000), d'une composante du manteau supérieur (40,000; Marty and Humbert, 1997). Cependant, la simple accumulation de ^{40}Ar radiogénique dans la croûte peut également produire de tels rapports élevés en $^{40}Ar/^{36}Ar$.

Les isotopes de l'hélium sont représentés par les masses 4 et 3. L'hélium-4 est produit sur Terre par la décroissance de $^{235, 238}U$ et ^{232}Th. En effet, les particules alpha émises lors de cette décroissance ne sont rien d'autres que des atomes de ^{4}He. L'hélium-3 est stable et représente la composante primordiale incorporée lors de l'accrétion de la Terre. Dans cette étude, seul l'hélium-4 a été analysé afin de définir le rapport $^{4}He/^{40}Ar^{*}$ qui représente un bon indicateur de phénomènes de dégazage des magmas (l'hélium est 10 fois plus soluble que l'argon dans les liquides silicatés), ainsi qu'un bon traceur de l'évolution du manteau. Le manteau supérieur (MORB) est caractérisé par un rapport $^{4}He/^{40}Ar^{*}$ actuel variant entre 1 et 5 (Graham, 2002).

L'azote est un des éléments volatiles les plus abondants sur Terre. Les isotopes stables de l'azote sont représentés par ^{14}N et ^{15}N et sont piégé dans le manteau terrestre, soit dans la structure des minéraux sous forme NH_4^+, soit dans les inclusions fluides des minéraux. L'azote représente un très bon traceur de croûte recyclée dans le manteau. Ainsi, une croûte aura un $\delta^{15}N$ positif de l'ordre de +7 ‰ (Sano et al., 1998), tandis qu'une composante mantellique supérieur comme celle mesurée dans les MORBs ou dans les

diamants aura un $\delta^{15}N$ négatif de l'ordre de -5 ±2 ‰ (Cartigny et al., 2001; Marty et Humbert, 1997). Le manteau profond représenté par les OIBs présente un $\delta^{15}N$ intermédiaire entre la croûte et le manteau supérieur, traduisant le recyclage de sédiments (+3 ‰; Marty and Dauphas, 2003). L'azote et l'argon étant tous deux des éléments incompatibles avec une faible solubilité dans les magmas (Libourel et al., 2003; Miyazaki et al., 2004), les rapports isotopiques $^{40}Ar/^{36}Ar$ et $\delta^{15}N$ traduisent ainsi les sources mantelliques.

Plan de la thèse

Cette thèse est présentée sous forme de trois articles rédigés en anglais, 1 publié et 2 en révision dans des revues scientifiques internationales à comités de lecture. Ces articles correspondent aux trois chapitres principaux de la thèse.

Le premier chapitre porte sur la géochimie et les isotopes du Sr et Nd dans les téphras italiens T21d et T32. Il a permis de caractériser le manteau source et la province volcanique source (Sabatini, Latium, Italie), ainsi que de contraindre l'âge de mise en place de ces produits volcaniques. L'article a été publié dans la revue *Quaternary International* en Aout 2009.

Le second chapitre traite des données géochimiques et isotopiques Nd, Sr, Hf et Pb obtenues pour les roches mafiques des intrusions des Montérégiennes. Il met en évidence un magmatisme résultant de la fusion du manteau lithosphérique subcontinental. Il montre aussi la présence d'une signature peu radiogénique en plomb-207, typique de la présence d'un manteau archéen. L'article est en révision pour être soumis dans la revue *Lithos*.

Le troisième chapitre est consacré à l'étude des gaz rares (He, Ar) et des gaz majeurs (N) préservés dans les inclusions fluides des clinopyroxènes et des amphiboles des roches mafiques des Montérégiennes. Il démontre la présence d'une signature isotopique similaire à celle observée dans un manteau supérieur. L'article est en révision pour être soumis dans la revue *Chemical Geology*.

Tous les chapitres de cette thèse ont également fait l'objet de conférences présentées lors de congrès internationaux, nationaux et locaux suivants :

- Mars 2010, Vitrine étudiante de l'UQAC, Chicoutimi, Québec ;
- Janvier 2010, 10^{éme} Congrès des étudiants du GEOTOP, Montréal, Québec ;
- Décembre 2009, AGU Fall Meeting, San Francisco, États-Unis ;
- Août 2008, IAVCEI General Assembly, Reykjavik, Islande (Chap.1 et 3) ;
- Juillet 2008, Goldschmidt, Vancouver, Colombie Britannique ;
- Février 2008, 8^{éme} Congrès des étudiants du GEOTOP, Rivière du Loup, Québec ;
- Mars 2007, 7^{éme} Congrès des étudiants du GEOTOP, LaChute, Québec.

Références

Blichert-Toft, J. and Albarede, F., 1997. The Lu-Hf isotope geochemistry of chondrites and the evolution of the mantle-crust system. Earth and Planetary Science Letters Vol.148, p.243-258.

Blichert-Toft, J., Chauvel C., Albarede, F., 1997. Separation of Hf and Lu for high-precision isotope analysis of rock samples by magnetic sector-multiple collector ICP-MS. Contributions to Mineralogy and Petrology Vol. 127 (Issue 3), p.248-260.

Brauer, A.W., S.; Mangili, C.; Moscariello, A., 2007. Tephrochronological dating of varved interglacial lake deposits from Pianico-Sellere (Southern Alps, Italy) to around 400 ka. Journal of Quaternary Science 22, 85-96.

Cartigny, P., Harris, J. W., and Javoy, M., 2001. Diamond genesis, mantle fractionations and mantle nitrogen content: a study of δ^{13}C-N concentrations in diamonds. Earth Planetary Science Letters 185, 85-98.

Cox, R.A., Wilton D.H.C. , 2006. U–Pb dating of perovskite by LA-ICP-MS: An example from the Oka carbonatite, Quebec, Canada. Chemical Geology In press, p.

De Paolo, D.J. and Wasserburg, G.J., 1976. Nd isotopic variations and petrogenetic models. Geophysical Research Letters 3 (5), 249-252.

Eby, N., 1984. Geochronology of the Monteregian Hills alkaline igneous province, Quebec. Geology 12, 468-470.

Eby, N., 1985. Age relations, chemistry and petrogenesis of mafic alkaline dikes from the Monteregian Hills and younger White Mountain igneous provinces. Canadian Journal of Earth Sciences 22, 1103-1111.

Eby, N., 2006. Carbonatites to alkali granites- Petrogenetic insights from Chilwa and Monteregians Hills-White Mountain Igneous Provinces, Congrés GAC-MAC, Montréal, pp. 45.

Esu, D. and Gianolla, D., 2009. The malacological record from the Plio-Pleistocene Leffe Basin (Bergamo, Northern Italy). Quaternary International.

Faure, S., Tremblay, A. and Angelier, J., 1996. State of intraplate stress and tectonism of northeastern America since Cretaceous times, with particular emphasis on the New England-Quebec igneous province. Tectonophysics 255, 111-134.

Foland, K.A., Gilbbert, L.A., Sebring, C.A. and Jiang-Feng, C., 1986. 40Ar/39Ar ages for plutons of the Monteregian Hills, Quebec: Evidence for a single episode of Cretaceous magmatism. Geological Society of America Bulletin 97, 966-974.

Foland, K.A., Jiang-feng, C., Gilbbert, L.A. and Hofmann, W.A., 1988. Nd and Sr isotopic signatures of Mesozoic plutons in northeastern North America. Geology 16, 684-687.

Furman, T., 2007. Geochemistry of East African Rift basalts: An overview. Journal of African Earth Sciences 48 (2-3), 147-160.

Furman, T. and Graham, D., 1999. Erosion of lithospheric mantle beneath the East African Rift system: geochemical evidence from the Kivu volcanic province. Lithos 48 (1-4), 237-262.

George, R.M. and Rogers, N.W., 2002. Plume dynamics beneath the African plate inferred from the geochemistry of the Tertiary basalts of southern Ethiopia. Contributions to Mineralogy and Petrology 144, 286-304.

Hart, A., 1988. Heterogeneous mantle domains: signatures, genesis and mixing chronologies. . Earth and Planetary Science Letters Vol.90 (3), p273-296.

Hart, S.R., Hauri, E.H., Oschmann, L.A. and Whitehead, J.A., 1992. Mantle plumes and entrainment: isotopic evidence. Science 256, 517-520.

Hofmann, A.W., 1988. Chemical differentiation of the Earth: the relationship between mantle, continental crust, and oceanic crust. Earth and Planetary Science Letters 90 (3), 297-314.

Hofmann, A.W. and White, W.M., 1982. Mantle plumes from ancient oceanic crust. Earth and Planetary Science Letters 57 (2), 421-436.

Izett, G.A., 1981. Volcanic ash beds: Recorders of upper Cenozoic silicic pyroclastic volcanism in the Western Unites States. Journal of Geophysical Research 86, 10200-10222.

Karner, D.B.M., F.; Renne,P.R., 2001. The history of the Monti Sabatini and Alban Hills volcanoes: ground work for assessing volcanic-tectonic hazards for Rome. Journal of Volcanology Geothermal Research 107, 185-215.

Libourel, G., Marty, B. and Humbert, F., 2003. Nitrogen solubility in basaltic melt. Part I. Effect of oxygen fugasity. Geochimica et Cosmochimica Acta 67 (21), 4123-4135.

Marty, B. and Dauphas, N., 2003. The nitrogen record of crust-mantle interaction and mantle convection from Archean to Present. Earth and Planetary Science Letters 206, 397-410.

Marty, B. and Humbert, F., 1997. Nitrogen and argon isotopes in oceanic basalts. Earth and Planetary Science Letters 152 (1-4), 101-112.

McHone, J.G., 1996. Constraints on the mantle plume model for Mesozoic alkaline intrusions in northeastern North America. The Canadian Minerlogist 34, 325-334.

Miyazaki, A., Hiyagon, H., Sugiura, N., Hirose, K. and Takahashi, E., 2004. Solubilities of nitrogen and noble gases in silicate melts under various oxygen fugasities: implications for the origin and degassing history of nitrogen and noble gases in the Earth. Geochimica et Cosmochimica Acta 68 (2), 387-401.

Moscariello, A. et al., 2000. A long lacustrine record from the Piànico-Sèllere Basin (Middle-Late Pleistocene, Northern Italy). Quaternary International 73-74, 47-68.

Ozima, M. and Podosek, F.A., 1983. Noble Gas Geochemistry.

Patchett, P.J., Kouvo, O. and al., 1981. Evolution of continental crust and mantle heterogeneity: Evidence from Hf isotopes. Contributions to Mineralogy and Petrology 78, 279-297.

Penck, A. and Bruckner, E., 1909. Die Alpen im Eiszeitaler, Bd 3, Chr. Her. Tauchnitz, Leipzig.

Pik, R., Deniel, C., Coulon, C., Yirgu, G., Marty, B., 1999. Isotopic and trace element signatures of Ethiopian flood basalts: Evidence for Plume-lithosphére interactions. Geochimica et Cosmochimica Acta 63 (15), 2263-2279.

Pik, R., Marty, B. and Hilton, D.R., 2006. How many mantle plumes in Africa? The geochemical point of view. Chemical Geology 226 (3-4), 100-114.

Pinti, D.L.Q., X.; Chiesa, S.; Ravazzi, C.; Gillot, P.Y., 2001. K-Ar dating of an early Middle Pleistocene distal tephra in the interglacial varved succession of Pianico-Sellere (Southern Alps, Italy). Earth and Planetary Science Letters 188, 1-7.

Sano, Y., Takahata, N., Nishio, Y. and Marty, B., 1998. Nitrogen recycling in subduction zones. Geophysical Research Letters 25 (13), 2289-2292.

Sarna-Wojcicki, A.M. and Davies, J.O., 1991. Quaternary tephrochonology. In: R.B. Morrison (Editor), Quaternary non-glacial geology. Geological Society of America, The Geology of North America, Boulder, colorado, pp. 93-116.

Sarna-Wojcicki, A.M., Lajoie, K.R., Meyer, C.E. and Adam, D.P., 1991. Tephrochronologic correlation of upper Neogene sediments along rge Pacific margin, comterminous Unated States. In: R.B. Morrison (Editor), Quaternary non glacial geology. Geologicl Society of America, The Geology of North America, Boulder Colorado, pp. 107-140.

Scardia, G. and Muttoni, G., 2009. Paleomagnetic investigations on the Pleistocene lacustrine sequence of Piànico-Sèllere (NorthernItaly). Quaternary International.

Self, S. and Sparks, R.S.J., 1981. Tephra studies. D.Reidel Publishing Co, Boston, 481 pp.

Sguigna, A.P., Larabee, A.J. and al., e., 1982. The half-life of 176Lu by a γ-γ coincidence measurement. Canadian Journal of Physics 60, 361-364.

Soderlund, U., Patchett, J., Vervoort, J., and Isachsen, C., 2004. The 176Lu decay constant determined by Lu-Hf and U-Pb isotope systematics of Precambrian mafic intrusions. Earth and Planetary Science Letters 219, 311-324.

Stracke, A., Hofmann, A.W. and Hart, A., 2005. FOZO, HIMU, and the rest of the mantle zoo. Geochemistry Geophysics Geosystems 6 (5), doi:10.1029/2004GC000824.

Thorarinsson, S., 1944. Tefrokronologiska studier på Island (Tephrochronological studies in Iceland) Geografiska Annaler 26, 1-217.

Trieloff, M., Kunz, J., Clague, D., Harrison, D. and Allègre, C.J., 2000. The Nature of Pristine Noble Gases in Mantle Plumes Science 288 (5468), 1036 - 1038.

White, W., 1985. Sources of oceanic basalts: Radiogenic isotopic evidence. Geology 13, 155-118.

Wilcox, R.E., 1965. Volcanic ash chronology. In: H.E. Wright, Jr. and Frey, D.G. (Editor), Quaternary of the United States. Princeton Univ. Press, Princeton, N.J., pp. 807-816.

Zindler, A. and Hart, S., 1986. Chemical geodynamics. Ann. Rev. Earth Planet. Sci 14, 493-571.

AVANT-PROPOS DU CHAPITRE 1

Contributions des auteurs

Le chapitre 1 est le résultat d'une collaboration entre l'Université du Québec à Montréal et le Laboratoire de Géochronologie de l'Université de Paris SUD XI, France. Je suis à l'origine de la majorité des analyses ainsi que de l'interprétation et la rédaction de l'article. Daniele Pinti a participé la rédaction de l'article ainsi qu'à sa relecture. Virgile Rouchon a échantillonné les roches de Roccamonfina et contribué à la géologie de la région étudiée. Il m'a fait parvenir les échantillons de Roccamonfina et celui de t32. Xavier Quidelleur et Pierre-Yves Gillot ont participé à la relecture ainsi qu'aux corrections de l'article.

CHAPITRE 1

Tephro-chronostratigraphy of the lacustrine interglacial record of Piànico, Italian Southern Alps: identifying the volcanic sources using radiogenic isotopes and trace elements

Emilie ROULLEAU[1], Daniele L. PINTI[1,*], Virgile ROUCHON[2], Xavier QUIDELLEUR[3] and Pierre-Yves GILLOT[3]

[1] GEOTOP and Département des Sciences de la Terre et de l'Atmosphère, Université du Québec à Montréal, Montréal, Qc, H2X 3Y7, Canada.

[2] Institut Français du Pétrole, 1-4 Avenue Bois Préau, 92500 Rueil-Malmaison, France.

[3] Laboratoire de Géochronologie Multi-Techniques, UMR IDES8148 (UPS-CNRS), Université Paris-Sud 11, 91405 Orsay Cedex, France.

Published in Quaternary International, August 2009

1.1. Abstract

The chronostratigraphic position of the Pianico carbonate sequence, Oroebic Alps, Italy remains controversial, notwithstanding that it is one of the best-preserved records of an alpine interglacial. Two distal tephra were discovered in the sequence. The lowermost (t21d) is a rhyolitic tephra dated by K–Ar at 779 ± 13 ka, different from the uppermost phonolitic tephra (t32) with an assigned age of 393 ± 12 ka. The volcanic source of t32 was recently interpreted as being the Brown Leucitic Tuff of the Roccamonfina volcano, southern Italy. New trace element and Nd and Sr isotopic composition of t32 and of 420–200 ka volcanic products of the Roccamonfina clearly indicate that this volcano is not the source of t32, but that it likely originated from the northern Roman Magmatic Province. The products of the initial explosive activity of Sabatini Mts., dated ca. 780–800 ka, isotopically match t32 and are proposed as its source. This indicates that the previously inferred age of ~400 ka for t32 is erroneous. New isotopic and geochemical data of t21d confirm it as being associated with the first pyroclastic eruptions (790–710 ka) of the Puy de Sancy volcano, French Massif Central. The Early-Middle Pleistocene K–Ar ages obtained previously for t21d, together with the isotopic attribution of volcanic sources to both tephra layers presented here, confirm Pianico as one of the best interglacial sequences of Cromerian age in the Western Alps.

1.2. Introduction

Distal tephra are excellent stratigraphic markers, providing material for both correlated and direct radiometric age determinations of the associated sedimentary deposits (e.g., Sarna-Wojcicki, 2000). Yet, radiometric ages are often hampered by the alteration state of the tephra and indirect qualitative dating approaches are needed. These are based on mineral and bulk chemistry comparison between the tephra and well-dated and chemically characterized volcanic sources. This method is not straightforward because it is generally based on major element chemistry, which for distal tephra can be deeply modified by weathering. Mineral fractionation during fall transport can also modify the chemical composition of the distal tephra (Sarna- Wojcicki et al., 1981). Comparison with trace

element contents and radiogenic isotopes would give more constrained indications on the volcanic sources. However, modern tephrochronology tends to be anchored on simple comparisons based on grain morphology and major element chemistry, and it is only recently that a few studies have used trace element geochemistry combined with statistical approaches (e.g., Pearce et al., 1996, 2008; Pouclet et al., 1999; Pinti et al., 2003).

Discovered more than one century ago, the long lacustrine carbonate varve sequence of the Piànico Formation, Oroebic Alps (Figs. 1 and 2) is one of the best-preserved records of an interglacial period in the Southern Alps (Moscariello et al., 2000). However, the chronostratigraphic position of this sequence has been only partially defined. Stoppani (1857) and Lepsius (1910) recognized the interglacial character of the carbonate sequences of Pia` nico and suggested a PlioPleistocene age, based on macroflora and on the number of observed glacial cycles. Since the discovery of *Rhinoceros merckii Jaeg* (Penck and Brückner, 1909), the Piànico carbonates have been attributed to the more recent Eemian interglacial or OIS 5e. Recently, Moscariello et al. (2000) carried out a more detailed sedimentological study of the Piànico Formation and proposed a Middle-Late Pleistocene age, although they recognized some discrepancies between the pollen record of Piànico and Eemian typical pollen records (Moscariello et al., 2000). Recently, Esu and Gianolla (2008) have discovered the occurrence of the genus *Tanousia* Servain (Mollusca) in the Piànico Formation, which has morphological resemblance with *Tanousia runtoniana-stenostoma* group observed in Northern Europe sediments of Bavelian and Cromerian age. The malacological records of *Tanousia* from Piànico combined with new mammal findings (Govoni et al., 2006) rather support an Early-Middle Pleistocene age for the Piànico Formation.

Wood fragments, dated with ^{14}C, were older than the upper age limit of the method (45 ka), indicating that Piànico is older than the Last Glacial Maximum (Alessio et al., 1978). Achim Brauer (GFZ, Potsdam) and his colleagues discovered a perfectly preserved tephra in the upper half of the Piànico Formation, the marker layer t21d (Fig. 2). Pinti et al. (2001) assigned an age of 779 ± 13 ka based on eight concordant K–Ar ages obtained on glass separates. A reverse to normal polarity paleomagnetic transition, recorded between the base and the top of the interglacial unit, and interpreted as the Matuyama–Brunhes reversal,

supported this age (Pinti et al., 2001). The reverse polarity has been recently confirmed by a new paleomagnetic survey of the lower half of the Piànico sequence (Scardia and Muttoni, in this issue) assigning the interglacial sequence to MIS 19. However, the chronostratigraphic position of the Piànico Formation is still strongly contested.

Brauer et al. (2007) discovered a new tephra layer (t32) in the uppermost sequence of the Piànico Formation. This second tephra is highly altered, preventing any precise isotopic dating. Brauer et al. (2007) compared the mineral content and the chemical composition of tephra t32 with those of the Roman Magmatic Province. They concluded that t32 tephra is a distal product of the Brown Leucitic Tuff (BLT) erupted from the Middle-Late Pleistocene Roccamonfina stratovolcano, located 600 km south of Piànico, between Rome and Naples (Fig. 1). They arbitrarily assigned the BLT to a parasitic structure of the Roccamonfina volcano, the Savone ravine dome dated at 393_12 ka (Giannetti, 2001), thereby suggesting that the interglacial carbonate sequence of Piànico was deposited during MIS 11. To support this hypothesis, they roughly compared the chemical composition of the t21d tephra with that of the Rivaux tephra, erupted from the Sancy volcano, Massif Central, France (Fig. 1) and poorly dated at 470 ± 200 ka (Pastre and Cantagrel, 2001). They concluded that the K-Ar age of t21d is erroneous and that this tephra belongs to the last activity phase of the Sancy volcano dated between 450 and 250 ka (Pastre and Cantagrel, 2001).

In the light of the following arguments, the assigned age of 393 ± 12 ka to t32 tephra is incorrect. The Savone ravine dome of the Roccamonfina has unclear stratigraphic relations with the BLT and is not directly related to the eruption of the BLT itself (Giannetti, 2001). It is thus not correct to use the age of the Savone ravine dome as equivalent to the emplacement age of the BLT. Ballini et al. (1990) and Luhr and Giannetti (1987) tentatively dated the BLT pyroclastic eruption between 335 and 385ka. Rouchon et al. (2008) precisely dated the BLT to 353±5 ka on the basis of three concordant K–Ar ages on sanidine and biotite. The eruptive age of the BLT corresponds to that of the glacial stage MIS10 (Pinti et al.,2007), thereby ruling out the age proposed by Brauer et al.(2007) for the Piànico interglacial sequence. This paper reports new trace element data on the t32 tephra plus new Sr and Nd isotopic ratios for both tephras and for the three major Roccamonfina plinian deposits. The Middle Pleistocene age of ~400ka suggested by Brauer et al. (2007) for the t32 tephra is not supported by the chemical and isotopic composition of the suggested volcanic sources.

1.3. The Piànico Formation: a brief stratigraphic guide and description of the tephra

The Piànico-Sellère basin (45° 48' 45" N, 10° 2' 58" E, 280-350 m a.s.l.) records a sequence of lacustrine, glacial and fluvial deposits cropping out along the Borlezza Valley, a western tributary of the Iseo Lake (Southern Alps, Bergamo, Italy).

The Piànico Formation (Moscariello et al., 2000; Ravazzi, 2006) consists of ~50 m of fine-grained laminated sediments corresponding to four lithostratigraphical units (from the base to the top; Fig. 2):

- the "Membro di Cascina Canneto" (MBC) - Cascina Canneto Member
- the "Banco Torbiditico Basale" (BTB) – Basal turbidite bed
- the "Silt e Argille Basale" (SAB) – Basal silt and clay
- the " Banco Varvato Carbonatico" (BVC) – carbonate Varved Bed
- the " Membro di La Palazzina" (MLP) – La Palazzina Member

Here, only a brief description of the SAB, BVC and the MLP is given, where the two tephra were discovered (Fig. 2). The SAB consists of carbonate, laminated mudstones interpreted as microturbidites. The BVC consists of about 10.5-m thick succession of carbonate varves formed during warm and cool temperate conditions dominated by endogenic calcite sedimentation. Thick coarser brownish layers occur within the varves and are interpreted as turbidity current deposits. These deposits have been used as ''marker layers'' during the painstaking work of varve counting and microstratigraphic correlation (Moscariello et al., 2000; Rossi et al., 2000; Mangili et al., 2005). Between the t0 and t22-labeled marker layers (Fig. 2), 15100 varves have been counted. Below t0, separated by an erosional debris flow and slump, there are 628 additional varves. The MLP member is a 30-m thick succession of i) lacustrine light/dark rhythmites dominated by endogenic precipitation of calcite, but enriched in clay and silt compared to the BVC, indicating detrital influx; and ii) massive/finely alternation of silt and sand resulting from high-density currents. Between marker layer t26 and TS0, an additional 1120 varves were counted (Ravazzi, 2006). The grayish t21d is a rhyolitic tephra located 896 varves (ca. 50 cm) below the upper termination of the BVC member (Fig. 2). It crops out with a constant thickness of 7–9 mm. It is composed of 85% of glass shards made of micro-vesicular pumice (average size of 46 mm;

Pinti et al., 2003). Primary magmatic minerals are plagioclase ($Ab_{64.1-72.4}$ $An_{21.1-25.6}Or_{6.5-10.2}$), alkali-feldspar ($Or_{53.9}Ab_{42.8-43.6}An_{2.5-3.3}$) and biotite (Pinti et al., 2001), together with zircon, sphene and apatite among the accessory minerals (Brauer et al., 2007). The t32 is an 8 mm thick continuous dark brown tephra outcropping mainly at the so-called ''Wall section'' (see Moscariello et al., 2000 for details on the outcrops) from where specimens were sampled for trace elements and radiogenic isotopes. The mineral assemblage of t32 is made up of two generation of clinopyroxenes (salite and diopside), plagioclase, sanidine, biotite, leucite phenocrysts and rare olivine xenocrysts (Brauer et al., 2007). The chemical composition of the glass is inhomogeneous (three subgroups have been observed by Brauer et al., 2007) and ranges from tephrophonolitic (the most abundant subgroup) to phono-tephritic (Fig. 3). The main juvenile phases are colorless low vesicular pumice fragments and brown blocky glass shards occurring in different states of alteration. The X-ray investigation on tephra t32 carried out at GEOTOP-UQAM revealed the occurrence of gypsum, kaolinite, pyrite, natrojarosite and barite as secondary minerals. Kaolinite and gypsum/natrojarosite/barite are classic products of weathering of plagioclase and pyrite, respectively, under acid conditions (Preda and Cox, 2004). Brauer et al. (2007) also observed leucite/analcime association, which could indicate analcimization.

1.4. Methods

Trace element composition of tephra t32 was analyzed at the SARM-CRPG in Vandœuvre, France. A few milligrams taken from a 10 g of crushed sample were fused with $LiBO_2$, dissolved with HNO_3, analyzed by ICP-MS Thermo Elemental X7 and calibrated with the international geostandards available at the SARM-CRPG. Details can be found in Carignan et al. (2001).

Isotopic analyses of Rb-Sr and Sm-Nd were performed on two glass separates of t21d at CRPG Vandœuvre by Laurie Raisberg. Approximately 100 mg of powder was spiked with tracer solutions. The samples were mixed with an HF–HNO_3–$HClO_4$ acid mixture in a teflon beaker and heated at 110°C for 72 hours. Rb and Sr isotopes were separated by cation-exchange techniques using AGX 50W resin with 2.5 N HCl. After rinsing with 2.9 N HNO_3,

REE were collected from the resin using 4.4 N HNO_3. Nd and Sm were extracted from the other REE using HDEHP-coated Teflon resin columns with 0.27 N and 0.5 N HCl, respectively. The Rb isotope composition was determined using an ELAN 6000 ICP–MS at the SARM-CRPG. The isotopic analyses of Sr, Nd and Sm were made in static multi-collection mode using a Finnigan MAT 262 mass spectrometer. Measured $^{87}Sr/^{86}Sr$ and $^{143}Nd/^{144}Nd$ ratios were normalized to $^{87}Sr/^{86}Sr = 0.1194$ and $^{143}Nd/^{144}Nd = 0.7219$, respectively. During the t21d analyses, the ratios obtained for La Jolla Nd and NBS987 SR standards were 0.511799 ± 22 and 0.710166 ± 48, respectively. Such ratios are slightly different than accepted values (La Jolla: 0.511854; NBS987: 0.71024) due to the well-known deviation produced when using Faraday cups (Solgadi et al., 2007). The results of t21d presented in Table 3 have been corrected in order to put the La Jolla and NBS987 standards into agreement with their internationally accepted values. The typical procedure blanks for Nd and Sr are about 0.4 ng and less than 2 ng, respectively. Initial $^{87}Sr/^{88}Sr$ and $^{143}Nd/^{144}Nd$ have been recalculated using the K-Ar age of 77 9± 13 ka obtained for t21d (Pinti et al., 2001). It is noteworthy that using the age of ca. 400 ka suggested by Brauer et al. (2007) would not change significantly the Sr and Nd isotopic composition (Table 3).

The Sm-Nd and Rb-Sr isotopic composition of t32 and Roccamonfina samples were determined at the GEOTOP-UQAM Radiogenic Isotope Laboratory in Montréal. Tephra t32 was powdered into three fractions (50 mg each), treated with three different protocols: (1) direct digestion of the sample without addition of Nd and Sr spikes to determine the isotopic composition; (2) digestion of the sample with addition of Sr and Nd spikes to obtain concentrations and parent daughter ratios and; (3) leaching of the sample to check whether the Sr and Nd isotopic composition of t32 was affected by the addition of carbonate/sulphate minerals produced by weathering. This latter process consisted in washing the fraction in 2 M HCl for 30 min and rinsed with distilled water. The sample was then heated in distilled water on a hotplate for 1 hour. For the Roccamonfina samples, about 50 mg of the powder underwent a direct digestion of the sample without addition of Nd and Sr spikes to determine the isotopic composition.

Chemical separation was conducted on powdered sample, weighed out into a Teflon Parr-bomb and spiked with ^{150}Nd-^{149}Sm and ^{87}Rb-^{84}Sr tracer solutions. A mixture of HF-HNO_3 was added to the powder and heated at 150°C for 1 week. Then, the samples were

evaporated in perchloric acid to break up the fluoride salt, dissolved again in 6 M HCL and heated again in the furnace for 12 hours. The resulting 6 M HCL solutions were loaded on cation-exchange columns containing 4 ml of AG1X8 resin in order to retain the Fe. 14 M HNO_3 was then added to transform the HCl salts into nitrates and evaporated. The REE separation was achieved using 1ml of Eichrom TRU Spec resin. Rb-Sr fractions were collected with 1M HNO_3 and REE fractions were collected with 0.05 M HNO_3. The Sm-Nd chemical separation was achieved using Eichrom LN Spec resin with procedures modified after Richard et al. (1976). Rb and Sr were separated using Eichrom Sr Spec resin. Rb fraction was collected using 6 ml of 3 M HNO_3 and Sr fraction was collected using 3 ml of distilled H_2O. The Sr fractions were passed twice through these columns to ensure a good separation of Rb and Sr.

The Nd, Sm and Sr samples were analyzed using a TIMS VG54 Sector. Nd and Sr were measured in dynamic mode and normalized to $^{146}Nd/^{144}Nd = 0.7219$ and $^{86}Sr/^{88}Sr = 0.1194$ assuming exponential fractionation, while Sm and Rb were measured in static mode. For this study, Nd standard JNdi yielded a value of $^{143}Nd/^{144}Nd = 0.512148 \pm 11$ (n=11), significantly lower than the published value of 0.512115 ± 7 (Tanaka et al., 2000). Tephra t32 analyses were then corrected using this offset of 0.000033. Sr isotopic measurements are reported to a value of $^{87}Sr/^{88}Sr=0.7102628 \pm 17$ (n=7) for NSB987 standard. Rb isotopic ratios were calculated from Rb contents and the natural abundance of ^{85}Rb and ^{87}Sr. The typical combined procedure blanks for Nd and Sm are under 150 pg. Initial $^{143}Nd/^{144}Nd$ and $^{87}Sr/^{88}Sr$ were calculated using an age of 779±13 ka for t21d (Pinti et al., 2007) and ages of 439 ± 9 ka (ante-BLT), 353 ± 5 ka (BLT) and 331 ± 2 ka (White Trachytic Tuff) for the Roccamonfina samples (Rouchon et al., 2008).

1.5. Results

Table 1 shows the average chemical composition for both t21d and t32 (Pinti et al., 2003; Brauer et al., 2007), while Table 2 contains new trace element data for the t32 layer (this study). Table 3 contains new Sr and Nd isotopic composition for both tephra layers and for seven Middle-Late Pleistocene volcanic products of the Roccamonfina volcano. The

Roccamonfina samples have been analyzed in order to test the hypothesis formulated by Brauer et al.(2007) of a genetic link between t32 tephra and the Roccamonfina volcanic complex (Rouchon et al., 2008).

In Fig. 3, the TAS diagram (Le Maitre et al., 1989) highlights the distinct chemical composition of the two tephras t21d and t32 (Table 1). Tephra t21d straddles at the boundary between the trachyte and the rhyolite fields (data from Pinti et al., 2003), while the average composition of the three populations of glass shards in t32 (the only data reported by Brauer et al., 2007) covers the fields from phono-tephrite to tephriphonolite. Fig. 3 shows that the chemical composition of volcanic rocks erupted from the Mont-Dore and Sancy volcanoes of Massif Central (France) is compatible with that of tephra t21d. Tephra t32 displays a bulk chemical composition compatible with several volcanic products from the Roman Magmatic Province (RMP hereafter) (Fig. 3). The phonotephrite to tephra-phonolite composition of t32 is compatible with those observed in the leucite-bearing rocks of Roccamonfina preceding the BLT (Rouchon et al., 2008; Conticelli et al., 2009), those erupted from the Sabatini Mts. (Conticelli et al., 1997, 2002; Sottili et al., 2004) and partially with those of Vico (Perini et al., 2004; Peccerillo, 2005; Avanzinelli et al., 2008) and the Alban Hills (Trigila et al., 1995; Freda et al., 1997; Peccerillo, 2005). The incompatible trace element compositions of t21d and t32 are reported in the primitive mantle-normalized diagrams of Wood et al. (1979) (Fig. 4a–c). Both tephra show an enrichment of Large Ion Lithophile Elements (LILE) compared to Heavy Rare Earth Elements (HREE) (Fig. 4a) which is characteristic of both alkali island-arc magmas and Oceanic Island Basalts (OIB) (Wilson, 1989). However, subtle differences exist which allow assigning each of these two tephra to a different geodynamic setting. Tephra t21d shows: 1) a large depletion in Ba and Sr compared to the other LILE; 2) an anomalous enrichment in Nb and Ta; and 3) a large depletion in P and Ti (Fig. 4a). The trough in Ba and Sr is possibly related to feldspar fractionation, while the trough at P may indicate apatite fractionation. The Ti trough, shared by both t21d and t32, is indicative of Fe–Ti oxides fractionation (Wilson, 1989). Tephra t32 is characterized by a marked Nb–Ta trough and enrichment in fluidmobile elements Ba and Sr (Fig. 4a). The Nb–Ta trough is characteristic of island-arc magmas and is explained by the Nb and Ta incompatibility in fluids released by the down-going slab during dehydration metamorphic reactions in subduction settings (e.g., Lustrino and Wilson, 2007). The incompatible trace element pattern

of t32 is typical of most of the Italian orogenic (subduction related) volcanism (e.g., Peccerillo, 2005 and references therein). On the other hand, the relative enrichment of Nb and Ta in tephra t21d is characteristic of anorogenic (intraplate-related) volcanism (e.g., Lustrino and Wilson, 2007). The Sr and Nd isotopic compositions of tephra t21d and t32 are presented in Table 3 and illustrated in Fig. 5a and b. The initial Sr and Nd ratios of the tephra t21d (Fig. 5a) are 0.705006–0.704986 and 0.512722, respectively. The more radiogenic Nd ratios and the less radiogenic Sr isotopic ratios of t21d compared to tephra t32 (Fig. 5b) are within those observed in Cenozoic anorogenic (intraplate-like) volcanism of Europe (Lustrino and Wilson, 2007). These values correspond to a dominant sub-lithospheric magma source region called Common Mantle Reservoir (CMR) (Lustrino and Wilson, 2007). In Fig. 5a, we compared the Nd and Sr isotopic composition of tephra t21d with those of the volcanic complex of Mont-Dore–Sancy (Massif Central, France) and Westerwald in Germany (Briot et al., 1991; Lustrino and Wilson, 2007 and references therein). These are the only anorogenic volcanic complex in Western Europe still active over the Quaternary (Nowell et al., 2006) together with the east-Eifel for which there are no Nd and Sr isotopic data for Quaternary products (Lustrino and Wilson, 2007). Pinti et al. (2003) noticed a strong similarity between the incompatible trace element composition of rhyolitic products erupted from the Euganean Hills, a volcanic complex of Oligocene age located 200 km east of Piànico (Fig. 1), and tephra t21d, hypothesizing whether a local reactivation of this volcanism over the Quaternary could have produced the fall deposits of Piànico. The completely different Nd and Sr isotopic composition between rhyolites from the Euganean Hills and t32 definitively ruled out this hypothesis and it shall not be discussed further (Fig. 5a).

Fig. 5b shows the comparison between the Nd and Sr isotopic composition measured in three different aliquots of tephra t32 and those measured in samples from the main explosive eruptions of the Roccamonfina volcano, spanning in age from 440 to 330 ka (Rouchon et al., 2008). The samples were selected in order to yield an overlook of the Nd and Sr isotopic variability of Roccamonfina volcanic products, proposed by Brauer et al. (2007) as the source of tephra t32. Samples are RMF14 (Rio Rava locality) and 89S (Campo), two trachytes predating the Brown Leucitic Tuff and dated by K–Ar at 439 ± 6 ka and 440 ± 6 ka, respectively (Rouchon et al., 2008); phonolite and shoshonite pumices 47Y3, 89I and 89J from the Brown Leucitic Tuff eruption dated (89I) at 353 ± 5 ka (Rouchon et al., 2008); and

finally RMF96 and RMF11, two samples of the most voluminous explosive eruption of the Roccamonfina volcano, the White Trachytic Tuff, which occurred at 331 ± 2 ka (Rouchon et al., 2008). For the sake of comparison, the Nd and Sr isotopic variability measured in other samples of the Roccamonfina volcano and the Ernici volcanic complex (Peccerillo, 2005; Frezzotti et al., 2007; Conticelli et al., 2009) and that of the main volcanic complexes of the Northern Roman Magmatic Province (N-RMP hereafter; Peccerillo, 2005 and references therein) are reported. The three analyzed aliquots of tephra t32 encompass a small range of $^{143}Nd/^{144}Nd_i$ (0.512198–0.512202) and $^{87}Sr/^{86}Sr_i$ values (0.710968–0.711031) (Fig. 5b). These isotopic compositions indicate the involvement of some crustal material in the genesis of the magma sources, a feature typical of the orogenic volcanism of Central Italy (Hawkesworth and Vollmer, 1979). However, the Nd and Sr isotopic composition of t32 is clearly different from those of the Roccamonfina volcanic products but similar to those of the NRMP, although the Nd isotopic composition is slightly more radiogenic (Fig. 5b).

1.6. Discussion

1.6.1. Alteration of the Piànico tephra and their "datability"

One of the major problems in tephro-chronostratigraphy is the weathering of tephra, which may prevent 1) the correct radiometric dating, 2) the stratigraphic correlation with other tephra markers, and 3) may cause misidentification (Pollard et al., 2003). Tephra t21d and t32 show very different conditions of preservation, which is possibly due to their different mineralogical and chemical composition. The t21d is a rhyolitic glass, which is more stable than the phonolitic glass composing t32 (Pollard et al., 2003). Here, following the empirical method of Pollard et al. (2003), we demonstrate that tephra t21d is perfectly preserved and thus we can assume radiometric dating by the K-Ar method meaningful. On the other hand, t32 is strongly altered, as indicated by the occurrence of secondary kaolinite and gypsum/natrojarosite/barite (this study) and advanced analcimization of the leucite (Brauer et al., 2007), thus rendering any radiometric dating dubious.

Pollard et al. (2003) proposed a simple empirical approach to quantify the capacity of a glass to resist to aqueous attack. Chemical alteration can take the form of cationic leaching

from the matrix, or complete destruction of the silica network. These two processes can be quantified by calculating three parameters of a glass: the 1) Si:O molar ratio, related to the number of non-bridging oxygens in the network structure, 2) NBO, and 3) the Gibb's free energy of hydration. In other words, the first two are a measure of the tendency of the silica network to disintegrate, and the third the potential for cationic exchange to occur (Doremus, 1994; White and Minser, 1984; Jantzen and Plodinec, 1984; Sterpenich and Libourel, 2006).

The Si:O molar ratio is a measure of the stability of the network. In a pure silica glass (which is chemically extremely stable) all four oxygens are linked to (and shared with) another silicon tetrahedron. The Si:O ratio is therefore 0.5 and the number of non-bridging oxygens (NBO) per silicon atom is zero. As network modifiers (Na_2O, K_2O, CaO, MgO) are added to the glass the ratio of Si:O falls, the network is disrupted, and the number of non-bridging oxygen ions increases. Basaltic tephra glass containing large amounts of CaO, Na_2O and MgO and less SiO_2 result in a more open network than rhyolitic glasses, facilitating network dissolution during hydration. The change in Gibb's free energy of hydration (ΔG_{Hydr}) determines the spontaneity and direction of a reaction with water. Negative free energies are associated with spontaneous reactions. Thus, more negative ΔG_{Hydr} results in more glass hydration.

The Si:O molar ratio, the NBO and the ΔG_{Hydr} have been calculated for tephra t32 and t21d (Figs. 6a and b) using equations by Pollard et al. (2003). In the same diagram, we reported the North-Atlantic tephra database (Haflidason et al., 2000) for comparison. These data have also been used by Pollard et al. (2003) to illustrate how these three parameters vary with increasing chemical instability of the glass. It is clear that tephra t21d has a chemical composition making it very resistant to weathering, while tephra t32, enriched in network modifiers such as Na, Ca and Mg, is extremely susceptible to hydration and alteration (Figs. 6a and b).

Brauer et al. (2007) have interpreted the Loss of Ignition (LOI) measured by Pinti et al. (2001) and the dissolved-water concentrations measured by EPMA in the glass shards of t21d (4-6.5 wt%; Pinti et al., 2003) as an evidence of advanced alteration of the tephra. The total absence of correlation between the EPMA dissolved-water concentrations, measured as the difference between 100% minus the sum of oxides and the alkali content (K_2O and Na_2O) of t21d (Fig. 7), suggests that this tephra has not suffered alteration with loss of alkali from

the glass (and consequent ageing of the sample). We can thus assume that the K-Ar age of t21d measured by Pinti et al. (2001) is meaningful.

1.6.2 Origin of t21d: anorogenic volcanism at the Brunhes-Matuyama reversal

The t21d volcanic layer has a geochemical anorogenic signature (Fig. 4a) restricting the quest of a volcanic origin for this tephra to a few volcanic complexes. Within the Western Alps, most of the distal tephra discovered erupted from the east-Eifel (Germany; e.g., van den Bogaard and Schmincke, 1985) and the Massif Central (e.g., Juvigné, 1991). East-Eifel volcanism can be discarded because its products are mainly phonolitic while t21d is distinctly rhyolitic and there is no recorded explosive activity around 780 ka (Nowell et al., 2006). The close volcanic field of Westerwald was active until 400 ka (Lustrino and Wilson, 2007; Nowell et al., 2006) but products were mostly alkali basalts. The Sr and Nd isotopic signature of these volcanic products is clearly different from that of t21d (Fig. 5a; Schreiber et al., 1999). Volcanism from France was particularly active in the Early-Middle Pleistocene with 32 recorded eruptions having ages compatible with that of t21d, most of them being from volcanic centers of the Massif Central (Mont Dore and Puy de Sancy; Nowell et al., 2006). Early activity of the Puy de Sancy stratovolcano shows trachy-rhyolitic explosive activity in the Early-Middle Pleistocene (Lavina, 1985; Pastre and Cantagrel, 2001). The Sr and Nd isotopic composition of the tephra t21d is within the isotopic variability observed for the Mont Dore-Sancy volcanic products (Fig. 5a; Briot et al., 1991).

The Puy de Sancy had two major explosive activities in its earlier phases of activity, producing two large pyroclastic deposits of trachytic pumices with thickness of 50-200 meters, the Rioubes-Hautes and Neschers deposits, dated at 720 ± 10 ka (Féraud et al., 1990) and 750 ± 40 ka (Cantagrel and Baubron, 1983), respectively. The former produced the first collapse of the Puy de Sancy caldera and it is not ruled out that the volume of the ejected tephra and the energy of the explosion could have carried ashes across Alps (Lavina, 2003; P. Lavina, written communication). Between 900 and 700 ka, the Puy de Sancy produced six explosive eruptions (Pastre and Cantagrel, 2001). Their CaO and FeO contents are all compatible with those measured in the t21d tephra (Fig. 8a). Alternatively, trachytic products of the last eruptive cycle of the Sancy, dated between 0.45 and 0.25 Ma (Pastre and

Cantagrel, 2001) have trace element composition clearly different from that of the tephra t21d (Fig. 4b). Note that the Rivaux tephra (470 ± 200 ka; Pastre and Cantagrel, 2001), which was erroneously indicated by Brauer et al. (2007) as the source of the t21d tephra, belongs to this latter stage of activity. The chemical composition of tephra t21d seems in agreement with that of earlier Mont Dore and Sancy eruptive cycles again supporting an Early-Middle Pleistocene age.

Tephra deposits close to the Brunhes-Matuyama reversal are not rare in the Mediterranean area. Cita et al. (1972) identified 33 tephra layers in the Middle Pleistocene sequence of ODP Leg 13, site 132 in the Tyrrhenian Sea and two layers in the contemporaneous sequence from the Ionian Sea (ODP Leg 13; site125). A correlative tephra was found lying just above the Brunhes-Matuyama reversal and recovered in four different cores (Narcisi and Vezzoli, 1999). McCoy and Cornell (1990) found two tephra layers, one rhyolitic and the other basalt-andesitic in the Tyrrheanian Sea Leg 107, site 650 A (core 48-X), with an assigned age between 780 and 731 ka, just above the Brunhes-Matuyama reversal (Boogard et al., 1999). More recently, a well traceable trachytic tephra layer (the Pitagora ash; Fig. 1) of unknown origin has been found in the Early Pleistocene marine records (OIS 19) available in outcrop in the Crotone basin, Calabria; southern Italy (Rio et al., 1996; Massari et al., 2002; Cita et al., 2006). Unfortunately, there are not yet available mineral chemistry data for the Pitagora ash to attempt a correlation with t21d.

1.6.3. Origin of t32: the northern Roman Magmatic Province

Deciphering the volcanic source of t32 is rather complicated because of the large alteration state of the tephra potentially causing misidentification. The t32 tephra was associated to the Roccamonfina products on the basis of its 1) mineralogy and petrology; 2) an anomalously low K_2O/Na_2O ratio from 0.9 to 1.2, which is rare among the ultrapotassic Italian volcanic rocks; and 3) the CaO vs. FeO ratio.

Brauer et al. (2007) already indicated that other RMP volcanic centers, such as the Sabatini Mts., erupted rocks with similar mineralogy and chemistry of t32. However, they discarded the Sabatini Mts. because pyroclastic units from this volcanic complex are generally ultrapotassic in composition (K_2O/Na_2O= 3-4; Conticelli et al., 1997) and

additionally bear sedimentary rock fragments. The occurrence of lithics cannot be used to discriminate volcanic sources of distal tephra because these heavier fragments are not transported more than a few km from the eruptive centers. Only weightless pumiceous glass shards of a few microns can be transported more than 600 km away from the source. The alkali content and the K_2O/Na_2O ratio cannot discriminate the source of t32 because the probable leucite analcimization of the tephra (Brauer et al., 2007). This process is always accompanied by alkali loss (Wilkinson, 1977) and drastic reduction of the K_2O/Na_2O ratio (Prelevic et al., 2004). Indeed, leucite-bearing rocks from Roccamonfina, the supposed volcanic origin of t32 (Brauer et al., 2007), have indistinctly K_2O/Na_2O ratios of 3-4 (Conticelli et al., 2009). This is a common value for all the RMP rocks of phonolitic composition (e.g., Conticelli et al., 1997; 2002; Sottili et al., 2004).

The CaO vs. FeO_{tot} ratio cannot be used to discriminate the source of t32. In Figs. 8b and c and d the CaO vs. FeO_{tot} measured in phonolite to tephra-phonolite products from the RMP volcanic complexes are reported, together with values measured in tephra t32 (data from Brauer et al., 2007). Except for the Alban Hills and Ernici (Fig. 8d) all the other volcanic centers (Sabatini, Vico, Vulsini, Roccamonfina) have CaO and FeO_{tot} values compatible with those measured in the t32 tephra, particularly the Sabatini Mts. (Fig. 8c). Unfortunately, incompatible trace element normalized diagrams (Fig. 4c) are also not very useful to discriminate the volcanic source of t32, because most of the RMP volcanic rocks have patterns very close to that of tephra t32. On the other hand, trace element bivariate plots (Fig. 9a) and Nd and Sr isotopic composition (Figs. 5b and 9b) can be more useful for that purpose.

The Nd and Sr isotopic composition of t32 (Fig. 5b) clearly indicates that this tephra was not erupted from the Roccamonfina volcanic complex. Its more radiogenic Sr and less radiogenic Nd isotopic compositions rather make it compatible with those of the N-RMP. Leucite-bearing tephra-phonolite to phonolite rocks from the Vico volcano, Northern Latium, show Nd and Sr isotopic signatures similar to t32, although the Nd isotopic composition of Vico volcanic products is slightly more radiogenic than t32 (Fig. 5b). The difference of isotopic composition between t32 and the supposed Roccamonfina source is not the product of an isotopic shift controlled by weathering of the tephra. Leached aliquot of t32 indeed shows the same Nd and Sr isotopic composition than bulk rock (Table 3). Furthermore,

studies of weathering of basaltic lavas and granite (Borg and Banner, 1996; Aubert et al., 2001) indicate that the residual product of the weathering (in our case t32) should have a lower Nd and Sr isotopic composition than the fresh source rock. This means that the theoretical ''fresh'' t32 tephra should be rather positioned in the upper right corner of the plot of Fig. 5b, which is in the opposite direction to the Roccamonfina rocks. Analcimization of leucite could provoke 87Sr/86Sr enrichment as observed in ultrapotassic rocks of Serbia (Prelevic et al., 2004). Yet, the possible enrichment in the $^{87}Sr/_{86}Sr$ ratio should not be higher than 0.07% of the initial value. For t32, we could thus have an initial, theoretically non-weathered $^{87}Sr/^{86}Sr$ value of 0.71047–0.71053, still more radiogenic than the values measured for the Roccamonfina BLT products ($^{87}Sr/^{86}Sr$ = 0.70882-0.70900; Table 3 and Fig. 5b).

In Fig. 9a the Th/Nb ratio is plotted against the Ta/Nb ratio for tephra t32, the volcanic rocks of Roccamonfina, the Ernici and the Northern-RMP. In Fig. 9b, the Th/Nb ratio is plotted against the $^{87}Sr/^{86}Sr$ isotopic ratio for the same rocks. Partial melting or crystal fractionation do not affect the highly incompatible element ratios and thus likely reflect the volcanic source composition. Results indicate the northern volcanic complexes of the RMP (Sabatini Mts., Vico and the Vulsini Volcanic District; Fig. 9a,b) as the possible source of tephra t32. The problem is to identify precisely an eruption of those volcanic complexes that could be the source of t32 in order to indirectly date this tephra. Geochronological (K–Ar and Ar–Ar) and petrological data allowed the identification of three main periods for the Vico activity (Perini et al., 2004). Only Period II (~305–138 ka) was dominated by effusion of intermediate to felsic leucite-bearing lavas followed by eruptions of voluminous leucite-bearing pyroclastic flows and falls. This was the most intense eruptive cycle of Vico with more than 50 km3 of material ejected (De Rita et al., 2002). Large-scale volcanic activity of the Vulsini Volcanic District occurred between 590 and 127 ka (e.g., Vezzoli et al., 1987; Nappi et al., 1994) and is related to five major volcanic complexes: the Paleo-Vulsini, Bolsena-Orvieto, Southern Vulsini, Latera and Montefiascone volcanic complexes. Volcanic activity was highly explosive and producing thick and widespread ignimbritic and fall deposits (e.g., Palladino and Agosta, 1997). Compositionally, the Vulsini eruption products encompass the entire spectrum of potassic rock types, with a predominance of trachytes and phonolites in terms of erupted volumes. Finally, the Sabatini Mts. developed over a wide area located just to the north of Rome (Fig. 1). The volcanism was there predominantly explosive

and generated widespread pyroclastic deposits with only minor lava flows, which were emitted from a large number of centers including several calderas (De Rita et al., 2002). Products are dominantly tephritic to tephri-phonolitic and were erupted mainly between 560 and 40 ka, with early activity characterized by large Plinian eruption (Sottili et al., 2004). Karner et al. (2001) dated the onset of the Sabatini volcanic activity back to w800 ka. Indeed, 40Ar/39Ar measurements performed on two buried volcanic layers recovered from a deep core yielded ages of 802 ± 4 ka and 783 ± 7 ka. More recently, Florindo et al. (2007) obtained 17 new $^{40}Ar/^{39}Ar$ ages on sanidine and/or leucite from tephra layers intercalated with aggradation terraces of the paleo-Tiber delta. These tephra were recovered from deep cores down around the town of Rome. Among these tephra, eight show 40Ar/39Ar ages ranging from 783.1 ± 9.9 ka to 804.6 ± 9.3 ka. Some of the tephra recovered are leucite-bearing rocks (Florindo et al., 2007). These ages are fully compatible with the K–Ar age of the Piànico Formation (Pinti et al., 2001). Thus, the tephra t32 could be an earlier phonolitic product of the Roman Magmatic Province, possibly from the Sabatini Mts. Unfortunately, chemical, mineral or isotopic information on the primitive volcanic activity of the Roman Volcanic province are not yet available to compare with tephra t32. Comparison of tephra t32 with other tephra layers of similar age and chemistry could be helpful in identifying the volcanic source. Brauer et al. (2007) noticed a strong similarity between the mineralogy and chemistry of tephra t32 and the Bag Tephra, a widespread volcanic layer interbedded in Quaternary loess deposits along the Danubian valley of Hungary and Slovakia (Pouclet et al., 1999). A paleomagnetic reversal, interpreted as the Brunhes–Matuyama, was found below this tephra layer (Juvigne´ et al., 1991). Interestingly, Pouclet et al. (1999) concluded, on the basis of trace and major elements chemistry that the most probable magmatic source for this tephrawas the N-RMP and more probably the Sabatini Mts. or the Alban Hills. The age of the tephra was tentatively fixed between 788 and 380 ka (Pouclet et al., 1999). Pouclet et al. (1999) even suggested the possibility that the 350 ka phono-tephritic Villa Senni eruption of the Alban Hills was a plausible source for the Bag Tephra. However, volcanic products of Alban Hills are mainly leucititic and, in a smaller extent, tephri-phonolitic, while true phonolitic products are nearly absent. If t32 is the Bag Tephra, thus Alban Hills can be eliminated as the volcanic source because both the Sr and Nd and the trace element

composition of t32 (Figs. 9a,b) do not match with those of this volcanic center. Thus, the Sabatini Mts. remain the most plausible volcanic source for tephra t32 (Figs. 9a,b).

1.7. Conclusions

This study shows that two tephra layers found interbedded within the interglacial carbonate deposits of the Piànico Formation, Oroebic Alps, belong to distinct volcanic sources located in different geodynamic contexts.

- Major, trace elements and Sr-Nd isotopic compositions of rhyolitic t21d tephra suggest the anorogenic French Massif Central as its source. More precisely, the earlier pyroclastic activity of the Mont-Dore Sancy volcanoes can be related to this tephra, an hypothesis supporting the previously K-Ar age of 779 ± 13 ka measured on t21d glass shards (Pinti et al., 2001).
- The chemistry, petrology and mineralogy of tephra t32 is similar to leucite-bearing volcanic rocks erupted from several Quaternary centers of the Southern-RMP (Roccamonfina, Ernici) and Northern-RMP (Alban Hills, Sabatini Mts., Vico and the Vulsini Volcanic District) (Figs. 3 and 8b-d).
- New trace element and Nd and Sr isotopic composition of tephra t32 (this study), together with new chemistry and isotopic data from Roccamonfina (Rouchon et al., 2008; Conticelli et al., 2009) exclude Roccamonfina as the volcanic source of this tephra.
- However, trace elements and Sr-Nd isotopic composition of tephra t32 (Fig. 5b) pointed out the N-RMP as the volcanic source of this tephra, most likely the Sabatini volcanic complex (Figs. 9a and b). This also supports the previously suggested volcanic source of other volcanic layers found in loess deposits of eastern Europe (the Bag Tephra; Pouclet et al., 1999) which are likely the same as t32 (Brauer et al., 2007; this study).
- Earlier volcanic activity of the Sabatini Mts. dated back between 802 ± 4 ka and 783 ± 7 ka (Karner et al., 2001) could be the volcanic origin of tephra t32. The limited knowledge on the earliest activity of the Roman Magmatic Province, buried under

hundred meters of more recent volcanic explosive and effusive products (Florindo et al., 2007; Mariucci et al., 2008), does not allow yet to assign an eruption source to tephra t32.

In conclusion, the measured K-Ar age of 779±13 ka of tephra t21d remains the only absolute dating of the Piànico Formation, now supported by two paleomagnetic studies of the Piànico sequence (Pinti et al., 2001; Scardia and Muttoni, 2009) which clearly indicate the presence of a reversal identified as the Brunhes-Matuyama. Such a conclusion implies that recent paleoclimatic reconstructions based on younger ages for the Piànico Formation need to be revaluated (Mangili et al., 2007; Brauer et al., 2008).

Acknowledgements

We wish to thank valuable comments and suggestions from Michele Lustrino and an anonymous reviewer for improving the manuscript. The large databases on the anorogenic volcanism of Europe of Lustrino and Wilson (2007) and on the Italian volcanism compiled by Peccerillo (2005) were a precious support for this study. L. Raisberg at CRPG kindly helped in measurements of Nd and Sr at CRPG-Nancy. C. Ravazzi and S. Chiesa were very helpful for the sampling of tephra t32 at Piànico in September 2006. We wish to thank A. Peccerillo, P. Lavina and D. de Rita for fruitful discussions on Italian volcanism and the Puy de Sancy. Michelle Leithier helped with illustrations and C. Chouinard polished the English. This is GEOTOP contribution no. 2009-0004 and LGMT no. 79.

References

Alessio, M., Allegri, L., Bella, F., Belluomini, G., Calderoni, G., Cortesi, C., Improta, S., Manfra, L., Orombelli, G. 1978. I depositi lacustri di Rovagnate, di Pontida e di Piànico in Lombardia: datazione con il ^{14}C. Geografia Fisica & Dinamica Quaternaria 1, 131-137.

Aubert, D., Stille, P., Probst, A. 2001. REE fractionation during granite weathering and removal by waters and suspended loads: Sr and Nd isotopic evidence. Geochimica et Cosmochimica Acta 65, 387-406.

Avanzinelli, R., Elliott, T., Tommasini, S., Conticelli, S. 2008. Constraints on the genesis of potassium-rich Italian volcanic rocks from U/Th disequilibrium. Journal of Petrology 49, 195-223.

Ballini, A., Barberi, F., Laurenzi, M.A., Mezzetti, F., Oddone, M., Villa, I.M. 1990. Chrono stratigraphy of Roccamonfina volcanic complex. SIMP, genesi e differenziazione del magmatismo potassico del bordo tirrenico (abstract), 15. Convegno Autunnale SIMP, 15–18 October 1990, Ischia, Italy.

Barbieri, M., Peccerillo, A., Poli, G., Tolomeo, L. 1988. Major, trace element and Sr isotopic composition of lavas from Vico volcano (Central Italy) and their evolution in an open system, Contributions to Mineralogy and Petrology. 99, 485-497.

van den Boogard, P., Schmincke, H.U. 1985. Laacher See Tephra: a widespread isochronous late Quaternary tephra layer in central and northern Europe. Geological Society of America Bulletin, 96, 1554–1571.

van den Boogard, P., Mocek, B., Stavesand, M. 1999. Chronology and composition of volcanic ash layers in the central Tyrrhenian basin (site 974). In "Proocedings of the Ocean Drilling Program, Scientific Results." (R. Zahn, M. C. Comas, and A. Klaus, Eds.), 137-156.

Borg, L.E., Banner, J.L. 1996. Neodymium and strontium isotopic constraints on soil sources in Barbados, West Indies. Geochimica et Cosmochimica Acta 60, 4193-4206.

Brauer, A., Wulf, S., Mangili, C., Moscariello, A. 2007. Tephrochronological dating of varved interglacial lake deposits from Piànico-Sèllere (Southern Alps, Italy) to around 400 ka. Journal of Quaternary Science 22, 85-96.

Brauer, A., Mangili, C., Moscariello, A., Witt, A. 2008. Palaeoclimatic implications from micro-facies data of a 5900 varves time series from the Pianico interglacial sediment record, Southern Alps Palaeogeography, Palaeoclimatology, Palaeoecology 259, 121-135.

Briot, D., Cantagrel, J.M., Dupuy, C., Harmon, R.S. 1991. Geochemical evolution in crustal magma reservoirs: Trace-element and Sr-Nd-O isotopic variations in two continental intraplate series at Mont Dore, Massif Central, France. Chemical Geology 89, 281-303.

Cantagrel, J.-M., Baubron, J.C. 1983. Chronologie K-Ar des éruptions dans le massif volcanique des Monts-Dore: implications volcanologiques. Bulletin Bureau de Recherches Géologiques et Minières (BRGM), Géologie de la France 2, 123-142.

Carignan, J., Hild, P., Mevelle, G., Morel, J., Yeghicheyan, D. 2001. Routine analyses of trace element in geological samples using flow injection and low pressure on-line liquid chromatography coupled to ICP-MS: a study of geochemical reference materials BR, DR-N, UB-N, AN-G and GH. Geostandards Newsletter 25, 187-198.

Cita, B.M., Capraro, L., Ciaranfi, N., Di Stefano, E., Marino, M., Rio, D., Sprovieri, R., Vai, G.B. 2006. Calabrian and Ionian: A proposal for the definition of Mediterranean stages for the Lower and Middle Pleistocene. Episodes 29, 107-114.

Cita, B.M., Chierici, M.A., Ciampo, G., Moncharmont Zei, M., d'Onofrio, S., Ryan, W.B.F. 1972. The Quaternary record in the Tyrrhenian and Ionian basins of the Mediterranean sea. In "Initial Reports of Deep Sea Drilling Project 13" (W. B. F. Ryan and K. J. Hsu, Eds.), 1263-1339.

Civetta L., Innocenti F., Manetti P., Peccerillo A., Poli G. 1981. Geochemical characteristics of potassic volcanics from Mt. Ernici (Southern Latium, Italy). Contributions to Mineralogy and Petrology 78, 37-47.

Conticelli, S., Francalanci, L., Manetti, P., Cioni, R., Sbrana, A. 1997. Petrology and geochemistry of the ultrapotassic rocks from the Sabatini Volcanic District, central Italy: The role of evolutionary processes in the genesis of variably enriched alkaline magmas. Journal of Volcanology Geothermal Research 75, 107-136.

Conticelli, S., D'Antonio, M., Pinarelli, L., Civetta, L. 2002. Source contamination and mantle heterogeneity in the genesis of Italian potassic and ultrapotassic volcanic

rocks: Sr-Nd-Pb isotope data from Roman Province and Southern Tuscany. Contributions to Mineralogy and Petrology 74, 189-222.

Conticelli, S., Marchionni, S., Rosa, D., Giordano, G., Boari, E., Avanzinelli, R. 2009. Shoshonite and sub-alkaline magmas from an ultrapotassic volcano: Sr–Nd–Pb isotope data on the Roccamonfina volcanic rocks, Roman Magmatic Province, Southern Italy. Contributions to Mineralogy and Petrology 157, 41–63.

De Rita, D., Fabbri, M., Mazzini, I., Paccara, P., Sposato, A., Trigari, A. 2002. Volcaniclastic sedimentation in coastal environments: the interplay between volcanism and Quaternary sea level changes (central Italy) Quaternary International 95-96, 141-154.

Doremus, R. H. 1994. "Glass Science." John Wiley & Sons Inc., New York.

Florindo, F., Karner, D.B., Marra, F., Renne, P.R., Roberts, A.P, Weaver, R. 2007. Radioisotopic age constraints for Glacial Terminations IX and VII from aggradational sections of the Tiber River delta in Rome, Italy. Earth and Planetary Science Letters 256, 61 – 80.

Freda, C., Gaeta, M., Palladini, D.M., Trigila, R. 1997. The Villa Senni eruption (Alban Hills, central Italy): the role of H_2O and CO_2 on the magma chamber evolution and on the eruptive scenario. Journal of Volcanology Geothermal Research 78,103-120

Frezzotti, M.L., De Astis, G., Dallai, L., Ghezzo, C. 2007. Coexisting calc-alkaline and ultrapotassic magmatism at Monti Ernici, Mid Latina Valley (Latium, central Italy). European Journal of Mineralogy 19, 479-497.

Ghiara, M.R., Lirer, L. 1977. Mineralogy and geochemistry of the "low potassium" series of the Roccamonfina volcanic suite (Campania, South Italy). Bulletin of Volcanology 40, 39-56

Giannetti, B., Ellam, R. 1994. The primitive lavas of Rocccamonfina volcano, Roman region, Italy: new coinstraints on melting processes and source mineralogy. Contributions to Mineralogy and Petrology 116, 21-31

Giannetti, B. 2001. Origin of the calderas and evolution of Roccamonfina volcano (Roman Region, Italy). Journal of Volcanology Geothermal Research 106: 301–319.

Gillot, P.Y., Cornette, Y., Max, N., Floris, B. 1992. Two reference materials, trachytes MDO-G and ISH-G, for argon dating (K-Ar and $^{40}Ar/^{39}Ar$) of Pleistocene and Holocene rocks. Geostandards Newsletter 16, 55-60.

Govoni, L., Paganoni, A., Sala, B. 2006. The mammal fauna of the Piànico-Sèllere Basin. In "INQUA-SEQS 2006: The Quaternary of the Italian Alps." 14-20. Piànico setting field trip guide SEQS 2006, Milano, Università Bicocca.

Haflidason, H., Eiriksson, J., van Kreveld, S. 2000. The tephrochronology of Iceland and the North Atlantic region during the Middle and Late Quaternary: a review. Journal of Quaternary Science 15, 3-22.

Hawkesworth, C.J., Vollmer, R. 1979. Crustal contamination vs. enriched mantle: $^{143}Nd/^{144}Nd$ and $^{87}Sr/^{86}Sr$ evidence from the Italian volcanics. Contributions to Mineralogy and Petrology 69, 151-165

Jantzen, C.M., Plodinec, M.J. 1984. Nuclear waste glass durability. Journal of Non-crystalline Solids 67, 207-223.

Juvigné, E., Horvath, E., Gabris, G. 1991. La Téphra de Bag: une retombée volcanique à large dispersion dans le loess pléistocène d'Europe centrale. Eiszeitalter Gegenwart Hannover 41, 107-118.

Juvigné, E., 1991. Distribution de vastes retombées volcaniques originaires de l'Eifel et du Massif Central aux temps post-glaciaires dans le NE de la France et les régions voisines. Compte REndus de l'Acadèmie de Sciences de Paris, Serie, II 312, 415–420.

Karner, D. B., Marra, F., Renne, P. R. 2001. The history of the Monti Sabatini and Alban Hills volcanoes: groundwork for assessing volcanic-tectonic hazards for Rome. Journal of Volcanology Geothermal Research 107, 185-215.

Lavina, P. 1985. "Le volcan du Sancy et le « Massif Adventif » (Massif des Monts Dore - Massif Central Français). Etudes Volcanologiques et structurales." Unpublished PhD thesis, Université Blaise Pascal, Clermont Ferrand.

Lavina, P. 2003. Les instabilités du strato-volcan du Sancy (Monts Dore, France) de -1 Ma à -0,2 Ma. L'avalanche de débris du Sancy. In "Volcano." Société Géologique de France.

Le Maitre, R.W., Bateman, P., Dudek, A., Keller, J., Lameyre Le Bas, M.J., Sabine, P.A., Schmid, R., Sorensen, H., Streckeisen, A., Woolley, A.R., Zanettin, B. 1989. A classification of the igneous rocks and glossary of terms. Blackwell, Oxford.

Luhr, J.F., Giannetti, B. 1987. The Brown Leucitic Tuff of Roccamonfina Volcano (Roman Region, Italy). Contributions to Mineralogy and Petrology 95, 420–436.

Lepsius, R. 1910. Die Einheit und die Ursachen der diluviale Eiszeit in der Alpen. In "Abd. D. Grossh. Hess. Geol. Landesanstalt zu Darmstadt." 136, Darmstadt.

Lustrino, M., Wilson, M. 2007. The circum-Mediterranean anorogenic Cenozoic igneous province. Earth-Science Reviews 81, 1-65.

Mangili, C., Brauer, A., Moscariello, A., Naumann, R. 2005. Microfacies of detrital event layers deposited in Quaternary varved lake sediments of the Pianico-Sellere basin (northern Italy). Sedimentology 52, 927-943.

Mangili, C., Brauer, A., Plessen, B., Moscariello, A. 2007. Centennial-scale oscillations in oxygen and carbon isotopes of endogenic calcite from a 15,500 varve year record of the Piànico interglacial. Quaternary Science Reviews 26, 1725-1735.

Mariucci, M.T., Pierdominici, S., Pizzino, L., Marra, F., Montone, P. 2008. Looking into a volcanic area: An overview on the 350 m scientific drilling at Colli Albani (Rome, Italy). Journal of Volcanology and Geothermal Research 176, 225–240.

Massari, F., Rio, D., Sgavetti, M., Prosser, G., D'Alessandro, A., Asioli, A., Capraro, L., Fornaciari, E., Tateo, F. 2002. Interplay between tectonics and glacio-eustasy: Pleistocene succession of the Crotone basin, Calabria (southern Italy). Geological Society of America, Bulletin 114, 1183-1209.

McCoy, F.W., Cornell, W. 1990. Volcanoclastic sediments in the Tyrrhenian basin. The Proceedings of the Ocean Drilling Program, Sciences Research 107, 291-305.

Milani, L., Beccaluva, L., Coltorti, M. 1999. Petrogenesis and evolution of the Euganean Magmatic Complex, Veneto region, North-East Italy. European Journal of Mineralogy 11, 379-399.

Moscariello, A., Ravazzi, C., Brauer, A., Mangili, C., Chiesa, S., Rossi, S., de Beaulieu, J.-L., Reille, M. 2000. A long lacustrine record from the Piànico-Sèllere Basin (Middle-Late Pleistocene, Northern Italy). Quaternary International 73/74, 47-68.

Nappi, G., Capaccioni, B., Mattioli, M., Mancini, E., Valentini, L. 1994. Plinian Fall Deposits from Vulsini Volcanic District (Central Italy). Bulletin of Volcanology 56, 502-515.

Narcisi, B., Vezzoli, L. 1999. Quaternary stratigraphy of distal tephra layers in the

Mediterranean--an overview. Global and Planetary Change 21, 31-50.

Nowell, D.G., Jones, C.M., Pyle, D. 2006. Episodic Quaternary volcanism in France and Germany. Journal of Quaternary Science 21, 645-675.

Palladino, D.M., Agosta, E. 1997. Pumice fall deposits of the western Vulsini Volcanoes (Central Italy). Journal of Volcanology Geothermal Research 78, 77-102.

Pastre, J.-F, Cantagrel, J.-M. 2001. Téphrostratigraphie du Mont Dore. Quaternaire 12, 249-267.

Pearce, N.J.G., Alloway, B.V., Westgate, J.A. 2008. Mid-Pleistocene silicic tephra beds in the Auckland region, New Zealand: Their correlation and origins based on the trace element analyses of single glass shards. Quaternary International 178, 16-43.

Pearce, N.J.G., Westgate, J.A., Perkins, W.T. 1996. Developments in the analysis of volcanic glass shards by laser ablation ICP-MS: quantitative and single internal standard-multi-element methods. Quaternary International 34-36, 213-227.

Peccerillo, A. 2005. Plio-Quaternary volcanism in Italy: Petrology, geochemistry, geodynamics. Springer-Verlag, Berlin.

Penck, A., Brückner, E. 1909. "Die Alpen im Eiszeitaler, Bd 3." Chr. Her. Tauchnitz, Leipzig.

Perini, G., Francalanci, L., Davidson, J.P., Conticelli, S. 2004. Evolution and genesis of magmas from Vico volcano, central Italy: Multiple differentiation pathways and variable parental magmas. Journal of Petrology 45, 139-182.

Pinti, D.L., Quidelleur, X., Chiesa, S., Ravazzi, C., Gillot, P.Y. 2001. K-Ar dating of an early Middle Pleistocene distal tephra in the interglacial varved succession of Pianico-Sellere (Southern Alps, Italy). Earth Planetary Science Letters 188, 1-7.

Pinti, D.L., Quidelleur, X., Lahitte, P., Aznar, C., Chiesa, S., Gillot, P.Y. 2003. The Piànico tephra: an early-middle Pleistocene record of intraplate volcanism in the Mediterranean. Terra Nova 15, 176-186.

Pinti, D.L., Rouchon, V., Quidelleur, X., Gillot, P. Y., Chiesa, S., Ravazzi, C. 2007. Comment: "Tephrochronological dating of varved interglacial lake deposits from Piànico-Sèllere (Southern Alps, Italy) to around 400 ka" by Brauer, A., Wulf, S., Mangili, C., Moscariello, A. Journal of Quaternary Science 22, 411-414.

Pollard, A.M., Blockey, S.P.E., Ward, K.R. 2003. Chemical alteration of tephra in the

depositional environment: theoretical stability modelling. Journal of Quaternary Science 18, 385-394.

Pouclet, A., Horvath, E., Gabris, G., Juvigné, E. 1999. The Bag tephra, a widespread tephrochronological marker in Middle Europe: chemical and mineralogical investigations. Bulletin of Volcanology 60, 265-272.

Preda, M., Cox, M.E. 2004. Temporal variations of mineral character of acid-producing pyritic coastal sediments, Southeast Queensland, Australia. Science of the Total Environment 326, 257-269.

Prelevic, D., Foley,, S.F., Cvetkovic, V., Romer, L. 2004. The analcime problem and its impact on the geochemistry of ultrapotassic rocks from Serbia. Mineralogical Magazine 68, 633–648.

Ravazzi, C. 2006. The stratigraphic setting of the Piànico-Sellère Basin. In:Ravazzi C. (Ed.) INQUA-SEQS 2006: The Quaternary of the Italian Alps, pp. 14-20. Piànico setting field trip guide SEQS 2006, Milano, Università Bicocca.

Richard, P., Shimizu, N., Allegre, C.J. 1976. $^{143}Nd/^{146}Nd$, a natural tracer: an application to oceanic basalts. Earth and Planetary Science Letters 31, 269-278.

Rio, D., Channell, J.E.T., Poli, M.S., Sgavetti, M., D'Alessandro, A., Prosser, G. 1996. Reading Pleistocene eustasy in a tectonically active siliciclastic shelf setting (Crotone peninsula, southern Italy). Geology 24, 743–746.

Rossi, S., Reille, M., Moscariello, A., Ravazzi, C., Beaulieu, J.L. De, Brauer, A., Chiesa, S., Mangili, C., 2000. The annually laminated record of Piànico-Sèllere (Northern Italy): an overview. The 1st ALDP/ELDP Joint Meeting 'Environmental Change in Eurasia'. Kyoto and Mikata, Japan, 20–25 March 2000 (Abstract) 80–82.

Rossi, S. 2003. "Analyse pollinique de la séquence lacustre Pleistocène de Pianico-Sellere (Italie)." Université de Aix Marseille III/Università degli studi di Milano.

Rouchon, V., Gillot, P.Y., Quidelleur, X., Chiesa, S., Floris, B. 2008. Temporal evolution of the Roccamonfina volcanic complex (Pleistocene), Central Italy. Journal of Volcanology Geothermal Research 177, 500–514.

Sarna-Wojcicki, A., 2000. Tephrochronology. In: Stratton, J., Sowers, J. M. and Lettis, W. R. (Eds.), Quaternary Geochronology. Methods and Applications, pp. 357-377. AGU, Washington, D.C.

Sarna-Wojcicki, A.M., Meyer, C.E., Woodward, M.J., Lamothe, P.J. 1981. Composition of air-fall ash erupted on May 18, May 25, June 12, July 22 and August 7. In: Lipman P. W. and Mullinaux D. R. (Eds.), The 1980 eruption of Mount St. Helens, Washington, 1250, pp. 670-681. Geological Survey of America, Washington.

Scardia, G. and Muttoni, G., 2009. Paleomagnetic investigations on the Pleistocene lacustrine sequence of Piànico-Sèllere (Northern Italy). Quaternary International, this volume. doi:10.1016/j.quaint.2008. 06.017.

Schreiber, U., Anders, D., Koppen, J., 1999. Mixing and chemical interdiffusion of trachytic and latitic magma in a subvolcanic complex of the Tertiary Westerwald (Germany). Lithos 46, 695–714.

Solgadi, F., Moyen, J.F., Sawyer, E.W., Reisberg, L. 2007. The role of crustal anatexis and mantle-derived magmas in the genesis of synorogenic hercynian granites of the Livradois area, French Massif Central. The Canadian Mineralogist 45, 581-606.

Sottili, G., Palladino, D.M., Zanon, V. 2004. Plinian activity during the early eruptive history of the Sabatini Volcanic District, Central Italy. Journal of Volcanology Geothermal Research 135, 361-379.

Sterpenich, J., Libourel, G. 2006. Water diffusion in silicate glasses under natural weathering conditions: evidence from buried medieval stained glasses. Journal of Non-Crystalline Solids 352, 5446-5451.

Stoppani, A. 1857. Studi geologici e paleontologici sulla Lombardia. Tipografia Turati, Milano.

Tanaka, T., Togashi, S., Kamioka, H., Amakawa, H., Kagami, H., Hamamoto, T., Yuhara, M., Orihashi, Y., Yoneda, S., Shimizu, H., Kunimaru, T., Takahashi, K., Yanagi, T., Nakano, T., Fujimaki, H., Shinjo, R., Asahara, Y., Tanimizu, M., Dragusanu, C. 2000. JNdi-1: a neodymium isotopic reference in consistency with LaJolla neodymium. Chemical Geology 168, 279-281

Trigila, R., Agosta, E., Currado, C., De Benedetti, A.A., Freda, C., Gaeta, M., Palladino, D.M., Rosa, C. 1995. Petrology. In: Trigila R. (Ed.), The volcano of the Alban Hills Tipografia SGS, Rome, 95-165.

Vezzoli, L., Conticelli, S., Innocenti, F., Landi, P., Manetti, P., Palladino, D.M., Trigila L. 1987. Stratigraphy of the Latera Volcanic Complex: proposal for a new nomenclature. Periodico di Mineralogia 56, 89-110.

White, W.B., Minser, D.G. 1984. Raman spectra and structure of natural glasses. Journal of Non-crystalline Solids 67, 45-59.

Wilkinson, J.F.G., 1977. Analcime phenocrysts in a vitrophyric analcimite - Primary or secondary? Contributions to Mineralogy and Petrology 64, 1-10.

Wilson M. 1989. Igneous petrogenesis. A global tectonic approach. Unwin Hyman, Boston, 466 pp.

Wood, D.A., Joron, J.-L., Treuil, M. 1979. A re-appraisal of the use of trace elements to classify and discriminate between magma series erupted in different tectonic settings. Earth Planetary Science Letters 45, 326-336.

Table 1
Major element chemistry of bulk rock and glass shards of t21d, t32 reported as wt%.

Element	t21d $n = 64$[a]			t32[b]			t32[b]			t32[b]		
	Glass shards			Type A $n = 24$			Type B $n = 3$			Type C $n = 3$		
	ARD	StD	AWF	ARD	StD	AWF	ARD	StD	AWF	ARD	StD	AWF
SiO_2	66.03	0.44	69.78	52.42	1.77	53.61	47.92	1.35	49.22	46.07	1.19	47.29
TiO_2	0.30	0.07	0.32	0.56	0.13	0.58	0.83	0.12	0.86	1.09	0.06	1.12
Al_2O_3	14.94	0.23	15.79	20.95	1.09	21.42	18.03	0.44	18.52	15.77	0.09	16.19
FeO_{total}	1.65	0.18	1.75	4.62	0.84	4.73	7.68	0.38	7.90	8.87	0.54	9.11
MnO	0.13	0.09	0.14	0.21	0.04	0.22	0.23	0.04	0.24	0.22	0.05	0.18
MgO	0.20	0.03	0.21	0.87	0.50	0.90	2.75	0.17	2.83	4.39	0.27	4.51
CaO	0.89	0.06	0.94	5.25	1.13	5.38	8.83	0.07	9.07	11.07	0.81	11.36
Na_2O	4.73	0.15	5.00	6.39	1.29	6.52	5.49	0.78	5.63	4.15	0.55	4.25
K_2O	5.76	0.14	6.09	6.32	1.24	6.48	5.00	0.62	5.14	5.05	1.07	5.20
P_2O_5				0.18	0.13	0.18	0.58	0.10	0.60	0.73	0.22	0.76
Total	94.62		100.00	97.78		100.00	97.34		100.00	97.40		100.00

Note. AWF = LOI-free corrected values.
[a]Data from Pinti et al. (2003).
[b]Data from Brauer et al. (2007).

Table 2. Trace elements analyses of t32.

Element	(ppm)
As	61.3
Be	9.7
Bi	2.36
Cd	0.38
Co	14.7
Cr	19.09
Cu	44.91
Dy	6.01
Er	2.4
Eu	3.34
Ga	17.6
Ge	1.2
Gd	10.83
Ho	0.927
Lu	0.29
Mo	31.53
Ni	31.35
Pr	32.54
Sb	2.9
Sn	3.5
Tm	0.311
V	129.4
W	8.6
Yb	2.00
Zn	72.7
Cs	28.0
Rb	248.2
Ba	3013
Th	103.0
U	22.0
K	57255
Ta	1.8
Nb	28.47
La	192.1
Ce	325.9
Sr	2095
Nd	107
P	1767
Hf	8.1
Zr	411
Sm	16.9
Ti	3195
Tb	1.35
Y	29.1

Table 3. Strontium and neodynium isotopic analyses of t21d and t32

Sample	Formation	phase/method/laboratory	Age ka	[Sr] ppm	[Rb] ppm	$[^{87}Sr/^{86}Sr]_0$	±2σ	$[^{87}Sr/^{86}Sr]_t$	[Sm] ppm	[Nd] ppm	$^{a}[^{143}Nd/^{144}Nd]_{0\to t}$	±2σ	εNd (t)
T21d	Pianico Formation	glass/spike/CRPG Nancy	780	149.08	5.52	0.705007	±48	0.705006	-	-	-	-	
T21d	Pianico Formation	glass/spike/CRPG Nancy	780	151.32	5.43	0.704987	±48	0.704986	6.25	1.29	0.512722	±32	1.64
T32a	Pianico Formation	bulk/GEOTOP	(780)			0.710969	±14	0.710969			0.512202	±11	-8.50
T32b	Pianico Formation	bulk/spike/GEOTOP	(780)	2297	248	0.710971	±17	0.710968	18.45	118.18	0.512188	±11	-8.78
T32c	Pianico Formation	bulk/acid digestion/GEOTOP	(780)			0.711031	±18	0.711031			0.512198	±7	-8.58
RMF96	White Trachityc Tuff (WTT)	bulk/spike/GEOTOP	331	513	456.3	0.708428	±15	0.708415	11.09	72.42	0.512298	±10	-6.63
RMF11	White Trachityc Tuff (WTT)	bulk/spike/GEOTOP	331	678	385	0.708422	±15	0.708414	10.97	71.04	0.512262	±9	-7.28
47Y3	Brown Leucitic Tuff (BLT)	bulk/spike/GEOTOP	354	1668	382.2	0.708919	±14	0.708916	12.74	69.73	0.512214	±10	-8.26
89I	Brown Leucitic Tuff (BLT)	bulk/spike/GEOTOP	354	1276	416	0.708827	±13	0.708822	12.61	76.60	0.512225	±8	-8.05
89J	Brown Leucitic Tuff (BLT)	bulk/spike/GEOTOP	354	1430	620.4	0.709012	±14	0.709006	11.61	65.11	0.512216	±9	-8.22
RMF14	Pre-BLT	bulk/spike/GEOTOP	440	673	413.6	0.708516	±14	0.708504	11.72	71.99	0.512264	±8	-7.29
89S	Pre-BLT	bulk/spike/GEOTOP	439	830	397	0.708556	±14	0.708548	11.03	67.90	0.512255	±9	-7.45

Note:
(1) Age correction (780 Ka) for both t21d and t32 Nd isotopic compositions are within uncertainties.
(2) $^{147}Sm/^{144}Nd$ has calculated for 89S sample to obtain the $[^{143}Nd/^{144}Nd]_t$

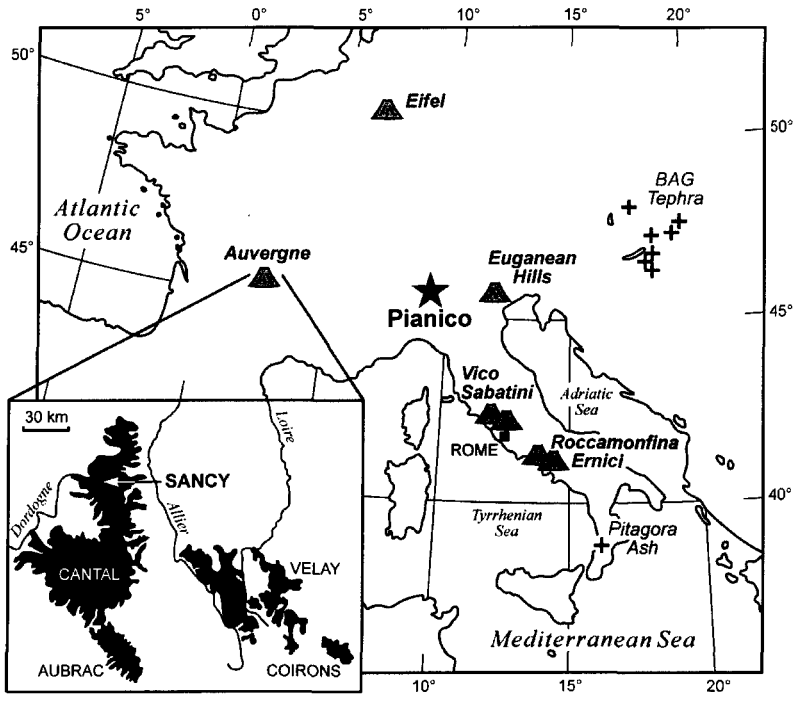

Figure 1. Simplified map of Europe and the Italian Peninsula with the location of Piànico, tephra layers (Pitagora Ash and Bag tephra) and volcanic centers discussed in the text. A detail of the Massif Central volcanic complex in Auvergne with position of the Puy de Sancy and Mont Dore volcanoes is also reported (redrawn and modified from Brauer et al., 2007).

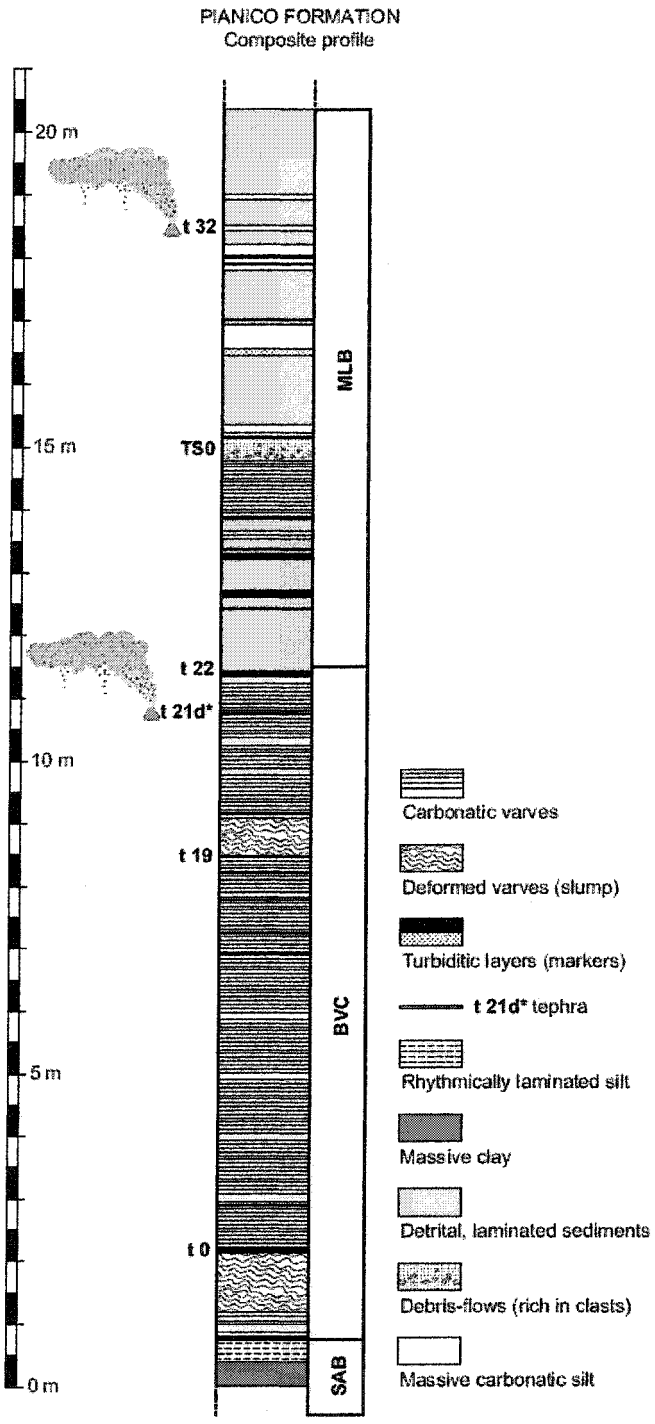

Figure 2. Simplified stratigraphy of the Piànico Formation with position of the two volcanic layers, t21d and t32 (redrawn and modified from Rossi, 2003).

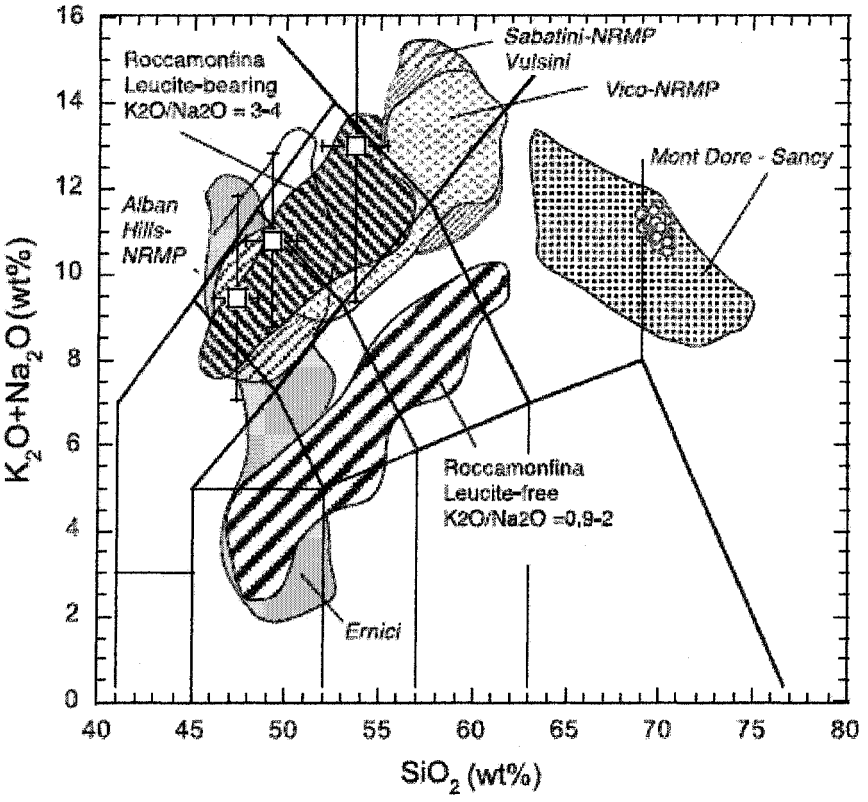

Figure 3. LOI-free TAS diagram (Le Maitre, 1989) for the t21d tephra (small circles), t32 (squares) compared to the chemical composition of volcanic rocks from the Northern Roman Magmatic Province (NRMP) centers of Alban Hills (Trigila et al., 1995; Freda et al., 1997; Peccerillo, 2005), Vico (Barbieri et al., 1988; Perini et al., 2004; Avanzinelli et al., 2007), Sabatini (Conticelli et al., 1997; 2002) and those of Roccamonfina (Luhr and Gianetti, 1987; Ghiara and Lirer, 1977; Giannetti and Ellam, 1994; Peccerillo, 2005; Conticelli et al., 2008; Rouchon et al., 2008), Ernici (Civetta et al., 1981; Conticelli et al., 2002; Frezzotti et al., 2007). Compositionally, the Vulsini eruption products encompass the entire spectrum of potassic rock types, with a predominance of trachytes and phonolites in terms of erupted volumes. Data of Mont-Dore and Sancy volcanoes are from Briot et al. (1991), Pastre and Cantagrel (2001) and Lavina (1985).

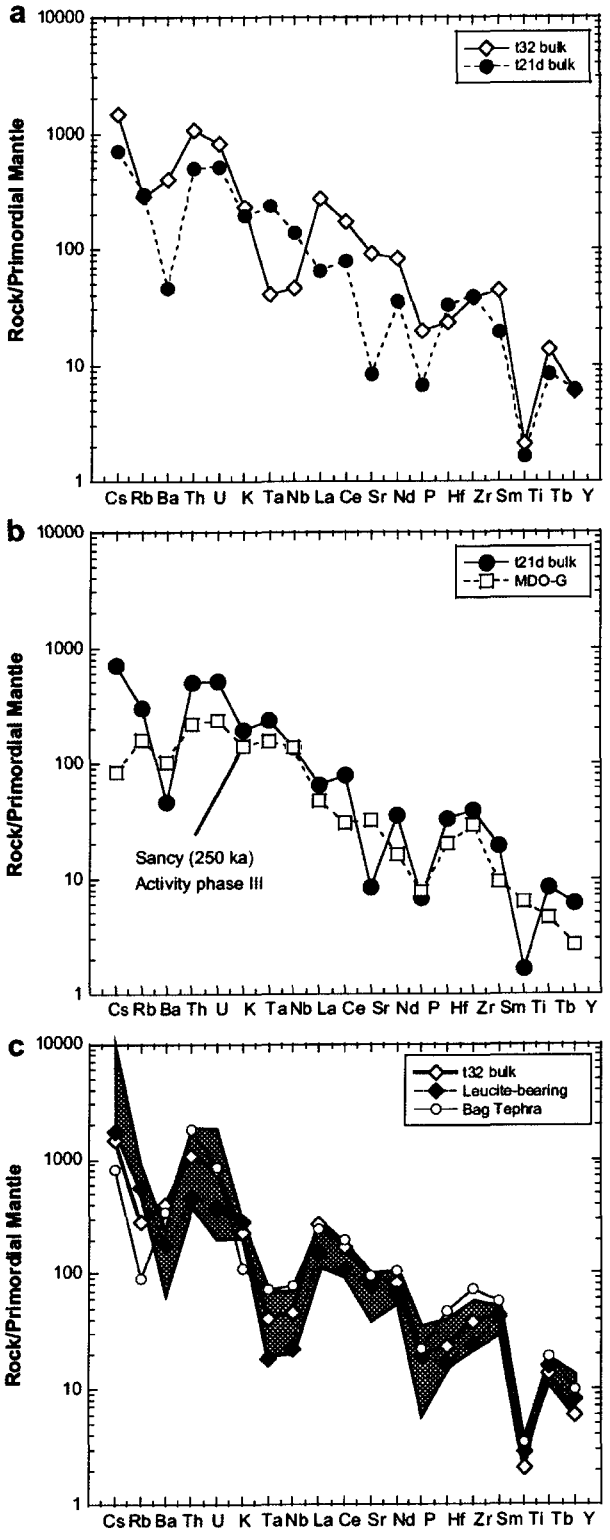
a
b
c
Rock/Primordial Mantle
10000
1000
100
10
1
Cs Rb Ba Th U K Ta Nb La Ce Sr Nd P Hf Zr Sm Ti Tb Y
t32 bulk
t21d bulk
MDO-G
Sancy (250 ka)
Activity phase III
Leucite-bearing
Bag Tephra

Figure 4. a) Trace elements composition of tephra t21d and t32, normalized to the primitive mantle of Wood (1979); **b**) trace element normalized diagram of tephra t21d and that of trachyte MDO-G dated at 250 Ka and typical of the products of the last eruptive cycle of the Sancy (data from Gillot et al., 1992); **c**) trace element normalized diagram of tephra t32 plotted against those of Roccamonfina leucite-bearing rocks (data from Conticelli et al., 2008) and those of the Northern Roman Magmatic Province (data source same as Fig. 3).

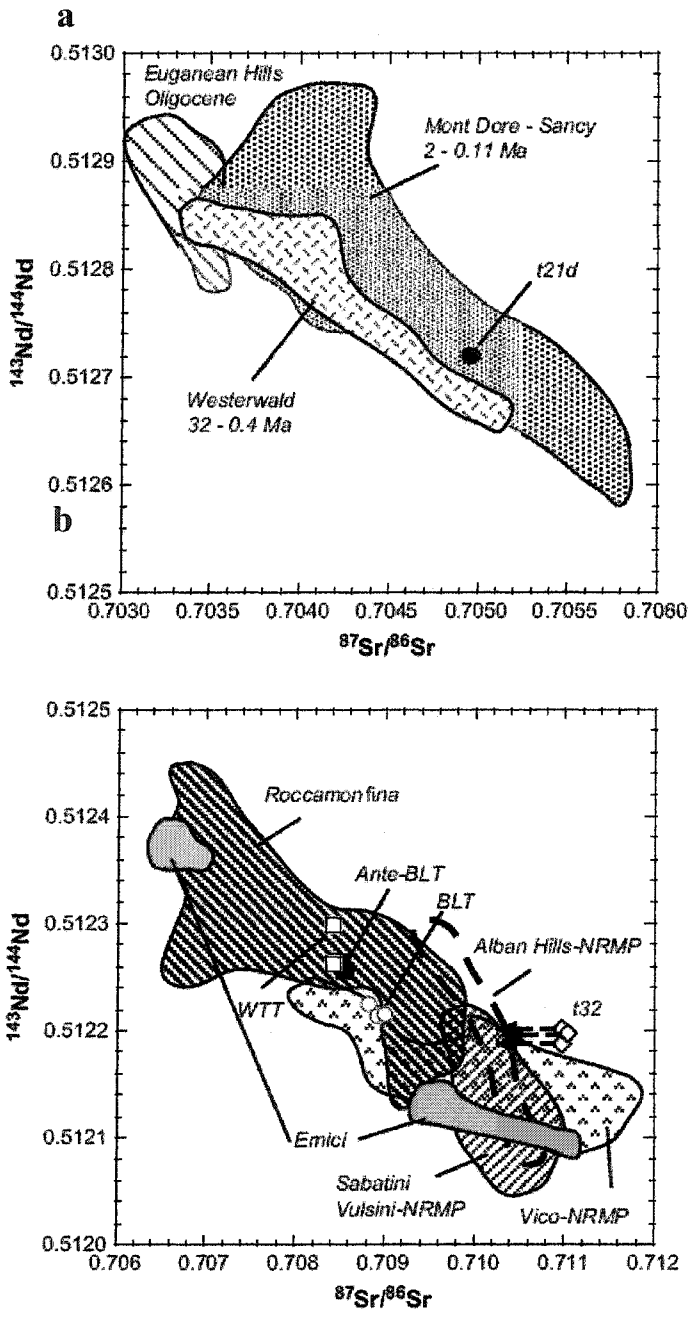
a
Euganean Hills
Oligocene
Mont Dore - Sancy
2 - 0.11 Ma
t21d
Westerwald
32 - 0.4 Ma
b
143Nd/144Nd
87Sr/86Sr
0.5130
0.5129
0.5128
0.5127
0.5126
0.5125
0.7030
0.7035
0.7040
0.7045
0.7050
0.7055
0.7060
Roccamonfina
Ante-BLT
BLT
Alban Hills-NRMP
WTT
t32
Emici
Sabatini
Vulsini-NRMP
Vico-NRMP
0.5125
0.5124
0.5123
0.5122
0.5121
0.5120
0.706
0.707
0.708
0.709
0.710
0.711
0.712

Figure 5. **a)** Sr and Nd isotopic composition of tephra t21d compared to that of the anorogenic volcanic complexes of Westerwald, Germany (Scheiber et al., 1994) and Massif central (Briot et al., 1991). The Nd and Sr isotopic composition of the Euganean Hills (Milani et al., 1999; Lustrino and Wilson, 2007 and references therein) was also reported to show the absence of relation between tephra t21d and the anorogenic Euganean Hill volcanic complex located nearby Piànico. **b**) Sr and Nd isotopic composition of tephra t32 (diamonds) compared to that of Roccamonfina main pyroclastic episodes predating the Brown Leucitic Tuff (black squares), the BLT (white circles) and the WTT (white squares) (this study). The Nd and Sr isotopic composition of Roccamonfina-Ernici and the Northern Roman Magmatic Province were also reported. Data source same as Fig. 3. The dashed arrows show the hypothetical position of t32 if analcimization had produced artificial $^{87}Sr/^{86}Sr$ enrichment (see text for details and Prelevic et al., 2004).

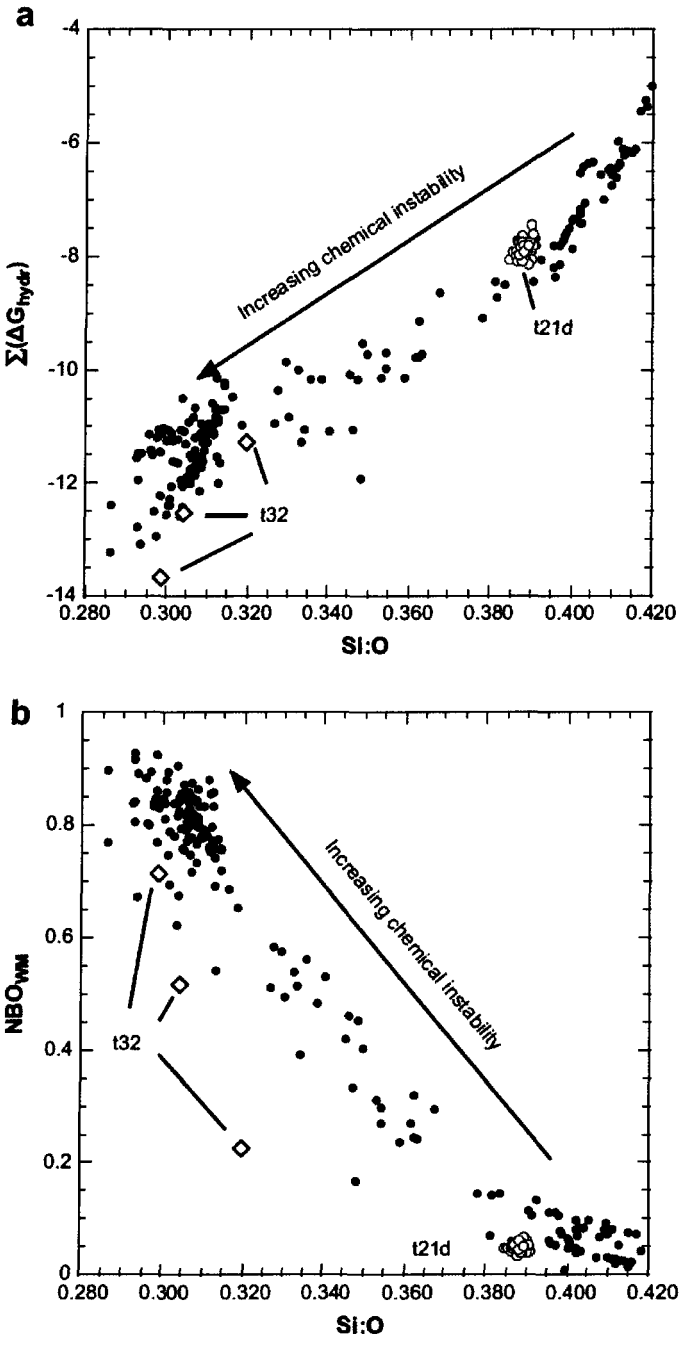

Figure 6. a, b) Empirical parameters Si:O, NBO and ΔG_{hydr} calculated for t21d, t32 compared to that of North Atlantic tephra (data from Haflidason et al. (2000) and Pollard et al. (2003)) in order to illustrate how a glass evolves during weathering. See text for details.

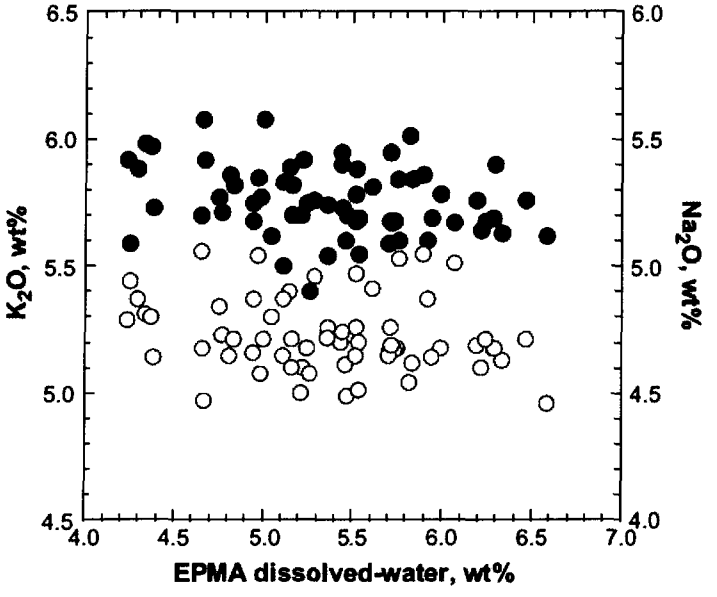

Figure 7. A double-Y plot illustrating the alkali (K_2O and Na2O) contents vs. the dissolved-water concentration in glass of tephra t21d, calculated from EPMA analyses (data from Pinti et al., 2003).

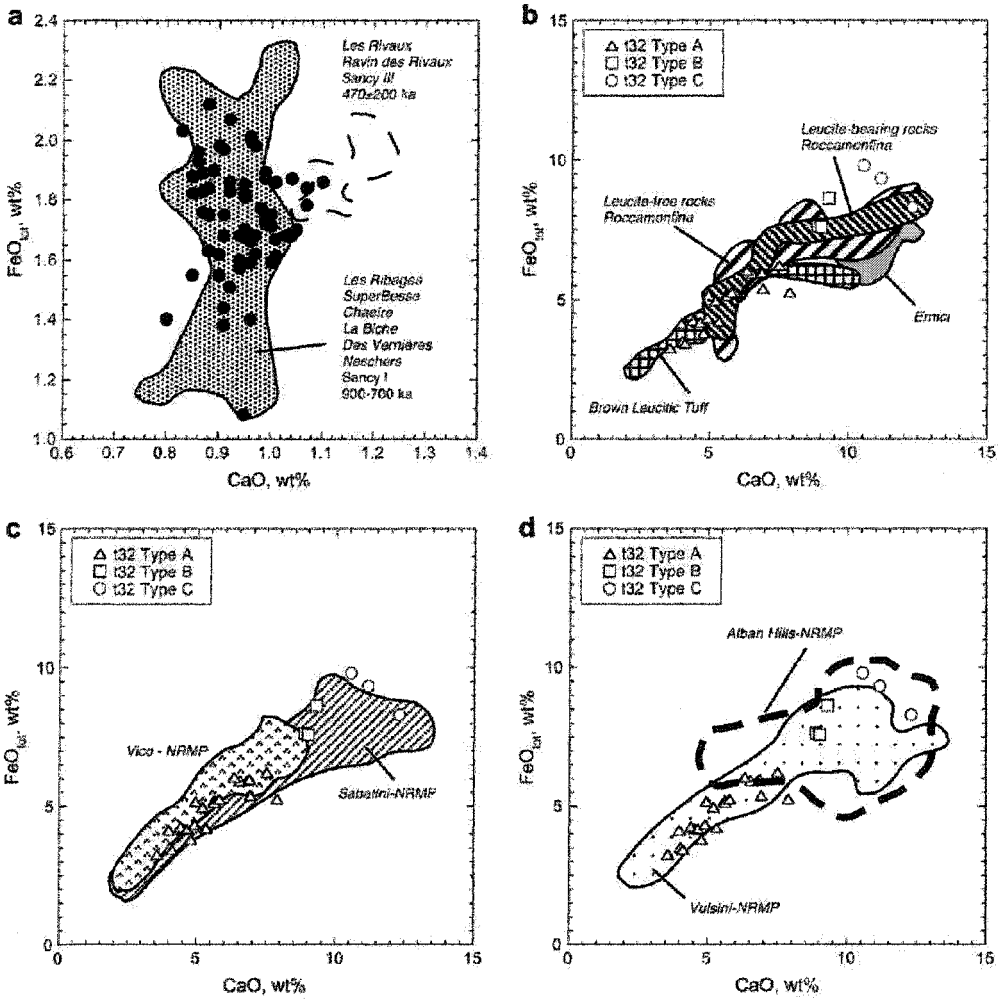

Figure 8. **a**) Plot of LOI-free CaO vs FeO_{tot} contents of tephra t21d (data from Pinti et al., 2003) against the values measured in trachytes of the first period of activity of the Puy de Sancy, French Massif central, dated between 900 to 700 ka and those of the Rivaux eruptions (dated at 470±200 ka). Data are from Pastre and Cantagrel (2001) and Lavina (1985). **b, c, d**) CaO vs FeO_{tot} contents of tephra t32 plotted against values from volcanic products of Ernici-Roccamonfina and Northern Roman Magmatic Province (data sources are the same as in Fig. 3).

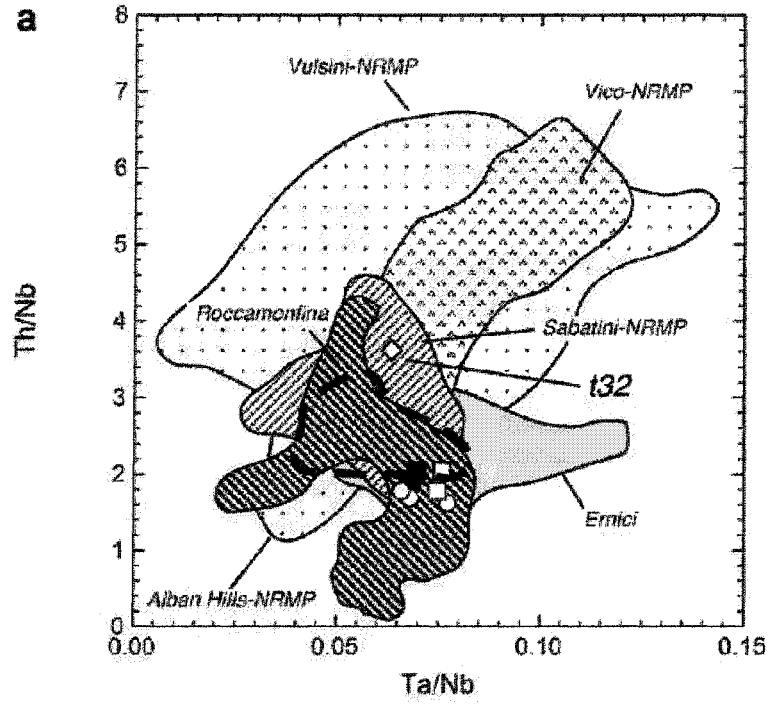
a
Vulsini-NRMP
Vico-NRMP
Roccamonfina
Sabatini-NRMP
t32
Ernici
Alban Hills-NRMP
Th/Nb
Ta/Nb
0
1
2
3
4
5
6
7
8
0.00
0.05
0.10
0.15

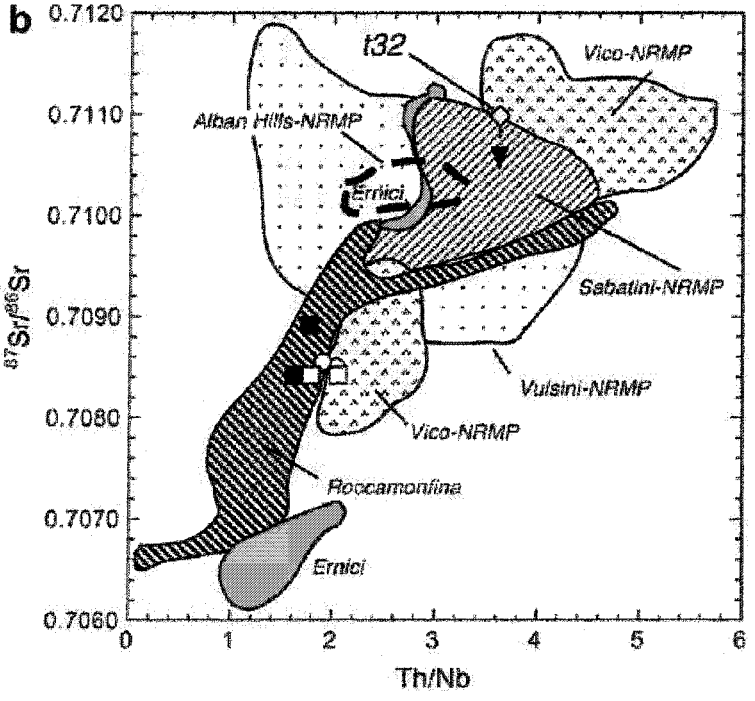
b
t32
Vico-NRMP
Alban Hills-NRMP
Ernici
Sabatini-NRMP
Vulsini-NRMP
Vico-NRMP
Roccamonfina
Ernici
$^{87}Sr/^{86}Sr$
0.7120
0.7110
0.7100
0.7090
0.7080
0.7070
0.7060
0
1
2
3
4
5
6
Th/Nb

Figure 9. **a**) Bivariate plot of incompatible element ratios Th/Nb and Ta/Nb and **b**) Th/Nb ratio against the $^{87}Sr/^{86}Sr$ ratios for tephra t32 and those of the Roccamonfina volcanic products (this study) compared with those of the Roccamonfina-Ernici and the Northern-RMP from literature data (data sources are the same as in Fig. 3). The dashed arrows show the hypothetical position of t32 if analcimization had produced artificial $^{87}Sr/^{86}Sr$ enrichment (see text for details and Prelevic et al., 2004).

TRANSITION

Dans le chapitre 1, j'ai identifié la source d'émission volcanique de dépôts distaux jeunes retrouvées dans des formations lacustres carbonatées d'âge Pleistocene au Nord de l'Italie (Formation de Piànico). Ceci n'était possible qu'en caractérisant isotopiquement les provinces magmatiques d'émission et les produits volcaniques éjectés. En plus d'identifier l'origine de la source volcanique de ces produits volcaniques jeunes, cette étude de téphrochronologie visait à approfondir nos connaissances des périodes interglaciaires du Pléistocène.

Après avoir étudié une province magmatique continentale jeune, j'ai appliqué l'utilisation des isotopes au traçage des sources mantelliques d'une province magmatique continentale ancienne et plus complexe, telle que celle des Montérégiennes (chapitres 2 et 3). Dans ce genre de contexte continental, la signature mantellique peut être partiellement effacer par l'altération hydrothermale tardive ou bien la contamination crustale. Le couplage de plusieurs systèmes isotopiques, chacun ayant des caractéristiques complémentaires à l'autre, est un moyen efficace pour contraindre la composition du manteau source. En particulier dans le chapitre 3 je montrerais de nouveaux couplages entre les isotopes de l'azote et du plomb qui permettraient de mieux contraindre la source mantellique de cette province complexe. Un nouvel outil isotopique à explorer dans le futur.

CHAPITRE 2

Geochemical and isotopic (Nd-Sr-Hf-Pb) evidence for lithospheric mantle source in the formation of the alkaline Monteregian Province (Québec)

Emilie ROULLEAU[1] and Ross STEVENSON[1]

[1] GEOTOP and Département des Sciences de la Terre et de l'Atmosphère, Université du Québec à Montréal, Montréal, Qc, H2X 3Y7, Canada.

In revision for submission to Lithos

2.1. Abstract

The origin of the Monteregian Igneous Province, of southern Québec (Canada), is controversial with proposed origins involving hot spot or continental rift models. In this study, we present new geochemical and isotopic (Nd-Sr-Hf-Pb) results and modelling from mafic rocks of the Monteregian intrusions in order to constrain the mantle source. The major and trace element geochemistry of the intrusions are consistent with the fractional crystallization of Ol ± Cpx (± Plag) from OIB-like magmas. A combination of high Th contents and Ba/Rb ratios, and lower K/Th* ratios indicate the presence of amphibole in the mantle source of Monteregian magmas. An amphibole-bearing mantle and high (La/Yb)n ratios argue in favour of metasomatized mantle source. Trace element ratio modelling shows that the geochemical character of Monteregian magmas can be reproduced by low percentage melting of a spinel/garnet lherzolite mantle enriched by the percolation of a carbonatitic fluid and containing 1% amphibole. Crustal contamination (up to 23%) of the intrusions is evident from variations in the Sr and Nd isotope compositions, although the bulk of the Nd-Sr-Hf and Pb isotopic data form a tight cluster of depleted values. The OIB character and depleted isotopic compositions represent a hybrid reservoir similar to the LCV or CMR lithospheric mantle observed under Europe. However, low $^{207}Pb/^{204}Pb$ and $^{208}Pb/^{204}Pb$ ratios indicate the potential incorporation of an Archean component via the lithospheric mantle. These results point towards the involvement of the lithospheric mantle in the generation of the Monteregian magmatism; possibly in response to lithospheric extension during the opening of the North Atlantic Ocean at ca. 124 Ma.

Keywords: Lithospheric Mantle; Archean Mantle; Rift; Sr, Nd, Hf and Pb isotopes; Monteregian Province (Québec).

2.2. Introduction

Magmas of continental igneous provinces range from large volume tholeiitic flood basalts such as the Deccan Province and Columbia River Basalts (e.g. Hawkesworth and Gallagher, 1993, and references therein) to smaller volume alkaline basalt/gabbro complexes such as the Okenyenya complex of Namibia (e.g. Milner and leRoex, 1996) and the Monteregian Igneous Province of south-eastern Quebec (Canada). The rocks of these provinces share similar geochemical features to those of Ocean Island Basalts (OIB), including evidence for an enriched mantle source. Thus, like OIB, magmas from many continental igneous provinces are believed to reflect mantle melts associated with a mantle plume. However, in many of these continental igneous provinces, the absence of a systematic age progression of magmatic activity and the lack of evidence for regional basement uplift argues against a mantle plume association (Furman and Graham, 1999; Furman, 2005; Lustrino and Wilson, 2007). Alternatively, the Cenozoic magmatic activity in the Mediterranean area has been ascribed to extensional tectonics through reactivation of ancient structural dislocations rather than advocating the passage of hot spots on continents (Lustrino and Wilson, 2007). Geochemical interpretations of the mantle origin of continental igneous provinces are clouded by possible interactions with other enriched reservoirs such as the sub-continental lithospheric mantle and passage of the magmas through and emplacement within continental crust. Magmas from continental igneous provinces inherently show greater geochemical and isotopic variability than OIBs due to magma interaction with the asthenospheric mantle, lithospheric mantle and continental crust (Lustrino and Wilson, 2007; McKenzies and O'Nions, 1995; Saunders et al., 1992; Tang et al., 2006). Thus, the magmas may be products of asthenospheric or lithospheric mantle sources or a mixture of both (Hawkesworth and Gallagher, 1993; Lustrino and Sharkov, 2006; Lustrino and Wilson, 2007; Milner and leRoex, 1996; Rogers et al., 2000; Shaw et al., 2003; Stein and Hofmann, 1992; Tang et al., 2006).

The Monteregian Igneous Province is composed of nine plutons and associated dykes of alkaline compositions that were emplaced in southern Québec, eastern Canada, by a continental magmatic event at ca. 124 Ma (Eby, 1984a; Foland et al., 1986). Like other Continental Igneous Provinces, the exact origin of these intrusions is controversial and has

been ascribed to melting of the lithospheric mantle at the time of the opening of North Atlantic Ocean (Faure et al., 1996; Bédard, 1985; Wen et al., 1987) or a deep mantle (plume) origin (Eby, 1985; Foland et al., 1988). In fact, this igneous province has been linked to the alkaline intrusions of the New Hampshire White Mountains and the New England seamount chain as expressions of an age-progressive hotspot track: the New England hotspot, analogous with the Hawaiian model (Eby, 1985; Foland et al., 1988). However, eastward chronological progression of such a hotspot track is not completely supported by a regular progression in ages of the Monteregian Igneous Province (ca. 110 to 140 Ma; Eby, 1984a; Eby, 1985; Foland and Faul, 1977; Foland et al., 1986), White Mountains (110 to 130 and 165 to 200 Ma; Foland and Faul, 1977) and New England Seamounts (80 to 110 Ma; Duncan, 1982).

Geochemical and isotopic studies (Sr, Nd and Pb) of the Monteregian intrusions yield depleted isotopic signatures that have been variably ascribed as OIB and HIMU signatures consistent with a deep mantle (plume) origin (Eby, 1985; Foland et al., 1988) or an mantle source related to rifting and formation of the North Atlantic Ocean (Faure et al., 1996; McHone 1996). The uncertainty in the geochemical and isotopic interpretation of the mantle origin of these melts arises from influence of crustal assimilation observed in the intrusions on the basis of Sr, Nd and Pb isotope data (Chen et al., 1994; Eby, 1984b; Eby, 1985a; Eby, 1985b; Foland et al., 1988; Landoll and Foland, 1996). This crustal assimilation obscures the origin of the enriched nature of these intrusions. Overall, these geochemical and isotopic studies concentrated largely on Sr and Pb isotopes (Eby, 1984b; Eby, 1985a; Eby, 1985b; Foland et al., 1988) and provided only limited Nd isotope data for selected Monteregian hills. In this paper, we present new geochemical and Nd, Sr, Hf and Pb isotope data for mafic rocks from eight of the Monteregian intrusions. These mafic samples were chosen in an effort to minimize the effects of crustal contamination and obtain a clearer signature of the mantle signature involved in the formation of the Monteregian Hills.

2.3. Geology

The Monteregian Igneous Province consists of a series of alkaline plutons and dikes emplaced along a linear east-west trend associated with the St. Lawrence graben and the

Ottawa-Bonnechere paleorift (Fig.1). The magmas intruded three different terrains including the Precambrian Grenville basement west of Montréal, the St. Lawrence Lowlands sediments and the metamorphosed sequences of the Appalachian Mountains, east of Montréal. The igneous intrusions reveal a large variety of rocks from strongly silica-undersaturated to moderately silica-saturated. At the western end of the Monteregian Igneous Province, Oka complex is characterized by strongly silica-undersaturated rocks, represented by carbonatites, okaites and meltegites. The Central Monteregian Igneous Province intrusions (Mont Royal, St Bruno, St Hilaire, St Grégoire, Yamaska and Rougemont) are principally composed of slightly silica-undersaturated (essexite) to moderately silica-oversaturated rocks (gabbros and pyroxenite) with minor felsic rocks (syenite). The St Hilaire and St Grégoire intrusions contain a higher proportion of felsic rocks represented by nepheline syenites. The eastern part of the Monteregian Igneous Province (Mounts Shefford and Brome) is mainly characterized by silica-oversaturated rocks (pulaskite, syenite) and minor mafic rocks (gabbro and diorite). The 140 Ma Mount Megantic intrusion has traditionally been considered part of the, Monteregian Igneous Province, but is also argued to belong to White Mountains alkaline series of New Hampshire because of its older age (200 to 165 and 110 to 130 Ma; Eby, 1985a; 1985b; Foland and Faul, 1977; Foland et al., 1988).

Mont Royal is mainly composed of gabbro and leucogabbro with a minor proportion of syenite and nepheline-diorite (Bancroft, 1923; Gelinas, 1972). The gabbro is composed of cumulus olivine (Fo74-68), Ti-augite and varying amounts of amphibole and plagioclase (An83-44). The St Bruno intrusion is primarily a gabbro body composed of olivine (Fo84-74), plagioclase (An84-55) and minor amounts of amphibole (Philpotts, 1976). A quartz-gabbro body associated with the St Bruno pluton is considered a product of crustal contamination of the gabbroic magma (Eby, 1984b). Mount St Hilaire is composed of two principal rock-types that form two halves of the intrusion; gabbro and nepheline syenite. Generally, the gabbros are pyroxene-rich but appear locally richer in amphibole and olivine is rare. Small bodies quartz syenite associated with the St Hilaire pluton are attributed to crustal contamination by the host rocks (Currie, 1983; 1986; Eby, 1988; Perrault, 1972). Mount Rougemont is essentially composed of pyroxenite and gabbro. Olivine can be abundant and plagioclase is present either as an interstitial phase in the pyroxenites or a major phase in the gabbros (Philpotts, 1972; Philpotts, 1976). Mount St Grégoire is a small circular intrusion

with a core of essexite surrounded sequentially by rings of essexite, pulaskite and nepheline syenite (Eby, 1988; Philpotts, 1972 and authors therein). The essexite consists of minor olivine and a varying amount of augite, hornblende and oligoclase. The Yamaska pluton is mainly composed of pyroxenites (yamaskite) and gabbro (Gandhi, 1966). The gabbro is composed of abundant plagioclase, Ti-augite and/or hornblende. The pyroxenites and gabbros are intruded by essexite and nepheline-syenite. The essexite consists of Ti-augite, kaersutite and plagioclase, and interstitial alkali feldspar or nepheline. Mount Shefford is composed of diorite, gabbro and minor intrusive breccias, sub-volcanic porphyries, nordmarkite and pulaskite (Valiquette, 1977). Mount Brome, the largest intrusion of the Monteregian Province, is composed of a gabbro body partly enclosing a core of pulaskite and nordmarkite. Small bodies of nepheline-diorites, monzonites, and foyaites are found intruded into the core syenite units. The gabbro is composed of plagioclase, clinopyroxene, hornblende and rare olivine. Previous studies showed that crustal contamination played a major role in the evolution the Mount Shefford and Brome intrusions (Chen et al., 1994; Landoll and Foland, 1996).

2.4. Samples and analytical methods

Samples were selected on the basis of their chemistry and mineralogical features from a large set of rocks (140) collected from Mounts Royal, St Bruno, St Hilaire, St Grégoire, Rougemont, Yamaska, Shefford and Brome. The Mount Royal samples include rocks collected in 1930 during the construction of a railway tunnel through the mountain (provided by R. Martin, McGill University). An effort was made to concentrate on samples of mafic character in order to minimize contamination and differentiation effects. A total of 49 samples were analyzed for major and trace element compositions and 44 samples were analyzed for their isotopic compositions.

The selected samples were ground to powder using a ceramic mill and whole rock major and minor elements and transition metals (Co, Cr, V, Sc) were analysed with a Philips PW 1400 X-ray fluorescence (XRF) spectrometer (McGill University). Analyses of major and minor elements were obtained using 10-15 grams of rock powder in the form of fused beads

prepared from ignited samples. Uncertainties for major and minor oxides are less than 1% of quoted values, respectively. Rare Earth Elements (REE) were determined using a Perkin Elmer ELAN DRCplus ICP-MS (McGill University) with a precision better than 5% for all the elements.

Chemical separation procedures for Nd and Sr isotopes were conducted under clean lab conditions and all acids were distilled. All samples were analysed at GEOTOP (UQAM). In each case, between 50 and 100 mg of powdered sample were weighed out into a Teflon Parr-bomb and spiked with ^{150}Nd – ^{149}Sm and ^{87}Rb – ^{84}Sr tracer solutions for the determination of Sm-Nd and Rb-Sr concentrations. A mixture of HF-HNO_3 acids was added and the mixture placed in an oven in order to dissolve the samples under pressure at a temperature of 150 °C. After one week, the samples were removed from the furnace and evaporated. The samples were subsequently evaporated in perchloric acid to break up the fluoride salts and redissolved in 6 M HCL in the oven again for 12 hours. The resulting 6 M HCL solution was loaded onto ion-exchange columns containing AG1X8 resin that retained the Fe in the sample but allowing the other elements to be eluted with 6 M HCL. The samples were evaporated and 0.5 ml of 14M HNO_3 was added to change the HCl salts into nitrates. The REE separation was achieved using Eichrom TRU Spec resin in which samples must be nearly Fe-free. About 1 ml of TRU Spec resin was placed in the column, washed with 3-4 ml of 0.05M HNO_3 and equilibrated using 2 ml of 1M HNO3 prior to loading 1 ml of the samples. A beaker was placed beneath the column to collect the first 2 ml of rinse with 1m HNO_3 in order to collect the Rb-Sr fractions. The column was then rinsed with 0.25 ml of 0.05M HNO_3 and then the REE fractions were collected using 1.75 ml of 0.05 M HNO_3.

The Sm-Nd separation was achieved using columns containing about 2 ml of Eichrom LN Spec resin. These columns were conditioned with 0.2M HCl prior to loading the samples in the same acid. Samples were eluted with 0.2 M HCl, then Nd was collected using 0.3 M HC and Sm was collected using 0.5 M HCl. Both the Nd and Sm fractions were successively evaporated while Rb and Sr were separated using Eichrom Sr Spec resin.

The isotopic composition and concentration of Nd, Sm, and Sr of Mt. Royal were analysed by thermal ionisation mass spectrometry (TIMS). Nd and Sm were measured using a triple filament assemblage with the samples evaporated on Ta side filaments and ionized by a Re centre filament. Sr samples were loaded and analysed on a single Re centre filament.

The Nd and Sr samples were measured in dynamic mode and normalized to $^{146}Nd/^{144}Nd$ = 0.7219 and $^{86}Sr/^{88}Sr$ = 0.1194 assuming exponential fractionation behaviour while Sm was measured in static mode. During the period of this study, repeated measurements of the Nd International Standard JNdi yielded a value of $^{143}Nd/^{144}Nd$ =0.512148 ± 11 (N=11) compared to the published value of 0.512115 ± 7 (Tanaka et al., 2000). Our samples were corrected by 0.000033 for taking into account the shift of the measured standard. Repeated analysis of the NBS 987 Sr standard yielded a value of $^{87}Sr/^{88}Sr$ = 0.710263 ± 17 (N=7). Rb isotopic ratios were calculated from Rb contents and the natural abundance of ^{85}Rb and ^{87}Sr. Epsilon Nd values were calculated using the present day CHUR value of 0.512635 for $^{143}Nd/^{144}Nd$. Initial $^{143}Nd/^{144}Nd$ and $^{87}Sr/^{88}Sr$ were calculated at ca. 124 Ma (± 1.5 Ma; Foland et al., 1986) based on Ar/Ar ages for Monteregian intrusions. The typical combined procedure blanks for Nd and Sm are <150 pg.

Lead isotopic compositions were determined on plagioclase separates, a mineral that is comparatively Pb-rich and generally contains very little U and Th. Typically, 10 to 30 mg of clear, inclusion-free plagioclase grains were hand-picked under a microscope from the 50 to 150 nm size fraction. The mineral grains were ulta-sonically washed in H_2O, acetone and dried down. They were then leached using hot 6N HCl acid for 24 to 48 hours. The mineral residue was then rinsed with distilled water, dried down and powdered in an agate mortar. The powders were further leached at room temperature using a dilute mixture of HF+HBr (~1N), for 30-60 minutes in an ultrasonic bath. The mineral residue was re-dissolved in concentrated HF. The leaching treatments were aimed at removing, as much as possible, labile radiogenic Pb held in crystalline defects, cleavage surfaces or foreign mineral inclusions. The mineral residues were processed through anion-exchange chromatography following the procedure of Manhès et al. (1980). Pb was analysed using multi-collector ICP-MS instrument (IsoProbe from Micromass) operated in "solution mode" with an Aridus nebulizer system at GEOTOP-UQAM and calibrated with the NIST-SRM-981 standard. Total procedural blank is smaller than 55 pg.

Hafnium and lutecium isotopic compositions were determined on bulk rocks. The selected samples were ground to powder using a ceramic mill at GEOTOP-UQAM. Chemical separation and isotopic composition of Lu-Hf were analyzed on a ThermoFinnigan Neptune™ multi-collector inductively coupled mass spectrometer (MC-ICP-MS) at

Washington State University (see Vervoort et al., 2004). Samples were dissolved using a 10:1 HF/HNO3 mixture in Teflon bombs in an oven at 160 °C for 4–5 days. All samples analyzed for isotopic composition were spiked with a mixed ^{176}Lu–^{180}Hf tracer in order to determine accurate parent/daughter ratios. Lu and Hf were separated from the same solution following methods described in Vervoort et al. (2004). During the course of this study, repeated measurements of the Hf International Standard JMC 475 yielded yielded a value of $^{176}Hf/^{177}Hf$=0.282147±12, $^{178}Hf/^{177}Hf$=1.467204±35, $^{180}Hf/^{177}Hf$=1.886670±73 (2σ SD, n=141). Hf isotope measurements were normalized to the accepted values for these standards, $^{176}Hf/^{177}Hf$=0.282160±12 (Vervoort and Blichert-Toft, 1999b). For calculation of □Hf values we used $^{176}Hf/^{177}Hf_{CHUR(0)}$ = 0.282772 and $^{176}Lu/^{177}Hf_{CHUR(0)}$ = 0.0332 (Blichert-Toft and Albarede, 1997). Decay constant values used were λ176Lu=1.867×10−11 y−1 (Söderlund et al., 2004). Rougemont samples are not included among the Lu-Hf results due to unsatisfactory analyses resulting from multiple interferences with others trace elements.

2.5. Results

2.5.1. Major oxides

Representative analyses are shown in Table 1 and major element diagrams are presented in Fig. 2. The rock range in composition is from phonolite-tephrite (essexite, nepheline-monzodiorite and nepheline-diorite) to picrite and basanite (gabbro and pyroxenite; c.f. TAS diagram; Le Maitre et al., 1989). Analyzed rocks have Loss On Ignition (LOI) values less than 1.3 wt.% indicating little or no alteration of the samples. The (K_2O + Na_2O) values range from 0.5 to 13 wt.% highlighting the alkaline and potassic character of the igneous intrusions. The rocks show low concentrations of SiO_2 (38.0-59.18 wt.%) and variable MgO contents (0.54-18.2 wt.%). The samples with low MgO (≤ 3 wt.%) are silica-undersaturated rocks such as nepheline diorites and monzodiorites, and essexites and samples with higher MgO (MgO ≥ 3 wt.%) are gabbros and pyroxenites (Table 1 and Fig. 2). The major element diagrams (Fig. 2) show one break in slope for all elements except for Al_2O_3 and P_2O_3. For the first slope, MgO plotted against TiO_2, CaO and Fe_2O_3 shows a positive correlation, although it is inversely correlated with SiO_2 (Fig. 2). This is a prominent feature

of the Monteregian hills and consistent with the fractionation of Fe-Mg silicates such as pyroxene, olivine and minor amphibole and/or biotite. The second trend affects principally Mts. Royal, Rougemont and St Bruno samples and shows small increases of CaO, TiO_2 and Fe_2O_3 and small decreases of SiO_2 with decreasing MgO (Fig. 2). This trend likely reflects the presence of cumulus pyroxene and olivine and is confirmed by the petrography of the samples. In fact, many samples of Mount Royal (MR17, MR24, 195+50-60, 298+03), Rougemont (MRG3) and St Bruno (MSB1, MSB4 and MSB5a) contain cumulus pyroxene in the rock samples. The negative correlation between Al_2O_3 and MgO (Fig. 2) suggests that plagioclase fractionation did not play a major role in the evolution of these magmas. The trend of decreasing CaO/Al_2O_3 with decreasing MgO confirms the role of clinopyronene and supports the absence of significant plagioclase fractionation (Fig.2). The P_2O_5 - TiO_2 plot reveals two groups: low P_2O_5 (0.0027-0.46) and high P_2O_5 (0.9-2.6). The high P_2O_5 group shows a positive correlation between P_2O_5 and TiO_2 and results from the fractionation of the apatite and Fe-Ti oxides. In samples with low P_2O_5, neither apatite nor Fe-Ti oxides play a significant role. If we compare the different intrusions, Mt. St Grégoire shows the smallest overall variations in major element contents compared to the other intrusions (Fig. 2) with Brome, Mount Royal, Rougemont, St Bruno showing the greatest overall variation in rock compositions. Overall, the geochemical range of samples is comparable to those of Eby (1984b; 1985a).

2.5.2. Trace and rare earth elements

The trace element and REE diagrams of Monteregian Igneous Province rocks (samples with MgO<10 % w.t.) are rather heterogeneous (Fig. 3 and 4). The REE profiles are variably light-REE enriched with La ranging from 70 to 200 times primitive mantle in samples from Mt. Royal, St Gregoire, Yamaska, St Hilaire, Shefford and Brome (one sample, MB18) and Lu ranging from 4.7 to 7.2. Less enriched samples from Brome, Yamaska, Rougemont and St Bruno have La contents of 20 to 50 times primitive mantle and Lu from 1.4 to 2.6 times primitive mantle (Fig. 3). Two samples from Rougemont (MRg1 and MRg4) are particularly low in La and Lu, ranging from 5 to 7 times and 0.6 times primitive mantle, respectively (Fig. 3). Most samples have normalized (La/Yb)n ratios ranging from 15-35,

with the exception of St Bruno and Rougemont, which range from 10.6-11.5. The REE profiles for Mts Shefford, St Grégoire and St Hilaire are particularly homogeneous. A camptonite from Mt. Royal (181+00; Table 2) yields a concave profile due to LREE and HREE enrichments (Fig. 3).

Large Ion Lithophile (LIL) elements such as Rb (4.2-80 ppm), Sr (568-5501 ppm) and Ba (36-2510 ppm) correlate positively with MgO, indicate the fractional crystallization of mafic mineral as pyroxene or amphibole. All the Monteregian Hills show a negative anomaly for K relative to neighbouring Nb and U (Fig.4). The systematic depletion of K could be explained by the presence of a residual K retaining phase in the source mantle (phlogopite or amphibole; Class and Goldstein, 1997).

Transition elements, such as Sc and Co show a positive correlation with MgO, and V shows a negative correlation with SiO_2, likely reflecting the fractionation of olivine and pyroxene (Table 1). High Field Strength (HFS) elements like Zr (45.1–605 ppm), Nb (1.6-162 ppm) and Y (5.8–54.7 ppm) show no correlation with MgO but a positive correlation with SiO_2 as a result of magma differentiation. Negative Nb anomalies are present in samples from Mts. Royal, Rougemont, St Hilaire, Shefford and Brome (Fig. 4). This depletion in Nb does not correlate with the degree of fractionation (e.g., MgO) and thus reflect either the chemistry of the mantle source or the involvement of crustal material. Other strongly incompatible elements such as U (up to 1000) and Th (up to 380) are highly enriched compared to primitive mantle and may indicate post-magmatic enrichment (e.g. U). The majority of the Tb/Yb ratios are <1, suggesting that most samples are depleted in heavy REE. There are no negative Eu anomalies which suggests that plagioclase fractionation did not play a role in the formation of these rocks (Fig. 4). However, samples from Mts. Royal, St Bruno, Rougemont, St Hilaire, Yamaska, Shefford and Brome show strong positive anomalies in Sr with either no Eu anomaly or a small positive Eu anomaly. This likely reflects the stabilization of pyroxene and/or amphibole in the fractionation assemblage at high water pressures (Bédard et al., 1987; Eby, 1984b; Yoder and Tilley, 1962). A number of samples possess either small negative or small positive anomalies for Zr and Ti reflecting the fractionation (negative anomalies) or accumulation (positive anomalies) of minute amounts of Ti-rich phases. Ti and Zr negative anomaly can be explained also by amphibole- bearing mantle source (Spath et al., 2001).

2.5.3. Nd, Sr, Pb and Hf isotopes

The Sm-Nd, Rb-Sr, Lu-Hf and Pb isotope compositions and elemental concentrations are reported in Table 3 and 4, and shown in Fig 5. The $(^{143}Nd/^{144}Nd)_i$ ratios measured in the Monteregian hills rocks range from 0.512571 to 0.512780 . The initial $(^{87}Sr/^{86}Sr)_i$ ratios vary from 0.70330 to 0.70472 (Table 3). There is a rough inverse correlation between $(^{143}Nd/^{144}Nd)_i$ and $(^{87}Sr/^{86}Sr)i$ ratios for the Monteregian hills rocks (Fig.5a). The low $(^{87}Sr/^{86}Sr)i$ and high $(^{143}Nd/^{144}Nd)_i$ ratios of the Monteregian intrusions fall within the domain of OIBs (Condie, 2001). Although there is a fair amount of variability within and between intrusions, the Mt. Royal rocks have the highest Nd ratios and the lowest Sr ratios. Samples from Rougemont and Yamaska have the lowest Nd and highest Sr isotope ratios (Fig. 5a). The $(^{176}Hf/\ ^{177}Hf)_i$ composition in Monteregian rocks range from 0.282937 to 0.282772 (Table 3) with considerable variation within a given intrusion. The $(^{176}Hf/\ ^{177}Hf)_i$ and $(^{143}Nd/^{144}Nd)_i$ ratios show a positive correlation similar to that of mantle array defined by Vervoort et al. (1999a ; Fig.5b). The Pb isotope compositions of Monteregian plagioclase separates show a range of values ($^{208}Pb/^{204}Pb$=39.65-37.27, $^{207}Pb/^{204}Pb$= 15.65-15.0, $^{206}Pb/^{204}Pb$=19.91-18.61) that differs from those of previous bulk rock studies (Eby, 1985b; Fig.5c-d). Here again, there are large isotopic variations within a given intrusion, particularly for Mounts Rougemont, St Gregoire, St Hilaire, Shefford and Brome. Two different trends are evident from the range of Pb isotope compositions of the Monteregian Hills (Fig. 5c-d): (1) one trend indicates $^{207}Pb/^{204}Pb$ vs $^{206}Pb/^{204}Pb$ compositions varying between mantle compositions and Appalachian/Grenville compositions suggesting mixing between mantle-derived magmas and the enclosing country rocks (Fig.5d); (2) A second trend is indicated by data varying between mantle compositions and samples with very low $^{207}Pb/^{204}Pb$ and $^{208}Pb/^{204}Pb$ ratios that cannot be explained by local rock contamination. This trend may reflect the involvement of an older component either in the mantle source (lithosphere) or during the ascent of magma (Fig.5c-d).

Figure 6 depicts the geographic distribution of Nd and Sr isotopic data from this study together with isotopic data from previous studies for comparison (Chen et al., 1994; Eby, 1984b; 1985a; 1985b; 1989; Foland et al., 1988; Landoll and Foland, 1996). A schematic profile of the geology of the Monteregian Igneous Province is included. It is evident that the εNd values of the Monteregian hills decrease from the West (highest values in Oka and Mt.

Royal) to the East (lowest values in Mt. Brome and Mt. Shefford). A corresponding increasingly radiogenic, but less clear trend is observed for the Sr isotope ratios for the intrusions. These coupled trends might reflect an enhanced crustal contamination from west to east.

2.6. Discussion

2.6.1. Alteration effect

Overall, the alteration of the Monteregian Igneous Province rocks is minimal and consists of surface oxidation of clinopyroxene, plagioclase and amphibole in hand samples. However, in the following sections the concentrations of mobile elements such as Rb, Sr, K, Ca, and Ba (Schiano et al., 1993; Swinden et al., 1990) are used for petrogenetic interpretations. Thus, a discussion of the robustness of the concentrations of these elements is warranted. In this regard, samples from six of the intrusions have unusually high Ba contents (>700 ppm); Mt Royal, St Hilaire, St Grégoire, Yamaska, Shefford and Brome (Table 2). However, the Ba concentrations form a positive correlation with Rb and K concentrations and there is no correlation between Ba contents and LOI (Table 1 and 2). Futhermore, plots of Ba, Rb, and K against Zr (an immobile element) yield mostly positive correlations except for some of the samples from Mounts Brome and Shefford. These correlations strongly suggest that the concentrations are magmatic in origin and not due to post-magmatic alteration. The behaviour of samples from Mounts Brome and Shefford likely reflect higher degrees of crustal contamination (Foland et al., 1988; Wen et al., 1987). Sr contents are more problematic because plots of Sr versus Zr or Rb begin with positive correlations for most of the intrusions but end with negative correlations for Mounts St. Hilaire, Shefford and Brome. However, the lack of correlation between Sr contents and LOI contents suggests that Sr is not affected by post-magmatic alteration. The plot of Sr concentration versus initial Sr isotope ratios (Fig 7a) suggests that while the majority of the intrusions are affected by crustal contamination that lowers Sr contents, Mounts Sheffords and Brome appear to have interacted with a Sr-rich contaminant. These latter samples are not included in the petrogenetic discussions.

2.6.2. Fractional crystallization and accumulation

In most of the major element diagrams of the Monteregian Igneous Province (Fig.2), the samples exhibit two different trends with the break between the two trends occurring at about 10 wt.% MgO that separates melt compositions (< 10% MgO) from cumulate compositions (> 10% MgO). For the melt compositions (MgO ≤ 10%), plots of SiO_2, Fe_2O_3, CaO, TiO_2 or K_2O against MgO indicate that fractional crystallization of olivine and clinopyroxene is a dominant process affecting the initial magma composition. The increase in Al_2O_3 content with decreasing MgO and the absence of Eu anomalies in the REE profiles (Fig. 2 and 3) indicate that fractional crystallization of plagioclase was not significant. The P_2O_5, TiO_2 and Zr contents indicate that apatite and Ti-oxides are minor residual (negative anomalies) or cumulus phases (positive anomalies; Eby, 1984b; Zhang, 2005; Fig. 2 and 4). The increasing K_2O contents with decreasing MgO among the samples (Fig. 2) suggest that fractional crystallization of amphibole or/and biotite in these magmas was not a significant factor in the evolution of the rocks.

For MgO ≥ 10%, the negative trend of SiO2, Fe2O3, CaO and TiO2 against MgO suggests the presence of accumulation of clinopyyroxene (± olivine). In fact, visible clinopyroxene cumulate are observed in Mts. Royal (MR24, MR17, 195+50-60 and 298+03), St Bruno (MSB1, MSB4, and MSB5a) and Rougemont (MRg3) rocks. Thus, samples with high MgO (≥ 10%) are excluded from the following petrogenetic discussions because they do not reflect the evolution of the magma.

2.6.3. Crustal contamination by wall rocks

The role of crustal contamination on the variations in incompatible trace elements and isotopic ratios needs to be evaluated in order to differentiate between possible mantle source(s). The crust beneath the Monteregian Igneous Province includes, from West to East, the Precambrian Grenville basement, limestones and shales of the St Lawrence Lowlands, and metamorphosed sequences of the Appalachian Mountains. The isotopic compositions of crustal material ($(^{87}Sr/^{86}Sr)i$ ~0,7085-0.71500 and $(^{143}Nd/^{144}Nd)i$ ~ 0.51200) are significantly different from those measured in the Monteregian magmas (Bell, 1982; Chakrabarti et al., 2007; Chen et al., 1994; Davies and Smith, 2006 and authors therein; Landoll and Foland,

1996). In Fig. 5, the Nd and Sr isotopic ratios from this study and previous studies clearly trend towards crustal compositions (Chen et al., 1994; Eby, 1984b; Landoll and Foland, 1996). Although the Oka carbonatites (not studied here) were intruded through the Grenville basement, they have the most depleted isotopic compositions of the Monteregian Hills (c.f. Fig.6). The relatively non radiogenic Sr and highly radiogenic Nd isotope ratios of the Oka carbonatites are interpreted to represent the upper mantle under the Monteregian Province (Bell, 1982). In figure 7, $(^{87}Sr/^{86}Sr)i$ and $(^{143}Nd/^{144}Nd)_i$ are plotted against the Sr contents of the Monteregian hills samples. Because $^{87}Sr/^{86}Sr$ and $^{143}Nd/^{144}Nd$ ratios are not affected by closed-system fractionation/differentiation, they are good indicators of crustal assimilation. There are clear correlations of decreasing Sr contents with increasing Sr and decreasing Nd isotope compositions for the majority of the intrusions that are consistent with the addition of crustal material in samples of Monteregian hills. The exceptions are samples from Mounts Shefford and Brome which have been shown to have suffered extensive crustal contamination (Chen et al., 1994; Landoll and Foland, 1996). The samples from this study appear to have been contaminated by a Sr-rich contaminant, possibly a fluid rich in Sr. Crustal contamination trends are also evident from the Pb isotope data (Figs. 5c-d) but are discussed in detail in the Pb isotope section further below. No clear evidence of crustal contamination is noted from the Hf isotopes, likely due to the fewer number of samples analysed. One notable exception of this is the presence of a slight trend towards the wall rocks in a plot $^{176}Hf/^{177}Hf$ versus $^{208}Pb/^{204}Pb$ (c.f. Fig. 14b).

There is an overall increasing degree of contamination from west to east in the Monteregian Igneous Province. Figure 6 shows a longitudinal geologic cross-section of the Monteregian Province with the relative thicknesses and distributions of the Grenville basement, sedimentary rocks of the St. Lawrence lowlands and the Appalachian Orogen along with the Nd and Sr isotope compositions of the Monteregian Hills. The εNd values show a clear decrease from west to east whereas the $(^{87}Sr/^{86}Sr)i$ show a less obvious increase, indicative of increasing contamination to the east. Mt. Royal is located within the thinnest portion of the St Lawrence sediments and shows only slight evidence of contamination whereas the easternmost intrusions, such as Rougemont or Brome, show more contamination. Similarly, the thickness of the sediments increases from West to East along with a change in the host rocks, passing from the St. Lawrence lowlands to Appalachian orogen (Fig.6). In

fact, Rougemont intrudes the St Lawrence sediments and shows less contamination than Brome which intrudes Appalachian orogen. Thus, increasing contamination in Monteregian Igneous Province can be associated with increasing thickness of sediments overlying the Grenville basement and the change of type of host rock. The higher degree of scatter in the Sr isotope data compared to the Nd isotope data likely reflects the greater mobility of Sr (Bienvenu et al., 1990; Swinden et al., 1990) and the greater variability of Sr contents among the contaminants (shales, limestones, schists) compared to Nd.

2.6.4. AFC Model

Although crustal contamination has been inferred for most of the Monteregian Hills, only the contamination of Mounts Brome and Shefford has been modelled in previous studies using host sediments (sandstone) and Grenville basement as the contaminants (Bell, 1982; Chen et al., 1994; Landoll and Foland, 1996). These studies showed that a maximum of 20% contamination by the host rocks could explain the Nd and Sr signature for mafic rocks. In figure 8, we present contamination models for each of the Monteregian intrusions.

To quantify the crustal contamination of our mafic samples, we used the coupled assimilation and fractional crystallization (AFC) model created by DePaolo (1981) for Sr and Nd isotopes. This AFC model assumes a single pulse of magma, without recharge, and crystal fractionation of solids from the liquid. For our modelling, we used the mass ratio of assimilated to fractionally crystallized material (R) and the bulk trace element distribution coefficients for the fractionating mineral assemblages (D). For the mafic rocks, we assume that clinopyroxene, plagioclase and apatite are the main fractionating phases for Sr and Nd, and assign representative bulk D values of 1 for Sr and 0.2 for Nd (e.g. Chen et al., 1994). The isotopic compositions of the initial uncontaminated magma are taken from the primitive isotopic compositions of Mt Royal (MR15) and St Gregoire (MSG6) and are similar to the isotopic compositions found at Oka. The primitive concentrations of Nd and Sr of the parental magma vary from 1200-2500 ppm for Sr and 25-95 ppm for Nd. The contamination of each Monteregian intrusion is modeled by a host rock appropriate to their location (c.f. Fig.7); granite for the Grenville basement, carbonate for the St Lawrence Lowlands (Trenton and Utica formations) and sandstone for the Appalachian Orogen (Gilman formation;

Chakrabarti et al., 2007; Chen et al., 1994; Davies and Smith, 2006, and authors therein). The contamination of Mount Royal was modeled using both the Grenville basement and St Lawrence sediments because the cover of the St Lawrence Lowlands sediments is relatively thin in the Montreal area.. The values used for the modelling are summarized in Table 4.

The results of the AFC model are illustrated in Fig.8 and indicate that the isotopic variation observed for Mt. Royal samples can be explained by up to 17% (R value) contamination by Grenville basement or up to 20 % contamination by St Lawrence sediments. Two samples from Mount St Bruno (MSB2, MSB8) also show contamination up to 20 % by St Lawrence sediments. Three samples from Mount Rougemont (MRG1, MRG4, MRG11) vary from 13-23% contamination by St Lawrence sediments and Mount Yamaska samples vary between 6 and 17 % contamination by Appalachian sediments. Brome and Shefford are characterized by the greatest contamination (10 to 19%) by Appalachian sediments (Fig.9). However, the majority of samples from this study show little (<6%) or no contamination and have isotopic values that fall within a relatively restricted range of $^{87}Sr/^{86}Sr_i$ = 0.7032-0.7037 and $^{143}Nd/^{144}Nd_i$ = 0.512788-0.51269. Bell et al. (1982) reported an initial Sr isotope ratio of 0.70318 for the Oka carbonatites and suggested a mean ratio of 0.7033 as representative of the upper mantle beneath the Monteregian Igneous Province. We propose that this range of $^{87}Sr/^{86}Sr_i$ (0.7032-0.7037) and $^{143}Nd/^{144}Nd_i$ (0.512788-0.51269) ratios may reflect a heterogeneous enriched Monteregian mantle similar to that described for the European magmatic province (Lustrino and Wilson, 2007).

2.6.5. Evidence for an amphibole-bearing mantle source: Metasomatism event?

The majority of Monteregian rocks are systematically depleted in K with respect to neighbouring Th and Nb in the trace element profiles (Fig.3). This suggests the presence of a residual K-bearing phase during melting in the mantle because bulk partition coefficients for K and Th are similar in spinel and garnet lherzolite (Furman, 2007). Amphibole and phlogopite are the most likely phases that could produce the observed K/Th fractionation. Although many of Monteregian rocks contain amphibole and/or biotite, they are not present in all rocks, whereas all Monteregian samples show negative K anomalies. Thus, the origin of the K depletion must lie in a residual hydrous phase(s) in the mantle (Class and Goldstein,

1997; Spath et al., 2001). Almost all the Monteregian hills samples have K_2O < 3% (one sample has 5% in K_2O) and TiO2 < 6%. In many of the samples, the K anomaly is associated with depletions in Zr and Ti. Spath et al. (2001) argued that these depletions in K_2O (≤ 2.5%), Zr and low TiO_2 (≤ 8.8%) are best reconciled by the presence of amphibole in mantle source. In a diagram of K/Th* versus Th (Fig. 9a), samples from the Monteregian Hills lie within the high Th field (>7ppm) of magmas generated by a low degree of melting of an amphibole-bearing source material (i.e., low K/Th*<2000). In addition, Furman and Graham (1999) explain that melting of peridotite with phlogopite in residue produces melts with high Rb/Sr (≥0.10) and low Ba/Rb (≤20) whereas peridotite with amphibole produces low Rb/Sr (≤0.06), high Ba/Rb (≥20), and low K_2O/Na_2O (≤0.75). The low Rb/Sr (0.005-0.058), high Ba/Rb (4.64-52.28), and low K_2O/Na_2O (≤0.88) ratios of the Monteregian Hills are compatible with melts derived from an amphibole-bearing lherzolite (Fig. 9b and Table 2). However, one sample from Mt. Royal (194+66; Table 2) shows high Rb/Sr (0.19) and low Ba/Rb (9.85), more consistent with the presence of phlogopite in the mantle source. These results indicate that the mantle source for the Monteregian Hills contained amphibole produced by a hydration event prior to melting (e.g. metasomatic fluid).

In order constrain the origin of the hydration event, we plotted $(La/Yb)_n$ vs Ti/Eu ratios for the Monteregian Igneous Province in Fig. 10 along with data from the Oka carbonatite (Gold and Eby, 1986) and mantle peridotites (lherzolite; McDonough, 1990). High $(La/Yb)_n$ ratios in mafic rocks, such as those of the Monteregian Hills, are often interpreted as the result of melting of fertile lherzolite (George and Rogers, 2002). The bulk of the Monteregian rocks lie on a mixing line between the Oka carbonatite and the mantle lherzolite (Fig. 10) indicating that enrichment of the Monteregian mantle required the addition of < 2% carbonatite melt (mixing-percolation model; Rudnick et al., 1993). Thus, the geochemistry of the Monteregian magmas is consistent with melting of a hydrated mantle that was enriched by the percolation of small fractions of a carbonatite (LILE-enriched) melt producing fertile peridotite.

2.6.6. Depth and degree of partial melting of Monteregian magmas

The depletion in heavy REE (low Tb/Yb ratios) of the Monteregian rocks suggests that their mantle source requires residual garnet in addition to amphibole. Figure 11 uses the Ce/Y and Zr/Nb ratios of the Monteregian rocks to model the degree of partial melting from a fertile garnet lherzolite containing 1% of amphibole for the Monteregian rocks. The majority of the Monteregian hills rocks require < 3% melting of a mantle source with modal garnet variations of 2-10%. Samples from Mounts Rougemont and St Bruno with particularly low Ce/Y ratios and variable Zr/Nb ratios indicate 0.3-1.5 % melting of a mantle source with no garnet. These samples suggest that spinel peridotite may also play a significant role in the magma formation. Some samples with very high Zr/Nb ratios result in higher and possibly aberrant degrees of melting (4-7%) due depletion of Nb. For samples from Mounts Shefford (MS-16) and Brome (MB-10 and MB-13) this is likely due to crustal contamination processes discussed above. For samples from Mount Rougemont (MRG-2 and MRG-4), the aberrant trace element profiles for these samples suggest that perturbation of the Nb contents of these samples also may be associated with crustal contamination.

In addition, high primitive mantle-normalized ratios of Dy/Yb_n (1-3.7), La/Yb_n (9.9-34), Sm/Y_n (2.89–12.2) and Tb/Yb_n (1.29-5.05) in the Monteregian samples are also consistent with melting of a garnet-bearing mantle (Karmalkar et al., 2005, and authors therein; Shaw et al., 2003). Eby (1984b; 1985a; 2006) previously argued that the Monteregian magmas formed from low degrees ($\leq$ 6 %) of melting of a garnet-bearing lherzolite mantle. Our model differs in the recognition of the important role of residual amphibole in the production of the magmas and the presence of spinel lherzolite.

The presence of spinel lherzolite implies that the partial melting zone of the Monteregian magmas may have been located near the transition zone from spinel to garnet lherzolitic mantle and in association with residual amphibole can be used to place constraints on the depth of melting. Amphibole is not stable in the asthenospheric upper mantle or in thermal plumes. In cold environments, the hydrous minerals can be stable to high pressures, thus both phlogopite and amphibole are stable in cold old continental and oceanic lithospheric mantle. The presence of water in mantle amphiboles suggests a low solidus temperature for the 'wet' lithospheric mantle (Class and Goldstein, 1997). Thus, the stability of amphibole is limited to a depth of <90 km (e.g. Weinsten et al., 2006, and references

therein). Although, the spinel-garnet transition is estimated by Lustrino and Sharkov (2006) at 80-90 km, we prefer the range of 60-80 km given by Furman and Graham (1999) that is consistent with our interpretations. In fact, the stability domain of garnet is generally accepted to be ≥60 km (e.g. Furman and Graham, 1999; Weinstein et al., 2006). These considerations strongly suggest that the signature of the Monteregian igneous rocks reflects subcontinental lithospheric mantle (SCLM) melting and not melting of the deeper asthenospheric mantle. This would place the melt zone near the boundary of garnet and spinel mantle stability domains, at the base of the lithospheric mantle (70-80 km; Hofstetter and Bock, 2004).

2.6.7. Monteregian mantle source(s)

2.6.7.1. Isotopic signature of SCLM

Radiogenic isotope (Nd, Sr, Pb) studies from the Monteregian intrusions have been interpreted to reflect melting of a mantle source similar to that feeding OIBs (Eby, 1985b) and deeper than the SCLM (Foland et al., 1988). Eby (1984b) proposed, on the basis of Sr isotope data that the mantle source of the Monteregian hills was equivalent to the present-day HIMU reservoir. In contrast, Wen et al. (1987) proposed that Sr and Nd isotope data from the Oka carbonatite complex reflect melting of the SCLM.

Once screened for the effects of crustal contamination, the remaining Nd and Sr isotope data (Table 4 and Fig. 5) suggest a somewhat heterogeneous mantle source with a range of $^{87}Sr/^{86}Sr_i$ = 0.7032-0.7037 and $^{143}Nd/^{144}Nd_i$ = 0.512788-0.51269 and confirm the strong OIB-like signature of the Monteregian intrusions. In Fig. 5, the Monteregian intrusion data (Nd, Sr, Hf and Pb) seem to suggest mixing between an enriched mantle, like EMI and a more depleted mantle, like-HIMU (Hofmann, 1988). This is supported by plots of Nd isotope ratios vs Zr/Nb and Sr isotope ratios against vs La/Nb (Fig. 12). In this figure, (samples with Nb depletion are excluded) Monteregian samples plot between depleted reservoirs (HIMU-like) and enriched mantle (EM1-like). The range of the Zr/Nb (2.5-7) and La/Nb (0.2-1.5) ratios are characteristic of continental alkaline rocks (Furman and Graham, 1999; Melluso and Morra, 2000; Späth et al., 1996) and, thus, consistent with the geochemical character of the continental lithospheric mantle (SCLM). Rather than a mixture of EM1 (lithospheric

mantle) and HIMU (asthenospheric mantle) sources, the Nd-Sr-Hf-Pb isotopic and geochemical signatures of Monteregian hills could represent a hybrid (mixing between EM1 and HIMU isotopic composition) lithospheric mantle.

The isotopic compositions of Cenozoic volcanic rocks in Europe are also interpreted to be derived from a HIMU-type reservoir (Fig. 13) within the SCLM (Hoernle et al., 1995; Lustrino and Sharkov, 2006; Lustrino and Wilson, 2007) as well as associated with a Low Velocity Component (LVC) in the underlying mantle (Hoernle et al., 1995). The mantle under the Monteregian Igneous Province shows a similar low velocity anomaly (Aktas and Eaton, 2006; Rondenay et al., 2000). Lustrino and Wilson (2007) defined a Common Mantle Reservoir (CMR) which represents the SCLM beneath the Circum-Mediterranean Anorogenic Cenozoic Igneous (CiMACI) province (Fig.13). They argued that this SCLM was subsequently partially melted in a variety of geodynamic settings related to lithospheric extension and continental collision. We suggest that the similarity in Nd, Sr, Hf and Pb isotopic signatures between the Monteregian hills and the above European provinces reflects the derivation of the Monteregian Hills from a similarly hybrid reservoir composition (EMI and HIMU-like), located in the lithospheric mantle.

2.6.7.2. Particular signature of Pb isotopes: Archean mantle or lower crust

The Pb isotope data potentially reveals important information regarding the shallow mantle under the Monteregian Hills. From Figure 5c and d, it is evident that the large compositional range in Pb isotope compositions reflects as many as three different sources. Crustal contamination by wall rocks is indicated by the whole-rock Pb isotope data (Eby 1985b) and a number of samples from this study that trend towards Appalachian crust/Grenville basement values in Figures 5c and d. The bulk of the data from this study form a cluster about the proposed depleted hybrid mantle reservoir. However, a third reservoir is indicated by a number of the Monteregian samples with lower $^{207}Pb/^{204}Pb$ and $^{208}Pb/^{204}Pb$ ratios indicating mixing between the SCLM and an older, unradiogenic Pb component. Two possible explanations are: (1) the involvement of an Archean lower crust or; (2) the involvement of Archean lithospheric mantle. The two possibilities are investigated

using figure 14 by comparing the correlations between Sr, Nd, Hf and Pb isotopic compositions of the Monteregian samples and those of Archean lower crust and mantle.
In the event that the parental magmas to the Monteregian Hills interacted with an Archean lower crust during their ascent from the mantle, the average isotopic compositions of an Archean lower crust are depicted in figure 14 (Griffin et al., 1980b; Rudnick and Goldstein, 1990b; Stuart et al., 2000; Zhang, 2002). The second possibility is the incorporation of an Archean mantle component in the SCLM of the Monteregian Hills. Assuming a depleted Archean mantle, the isotopic compositions would also be characterised by non-radiogenic Pb, Nd and Hf, but also non-radiogenic Sr isotopic compositions (Bell, 1987; Griffin et al., 2000; Pearson, 2004; Schmidberger et al., 2007).

In the Nd and Hf versus Pb isotope plots of Fig. 14 (a and b) the Archean mantle and lower crust end members both plot in the lower left-hand side of the diagrams and in each of these diagrams there is a clear trend of a number of the Monteregian samples towards this quadrant. In each of the Nd and Hf versus Pb isotope diagrams (Fig. 14a and b), there appears to be a stronger correlation with the Archean mantle end-member than with the Archean lower crust end-member due to the non-radiogenic Pb isotope compositions of samples from Mounts St Hilaire, St Gregoire, Mount Royal, Shefford, Yamaska and Rougemont. A stronger case for a correlation between the Monteregian data and an Archean mantle component can be made from the Sr versus Pb isotope diagram which clearly distinguishes between the Archean mantle and lower crust end-members (Fig. 14c). Further support for the presence of an Archean lithospheric mantle component and against an Archean lower crust component is found in two separate studies. Trzcienski and Marchildon (1989) identified granulite xenoliths in an alnoite dyke from Ayers Cliff in southwest Quebec that suggested that the lower crust was consistent with granulites of the Grenville province. Nd isotope data from granulite xenoliths from the same dyke yield Mesoproterozoic Nd model ages (1.7-1.9 Ga; Stevenson unpublished Nd data). This suggests the absence of an Archean component in the lower crust of southwest Quebec. Additionally, in a geochemical study of a large suite of mantle xenoliths from across North America, Griffin et al (2004) proposed that the Proterozoic lithosphere surrounding the Canadian Shield was underlain by a wedge of Archean lithospheric mantle protruding from beneath the Superior province (and towards southwest Quebec). The authors also proposed that splinters of the Archean lithospheric

mantle could be distributed even farther from the Archean craton. Thus, the Monteregian data are compatible with an Archean component within the SCLM beneath southwestern Quebec.

The second possibility is the incorporation of Archean mantle in the SCLM of the Monteregian Hills. (Bell, 1987; Griffin et al., 2000; Pearson, 2004; Schmidberger et al., 2007). Based on geochemical data of a large panel of North American rocks, Griffin et al. (2004) show that there is an Archean mantle under the Canadian craton, composed by infertile peridotites and eclogites. They proposed a model in which there is a "wedge of Archean mantle separating Proterozoic upper SCLM from a mixed Archean-Proterozoic lower SCLM, produced by Proterozoic collisional tectonics". Further, in their model Archean mantle fragments are also supposed to lie in younger SCLM. Consequently, it is proposed that a part of the mantle isotopic composition under the Monteregian Hills may result from a heterogeneous produced by mixing of Archean mantle fragments and Proterozoic SCLM.

The higher-than-normal Sr isotope composition of the Rougemont samples could be explained by the presence of fertile Archean mantle fragments, with $^{87}Sr/^{86}Sr$ varying between 0.7043 and 0.7080, in SCLM (Pearson and Shirey, 2004; Schmidberger et al., 2007). Alternatively, the increase in the $^{87}Sr/^{86}Sr$ isotope composition could reflect mixing between the three end-members: SCLM, Archean mantle and local wall rocks. For example, petrological evidence of contamination by wall rocks is observed in MRG9, MRG11 and MB15, from Mounts Brome and Rougemont. In fact, these rocks show the presence of quartz in the gabbro (MRG11) or the formation of secondary amphibole.

2.7. Conclusions

New geochemical and isotopic (Nd, Sr, Hf, Pb) data obtained from mafic rocks of the Monteregian Igneous Province place important constraints on the mantle source(s) that formed this continental igneous province in eastern North America. These data indicate that, (1) Monteregian magmas were generated near the boundary of garnet and spinel mantle stability domains (60-80 km depth), at the base of the lithospheric mantle (Hofstetter and Bock, 2004), (2) that the compositions of the Monteregian magmas are consistent with derivation from a lithospheric mantle that was metasomatised by carbonatite melts, and (3)

that the sub-continental mantle lithosphere beneath the Monteregian Hills contained an Archean component.

Although a mantle plume component for the Monteregian Igneous Province cannot be completely ruled out, the accumulated geochemical, isotopic, geochronological and geophysical data are more consistent with an origin produced by lithopheric rifting. Structural reactivation of two paleorifts (the Ottawa-Bonnechere and St Lawrence) during the Cretaceous opening of North Atlantic Ocean (ca. 120Ma) is indicated by the emplacement of large dikes in Québec, (Faure et al., 1996 and authors therein) orientated W-E as a result of a N-S extension (Bédard, 1985; Faure et al., 1996 and references therein). Thus, the Monteregian magmatism would be the result of the reactivation of these two paleorifts during the opening of North Atlantic Ocean.

Acknowledgements

We wish to thank B. Lefevre, M.d.N. Gagnon, R. Lamziouaq and O. Matton for their help in laboratory work and in Nd and Sr measurements with the TIMS and ICP-MS. Also, we thank R. Martin for providing Mount Royal samples from Earth Science Department of McGill. We are grateful to D. Pinti for his support and comments on an early version of the manuscript. We thank J. David for his support and comments about Pb isotopes. We wish to thank R. Lapointe for his technical assistance with the TIMS. This study was supported by an NSERC grant to R. Stevenson. This is GEOTOP contribution no. 2010-XXX

References

Aktas, K. and Eaton, D.W., 2006. Upper-mantle velocity structure of the lower Great Lakes region. Tectonophysics 420, 267-281.

Bancroft, J., Howard, W., 1923. The essexites of Mount Royal, Montréal , Québec. The royal Society of Canada Section 4, 13-43.

Bédard, J.H., 1985. The opening of the Atlantic: The Mesozoic New England Igneous province, and mechanisms of continental breakup. Tectonophysics Vol. 113, p.209-232.

Bédard, J.H., Ludden, N.J.F. and Francis, D.M., 1987. The Mégantic Intrusive complex, Quebec: a study of the derivation of silica-oversaturated anorogenic magmas of alkaline affinity. Journal of Petrology 28 (2), 355-388.

Bell, K., 1982. Evidence from Sr isotopes for long-lived heterogeneities in the upper mantle. In: J. Blenkinsop, T.J.S. Cole and D.P. Menagh (Editors), Nature London. Macmillan Journals : London, United Kingdom, United Kingdom, pp. 251.

Bell, K. and Blenkinsop, J., 1987. Archean depleted mantle: Evidence from Nd and Sr initial isotopic ratios of carbonatites. Geochimica et Cosmochimica Acta 51 (2), 291-298.

Bell, K.B., J., 1987. Archean depleted mantle: Evidence from Nd and Sr initial isotopic ratios of carbonatites. Geochimica et Cosmochimica Acta 51, 291-298.

Bienvenu, P., Bougault, H., Joron, J.L., Treuil, M. and Dmitriev, L., 1990. MORB alteration: Rare-earth element/non-rare-earth hygromagmaphile element fractionation. Chemical Geology 82, 1-14.

Blichert-Toft, J. and Albarede, F., 1997. The Lu-Hf isotope geochemistry of chondrites and the evolution of the mantle-crust system. Earth and Planetary Science Letters Vol.148, p.243-258.

Chakrabarti, R., Abanda, P.A., Hannigan, R.E. and Basu, A.R., 2007. Effects of diagenesis on the Nd-isotopic composition of black shales from the 420 Ma Utica Shale Magnafacies. Chemical Geology 244 (1-2), 221-231.

Chazot, G., Menzies, M.A. and Harte, B., 1996. Determination of partition coefficients between apatite, clinopyroxene, amphibole, and melt in natural spinel lherzolites from Yemen: Implications for wet melting of the lithospheric mantle. Geochimica et Cosmochimica Acta 60 (3), 423-437.

Chen, J., Henderson, C.M.B. and Foland, K.A., 1994. Open-system, sub-volcanic Magmatic evolution:Constraints on the petrogenesis of the Mount Brome Alkaline Complex, Canada. Journal of Petrology 35 (4), 1127-1153.

Class, C. and Goldstein, S.L., 1997. Plume-lithosphere interactions in the ocean basins: constraints from the source mineralogy. Earth and Planetary Science Letters 150 (3-4), 245-260.

Condie, K.C., 2001. Mantle plumes and their record in earth history, Cambridge University Press, Cambridge, UK, 305 pp.

Currie, K.L., 1983. An interim report on the geology and petrology of the Mont St Hilaire pluton, Québec: Current Research, Part B. Geological Survey of Canada 83-1B, 39-46.

Currie, K.L., Eby, N. and Gittins, J., 1986. The petrology of the Mont St Hilaire complex, southern Quebec: An alcaline gabbro-peralkaline syénite association. Lithos 19, 65-81.

Davies, G.R. and Smith, J.L.B., 2006. Structurally controlled hydrothermal dolomite reservoir facies: An overview. American Association of Petroleum Geologists (AAPG) 90 (11), 1641-1690.

DePaolo, D.J., 1981. Trace element and isotopic effects of combined wall rock assimilation and fractional crystallization. Earth and Planetary Science Letters 53 (2), 189-202.

Duncan, R.A., 1982. The New England Seamounts and the absolute motion of the North America since mid-Cretaceous time. EOS 63, 1103-1104.

Eby, N., 1984a. Geochronology of the Monteregian Hills alkaline igneous province, Quebec. Geology 12, 468-470.

Eby, N., 1984b. Monteregian Hills I. Petrography, major and trace element geochemistry and strontium isotopic chemistry of the western intrusions: Mont Royal, St. Bruno and Johnson. Journal of Petrology 25 (Part.1), 421-452.

Eby, N., 1985. Age relations, chemistry and petrogenesis of mafic alkaline dikes from the Monteregian Hills and younger White Mountain igneous provinces. Canadian Journal of Earth Sciences 22, 1103-1111.

Eby, N., 1985a. Monteregian Hills II. Petrography, major and trace element geochemistry and strontium isotopic chemistry of the western intrusions: Mont Royal, St. Bruno and Johnson. Journal of Petrology 26 (Part.2), 418-448.

Eby, N., 1985b. Sr and Pb isotopes, U and Th chemistry of alkaline Montregian and white Mountain igneous provinces, eastern North America. Geochimica et Cosmochimica Acta 49, 1143-1153.

Eby, N., 1988. Geology and petrology of Mounts Johnson & St.-Hilaire, Monteregian Hills Petrographic Province. Annual Meeting (New York): Guidebook, 29-43.

Eby, N., 1989. Petrology and geochemistry of Mount Yamaska, Quebec, Canada: a mafic representative of the Monteregian Hills igneous province. Geological Society of India Memoir 15. B. B. D, 63-82.

Eby, N., 2006. Carbonatites to alkali granites- Petrogenetic insights from Chilwa and Monteregians Hills-White Mountain Igneous Provinces. Congrés GAC-MAC-Montréal, 45.

Faure, S., Tremblay, A. and Angelier, J., 1996. State of intraplate stress and tectonism of northeastern America since Cretaceous times, with particular emphasis on the New England-Quebec igneous province. Tectonophysics 255, 111-134.

Fisher, C.M., 2006. AN EXOTIC SOUTHERN AND CENTRAL APPPALACHIAN BASEMENT: PB AND ND ISOTOPIC EVIDENCE, Faculty of the Graduate School of Vanderbilt University, Nashville, Tennesse, 54 pp.

Foland, K.A. and Faul, H., 1977. Ages of the White Mountain intrusives; New Hampshire, Vermont, and Maine, USA. American Journal of Science 277, 888-904

Foland, K.A., Gilbbert, L.A., Sebring, C.A. and Jiang-Feng, C., 1986. 40Ar/39Ar ages for plutons of the Monteregian Hills, Quebec: Evidence for a single episode of Cretaceous magmatism. Geological Society of America Bulletin 97, 966-974.

Foland, K.A., Jiang-feng, C., Gilbbert, L.A. and Hofmann, W.A., 1988. Nd and Sr isotopic signatures of Mesozoic plutons in northeastern North America. Geology 16, 684-687.

Furman, T., 2007. Geochemistry of East African Rift basalts: An overview. Journal of African Earth Sciences 48 (2-3), 147-160.

Furman, T. and Graham, D., 1999. Erosion of lithospheric mantle beneath the East African Rift system: geochemical evidence from the Kivu volcanic province. Lithos 48 (1-4), 237-262.

Furman, T., Rooney, T., Bryce, J., Yirgu, G., Ayalew, D., Hanan, B., 2005. Continental rupture in the main Ethiopian Rift: Constraints from magma sources Compositions.

Gandhi, S.S., 1966. Igneous petrology of Mount Yamaska, Québec. Ph.D. Thesis, McGill University, Montreal, 267 pp.

Gelinas, L., 1972. La géologie du Mont Royal. Congrés Geologique International EX.B12.

George, R.M. and Rogers, N.W., 2002. Plume dynamics beneath the African plate inferred from the geochemistry of the Tertiary basalts of southern Ethiopia. Contributions to Mineralogy and Petrology 144, 286-304.

Gold, D. and Eby, N., 1986. Carbonatites, diatremes and ultra-alkaline rocks in the Oka Area, Québec. Joint Annual Meeting (Ottawa): Guidebook GAC-MAC Field Trip 21, 1-34.

Griffin, W.L. et al., 1980a. Early archean granulite-facies metamorphism south of Ameralik, West Greenland. Earth and Planetary Science Letters 50, 59-74.

Griffin, W.L., McGregor, V.R., Nutman, A., Taylor, P.N. and Bridgwater, D., 1980b. Early Archaean granulite-facies metamorphism south of Ameralik, West Greenland. Earth and Planetary Science Letters 50 (1), 59-74.

Griffin, W.L., O'Reilly, S.Y., Doyl, B.C., Pearson, N. J., Coopersmith, H., Kivi, K., Malkovets, V. , Pokhilenko, N., 2004. Lithosphere mapping beneath the North American plate. Lithos 77, 873– 922.

Griffin, W.L., Pearson, N. J., Belousova, E., Jackson, S. E., van Achterbergh, E., O'Reilly, Suzanne Y., Shee, S. R., 2000. The Hf isotope composition of cratonic mantle: LAM-MC-ICPMS analysis of zircon megacrysts in kimberlites. Geochimica et Cosmochimica Acta 64 (1), 133-147.

Halliday, A.N., Lee, D.-C., Tommasini, S., Davies, G.R.; Paslick, C.R., Godfrey Fitton, J., James, D.E., 1995. Incompatible trace elements in OIB and MORB and source enrichment in the sub-oceanic mantle. Earth and Planetary Science Letters 133 (3-4), 379-395.

Hart, S.R., 1984. A large-scale isotope anomaly in the southern hemisphere mantle. . Nature 309, 753-757.

Hawkesworth, C.J. and Gallagher, K., 1993. Mantle hotspots, plumes and regional tectonics as causes of intraplate magmatism. Terra Nova vol.5 (6), p.552-559.

Hoernle, K., Zhang, Y.-C. and Graham, D., 1995. Seismic and geochemical evidence for large-scale mantle upwelling benneath the eastern Atlantic and western and central Europe. Nature vol.374, p. 34-39.

Hofmann, A.W., 1988. Chemical differentiation of the Earth: the relationship between mantle, continental crust, and oceanic crust. Earth and Planetary Science Letters 90 (3), 297-314.

Hofstetter, A. and Bock, G., 2004. Shear-wave velocity structure of the Sinai subplate from receiver function analysis. Geophysical Journal International 158 (1), 67-84.

Karmalkar, N.R., Rege, S., Griffin, W.L. and O'Reilly, S.Y., 2005. Alkaline magmatism from Kutch, NW India: implications for plume-lithosphere interaction. Lithos 81 (1-4), 101-119.

Landoll, J.D. and Foland, K.A., 1996. The formation of quartz syenite by crustal contamination: Mont Shefford and other Monteregian complexes, Quebec. The Canadian Mineralogist 34, 301-324.

Latourrette, T., Hervig, R.L. and Holloway, J.R., 1995. Trace-Element Partitioning between Amphibole, Phlogopite, and Basanite Melt. Earth and Planetary Science Letters 135 (1-4), 13-30.

Le Maitre, R.W. et al., 1989. A classification of the igneous rocks and glossary of terms Blackwell, Oxford.

Lustrino, M. and Sharkov, E., 2006. Neogene volcanic activity of western Syria and its relationship with Arabian plate kinematics. Journal of Geodynamics 42 (4-5), 115-139.

Lustrino, M. and Wilson, M., 2007. The circum-Mediterranean anorogenic Cenozoic igneous province. Earth-Science Reviews 81 (1-2), 1-65.

Manhes, G., Allègre, C.J., Dupré, B. and Hamelin, B., 1980. Lead isotope study of basic-ultrabasic layered complexes: Speculations about the age of the earth and primitive mantle characteristics. Earth and Planetary Science Letters 47 (3), 370-382.

Matsui, Y., Onuma, N., Nagasawa, H., Higuchi, H. and Banno, S., 1977. Crystal structure control in trace element partition between crystal and magma. Tectonics 100, 315-324.

McDaniel, D.K. and McLennan, S.M., 1997. A Comparaison of Provenance information obtained from detrital zircon and feldspar grains in a sandstone from the devonian Catskill clastic wedge. Goldschmidt Conference.

McDonough, W.F., 1990. Constraints on the composition of the continental lithospheric mantle. Earth and Planetary Science Letters 101, 1-18.

McDonough, W.F. and Sun, S.S., 1995. The composition of the Earth. Chemical Geology 120 (3-4), 223-253.

McKenzies, D. and O'Nions, R.K., 1995. The source Regions of Ocean island Basalts. Journal of Petrology 36 (1), p.133-159.

Melluso, L. and Morra, V., 2000. Petrogenesis of Late Cenozoic mafic alkaline rocks of the Nosy Be archipelago (northern Madagascar): relationships with the Comorean magmatism. Journal of Volcanology and Geothermal Research 96 (1-2), 129-142.

Miller, B. and Barr, S., 2000. Petrology and Isotopic Composition of a Grenvillian Basement Fragment in the Northern Appalachian Orogen: Blair River Inlier, Nova Scotia, Canada Journal of Petrology 41 (12), 1777-1804.

Milner, S.C. and leRoex, A.P., 1996. Isotope characteristics of the Okenyenya igneous complex, northwestern Namibia: Constraints on the composition of the early Tristan plume and the origin of the EM 1 mantle component. Earth and Planetary Science Letters 141 (1-4), 277-291.

Pearson, D.G.C., D. and Shirey, S.B., 2004. Mantle samples included in volcanic rocks: xenoliths and diamonds. In: R.W. Carlson (Editor), Treatise on Geochemistry. Elsevier.

Perrault, G., Mandarino, J. A., 1972. Les collines Montérégiennes: Minéralogie du Mont St Hilaire. Congrés Geologique International EX. B15.

Philpotts, A.R., 1972. Les collines montérégiennes: Les monts Johnson et Rougemont. Congrés Geologique International Ex. B14.

Philpotts, A.R., 1976. Petrography of Mounts Saint Bruno and Rougemont. Ministére des richesses naturelles du Québec E.S. 16.

Rogers, N. et al., 2000. Two mantle plumes beneath the East African rift system: Sr, Nd and Pb isotope evidence from Kenya Rift basalts. Earth and Planetary Science Letters 176 (3-4), 387-400.

Rondenay, S., Bostock, M., Hearn, T., White, D. and Ellis, R., 2000. Lithospheric assembly and modification of SE Canadian shield: Abitibi-Grenville teleseismic experiment. Journal of geophysical research 105 (B6), p.13,735-13,754.

Rudnick, R.L. and Goldstein, S.L., 1990a. The Pb isotopic compositions of lower crustal xenoliths and the evolution of lower crustal Pb. Earth and Planetary Science Letters 98, 192-207.

Rudnick, R.L. and Goldstein, S.L., 1990b. The Pb isotopic compositions of lower crustal xenoliths and the evolution of lower crustal Pb. Earth and Planetary Science Letters 98 (2), 192-207.

Rudnick, R.L., McDonough, W.F. and Chappell, B.W., 1993. Carbonatite metasomatism in the northern Tanzanian mantle: Petrographic and geochemical characteristics. Earth and Planetary Science Letters 114 (4), 463-475.

Saunders, A.D., Storey, M., Kent, R.W. and Norry., M.J., 1992. Consequences of Plume-lithosphere interactions. The geological society Special n.68, p.41-60.

Schiano, P., Dupré, B. and Lewin, E., 1993. Application of element concentration variability to the study of basalt alteration (Fangataufa atoll, French Polynesia). Chemical Geology 104 (1-4), 99-124.

Schmidberger, S., Simonetti, A., Heaman, H., Creaser, A. and Whiteford, S., 2007. Lu–Hf, in-situ Sr and Pb isotope and trace element systematics for mantle eclogites from the Diavik diamond mine: Evidence for Paleoproterozoic subduction beneath the Slave craton, Canada. Earth and Planetary Science Letters 254, 55-68.

Shaw, J.E., Baker, J.A., Menzies, M.A., Thirlwall, M.F. and Ibrahim, K.M., 2003. Petrogenesis of the largest intraplate volcanic field on the Arabian plate (Jordan): a mixed lithosphere-asthenosphere source activated by lithospheric extension. Journal of Petrology 44 (9), 1657-1679.

Söderlund, U., Patchett, P.J., Vervoort, J.D. and Isachsen, C.E., 2004. The Lu-Hf decay constant determined by Lu-Hf and U-Pb isotope systematics of Precambrian mafic intrusions. Earth and Planetary Science Letters 219, 311-324.

Späth, A., le Roex, A.P. and Duncan, R.A., 1996. The geochemistry of lavas from the Comores archipelago, western Indian ocean: petrogenesis and mantle source region characteristics. . Journal of Petrology 37, 961-991.

Spath, A., Le Roex, A.P. and Opiyo-Akech, N., 2001. Plume - Lithopheric interaction and origin of continental rift-related alkaline volcanism- The Chyulu Hills Volcanic Province, Southern Kenya. Journal of Petrology 42 (4), 765-787.

Stein, M. and Hofmann, A.W., 1992. Fossil Plume Head beneath the Arabian Lithosphere. Earth and Planetary Science Letters 114 (1), 193-209.

Stracke, A., Hofmann, A.W. and Hart, A., 2005. FOZO, HIMU, and the rest of the mantle zoo. Geochemistry Geophysics Geosystems 6 (5), doi:10.1029/2004GC000824.

Stuart, F.M., Ellam, R.M., Harrop, P.J., Fitton, J.G. and Bell, B.R., 2000. Constraints on mantle plumes from the helium isotopic composition of basalts from the British Tertiary Igneous Province. Earth and Planetary Science Letters 177 (3-4), 273-285.

Stuart, F.M., Ellam, R.M., Harrop, P.J., Fitton, J. G., Bell, B.R., 2000. Constraints on mantle plumes from the helium isotopic composition of basalts from the British Tertiary Igneous Province. Earth and Planetary Science Letters Vol.177, p.273-285.

Swinden, H.S., Jenner, G.A., Fryer, B.J., Hertogen, J. and Roddick, J.C., 1990. Petrogenesis and paleotectonic history of the Wild Bight Group, an Ordovician rifted island arc in central Newfoundland. Contributions to Mineralogy and Petrology 105 (2), 219-241.

Tanaka, T. et al., 2000. JNdi-1: a neodymium isotopic reference in consistency with LaJolla neodymium. Chemical Geology 168 (3-4), 279-281.

Tang, Y.-J., Zhang, H.-F. and Ying, J.-F., 2006. Asthenosphere-lithospheric mantle interaction in an extensional regime: Implication from the geochemistry of Cenozoic basalts from Taihang Mountains, North China Craton. Chemical Geology 233 (3-4), 309-327.

Trzcienski , J.W.E. and Marchildon, N., 1989. Kyanite-garnet-bearing Cambrian rocks and Grenville granulites from the Ayer's Cliff, Quebec, Canada, lamprophyre dike suite: Deep crustal fragments from the northern Appalachians. Geological Society of America 17 (7), 637-640.

Valiquette, G., Pouliot, G., 1977. Geology of Mounts Brome and Shefford. Ministére des richesses naturelles du Québec E. S. 28.

Vervoort, J.D. and Blichert-Toft, J., 1999b. Evolution of the depleted mantle: Hf isotope evidence from juvenile rocks through time. Geochimica et Cosmochimica Acta 63, 533-556.

Vervoort, J.D., Blichert-Toft, J., Patchett, P.J. and Albaréde, F.A., 1999a. Relationships between Lu-Hf and Sm-Nd isotopic systems in the global sedimentary system. Earth and Planetary Science Letters 168, 79-99.

Vervoort, J.D., Patchett, P.J., Söderlund, U. and Baker, M., 2004. Isotopic composition of Yb and the determination of Lu concentrations and Lu/Hf ratios by isotope dilution using MC-ICPMS. Geochemistry, Geophysics, Geosystems 5 (Q11002).

Villemant, B., Jaffrezic, H., Joron, J.L. and Treuil, M., 1981. Distribution Coefficients of Major and Trace-Elements - Fractional Crystallization in the Alkali Basalt Series of Chaine-Des-Puys (Massif Central, France) Geochimica et Cosmochimica Acta 45 (11), 1,997-2,016.

Wareham, C.D. et al., 1998. Pb, Nd, and Sr Isotope Mapping of Grenville-Age Crustal Provinces in Rodinia. The Journal of Geology(106), 647–659.

Weinstein, Y., Navon, O., Altherr, R. and Stein, M., 2006. The Role of Lithospheric Mantle Heterogeneity in the Generation of Plio- Pleistocene Alkali Basaltic Suites from NW Harrat Ash Shaam (Israel). Journal of Petrology 47 (5), 1017–1050.

Wen, J., Bell, K. and Blenkinsop, J., 1987. Nd and Sr isotope systematics of the Oka complex, Quebec, and their bearing on the evolution of the sub-continental upper mantle. Contributions to Mineraloy and Petrology 97, 433-437.

Yoder, H.S.J. and Tilley, C.E., 1962. Origin of Basalt Magmas: An Experimental Study of Natural and Synthetic Rock Systems, pp. 342-532.

Zhang, H.-F., 2005. Transformation of lithospheric mantle through peridotite-melt reaction: A case of Sino-Korean craton. Earth and Planetary Science Letters 237, 768- 780.

Zhang, H.F. et al., 2002. Mesozoic lithosphere destruction beneath the North China Craton: evidence from major-, trace-element and Sr–Nd–Pb isotope studies of Fangcheng basalts. Contributions to Mineralogy and Petrology 144, 241–253.

Zindler, A. and Hart, S., 1986. Chemical geodynamics. Ann. Rev. Earth Planet. Sci 14, 493-571.

Table 1: Major element data for Monteregian Igneous Province

Sample	MR 15	MR 17	MR 24	MR 5b	181+00	194+66	195 +50-60	215+00	229+08	298+03	MSB-1	MSB-2	MSB-3
Rock type	**Essexite**	**Gabbro**	**Gabbro**	**Gabbro**	**Camptonite**	**Diorite**	**Gabbro**	**Gabbro**	**Diorite**	**Gabbro**	**Pyroxene gabbro**	**Quartz gabbro**	**Felsic gabbro**
wt.%													
SiO2	45.46	44.19	43.24	42.96	41.32	59.18	44.57	36.07	53.61	40.21	46.71	42.32	42.61
TiO2	2.94	3.09	3.05	3.56	3.20	0.50	2.47	5.01	1.73	2.11	1.62	5.19	4.08
Al2O3	18.620	11.900	9.660	17.430	15.430	18.390	11.210	14.680	19.250	7.370	5.93	16.27	12.91
Fe2O3	12.54	13.11	13.47	12.88	12.47	3.23	10.57	15.91	7.81	15.45	13.46	12.68	14.06
MnO	0.17	0.18	0.20	0.20	0.22	0.07	0.14	0.20	0.21	0.19	0.18	0.14	0.17
MgO	5.650	10.910	10.960	4.990	5.180	0.540	11.060	7.590	2.190	18.140	18.22	7.26	9.51
CaO	9.43	13.82	15.19	10.55	10.94	2.67	17.22	13.25	6.67	10.98	13.03	13.95	15.53
Na2O	4.01	2.22	2.23	3.77	3.68	6.47	1.53	2.75	6.06	1.35	1.04	1.79	1.63
K2O	1.24	0.79	1.23	1.70	1.69	5.72	0.55	1.02	1.67	0.73	0.54	0.37	0.37
P2O5	0.45	0.29	0.37	1.38	0.91	0.12	0.13	2.66	0.46	0.24	0.20	0.13	0.17
LOI	<d/l	0.13	1.09	1.02	4.78	2.58	1.15	1.02	0.47	3.27	-	0.49	-
Total	100.63	100.81	100.9	100.58	99.96	99.63	100.7	100.27	100.28	100.21	100.98	100.65	101.12
ppm													
Ba	418	376	346	641	565	1271	95	304	848	104	162	116	142
Co	45	50	56	25	34	-	41	44	-	84	72	45	50
Sc	-	37	41	10	-	-	27	18	-	32	40	28	32
V	313	359	380	276	303	49	313	397	82	262	216	352	502
K_2O/Na_2O	0.31	0.35	0.55	0.45	0.46	0.88	0.36	0.37	0.28	0.54	0.52	0.21	0.23

Sample	MSB-4	MSB-5a	MSB-8	MSH-3	MSH-10	MSH-12	MSH-13	MSH-15	MSH-18	MSG-3	MSG-5
Rock type	**Felsic gabbro**	**Pyroxene gabbro**	**Felsic péridotite**	**Nepheline diorite**	**Gabbro**	**Nepheline diorite**	**Anorthositic gabbro**	**Nepheline diorite**	**Amphibole gabbro**	**Essexite**	**Essexite**
wt.%											
SiO2	44.19	45.07	43.80	48.31	43.83	47.96	46.53	44.96	40.49	49.66	50.06
TiO2	1.96	3.37	4.47	2.75	4.01	2.77	3.01	3.88	3.88	2.38	2.36
Al2O3	7.57	8.26	15.29	17.48	18.90	18.87	18.65	17.53	19.33	18.54	18.62
Fe2O3	11.71	13.49	12.86	11.10	9.75	9.51	9.98	11.85	12.05	9.35	9.20
MnO	0.15	0.18	0.16	0.30	0.23	0.26	0.24	0.32	0.23	0.24	0.24
MgO	17.22	14.17	7.78	3.26	4.86	3.29	3.68	3.75	5.24	2.91	2.90
CaO	14.00	14.05	13.01	6.10	10.91	7.70	9.15	10.09	13.79	6.25	6.37
Na2O	1.41	1.49	2.65	6.20	4.26	5.83	5.23	4.47	2.75	6.55	6.54
K2O	0.56	0.69	0.51	2.92	1.13	2.29	1.59	1.30	0.51	2.91	2.97
P2O5	0.26	0.24	0.09	1.41	1.60	1.21	1.37	1.77	1.71	1.16	1.16
LOI	1.21	-	0.30	0.35	0.74	0.81	0.53	0.57	0.38	0.09	0.05
Total	100.28	101.07	100.98	100.31	100.32	100.62	100.08	100.59	100.43	100.14	100.57
ppm											
Ba	114	146	137	1015	826	986	849	705	451	873	860
Co	66	63	42	10	17	13	12	10	-	-	-
Sc	41	39	22	-	-	-	-	-	-	-	-
V	229	349	361	113	161	86	109	164	162	95	88
K_2O/Na_2O	0.40	0.46	0.19	0.47	0.27	0.39	0.30	0.29	0.19	0.44	0.45

Sample	MSG-6	MSG-7	MSG-8	MSG-9	MRg-1	MRg-3	MRg-4	MRg-6	MRg-9	MRg-11	MY-1	MY-3
Rock type	**Essexite**	**Essexite**	**Essexite**	**Striped essexite**	**Striped gabbro**	**Pyroxene gabbro**	**Striped gabbro**	**Striped gabbro**	**Gabbro**	**Quartz gabbro**	**Gabbro**	**Gabbro**
wt.%												
SiO2	50.14	49.62	50.44	45.57	42.22	43.24	41.92	40.53	41.54	45.34	45.64	47.51
TiO2	2.30	2.44	2.20	3.01	1.55	1.81	1.73	3.80	4.13	2.84	3.90	3.37
Al2O3	18.50	18.39	18.81	17.96	25.29	9.94	24.82	14.11	18.63	19.92	19.58	16.48
Fe2O3	9.11	9.59	8.62	12.00	8.35	11.08	9.22	17.62	14.04	11.39	9.59	12.12
MnO	0.25	0.25	0.24	0.25	0.07	0.13	0.07	0.16	0.14	0.20	0.14	0.29
MgO	2.76	2.95	2.70	3.68	4.32	16.31	4.01	8.16	5.64	4.34	4.65	4.09
CaO	6.12	6.32	6.20	8.74	16.85	17.26	16.78	14.45	13.30	9.90	12.82	9.17
Na2O	6.56	6.46	6.55	5.24	1.20	0.49	1.30	1.40	2.02	3.69	3.05	3.82
K2O	2.98	2.94	2.89	1.88	0.08	0.02	0.11	0.43	0.49	0.90	0.61	1.71
P2O5	1.10	1.17	1.06	1.63	0.03	0.02	0.03	0.13	0.12	1.06	0.22	1.50
LOI	0.45	0.12	0.44	0.42	0.50	0.45	0.80	0.06	0.62	0.49	0.19	0.28
Total	100.39	100.36	100.27	100.49	100.49	100.79	100.83	100.93	100.74	100.14	100.45	100.42
ppm												
Ba	904	862	925	777	37		52	126	128	343	259	473
Co	13	-	-	15	40	77	39	67	63	16	25	15
Sc	-	-	-	-	17	47	13	24	19	20	10	-
V	96	96	83	130	280	271	313	578	427	224	316	208
K_2O/Na_2O	0.45	0.46	0.44	0.36	0.07	0.04	0.08	0.31	0.24	0.24	0.20	0.45

Sample	MY-6	MY-9	MS-5a	MS-5b	MS-10	MS-12a	MS-14	MS-16	MB-7	MB-10	MB-13	MB-15	MB-18
Rock type	**Essexite**	**Essexite**	**Gabbro**	**Gabbro**	**Gabbro**	**Gabbro**	**Gabbro**	**Gabbro**	**Gabbro**	**Gabbro**	**Gabbro**	**Gabbro**	**Nepheline monzodiorite**
wt.%													
SiO2	38.96	42.00	45.83	41.38	48.55	51.77	46.75	42.94	38.53	47.40	42.52	45.95	51.57
TiO2	5.74	4.71	3.16	3.78	2.45	2.14	2.93	2.76	4.83	1.54	3.89	2.03	2.16
Al2O3	13.03	15.17	16.90	15.40	18.97	17.71	18.00	21.81	15.95	24.54	18.38	24.31	20.11
Fe2O3	15.27	12.90	11.29	13.89	10.16	9.39	11.42	9.01	16.92	6.00	10.85	6.76	6.24
MnO	0.27	0.25	0.19	0.20	0.21	0.27	0.30	0.19	0.18	0.10	0.17	0.10	0.18
MgO	6.60	5.14	4.65	5.85	3.96	3.05	3.23	3.65	5.99	1.91	4.60	2.77	1.51
CaO	14.01	11.41	9.15	11.25	8.61	6.55	9.04	12.81	12.95	13.14	12.36	12.87	6.00
Na2O	3.09	4.52	4.61	3.65	4.55	5.59	4.29	3.04	2.34	3.26	3.34	3.24	7.05
K2O	1.22	2.04	1.66	1.27	1.26	2.21	2.07	1.03	0.21	0.51	0.32	0.46	3.05
P2O5	1.83	1.51	1.46	1.90	0.97	1.02	1.22	1.07	2.22	0.90	1.85	0.91	0.35
LOI	0.17	0.21	0.91	1.28	0.47	0.25	0.76	1.29	0.20	0.74	1.33	0.52	0.97
Total	100.29	99.97	99.94	99.95	100.26	100.05	100.12	99.68	100.38	100.09	99.67	100.02	99.49
ppm													
Ba	587	730	967	711	809	942	930	506	270	403	342	710	2511
Co	37	21	23	20	17	-	12	13	15	-	-	-	-
Sc	-	-	16	16	-	-	-	-	11	-	-	-	-
V	373	289	174	229	156	72	128	148	299	79	137	114	116
K_2O/Na_2O	0.40	0.45	0.36	0.35	0.28	0.40	0.48	0.34	0.09	0.16	0.10	0.14	0.43

Note: The totals of the major element oxides are normalised to 100 wt%.

Table 2: Trace element data for Monteregian Igneous Province

Sample	MR15	MR17	MR24	MR5b	181+00	194+66	195 +50-60	215+00	229+08	298+03	MSB1	MSB2	MSB3	MSB4	MSB5a
ppm															
Rb	36.87	30.07	34.85	53.93	52.12	127.98	13.31	19.66	45.85	25.09	18.30	10.00	13.00	13.20	21.70
Ba	429	372	337	611	546	1261	122	321	789	107	169	130	153	135	168
Th	9.66	6.81	7.19	8.33	13.74	16.12	4.17	7.27	13.43	5.15	7.20	9.00	9.40	7.20	7.20
U	4.79	2.31	2.84	5.34	5.59	4.13	1.46	3.78	5.50	1.19	1.40	3.50	3.90	2.10	2.20
K	5145	3267	5103	7053	7012	23732	2282	4232	6929	3029	2240	1535	1535	2323	2863
Nb	64.29	69.52	52.19	77.56	103.64	58.11	14.38	48.91	156.83	24.74	17.20	23.00	20.50	23.50	24.80
La	46.44	37.03	43.19	82.66	91.01	66.07	15.98	66.23	135.36	20.23	17.96	12.14	21.51	20.89	23.27
Ce	90.60	79.53	85.86	174.67	177.04	90.22	36.36	150.22	287.12	43.15	40.57	28.13	50.72	45.60	52.03
Pr	10.63	9.96	10.42	21.72	20.54	8.09	5.19	20.23	33.78	5.66	5.66	4.07	7.33	6.12	7.17
Sr	1126	648	566	1446	1186	677	471	1054	1363	345	194	771	765	297	328
Nd	40.91	40.17	41.95	88.08	78.00	25.30	23.74	87.61	123.61	24.06	25.43	18.88	33.74	26.58	31.17
Sm	7.16	7.87	7.93	15.84	13.02	3.58	5.56	16.81	19.46	4.93	5.82	4.50	7.47	5.60	6.83
Zr	292	264	285	225	387	375	142	197	820	141	150	133	207	130	167
Eu	2.46	2.32	2.34	4.52	3.76	1.04	1.82	4.89	5.46	1.53	1.70	1.60	2.45	1.73	2.00
Gd	5.81	6.85	6.83	13.04	10.16	2.63	5.41	14.55	13.77	4.35	5.39	3.94	6.75	4.87	6.09
Ti	17634	18545	18300	21357	19181	2991	14811	30018	10364	12617	9692	31109	24479	11760	20224
Tb	0.79	0.90	0.90	1.67	1.30	0.39	0.73	1.83	1.95	0.59	0.74	0.53	0.88	0.66	0.84
Dy	4.22	4.87	4.81	8.87	6.98	2.20	3.84	9.43	10.62	3.15	3.98	2.93	4.72	3.54	4.41
Y	22.52	24.36	24.01	45.05	33.68	14.21	18.13	45.58	54.71	15.52	17.60	13.20	21.70	14.90	19.80
Ho	0.74	0.85	0.83	1.53	1.20	0.43	0.65	1.61	1.90	0.55	0.68	0.50	0.79	0.60	0.78
Er	1.88	2.06	2.07	3.78	2.99	1.26	1.55	3.83	5.02	1.34	1.69	1.20	1.88	1.47	1.92
Tm	0.24	0.27	0.26	0.46	0.38	0.19	0.19	0.45	0.68	0.17	0.22	0.15	0.24	0.18	0.25
Yb	1.52	1.54	1.60	2.63	2.19	1.37	1.11	2.55	4.09	1.02	1.27	0.87	1.33	1.04	1.38
Lu	0.20	0.21	0.23	0.35	0.31	0.21	0.15	0.34	0.55	0.14	0.17	0.11	0.19	0.14	0.19
Rb/Sr	0.03	0.05	0.06	0.04	0.04	0.19	0.03	0.02	0.03	0.07	0.09	0.01	0.02	0.04	0.07
Ba/Rb	11.64	12.38	9.67	11.34	10.48	9.85	9.19	16.32	17.21	4.25	9.22	12.99	11.74	10.20	7.72

Sample	MSB8	MSH3	MSH10	MSH12	MSH13	MSH15	MSH18	MSG3	MSG5	MSG6	MSG7	MSG8	MSG9	MRg1	MRg3
ppm															
Rb	13.10	76.50	28.60	61.00	41.10	38.00	16.40	80.30	81.40	80.20	80.40	79.30	48.80	4.20	1.20
Ba	148	983	808	958	829	665	465	928	885	957	850	898	819	66	15
Th	9.20	22.70	19.60	24.90	21.80	20.60	22.00	23.30	22.40	22.30	22.90	21.90	21.20	8.80	5.20
U	4.40	9.00	10.00	11.10	11.50	10.80	11.80	9.40	9.00	9.00	8.40	8.40	10.40	4.50	0.90
K	2116	12115	4688	9501	6597	5394	2116	12073	12322	12364	12198	11990	7800	332	83
Nb	21.20	127.40	90.10	127.80	86.70	78.50	45.00	107.50	112.30	117.40	107.60	116.40	111.60	1.90	0.80
La	12.62	113.13	86.42	100.74	89.40	88.03	62.56	89.97	88.72	93.19	83.40	85.31	104.34	4.37	3.67
Ce	28.03	221.96	182.96	205.58	184.79	178.25	138.69	173.04	171.05	177.40	160.42	162.35	208.02	9.64	11.67
Pr	4.02	26.21	23.70	25.25	23.41	22.42	19.04	20.59	20.51	20.88	19.06	19.13	25.41	1.42	2.13
Sr	979	1334	2549	2233	2657	2326	3100	1519	1504	1477	1501	1586	2226	1067	268
Nd	18.63	102.48	101.01	100.95	96.59	93.38	87.42	80.99	80.39	81.33	75.77	74.73	101.82	6.82	11.59
Sm	4.38	17.64	18.57	17.57	17.16	17.00	17.68	14.00	13.92	13.95	13.05	12.83	17.79	1.64	3.33
Zr	130	605	287	481	367	315	227	480	498	487	469	481	373	45	66
Eu	1.75	5.39	6.28	5.30	5.49	5.71	5.66	4.36	4.31	4.34	4.05	4.00	5.48	0.75	1.13
Gd	4.09	14.07	15.71	13.95	13.79	14.53	15.92	11.31	11.31	11.24	10.58	10.32	14.71	1.60	3.38
Ti	26793	16483	24006	16609	18054	23275	23263	14266	14122	13804	14631	13211	18066	9309	10849
Tb	0.55	1.84	1.97	1.84	1.75	1.82	1.95	1.50	1.51	1.50	1.40	1.36	1.89	0.22	0.46
Dy	2.94	9.61	10.17	9.61	9.00	9.24	9.77	8.05	8.05	8.03	7.51	7.32	10.00	1.14	2.53
Y	13.90	50.30	50.00	48.80	45.90	47.30	48.50	39.20	39.70	38.80	39.90	38.40	49.90	5.80	10.50
Ho	0.50	1.67	1.70	1.64	1.52	1.52	1.60	1.41	1.41	1.42	1.32	1.27	1.76	0.19	0.42
Er	1.24	4.23	4.02	4.10	3.70	3.71	3.70	3.71	3.66	3.71	3.43	3.36	4.37	0.47	1.01
Tm	0.16	0.55	0.49	0.52	0.45	0.44	0.43	0.49	0.49	0.50	0.45	0.45	0.55	0.06	0.12
Yb	0.91	3.28	2.72	3.11	2.59	2.50	2.31	3.03	3.06	3.05	2.81	2.78	3.31	0.31	0.66
Lu	0.13	0.47	0.36	0.42	0.35	0.35	0.30	0.42	0.44	0.45	0.40	0.40	0.46	0.04	0.09
Rb/Sr	0.01	0.06	0.01	0.03	0.02	0.02	0.01	0.05	0.05	0.05	0.05	0.05	0.02	0.00	0.00
Ba/Rb	11.33	12.84	28.24	15.70	20.17	17.49	28.38	11.55	10.87	11.93	10.57	11.32	16.78	15.68	12.63

Sample	MRg4	MRg6	MRg9	MRg11	MY1	MY3	MY6	MY9	MS5a	MS5b	MS10	MS12a	MS14	MS16	MB7	MB10	MB13
ppm																	
Rb	4.70	12.90	14.50	25.70	17.30	53.20	34.00	65.10	40.10	32.00	35.90	71.80	30.00	10.60	63.60	20.50	22.90
Ba	78	150	146	321	247	439	534	717	1059	754	838	977	939	518	296	424	370
Th	8.60	6.90	9.40	10.50	11.20	17.70	19.20	21.00	17.30	15.80	18.20	19.00	19.30	16.40	18.90	22.50	32.80
U	4.50	2.80	4.10	5.10	5.80	6.60	7.40	9.00	7.60	6.90	8.40	7.00	9.90	10.20	8.00	12.70	21.00
K	456	1784	2033	3734	2531	7095	5062	8464	6887	5269	5228	9169	8588	4273	871	2116	1328
Nb	1.60	16.50	19.60	60.00	21.30	67.50	94.20	105.10	60.30	61.50	56.80	105.00	43.00	6.60	108.60	10.30	10.30
La	4.63	15.66	13.29	49.88	21.88	68.60	96.18	97.29	73.22	65.87	61.67	95.29	85.46	44.88	26.82	27.66	36.66
Ce	10.08	34.97	29.04	114.32	45.19	142.49	200.21	195.85	158.20	142.63	122.70	185.92	165.77	97.13	66.46	57.11	82.72
Pr	1.46	4.93	4.04	16.01	5.97	17.86	25.38	24.07	20.40	18.57	14.94	21.78	19.57	12.80	10.36	7.42	11.71
Sr	1074	568	894	1104	1229	1248	1541	1544	1704	1680	1822	1227	2442	2717	1335	3327	5502
Nd	6.98	22.26	17.71	72.66	25.68	75.75	106.39	97.96	85.99	79.55	59.87	83.22	76.79	55.63	52.15	32.33	55.90
Sm	1.71	5.07	3.95	15.10	5.38	14.63	20.63	18.41	14.86	14.38	10.36	13.67	13.32	10.58	10.65	5.59	10.61
Zr	46	116	107	151	147	325	442	487	235	207	166	417	188	74	409	127	150
Eu	0.75	1.66	1.45	4.55	2.17	4.14	6.14	5.45	4.60	4.59	3.64	4.13	4.16	3.42	4.17	2.79	4.63
Gd	1.63	4.62	3.58	13.95	4.71	12.93	17.57	15.38	11.95	12.17	8.44	10.78	10.99	9.18	9.31	4.57	9.13
Ti	10346	22777	24755	17047	23377	20200	34388	28244	18947	22645	14685	12815	17556	16561	28939	9219	23329
Tb	0.22	0.65	0.50	1.84	0.65	1.67	2.19	1.95	1.49	1.49	1.12	1.44	1.43	1.17	1.07	0.54	1.01
Dy	1.21	3.46	2.72	9.90	3.39	8.84	10.94	9.88	7.62	7.80	5.96	7.82	7.55	6.03	5.06	2.70	4.81
Y	6.20	16.50	13.10	48.60	15.60	45.60	51.10	45.20	36.90	37.90	30.90	37.90	30.20	24.60	41.30	16.10	27.10
Ho	0.20	0.60	0.48	1.72	0.58	1.54	1.78	1.60	1.28	1.33	1.05	1.40	1.30	1.01	0.83	0.44	0.75
Er	0.49	1.49	1.19	4.25	1.45	3.86	4.10	3.78	3.06	3.16	2.64	3.66	3.31	2.43	1.78	1.04	1.65
Tm	0.06	0.19	0.15	0.53	0.18	0.49	0.49	0.45	0.36	0.38	0.34	0.49	0.43	0.29	0.20	0.12	0.18
Yb	0.33	1.10	0.88	3.00	1.05	2.91	2.68	2.57	1.99	2.19	1.99	2.95	2.58	1.63	0.96	0.68	0.89
Lu	0.04	0.15	0.12	0.40	0.15	0.41	0.35	0.33	0.26	0.29	0.28	0.41	0.36	0.22	0.12	0.09	0.11
Rb/Sr	0.00	0.02	0.02	0.02	0.01	0.04	0.02	0.04	0.02	0.02	0.02	0.06	0.01	0.00	0.05	0.01	0.00
Ba/Rb	16.59	11.62	10.07	12.47	14.28	8.26	15.70	11.02	26.41	23.56	23.34	13.61	31.29	48.84	4.65	20.66	16.14

Sample	MB15	MB18
ppm		
Rb	14.20	72.50
Ba	742	2511
Th	20.40	32.70
U	12.00	12.70
K	1909	12654
Nb	12.30	162.00
La	23.03	114.80
Ce	51.37	213.27
Pr	7.31	23.20
Sr	3057	2480
Nd	33.65	82.00
Sm	6.59	12.15
Zr	111	466
Eu	3.06	3.90
Gd	5.56	8.95
Ti	12192	12971
Tb	0.66	1.22
Dy	3.20	6.67
Y	17.30	36.00
Ho	0.54	1.20
Er	1.23	3.19
Tm	0.15	0.44
Yb	0.79	2.61
Lu	0.10	0.35
Rb/Sr	0.00	0.03
Ba/Rb	52.29	34.63

Table 3: Sr, Nd and Hf isotopic data for Monteregian Igneous Province

Samples	Sr	Rb	$^{87}Sr/^{86}Sr_m$	2 δ	$(^{87}Sr/^{86}Sr)_i$	Nd	Sm	$^{143}Nd/^{144}Nd_m$	2 δ	εNd	$(^{143}Nd/^{144}Nd)_i$	Lu	Hf	$^{176}Hf/^{177}Hf_m$	2 δ	$(^{176}Hf/^{177}Hf)_i$	εHf
	ppm	ppm				ppm	ppm					ppm	ppm				
MR 15	1096	36.87	0.703619	± 18	0.703447	43.79	7.78	0.512876	± 7	6.1	0.512789	0.22	5.81	0.282936	± 9	0.282923	7.7
MR 5b	1440	53.93	0.704642	± 18	0.704451	92.87	16.74	0.512748	± 8	4.0	0.512659						
181+00	1216	52.12	0.703959	± 18	0.703740	79.72	13.32	0.512811	± 8	4.9	0.512729						
194+66	687	127.98	0.705370	± 19	0.704419	24.07	3.52	0.512734	± 8	3.6	0.512663						
215+00	1061	19.66	0.703703	± 20	0.703609	91.74	17.82	0.512834	± 12	5.1	0.512739						
229+08	1320	45.85	0.703573	± 26	0.703395	124.69	19.74	0.512818	± 9	5.1	0.512741	0.57	5.38	0.282945	± 8	0.282910	7.2
MSB2	771	10	0.704195	± 22	0.704128	18.51	4.31	0.512729	± 8	2.7	0.512615	0.11	1.49	0.282896	± 8	0.282871	5.8
MSB3	765	13	0.703521	± 36	0.703434	31.20	6.79	0.512824	± 10	4.7	0.512718						
MSB8	979	13.1	0.703903	± 30	0.703834	17.13	3.94	0.512792	± 11	3.9	0.512680	0.12	3.33	0.282850	± 4	0.282837	4.6
MSH3	1334	76.5	0.703770	± 23	0.703477	116.35	20.23	0.512805	± 12	4.7	0.512720						
MSH10	2549	28.6	0.703396	± 28	0.703338	106.34	20.21	0.512842	± 10	5.3	0.512749	0.28	2.56	0.282851	± 8	0.282815	3.8
MSH12	2233	61	0.703517	± 35	0.703378	97.88	17.22	0.512822	± 9	5.0	0.512736						
MSH13	2657	41.1	0.703397	± 26	0.703318	94.14	17.22	0.512829	± 10	5.1	0.512741	0.38	7.16	0.282946	± 6	0.282928	7.8
MSH15	2326	38	0.703503	± 25	0.703420	104.57	19.24	0.512839	± 10	5.3	0.512748						
MSH18	3100	16.4	0.703324	± 30	0.703297	96.63	19.58	0.512859	± 8	5.5	0.512760						
MSG3	1519	80.3	0.703640	± 30	0.703370	79.84	13.92	0.512836	± 9	5.3	0.512750	0.43	9.59	0.282930	± 8	0.282916	7.4
MSG5	1504	81.4	0.703669	± 24	0.703393	78.22	13.62	0.512814	± 10	4.9	0.512729						
MSG6	1477	80.2	0.703624	± 23	0.703347	81.34	14.06	0.512836	± 11	5.3	0.512751	0.42	1.65	0.282891	± 9	0.282807	3.5
MSG7	1501	80.4	0.703698	± 34	0.703425	81.70	14.29	0.512826	± 11	5.1	0.512740						
MSG8	1586	79.3	0.703577	± 40	0.703322	79.40	13.67	0.512816	± 10	4.9	0.512731						
MSG9	2226	48.8	0.703482	± 26	0.703370	45.39	7.96	0.512829	± 10	5.2	0.512743						
MRg1	1067	4.2	0.703860	± 24	0.703840	6.34	1.55	0.512825	± 7	4.4	0.512705	-	-	-	-	-	-
MRg4	1074	4.7	0.703875	± 24	0.703853	6.70	1.60	0.512802	± 11	4.0	0.512685						
MRg6	568	12.9	0.704273	± 28	0.704157	21.93	5.03	0.512737	± 14	2.8	0.512624						
MRg9	894	14.5	0.704209	± 24	0.704126	16.68	3.66	0.512755	± 10	3.3	0.512647	-	-	-	-	-	-
MRg11	1104	25.7	0.704608	± 41	0.704489	75.74	16.01	0.512693	± 10	2.2	0.512589						
MY1	1229	17.3	0.704029	± 34	0.703957	23.29	4.87	0.512802	± 9	4.3	0.512699						
MY3	1248	53.2	0.704953	± 25	0.704735	82.19	16.00	0.512696	± 8	2.4	0.512600	0.43	7.17	0.282836	± 7	0.282816	3.9
MY6	1541	34	0.703853	± 35	0.703740	114.19	22.15	0.512813	± 14	4.7	0.512718	0.35	10.28	0.282902	± 7	0.282891	6.5
MY9	1544	65.1	0.703950	± 38	0.703734	104.54	19.66	0.512790	± 16	4.3	0.512698						

Note : (1) Age correction for $(^{87}Sr/^{86}Sr)_i$, $(^{143}Nd/^{144}Nd)_i$, $(^{176}Hf/^{177}Hf)_i$, εNd and εHf is 124 Ma
(2) Rb isotopic ratios were calculed from Rb contents and the naturel abundance of ^{85}Rb and ^{87}Sr
(3) dash symbols represent weakening analyzes

Table 3: continued

Samples	Sr	Rb	$^{87}Sr/^{86}Sr_m$	2 δ	$(^{87}Sr/^{86}Sr)_i$	Nd	Sm	$^{143}Nd/^{144}Nd_m$	2 δ	εNd	$(^{143}Nd/^{144}Nd)_i$	Lu	Hf	$^{176}Hf/^{177}Hf_m$	2 δ	$(^{176}Hf/^{177}Hf)_i$	εHf
	ppm	ppm				ppm	ppm					ppm	ppm				
MS5a	1704	40.1	0.703537	± 26	0.703417	93.56	16.25	0.512789	± 7	4.4	0.512703	0.27	2.61	0.282938	± 9	0.282904	7.0
MS5b	1680	32	0.703520	± 30	0.703423	84.81	15.48	0.512801	± 7	4.6	0.512712						
MS10	1822	35.9	0.703894	± 29	0.703794	64.12	11.20	0.512771	± 7	4.0	0.512685	0.27	2.85	0.282968	± 7	0.282937	8.1
MS12a	1227	71.8	0.703846	± 27	0.703548	101.13	11.20	0.512803	± 10	4.8	0.512722						
MS14	2442	30	0.703811	± 18	0.703748	83.13	14.55	0.512810	± 10	4.8	0.512725						
MS16	2717	10.6	0.704023	± 20	0.704003	-	-	-	-	-	-						
MB7	1335	63.6	0.704045	± 36	0.703802	48.32	9.89	0.512672	± 10	1.8	0.5125714						
MB10	3327	20.5	0.704076	± 32	0.704045	35.54	6.16	0.512696	± 8	2.6	0.5126109						
MB13	5502	22.9	0.703960	± 36	0.703939	58.49	11.14	0.512759	± 10	3.7	0.5126659						
MB15	3057	14.2	0.703994	± 33	0.703970	27.54	5.21	0.512715	± 9	2.8	0.5126221	0.10	0.32	0.282878	± 10	0.282772	2.3
MB18	2480	72.5	0.703711	± 36	0.703562	85.16	12.75	0.512765	± 9	4.2	0.5126911	0.36	5.67	0.282841	± 11	0.282821	4.0

Note : (1) Age correction for $(^{87}Sr/^{86}Sr)_i$, $(^{143}Nd/^{144}Nd)_i$, $(^{176}Hf/^{177}Hf)_i$, εNd and εHf is 124 Ma
(2) Rb isotopic ratios were calculed from Rb contents and the naturel abundance of ^{85}Rb and ^{87}Sr
(3) dash symbols represent weakening analyzes

Table 4: Pb isotopic composition for Monteregian Hills

Samples	$^{206}Pb/^{204}Pb$	2δ	$^{207}Pb/^{204}Pb$	2δ	$^{208}Pb/^{204}Pb$	2δ
MR15	19.61	0.005	15.49	0.004	39.02	0.010
MR15 duplicate	19.69	0.004	15.56	0.002	39.24	0.006
MR5b	19.36	0.010	15.65	0.009	39.30	0.020
MR5b duplicate	19.34	0.010	15.63	0.008	39.24	0.026
229+00	19.64	0.004	15.64	0.003	39.38	0.008
229+00 duplicate	19.62	0.005	15.63	0.004	39.35	0.009
MSB2	19.51	0.003	15.61	0.002	39.13	0.005
MSB8	19.46	0.005	15.59	0.005	39.26	0.014
MSH3*	19.65	0.021	15.45	0.018	38.93	0.046
MSH3	19.48	0.004	15.45	0.004	38.80	0.010
MSH3 duplicate	19.50	0.008	15.47	0.009	38.88	0.030
MSH10	19.92	0.008	15.64	0.006	39.65	0.013
MSH10 duplicate	19.93	0.003	15.63	0.003	39.64	0.007
MSH12	19.58	0.004	15.34	0.003	38.58	0.009
MSH13	19.61	0.006	15.40	0.004	38.87	0.011
MSH15	19.98	0.003	15.64	0.003	39.57	0.007
MSG3*	19.47	0.024	15.46	0.017	38.81	0.039
MSG3	19.46	0.002	15.50	0.003	38.82	0.005
MSG3 duplicate	19.53	0.002	15.58	0.002	39.07	0.005
MSG6	19.30	0.002	15.43	0.002	38.64	0.005
MSG6 duplicate	19.29	0.003	15.40	0.004	38.58	0.014
MSG7	19.53	0.007	15.65	0.006	39.26	0.017
MSG7 duplicate	19.47	0.008	15.59	0.006	39.08	0.016
MSG8	19.57	0.001	15.61	0.002	39.23	0.005
MRg1	19.61	0.004	15.69	0.003	39.53	0.010
MRg4	19.77	0.004	15.65	0.003	39.51	0.008
MRg9	18.79	0.012	15.01	0.008	37.59	0.015
MRg11	18.61	0.007	15.00	0.004	37.27	0.010
MY3	19.08	0.004	15.60	0.003	38.76	0.009
MY3 duplicate	19.04	0.001	15.55	0.001	38.65	0.003
MY6	19.40	0.002	15.54	0.002	38.93	0.009
MY6 duplicate	19.43	0.000	15.59	0.000	39.04	0.000
MY9	19.34	0.002	15.49	0.003	38.75	0.011
MS5a	19.45	0.003	15.60	0.003	39.12	0.006
MS5b	19.03	0.004	15.18	0.003	37.95	0.007
MS10	19.32	0.001	15.61	0.001	39.05	0.004
MS10 dulpicate	19.31	0.002	15.61	0.002	39.02	0.006
MS16	19.20	0.004	15.63	0.003	39.04	0.010
MS16 duplicate	19.20	0.005	15.63	0.004	39.04	0.010
MB10	19.37	0.014	15.55	0.011	39.15	0.029
MB15	19.01	0.005	15.25	0.004	38.30	0.009
MB18	19.63	0.010	15.59	0.010	39.26	0.029

Note: (1) Star symbols represent samples which have been analyzed by TIMS instrument during test period.

Table 5: Parameters using for AFC modelling

Legend #	Magma			Crust	D_{Sr}	D_{Nd}	R
		Sr (ppm)	Nd (ppm)				
1	MR15	1500	35	Grenville basm.	1	0.2	0.01-0.17
3	MSG6	1500	70	Appalachian sed.	1	0.2	0.01-0.12
4	MSG6	1600	32	Appalachian sed.	1	0.2	0.01-0.14
5	MSG6	1900	30	Appalachian sed.	1	0.2	0.01-0.17
6	MSG6	2500	25	Appalachian sed.	1	0.2	0.01-0.20
8	MSG6	1300	75	Appalachian sed.	1	0.2	0.01-0.07
12	MSG6	1500	45	Appalachian sed.	1	0.2	0.01-0.15
11	MR15	1200	75	St Lawrence sed.	1	0.2	0.01-0.20
13	MSG6	1200	95	St Lawrence sed.	1	0.2	0.01-0.13
14	MSG6	1500	67	St Lawrence sed.	1	0.2	0.01- 0.23
15	MSG6	1200	75	St Lawrence sed.	1	0.2	0.01-0.24
16	MSG6	1200	70	St Lawrence sed.	1	0.2	0.01-0.13

Magma	$^{86}Sr/^{87}Sr$	Sr (ppm)	$^{143}Nd/^{144}Nd$	Nd (ppm)
MR15	0.70344	above	0.512788642	above
MSG6	0.70333	above	0.512759	above
Crust				
Appalachian sed.	0.73800	100	0.51200	40
St Lawrence Sed.	0.7085	300	0.51185	40
Grenville basm.	0.71500	200	0.51200	30

Note: This AFC model assumes a single pulse of magma, without recharge, and crystallized material separated from liquid. In our modelling, we used the mass ratio of assimilated to fractionally crystallized material (R), varing from 0.01 to 0.23, and the bulk trace element distribution coefficients for the fractionating mineral assemblages (D). For the mafic rocks, we assume that clinopyroxene, plagioclase and apatite are the main fractionating phases of Sr and Nd elements, and assign representative bulk D values of 1 for Sr and 0.2 for Nd (e.g. Chen et al., 1994). The isotopic composition of the initial uncontaminated magma is taken from the primitive isotopic compositions of Mt Royal (MR15) and St Gregoire (MSG6) with primitive concentrations of Nd and Sr of the parental magma vary from 1200-2500 ppm for Sr and 25-95 ppm for Nd. Three crustal rocks represent the host rocks, Grenville basement (granite), Trenton and Utica series (carbonates) for St Lawrence sediments and Gilman formation for Appalachian orogen (Sandstone; Chakrabarti et al., 2007; Chen et al., 1994; Davies and Smith, 2006, and authors therein)

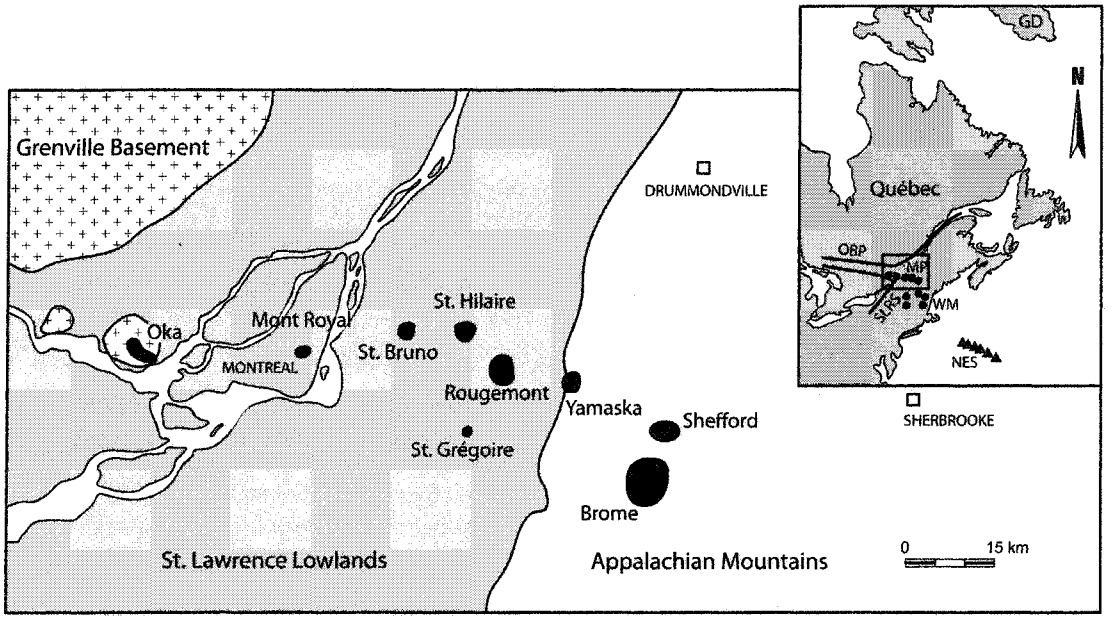

Figure 1 : Map of the Monteregian Igneous Province showing the distribution of the Cretaceous Monteregian intrusions. GD : Groenland ; NES : New England Seamounts ; WM : White Mountains ; SLRS : St Lawrence Rift System ; OBP : Paleo-rift Ottawa-Bonnechere ; MP : Province des Montérégiennes.

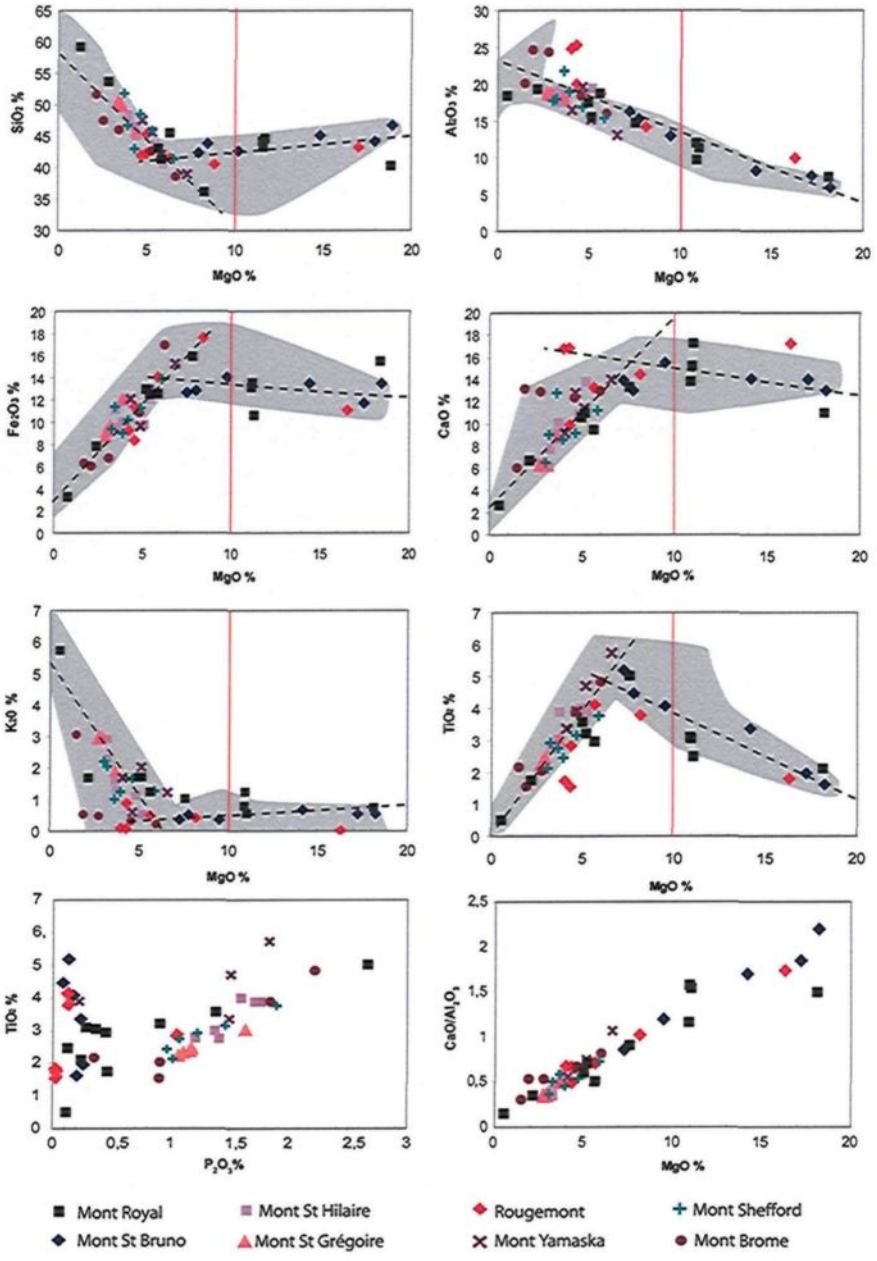

Figure 2 : Major element diagrams illustrating the composition of the Monteregian igneous intrusions as a function of MgO contents (wt%). Large symbols represent Monteregian data for each intrusion from this study. The grey domain represents literature data from Eby (1984b; 1985a) and Currie (1986). The red line separates samples with > 10 wt% MgO.

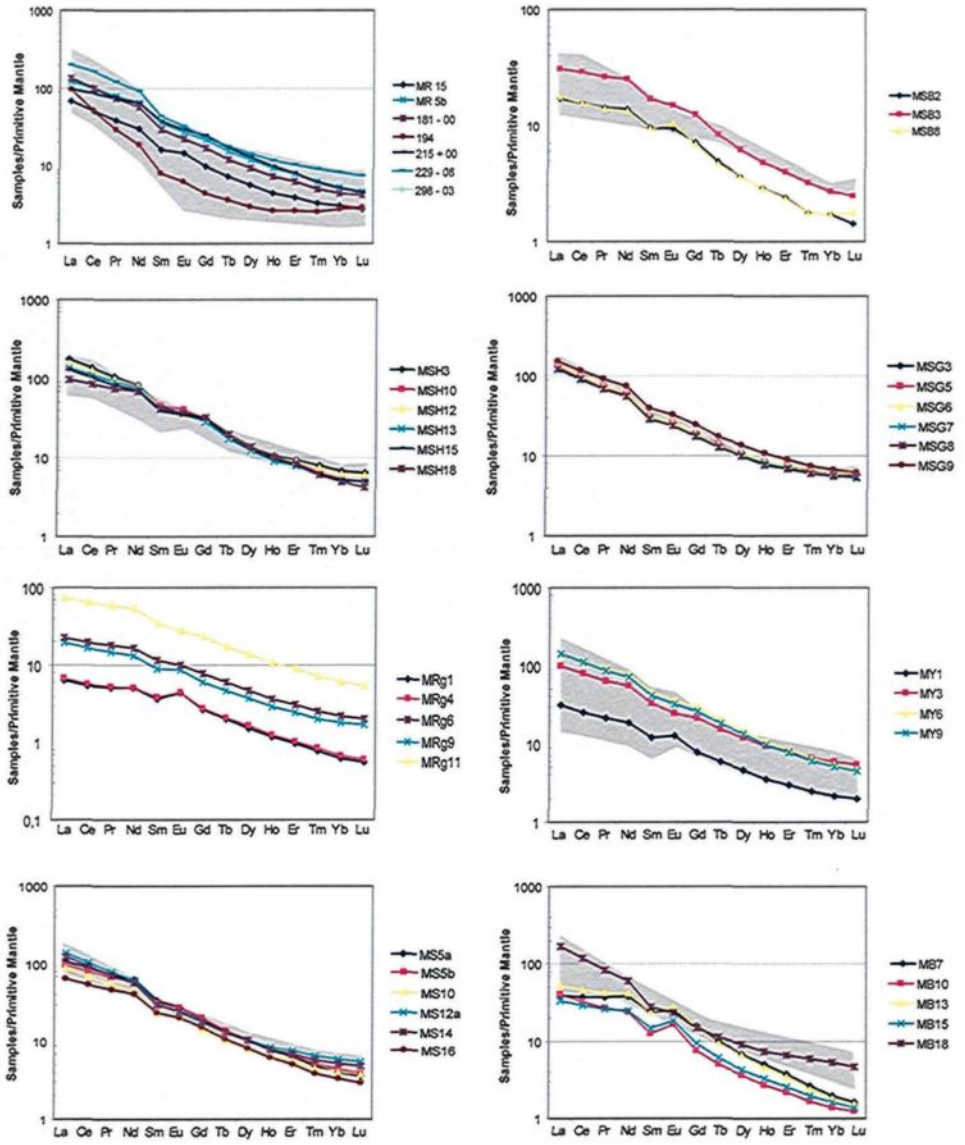

Figure 3 : REE patterns of the Monteregian Intrusions normalized to Primitive Mantle (McDonough and Sun, 1995). Each of the Monteregian intrusions are defined by their acronym: MR: Mont Royal, MSB: St Bruno, MSH: St Hilaire, MSG: St Grégoire, MRG: Rougemont, MY: Yamaska, MS: Shefford and MB: Brome. The grey domain represents literature data from Eby (1984b; 1985a) and Currie(1986). Only samples with MgO<10 wt.% are shown.

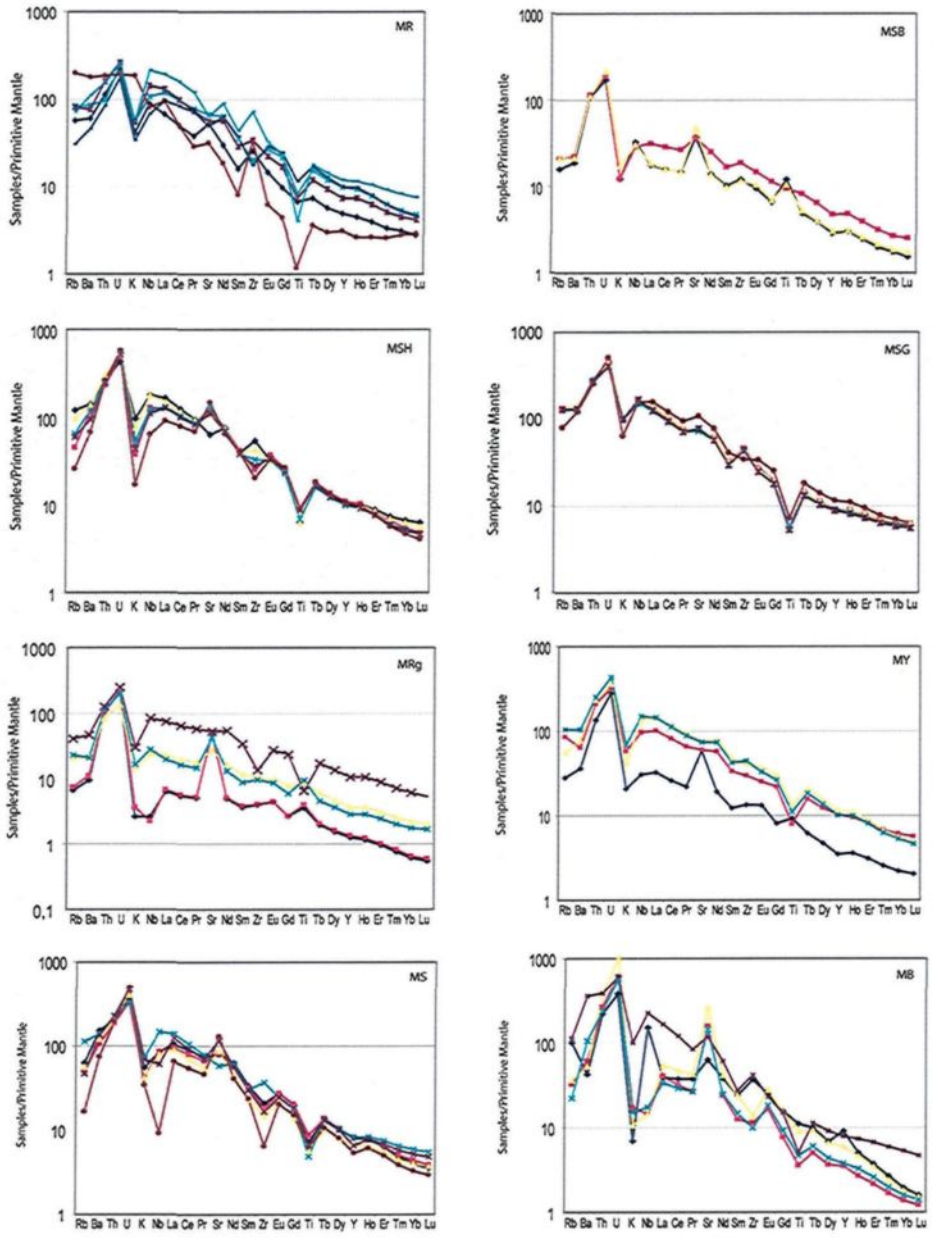

Figure 4 : Trace elements patterns of the Monteregian Hills normalized to Primitive Mantle (McDonough and Sun, 1995). Each of the Monteregian intrusions are defined by their acronym: MR: Mont Royal, MSB: St Bruno, MSH: St Hilaire, MSG: St Grégoire, MRG: Rougemont, MY: Yamaska, MS: Shefford and MB: Brome. Only samples with MgO<10 wt% are shown.

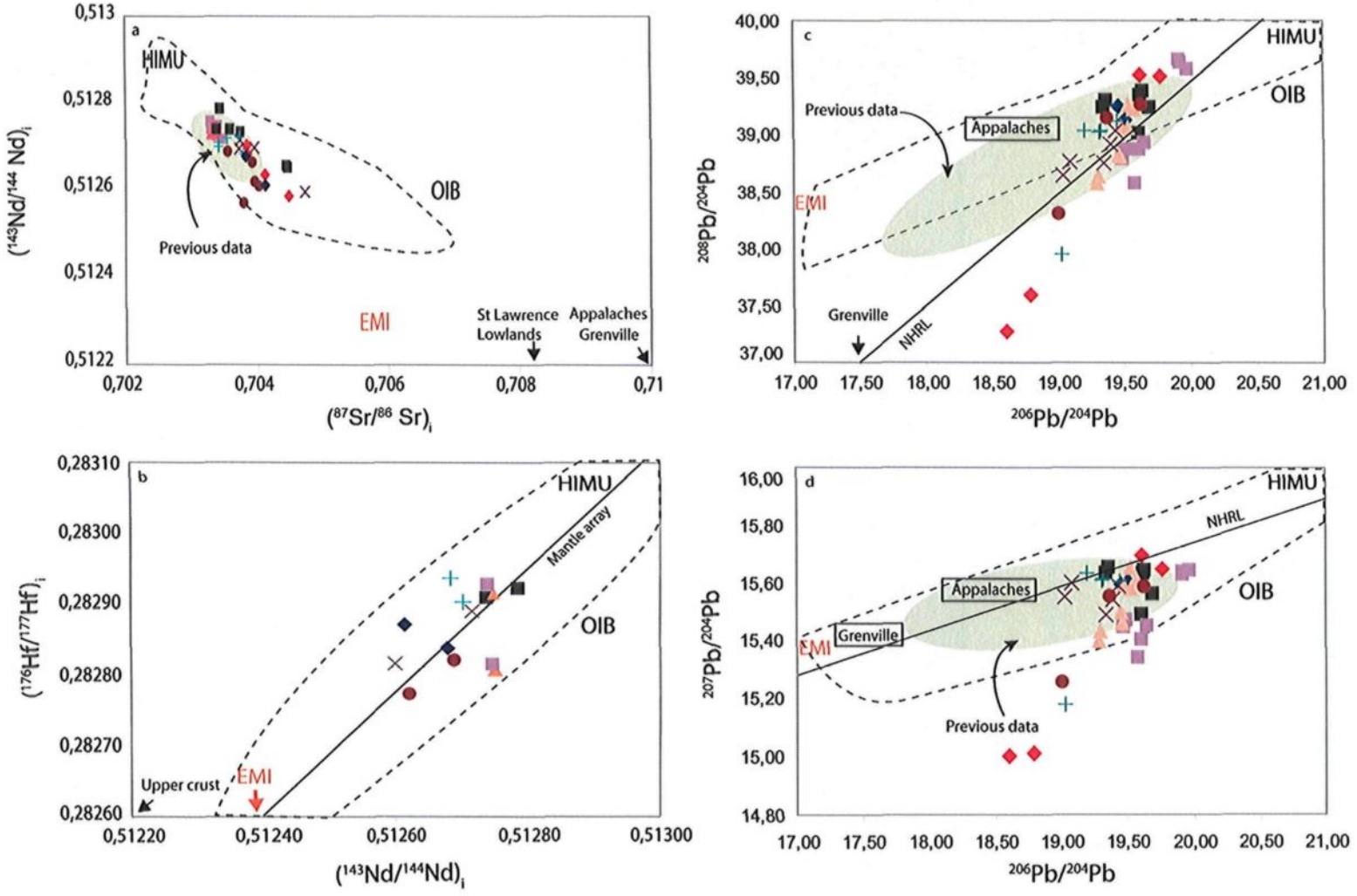
a
HIMU
OIB
Previous data
EMI
St Lawrence Lowlands
Appalaches Grenville
0,513
0,5128
0,5126
0,5124
0,5122
0,702
0,704
0,706
0,708
0,71
$(^{143}Nd/^{144}Nd)_i$
$(^{87}Sr/^{86}Sr)_i$
b
HIMU
Mantle array
OIB
Upper crust
EMI
0,28310
0,28300
0,28290
0,28280
0,28270
0,28260
0,51220
0,51240
0,51260
0,51280
0,51300
$(^{176}Hf/^{177}Hf)_i$
$(^{143}Nd/^{144}Nd)_i$
c
HIMU
OIB
Previous data
Appalaches
EMI
Grenville
NHRL
40,00
39,50
39,00
38,50
38,00
37,50
37,00
17,00
17,50
18,00
18,50
19,00
19,50
20,00
20,50
21,00
$^{208}Pb/^{204}Pb$
$^{206}Pb/^{204}Pb$
d
HIMU
NHRL
Appalaches
OIB
Grenville
EMI
Previous data
16,00
15,80
15,60
15,40
15,20
15,00
14,80
17,00
17,50
18,00
18,50
19,00
19,50
20,00
20,50
21,00
$^{207}Pb/^{204}Pb$
$^{206}Pb/^{204}Pb$

Figure 5 : a) $(^{143}Nd/^{144}Nd)_i$ vs. $(^{87}Sr/^{86}Sr)_i$; b) $(^{176}Hf/^{177}Hf)_i$ vs. $(^{143}Nd/^{144}Nd)^i$; c) $^{208}Pb/^{204}Pb$ vs. $^{206}Pb/^{204}Pb$ from plagioclase separates; d) $^{207}Pb/^{204}Pb$ vs. $^{206}Pb/^{204}Pb$ from plagioclase separates, of the Monteregian Hills. Only samples with MgO<10 wt.% are shown. Same symbols as in figure 2. The grey domain represents data from Eby (1985b) and Foland et al. (1988). The inital Nd, Sr and Hf isotopic ratios are calculated for an age of 124 Ma. Data sources: The mantle array is defined by Vervoort et al. (1999a). NHRL denotes the Northern Hemisphere Reference Line after Hart (1984). The compilation of OIB data are from Zindler and Hart (1986), Vervoort et al. (1999a) and Stracke et al. (2005). The EMI, HIMU and OIB fields are enriched mantle I, mantle with high U/Pb ratios, and ocean island basalts, respectively, and are from Hofmann (1988) and Zindler and Hart (1986). Appalachian data are from Chen et al. (1994), Fisher (2006 and therein authors) and McDaniel and McLennan (1997). Grenville basement data are from McDaniel and McLennan (1997), Wareham et al. (1998), Miller and Barr (2000) and Bell (1982). St Lawrence lowlands data are from Chakrabarti et al. (2007) and Davies and Smith (2006). Upper crust data are from Vervoort and Blichert-Toft (1999b).

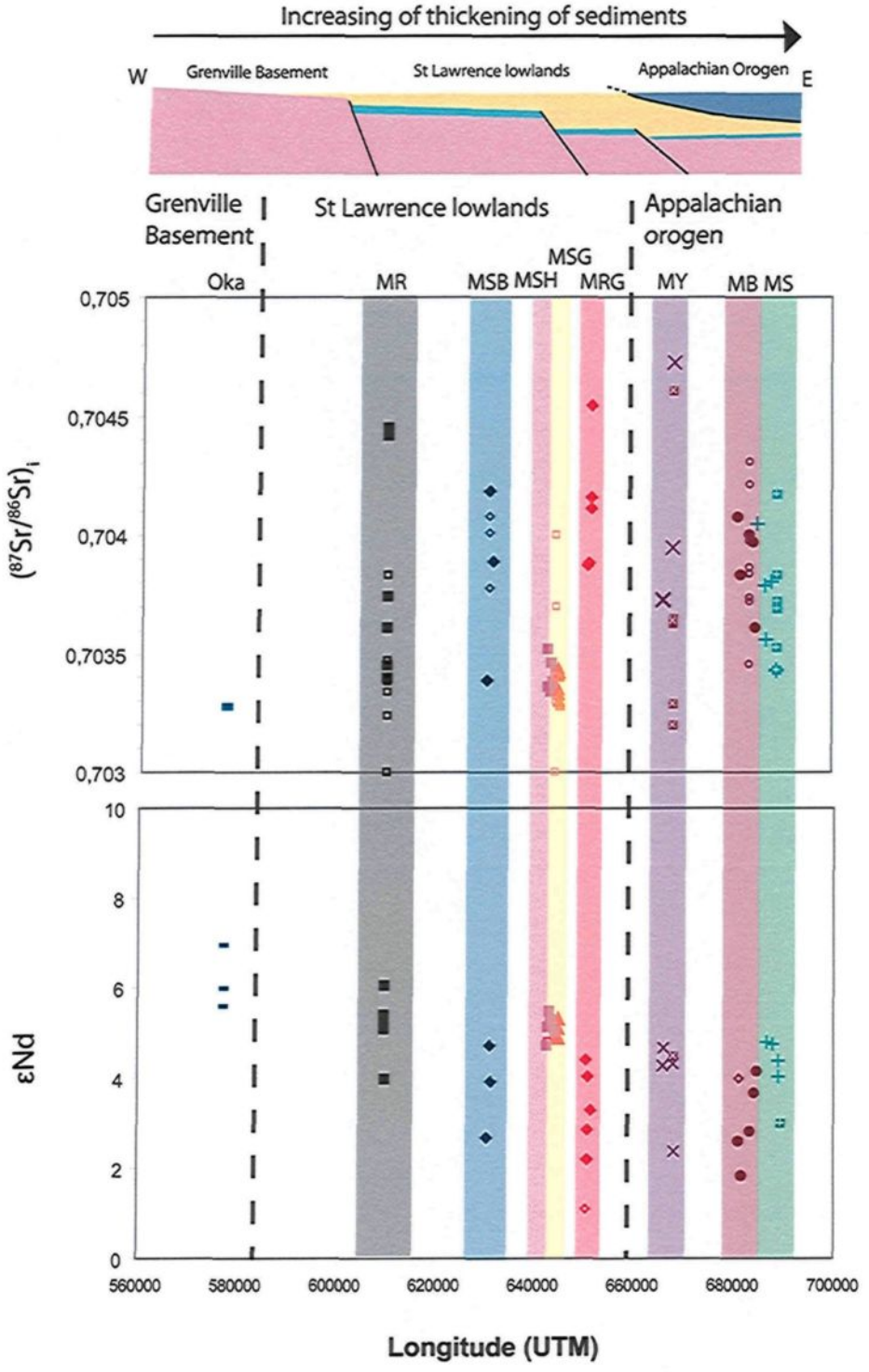
Increasing of thickening of sediments
W
Grenville Basement
St Lawrence lowlands
Appalachian Orogen
E
Grenville Basement
St Lawrence lowlands
Appalachian orogen
Oka
MR
MSB
MSH
MSG
MRG
MY
MB
MS
0,705
0,7045
0,704
0,7035
0,703
$(^{87}Sr/^{86}Sr)_i$
10
8
6
4
2
0
εNd
560000
580000
600000
620000
640000
660000
680000
700000
Longitude (UTM)

Figure 6: A schematic geological profile of the Monteregian area showing correlation with initial Sr ratio and εNd vs longitude (UTM) of the Monteregian intrusions. Each of the Monteregian intrusions are represented by different color symbols and defined by their acronym; black: Mont Royal (MR), blue: St Bruno (MSB), pink: St Hilaire (MSH), yellow: St Grégoire (MSG), red: Rougemont (MRG), purple: Yamaska (MY), green: Shefford (MS) and brown: Brome (MB). Large symbols as in figure 2 and small symbols represent literature data (Chen et al., 1994; Eby, 1984b; Eby, 1985a; Eby, 1989; Landoll and Foland, 1996). Oka data are represented by light blue lines (Wen et al., 1987). Only samples with MgO<10 wt.% are shown

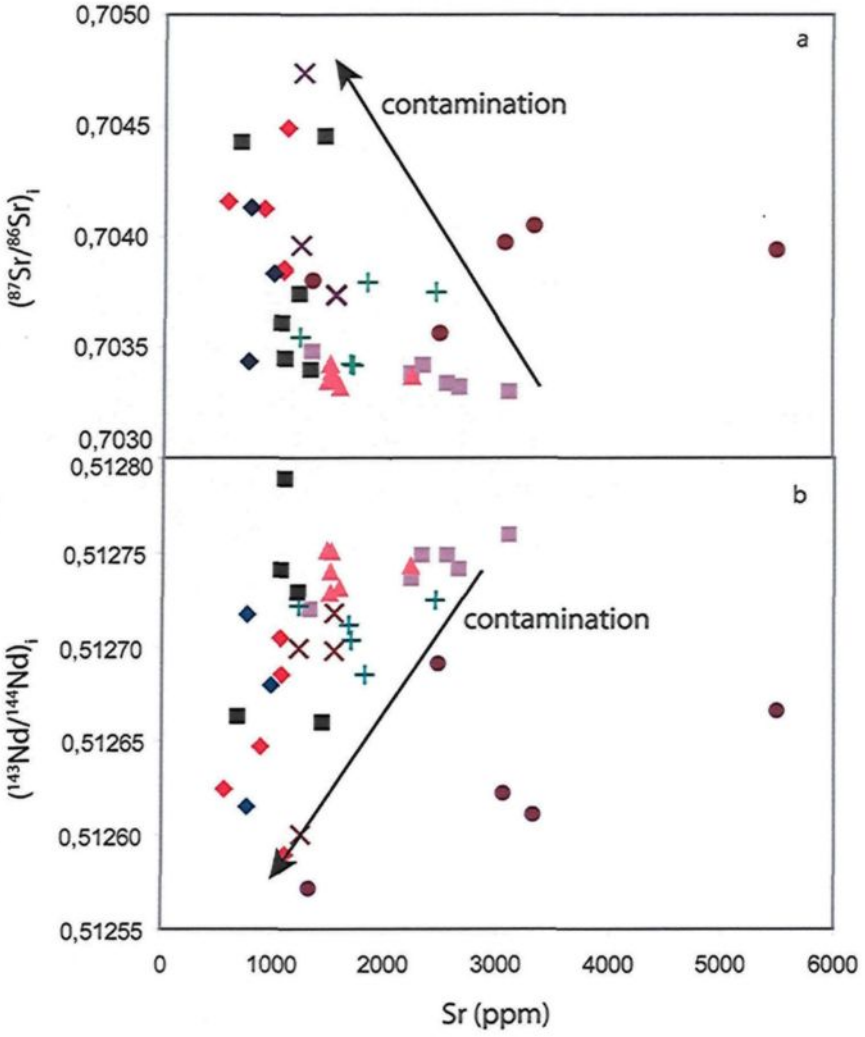

Figure 7: a) $(^{87}Sr/^{86}Sr)_i$ vs Sr (ppm) and b) $(^{143}Nd/^{144}Nd)_i$ vs Sr (ppm) from the Monteregian rocks. Same symbols as in figure 2. The increasing $(^{87}Sr/^{86}Sr)_i$, and decreasing $(^{143}Nd/^{144}Nd)_i$ with decreasing 1000/Sr indicates crustal contamination of the intrusions. Only samples with MgO<10 wt.% are shown.

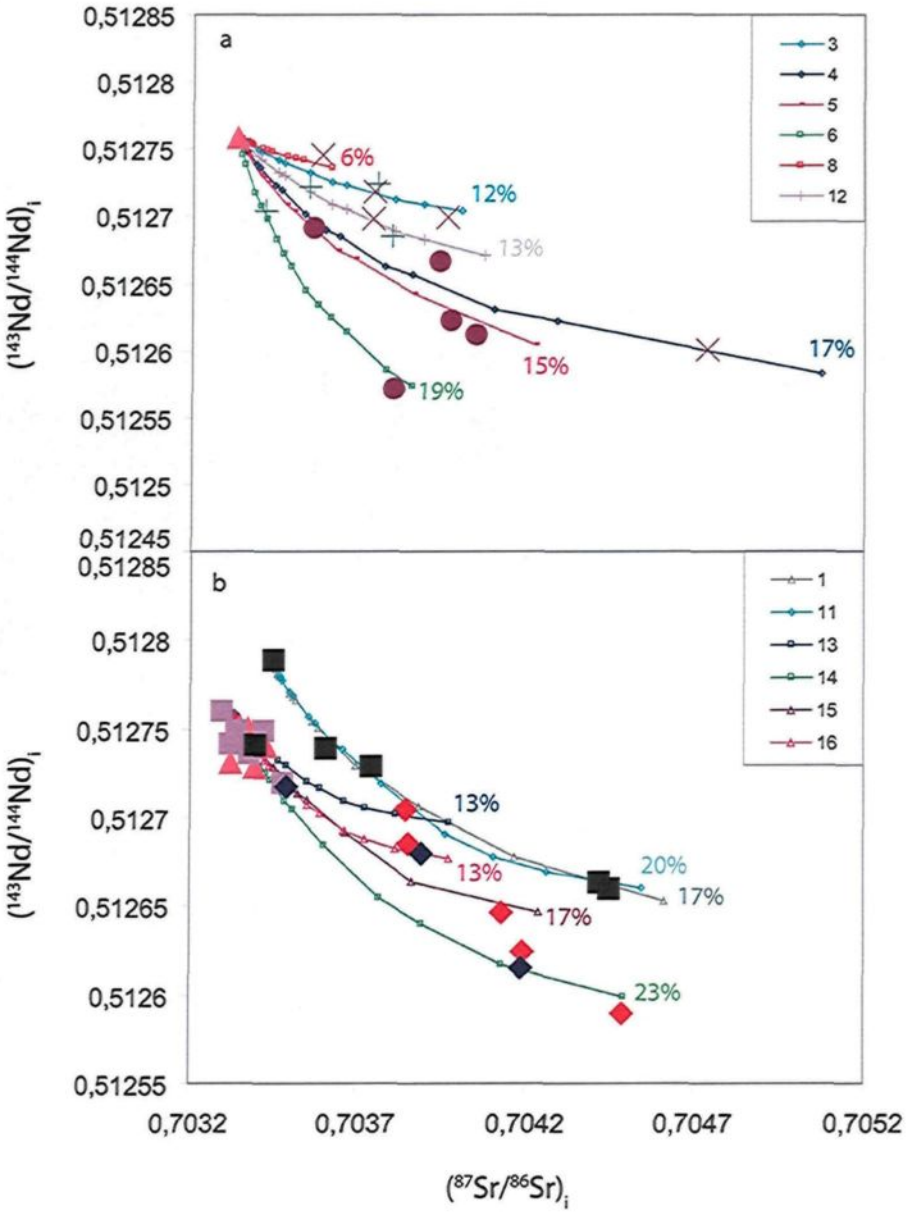
a
b
3
4
5
6
8
12
1
11
13
14
15
16
6%
12%
13%
15%
17%
19%
13%
13%
17%
20%
17%
23%
0,51285
0,5128
0,51275
0,5127
0,51265
0,5126
0,51255
0,5125
0,51245
0,7032
0,7037
0,7042
0,7047
0,7052
(143Nd/144Nd)i
(87Sr/86Sr)i

Figure 8: $(^{143}Nd/^{144}Nd)_i$ vs. $(^{87}Sr/^{86}Sr)_i$ illustrating assimilation-fractional crystallisation modeling (AFC; DePaolo (1981)) of the Monteregian parental magma by wall rocks. a) The model of contamination for Monteregian intrusions located in Gilman formation (Yamaska, Shefford and Brome). b) The model of contamination for Monteregian intrusions located in Grenville basement and Trenton formation (Mont Royal, St Bruno, St Hilaire, St Grégoire and Rougemont). The parental magma is represented by the two most radiogenic Sr isotope (MSG6: 0.7033 and MR15: 0.7034) and least radiogenic Nd (MSG6: 0.512759 and MR15:0.51278) isotope compositions. Three different contaminants are used: a sedimentary unit from the Appalachian orogen (Gilman formation; Chen et al., 1994), a sedimentary formation from the St Lawrence platform (Trenton formation; Chakrabarti et al., 2007; Davies and Smith, 2006) and a granite gneiss from the Grenville basement (Bell, 1982). The thin lines represent degree of assimilation/ contamination ratios and small points illustrate the percent of contamination (R values). Same symbols as in figure 2. The numbers in the legend at right refer to parameter model in Table 4. Only samples with MgO<10 wt.% are shown

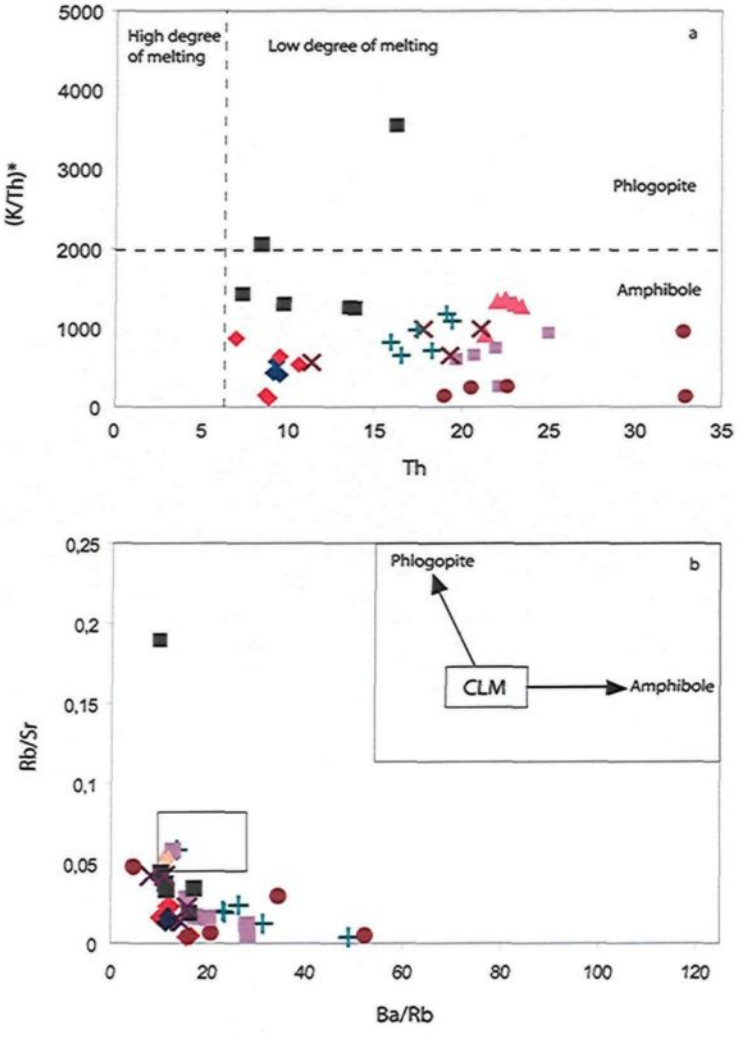

Figure 9: Variations in incompatible trace elements in order to constrain the mineralogical source in the Monteregian mantle. a) K/Th* (K_20*10,000/Th) vs. K shows the effect of melting of amphibole and phlogopite-bearing mantle source. Potassium is an essential structural constituent of these phases, so it will be retained in the source region until they are consumed through progressive melting. Very low degrees of melting are indicated by high Th (>7ppm) and low K/Th* (<2000) and are indicative of an amphibole-bearing source mantle (Furman, 2007). b) Rb/Sr vs. Ba/Rb. The mineralogy of the continental lithospheric mantle (CLM) source includes minor amounts of both amphibole and phlogopite (Furman and Graham, 1999). Thus samples plotting close to the CLM field are derived of the CLM source. Same symbols as in figure 2. Only samples with MgO<10 wt.% are shown

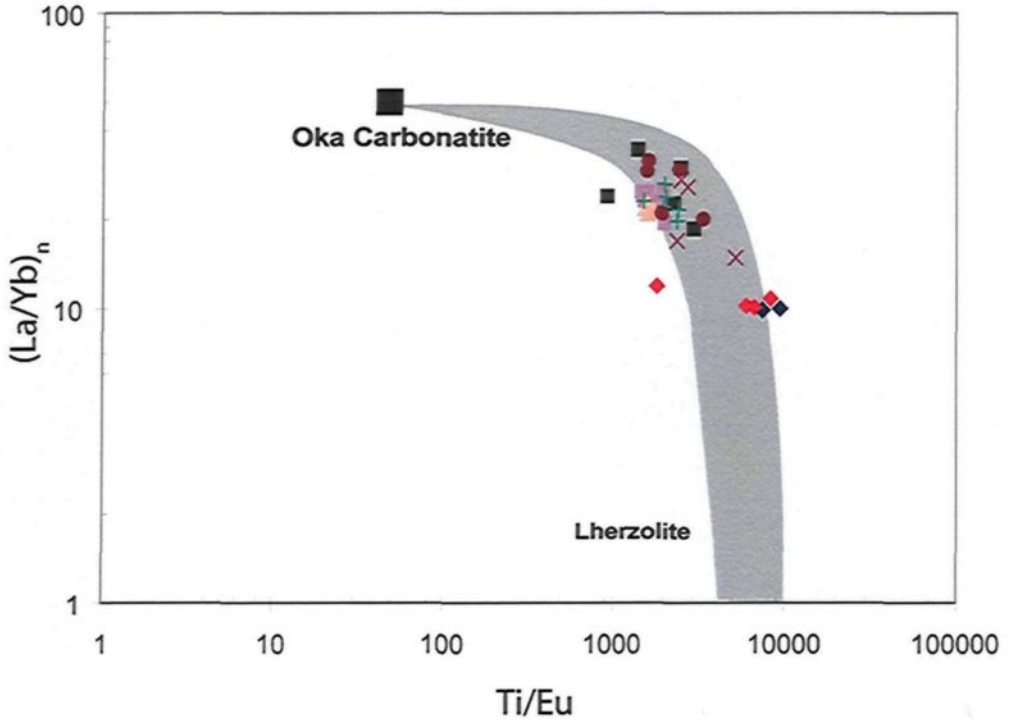

Figure 10: $(La/Yb)_N$ vs. Ti/Eu illustrate the effect of mixing between carbonatite melts and peridotite mantle. Data for Oka carbonatite and lherzolite mantle are respectively from Gold and Eby (1986), and McDonough (1990). Same symbols as in figure 2. The grey domain represents mixing between Oka carbonatite and lherzolite. Using the mixing-percolation model from Rudnick et al., (1993), only 2% of carbonatite melts is needed to explain the chemical and mineralogical modifications in the mantle beneath the Monteregian Igneous Province. Only samples with MgO<10 wt.% are shown.

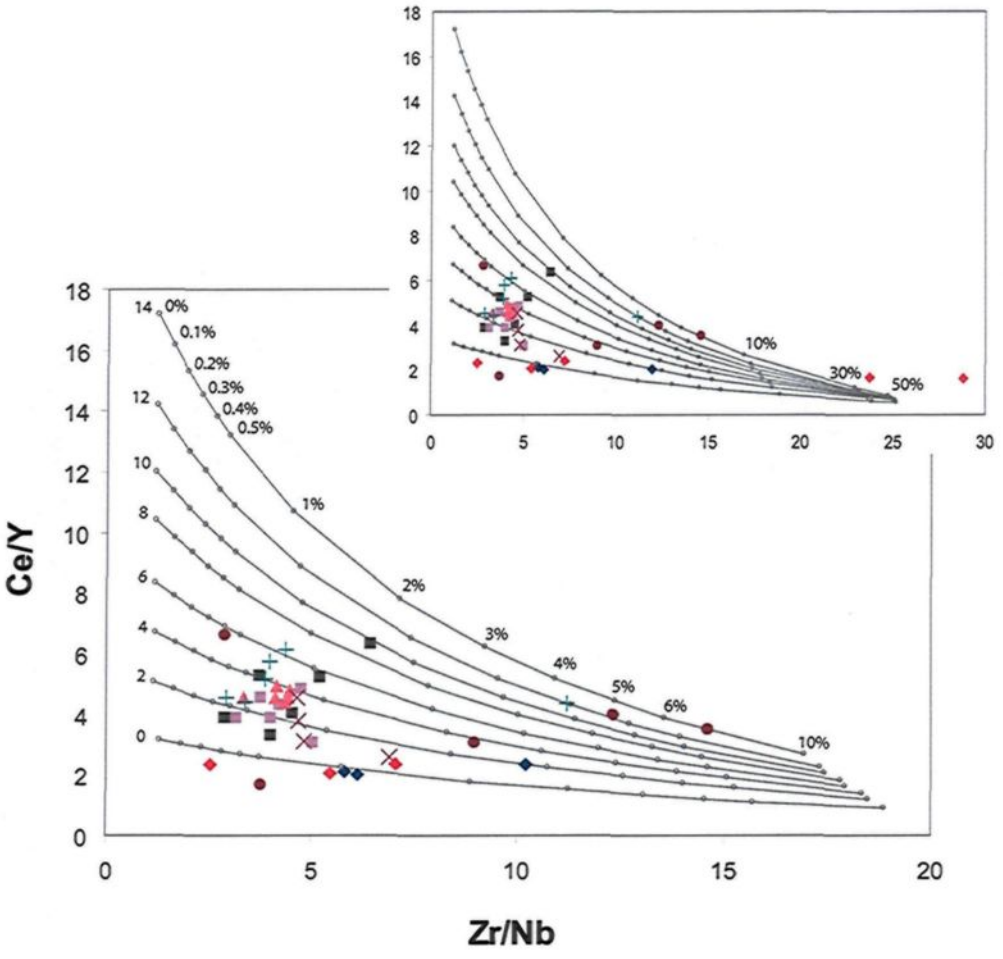

Figure 11: Ce/Y vs. Zr/Nb. This plot indicates partial melting and mineralogical compositions of original mantle under Monteregian Hills. Same symbols as in figure 2. Curved lines denote calculated fractional melts from a fertile peridotite with ca. 2× chondritic abundances of the elements. D-values are from Halliday et al. (1995) and for amphibole, D-values from GERM (http://earthref.org/GERM/: Chazot et al., 1996; Latourrette et al., 1995; Matsui et al., 1977; Villemant et al., 1981). Tick marks denote melt fraction and numbers at the start of each curve indicate the modal abundance of garnet in the source. The samples with MgO>10%w.t. are not presented.

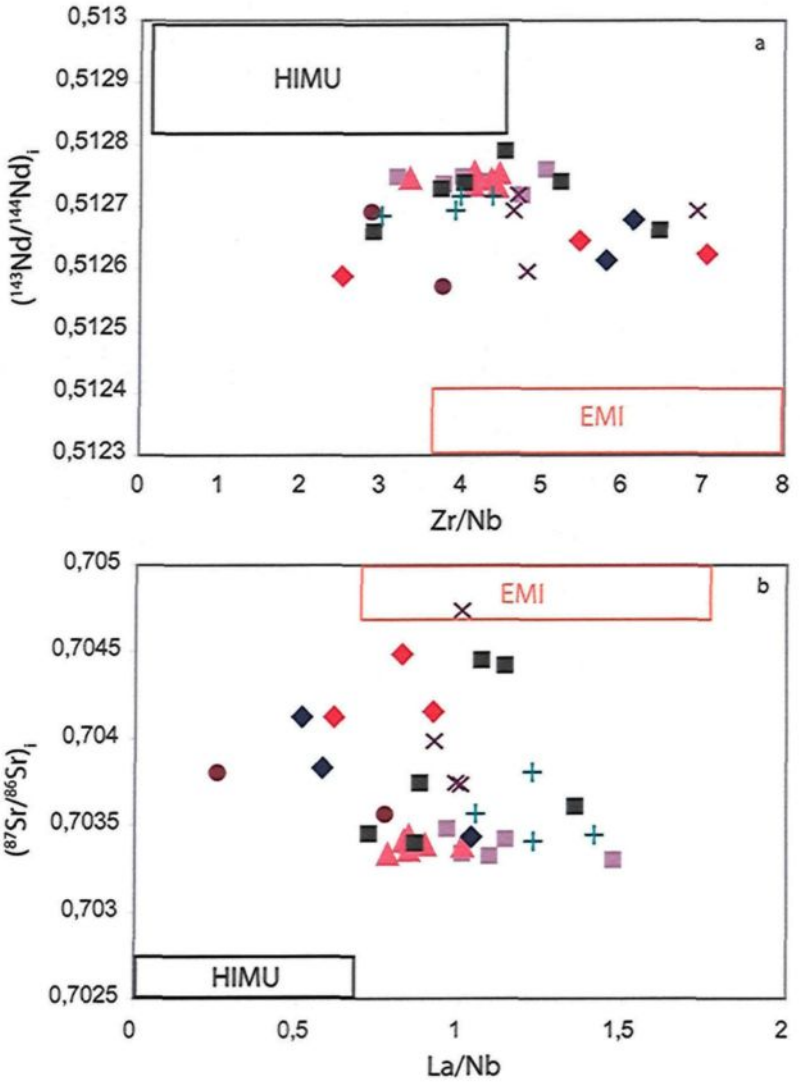

Figure 12: a) $(^{87}Sr/^{86}Sr)_i$ vs. La/Nb and b) $(^{143}Nd/^{144}Nd)_i$ vs. Zr/Nb indicate a mixing between EMI and HIMU end-members for Monteregian magmas. Same symbols as in figure 2. Data sources: EMI and HUMI fields are from Hofmann (1988) and Zindler and Hart (1986). Only samples with MgO<10 wt.% are shown

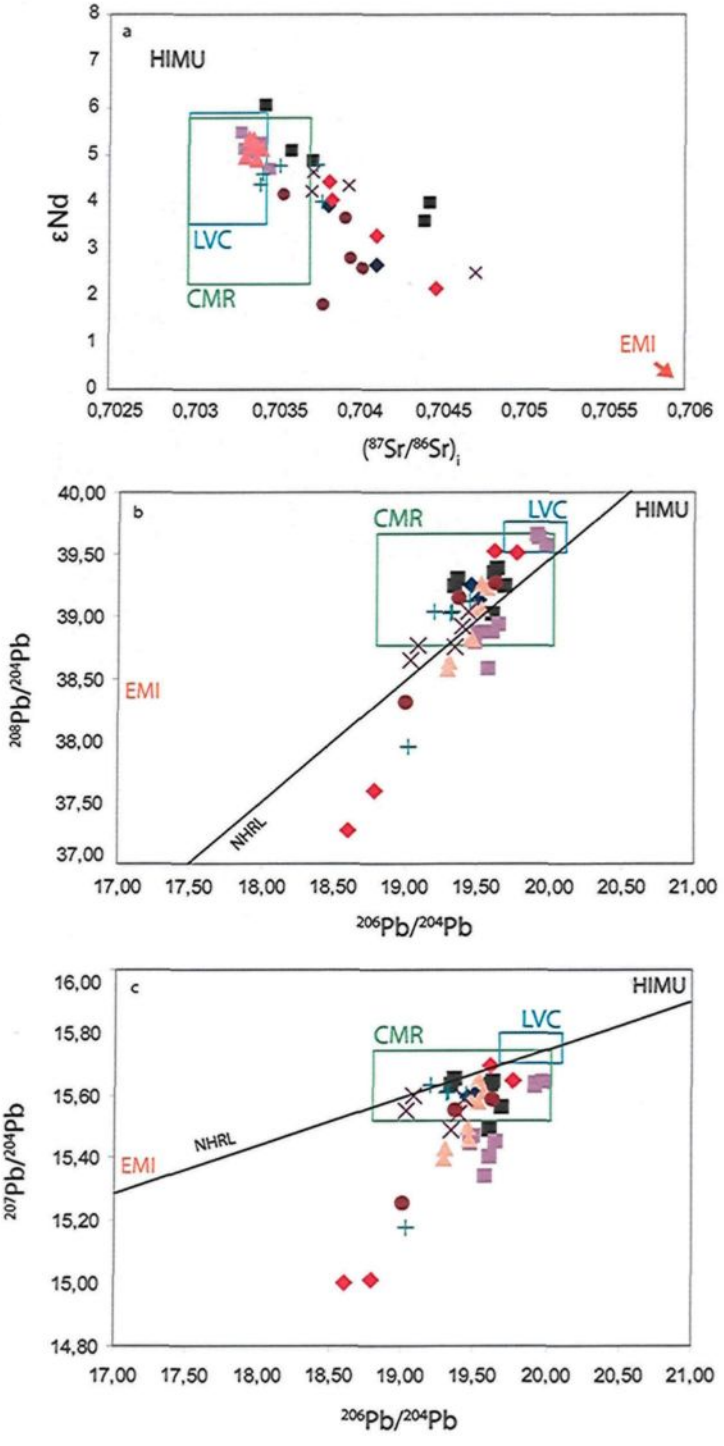
a
HIMU
LVC
CMR
EMI
εNd
$(^{87}Sr/^{86}Sr)_i$
b
CMR
LVC
HIMU
EMI
NHRL
$^{208}Pb/^{204}Pb$
$^{206}Pb/^{204}Pb$
c
HIMU
CMR
LVC
NHRL
EMI
$^{207}Pb/^{204}Pb$
$^{206}Pb/^{204}Pb$

Figure 13: a) εNd and $(^{87}Sr/^{86}Sr)_i$, b) $^{208}Pb/^{204}Pb$ vs. $^{206}Pb/^{204}Pb$ and c) $^{207}Pb/^{204}Pb$ vs. $^{206}Pb/^{204}Pb$ of the Monteregian igneous rocks. The Monteregian magmas result from unique hybrid reservoir located in sub-continental lithospheric mantle similar to European lithospheric mantle. Same symbols as in figure 2. Data sources: HIMU and EM1 end-members are from Hofmann (1988) and Zindler and Hart (1986). Literature data for the European mantle, Low Velocity Component (LVC) from Hoernle (1995) and Common Mantle Reservoir (CMR) from Lustrino and Wilson (2007). NHRL denotes the Northern Hemisphere Reference Line after Hart (1984). Only samples with MgO<10 wt.% are shown.

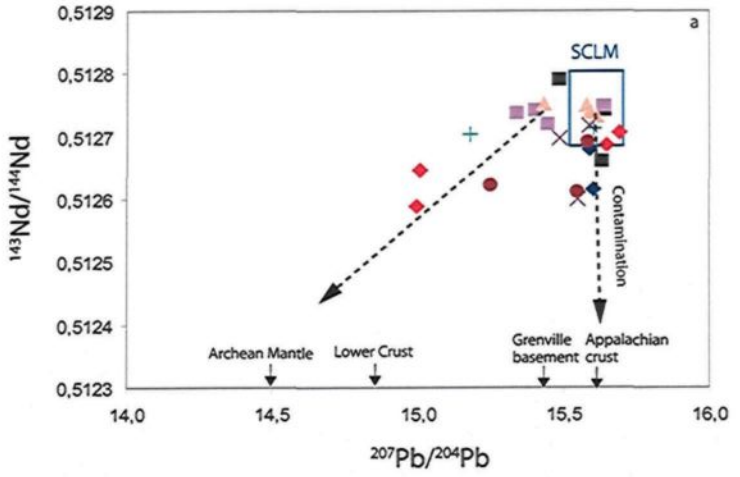
a
SCLM
Contamination
Archean Mantle
Lower Crust
Grenville basement
Appalachian crust
$^{143}Nd/^{144}Nd$
$^{207}Pb/^{204}Pb$
0,5129
0,5128
0,5127
0,5126
0,5125
0,5124
0,5123
14,0
14,5
15,0
15,5
16,0

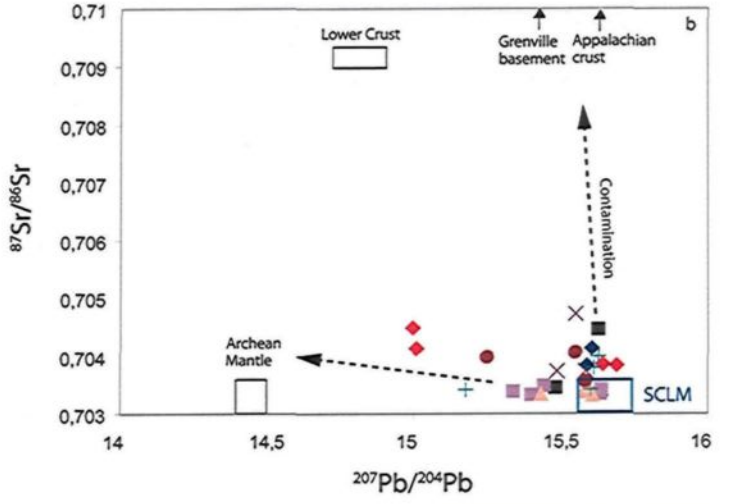
b
Lower Crust
Grenville basement
Appalachian crust
Contamination
Archean Mantle
SCLM
$^{87}Sr/^{86}Sr$
$^{207}Pb/^{204}Pb$
0,71
0,709
0,708
0,707
0,706
0,705
0,704
0,703
14
14,5
15
15,5
16

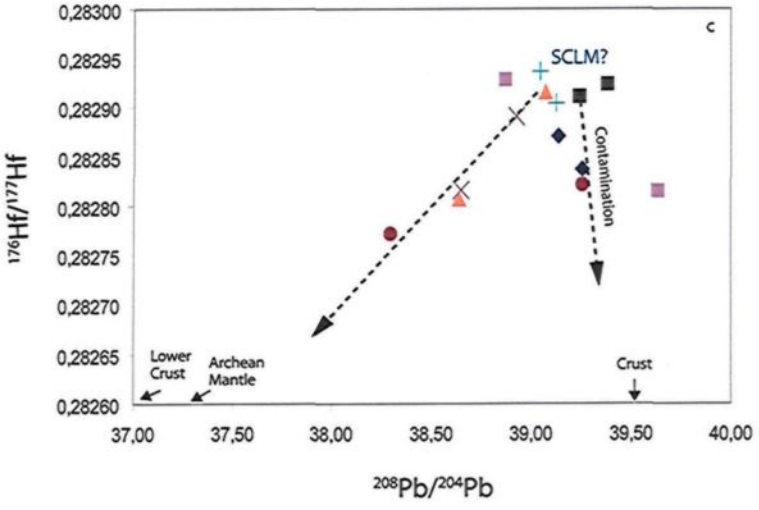
c
SCLM?
Contamination
Lower Crust
Archean Mantle
Crust
$^{176}Hf/^{177}Hf$
$^{208}Pb/^{204}Pb$
0,28300
0,28295
0,28290
0,28285
0,28280
0,28275
0,28270
0,28265
0,28260
37,00
37,50
38,00
38,50
39,00
39,50
40,00

Figure 14: a) ($^{143}Nd/^{144}Nd)_i$ vs. $^{207}Pb/^{204}Pb$ b) ($^{87}Sr/^{86}Sr)_i$ vs. $^{207}Pb/^{204}Pb$ and c) $^{176}Hf/^{177}Hf$ vs. $^{208}Pb/^{204}Pb$ contrast the impact of an Archean mantle component and wall-rock contamination in the formation of Monteregian magmas. The depleted Archean mantle data indicate unradiogenic Pb ($^{207}Pb/^{204}Pb$= 14.5-15.30, $^{208}Pb/^{204}Pb$= 34.46-36.42 and $^{206}Pb/^{204}Pb$=15.08-15.58), Nd (0.50921) and Hf (0.2817), and moderate radiogenic Sr (0.7012-0.7034) isotopic compositions The Archean lower crust compositions are non-radiogenic for Pb ($^{207}Pb/^{204}Pb$=14.8, $^{208}Pb/^{204}Pb$ = 34 and $^{206}Pb/^{204}Pb$=14.5), Nd (0.5116-0.5124) and Hf (0.2810)isotopes, but moderately radiogenic for Sr isotopes (0.709). Same symbols as in figure 2. Data sources: Appalachian data are from Chen et al. (1994), Fisher (2006 and therein authors) and McDaniel and McLennan (1997). Grenville basement data are from McDaniel and McLennan (1997), Wareham et al. (1998), Miller and Barr (2000) and Bell (1982). Lower crust data are from Griffin et al. (1980a); Rudnick and Goldstein (1990a); Stuart et al. (2000); Zhang (2002), and crust data is from Vervoort and Blichert-Toft (1999b). Archean mantle data are from Bell and Blenkinsop (1987); Griffin et al. (2000); Pearson (2004); Schmidberger et al. (2007). SCLM data are from Hoernle et al. (1995) and Lustrino and Wilson (2007)

AVANT-PROPOS DU CHAPITRE 3

Contributions des auteurs

Le chapitre 3 est le résultat d'une collaboration entre l'Université du Québec à Montréal et l'Université de Tokyo, Japon. Je suis à l'origine des analyses ainsi que de l'interprétation et la rédaction de l'article Daniele Pinti a participé à la rédaction de l'article ainsi quà la relecture. Ross Stevenson a participé à la correction de l'anglais ainsi qu'à la relecture. Naoto Takahata et Yuji Sano m'ont invité dans leur laboratoire afin de mesurer l'azote dans mes échantillons et ont participé à la relecture du chapitre. Fabien Pitre a participé à l'analyse de l'hélium et de l'argon ainsi qu'à la rédaction de la partie Méthodologie.

CHAPITRE 3

Nitrogen, helium and argon isotopes in minerals from alkaline intrusions of the Monteregian Hills, Québec: Evidence for an upper mantle origin

Emilie ROULLEAU[1]*, Daniele L. PINTI[1], Ross K. STEVENSON[1], Naoto TAKAHATA[2], Yuji SANO[2], Fabien PITRE[1]

[1] GEOTOP and Département des Sciences de la Terre et de l'Atmosphère, Université du Québec à Montréal, Succ. Centre Ville CP 8888, Montréal, QC, H2X 3Y7, Canada.

[2] AORI, Atmosphere and Ocean Research Institute, The University of Tokyo, Kashiwa, Japan

In Revision for submission to Chemical Geology

3.1. Abstract

The isotopic compositions of N and noble gases He and Ar were measured by crushing mineral separates from the Monteregian Hills Igneous Province in southwestern Quebec, Canada. Based on isotopic, petrologic and structural studies, this largely east-west alignment of intrusions have been previously interpreted as either the surface expression of the Great Meteor hot spot or the product of lithospheric mantle melts uprising through reactivated faults of Proterozoic grabens (Ottawa-Bonnechère rift). The N isotopic compositions of the Monteregian Hills ($\delta^{15}N$) range from -7.6±0.5‰ to +10.5±1.9‰ and they do not correlated with the N content. The radiogenic $^{4}He/^{40}Ar^{*}$ ratio plotted against the $^{4}He/^{36}Ar$ ratio indicate that the noble gasses are derived from a melt that was strongly degassed (85%) and air/crustal contaminated during its ascent. Melt degassing did not alter the N and Ar isotopic composition which can be used for tracing the mantle sources feeding the Monteregian Hills. Plots of $\delta^{15}N$ vs. $^{40}Ar/^{36}Ar$ and vs. $N_2/^{36}Ar$ ratios are consistent with upper mantle sources but seem to exclude involvement of the lower mantle (OIB noble gas signatures) in the origin of the Monteregian Hills. We show for the first time a co-variation between $\delta^{15}N$ values and $^{207}Pb/^{204}Pb$ and $^{208}Pb/^{204}Pb$ ratios which suggest binary mixing of two sources: upper mantle-derived melts and crustal contamination. In addition, correlations between $\delta^{15}N$ and trace elements ratios such as Ba/Nb and La/Nb indicate that the Monteregian Hills formed by melting of enriched subcontinental lithospheric mantle.

3.2. Introduction

Understanding the processes of material transfer between the surface and interior of the Earth is of great importance in constraining the chemical evolution of the mantle and formation of the mantle chemical heterogeneities (e.g., primordial, enriched and depleted reservoirs). Nitrogen, helium and argon isotopes are potentially important tracers of these transfer processes because they show specific isotopic signatures in each of the earth's reservoirs. The upper mantle shows a $\delta^{15}N$ (= $[(^{15}N/^{14}N)_{sample}/(^{15}N/^{14}N_{air})]$-1 x 1000) of -5±2‰ (Marty and Humbert, 1997; Sano et al., 1998; Cartigny et al., 2001), a $^{40}Ar/^{36}Ar$ of

27,000±4000 with an upper limit of 40,000 (Moreira et al., 1998; Raquin et al., 2008) and a radiogenic $^{4}He/^{40}Ar^{*}$ = 2.5 (Graham, 2002). The crust has a $\delta^{15}N \geq +7$ ‰ (Javoy, 1997), a $^{40}Ar/^{36}Ar \geq 300$ (Sano et al., 1998) and a $^{4}He/^{40}Ar^{*} >> 5$ (Ballentine et al., 1994). Finally, the atmosphere-hydrosphere is characterized by a $\delta^{15}N = 0$‰ (Mariotti, 1984), $^{40}Ar/^{36}Ar = 295.5$ (Ozima and Podosek, 1983) and a $^{4}He/^{40}Ar = 5.6 \times 10^{-4}$. The lower mantle is also characterized by specific isotopic signatures, though there is an ongoing debate concerning the isotopic compositions that constitute primordial "undegassed" mantle. Several measurements of Ocean Island Basalts (OIBs) suggest a ^{15}N-enriched reservoir with a measured $\delta^{15}N$ of +3±2‰ (Dauphas and Marty, 1999; Marty and Dauphas, 2003), $^{40}Ar/^{36}Ar \leq$ 8000 (Trieloff et al., 2000; Matsumoto et al., 2008) and a $^{4}He/^{40}Ar^{*}$ of ~0.1 (Graham, 2002). However, $\delta^{15}N$ values as low as -25‰ have been proposed (Mohapatra et al., 2009).

Mid-Ocean Ridge Basalts (MORBs), OIBs, and diamonds are the preferred probes to measure mantle-derived N and noble gases and thus to trace mantle chemical heterogeneities (e.g., Graham, 2002 and references therein). More recently, mantle xenoliths from continental igneous provinces have been the focus of recent research on N (Matsumoto et al., 2002; Fischer et al., 2005). Indeed, studies of continental magmatic suites are often hampered by crustal contamination (both during magma ascent and later superficial alteration), magma degassing and phase separation processes (e.g., Fischer et al., 2009) and thus require a multi-isotopic approach.

The Cretaceous Monteregian Hills Igneous Province (Québec, Canada), which is composed of nine alkaline intrusions, is one of these case studies. The mantle source that formed these intrusions is highly controversial. An alkaline character, a spatial distribution and OIB-like Sr and Pb isotopic signatures characterize this magmatic province. These studies suggest the presence of EM1 and HIMU components (Eby, 1985; Foland et al., 1988) and the involvement of the lower mantle associated with the passage of the Great Meteor hot spot track (Sleep, 1990). However, based on the Sr-Nd isotopic compositions of the Oka carbonatitic complex, Wen et al. (1987) argued in favor of the melting of a sub-continental lithospheric mantle (SCLM hereafter). A tectonic study of the region showed that dykes associated with the Monteregian Hills can be related to magma ascent during the reactivation of Paleozoic faults of the Ottawa-Bonnechère rift, during the opening of the North Atlantic

Ocean (180-150 Ma). These studies argue for the involvement of SCLM melts rather than a deeper source from the lower mantle (Faure et al., 1996).

A new study of the geochemistry and Sr, Nd, Hf and Pb isotopes of mafic rocks of the Monteregian Hills found isotopic heterogeneities that can be interpreted as a mixing of SCLM melts and local crustal contamination (Roulleau and Stevenson, 2010). In addition, the mineralogical assemblage (garnet, spinel and amphibole) of the mantle source defined by partial melting models suggests that melting occurred at the boundary of the spinel-garnet stability domain (ca. 70-80 km), at the base of the lithospheric mantle (Hofstetter and Bock, 2004).

In order to discriminate between the potential mantle sources of the Monteregian Hills (lower vs. upper mantle/SCLM) behind the veil of crustal contamination, we analyzed the $\delta^{15}N$ values and the $^{36,38,40}Ar$ and ^{4}He isotopic abundances preserved in inclusions in clinopyroxene and amphibole mineral separates. The N and noble gases were released by crushing the minerals rather than by stepwise heating because it has been previously found that the mineral matrix/groundmass frequently contains N from heterogeneous sources, including surface-derived N (e.g., Marty and Zimmermann, 1999). It has been found that crushing of the mineral separates releases N and Ar within the mineral inclusions and avoids the heterogeneity found within the mineral groundmass (Marty and Zimmerman, 1999).

3.3. Geological setting

The Monteregian Hills, dated at 124±1.5 Ma (Foland et al., 1986) were emplaced along a linear E-W trend, which follows the Ottawa-Bonnechere paleorift (Fig. 1). This half-graben has been interpreted as a Late Proterozoic to Early Paleozoic failed arm of the Iapetus Ocean, the precursor to the Atlantic Ocean (Pinet and Tremblay, 1995). The Ottawa-Bonnechere rift was reactivated during the breakup of the supercontinent Pangaea and the opening of the North-Atlantic, some 180-150 Ma ago (Faure et al., 1996). Moving eastward, the magmas intruded three different terrains: the Grenville-Province crystalline rocks (gneiss and amphibolites); the St-Lawrence Lowlands Cambrian-Ordovician dolostones, carbonates

and shales; and finally metasediments (quartzite) and metamorphic rocks of the Appalachians Mts. (Fig.1).

The igneous intrusions reveal a large variety of rocks from strongly silica-undersaturated to moderately silica-saturated (Eby, 1984; Eby, 1985). At the western end of the Monteregian Hills, Oka is characterized by carbonatites. The central intrusions (Mts Royal, St Bruno, St Hilaire, St Grégoire, Yamaska and Rougemont) are mainly composed of slightly silica-undersaturated (essexite) to moderately silica-oversaturated rocks (gabbros and pyroxenite) with minor felsic rocks (syenite). Silica-oversaturated rocks (pulaskite and syenite) and minor mafic rocks (gabbro and diorite) characterize the eastern portion of the Monteregian Hills (Mts Shefford and Brome).

Mineral separates for N and noble gas isotopic analyses were selected from mafic rocks (gabbros) of the following Monteregian Hills. Mt Royal has gabbros containing cumulus olivine (Fo74-68), Ti-augite, amphibole and plagioclase (An83-44); the Mt St Bruno intrusion is a gabbro containing olivine (Fo84-74), plagioclase (An84-55) and minor amounts of amphibole. Mt St Hilaire is composed of pyroxene-rich gabbros, locally richer in amphibole and with rare olivine (Eby, 1988). Mt Rougemont is essentially composed of pyroxenite and gabbro containing abundant olivine, while plagioclase is present either as an interstitial phase in the pyroxenites or a major phase in the gabbro. Mt St Grégoire has a core of essexite (minor olivine and varying amount of augite, hornblende and oligoclase (Eby, 1988). Mt Yamaska is mainly composed of pyroxenites and gabbros containing abundant plagioclase, Ti-augite and/or hornblende. Mt Shefford is composed of diorite, gabbro and minor intrusive breccias, sub-volcanic porphyries, nordmarkite and pulaskite. Mt Brome, the largest intrusion of the Monteregian Hills, is composed of a gabbro body containing plagioclase, clinopyroxene, hornblende and rare olivine (Landoll and Foland, 1996).

3.4. Samples and analytical methods

Nine clinopyroxenes (augite: samples MSB3, MSH13, MSG3, MRG1, MRG9 and MY3) and amphiboles (hornblende: samples MS10, MB15 and MR15) separates (0.2 to 1g) were picked from gabbros (40 % to 45% of SiO_2) and essexites (50 % of SiO_2) of the Monteregian Hills

for N, He and Ar elemental and isotopic measurements (Table 1). Mineral separates were ultrasonically cleaned in water, ethanol and acetone for 20 minutes, dried overnight, and loaded in a ball mill type crusher. The crusher is made of a stainless steel cylinder containing a steel ball and it is connected to an extraction line by a bellow. The crusher and the samples were baked at 80 °C overnight. Samples were manually crushed for 5 minutes. Recovery of crushed samples after each analysis showed that mm-scale minerals were reduced to a powder..

Nitrogen isotopic analyses were carried out at the Ocean Research Institute of the University of Tokyo. Gases released from the samples were expanded into a stainless steel high-vacuum line (Takahata et al., 1998). Gases were completely recovered from the crushing mill by adsorption onto a NUPRO® sintered stainless steel filter (0.5 μm pores) at liquid nitrogen temperature. After 20 minutes, the trap was heated at ambient temperature for 15 minutes to release the absorbed gas. Water, CO_2 and other condensable gases were removed by condensation on a Pyrex cold trap at liquid nitrogen temperature. To remove hydrocarbons from nitrogen, the non-condensable fraction reacted with O_2 produced by heating a CuO trap at 850°C for 5 minutes. The gas mixture was then exposed to a platinum foil heated at 1000°C. Hydrocarbons were then oxidized to CO_2, and hydrogen to water and adsorbed on the Pyrex cold trap. Oxygen was resorbed into the CuO trap at 600°C and then at 450°C. Purified N was concentrated in the final section of the line by adsorbing on a second NUPRO® sintered steel filter at liquid N temperature prior to the isotopic analyses. Nitrogen isotopes were measured in a static magnetic-sector mass spectrometer VG3600 equipped with a Faraday cup, calibrated against a purified atmospheric N standard measured at the same N amount than the sample, to avoid mass fractionation corrections. Generally, 1 nanomole of N_2 gives an ion current of 4 V on the Faraday cup on mass 28. Details on the extraction procedures and general performances of the instruments are given in Takahata et al., 1998. Measured nitrogen blanks were from 30 to 700 times lower than the amount of N released from the mineral separates. The error on the $\delta^{15}N$ values reported in Table 1 is the propagated error on the isotopic measurement of N on the sample and on the standard, both assumed at 2σ. The total error on the N amount is estimated at 5%.

The ^{40}Ar was also measured on the Faraday cup of the GV3600 but the low amount measured in our samples was between 1.5 to 5 times the blanks and thus rejected. Thus,

analysis of the ^{4}He, ^{36}Ar, ^{38}Ar and ^{40}Ar isotopes were done at the Noble Gas Laboratory of the GEOTOP-UQAM, Montréal. Mineral separates were crushed for about 5 minutes in a copy of the ball mill type crusher mentioned earlier in this section. Gases were then released in a stainless steel extraction and purification line. Reactive gases were removed using 99.8% pure Ti and ST-707 alloy (SAES) getters heated to 650°C and 250°C respectively and subsequently cooled to room temperature. Isotopic measurements were done on a quadrupole mass spectrometer Prisma-200C from Pfeiffer®, equipped of a Faraday cup and a channeltron. The instrument was calibrated for isotopic composition and gas concentration using a purified air standard. Measured argon blanks were from 8 to 60 times lower than the amount of Ar released from the mineral separates. The analytical uncertainties on the He and Ar amounts and isotopic ratios reported in Table 1 are the propagated error on the elemental and isotopic measurement of the sample and of the standard, both assumed at 2σ.

3.5. Results

The N_2 content and $\delta^{15}N$ values measured in gas inclusions from clinopyroxenes and amphiboles are reported in Table 1. The N_2 content in the released gasses range from 8.8 x 10^{-11} to 5.9 x 10^{-9} mol/g and do not correlate with the $\delta^{15}N$ values (Fig. 2). The measured $\delta^{15}N$ (and the Ar isotopic ratios) are not related to the mineral phase analyzed (Yokochi et al., 2009). Clinopyroxenes from Mts Rougemont and Yamaska (MGR9 and MY3) show the lowest $\delta^{15}N$ values (respectively -7.6±0.5‰ and -7.4±1.4‰). Higher $\delta^{15}N$ values (+7.0±0.8‰, +8.1±1.2‰ and +10.5±1.9‰) have been measured in two amphiboles (MS10, MB15) of Mts Shefford and Brome and one clinopyroxene from Mt Rougemont (MGR1). Clinopyroxene separates of Mts St Bruno (MSB3), St Hilaire (MSH13) and St Gregoire (MSG3) and an amphibole separate from Mt Royal (MR15) have intermediate $\delta^{15}N$ values ranging from -5.8±1.7‰ to -1.0±0.4‰ (Table 1). No geographic distribution of the $\delta^{15}N$ values is observed in contrast to Nd and Sr isotopes that show an eastward evolution in their isotopic signature (Roulleau and Stevenson, 2010).

The ^{4}He amounts range from 5.09 x 10^{-12} to 3.8 x 10^{-11} mol/g (Table 1). These values are 1-2 orders of magnitude higher than those measured by crushing mineral separates

representing SCLM and OIB sources (Fischer et al., 2005). However, Marty and Zimmermann (1999) measured similar He amounts in MORBs. The calculated $^{4}He/^{40}Ar^{*}$ ratios range from as high as 10 (MSG3 and MS10; Table 1) to as low as 1.9 (MSB3; Table 1). The radiogenic production ratio of the mantle for $^{4}He/^{40}Ar^{*}$ range from 1.6 to 4.2, reflecting production over 4.5 Ga and for present day, respectively with assumed K/U ratios of 12700 and Th/U ratios of 3.5 (Graham, 2002).

The ^{40}Ar amounts range from 3.28×10^{-12} to 1.9×10^{-11} mol/g (Table 1). The $^{40}Ar/^{36}Ar$ ratios range from 332±20 (MSG3) to 632±38 (MY3). The $^{40}Ar/^{36}Ar$ ratios in our samples are relatively low compared to those obtained from continental xenoliths (from 300 up to 16,000; Matsumoto et al., 2002; Fischer et al., 2005; Yokochi et al., 2009) but significantly higher than the atmospheric ratio of 295.5 (Ozima and Podosek, 1983). The measured $^{38}Ar/^{36}Ar$ ratios are significantly higher (from 0.1986±0.0222 to 0.2485±0.0154) than the atmospheric value of 0.1880 (Ozima and Podosek, 1983). Interestingly, the excess of ^{40}Ar compared to the atmospheric value (namely the $^{40}Ar^{*} = {}^{40}Ar - 295.5 \times {}^{36}Ar$) is correlated with excesses of ^{38}Ar compared to the atmospheric value (here reported as $^{38}Ar^{*}$; Fig. 3). High $^{38}Ar/^{36}Ar$ ratios are reported for diamonds samples from Zaire (Wada and Matsuda, 1998), Archean cherts (Sano et al., 1994) and natural gases which show mantle-like Ne and Xe isotopic signatures (Xu et al., 1995). High $^{38}Ar/^{36}Ar$ ratios are generally attributed to excess ^{38}Ar produced by nuclear reactions such as $^{35}Cl\ (\alpha,p)^{38}Ar$ (e.g., Wada and Matsuda, 1998).

3.6. Discussion

3.6.1. Elemental and isotopic fractionation: degassing or source effects?

Before using the isotopic compositions of this study to discriminate possible mantle sources in our samples we need to evaluate whether the isotopic ratios have been fractionated during the physical processes related to melt degassing and gas inclusion formation (e.g., Marty and Zimmermann, 1999; Cartigny et al., 2001). The $^{4}He/^{40}Ar^{*}$ ratio is one of the most sensitive indicators of degassing because the solubility of He and Ar in silicate melts differs by one order of magnitude (Carroll and Stolper, 1993), resulting in an increase of the

$^4He/^{40}Ar^*$ ratio in residual gas with increasing the degree of degassing. Moreira and Sarda (2000) observed an inverse correlation between the $^4He/^{40}Ar^*$ and the $^{40}Ar^*$ which is typical of the degassing of a melt with preferential loss of Ar and simultaneous increase of the $^4He/^{40}Ar^*$ ratio. A similar, but very rough relation is observed in our samples (Fig. 4) where the inverse of the $^{40}Ar^*$ concentration increases with an increasing $^4He/^{40}Ar^*$ ratio (except for sample MSG3). The process of melt degassing and $^4He/^{40}Ar^*$ fractionation can be modeled by using a "Rayleigh"-type distillation equation (Sarda and Graham, 1990):

$$R = R_0 \times F^{(\alpha-1)} \quad (1)$$

where R is the $^4He/^{40}Ar^*$ ratio in the residual gas phase after melt degassing, R_0 is the initial $^4He/^{40}Ar^*$ in the melt, F the fraction of remaining Ar in the residual gas phase and α is the fractionation factor that is equal to the ratio of the solubility constant S_{He}/S_{Ar} (Sarda and Graham, 1990). In Fig. 4, the evolution of the $^4He/^{40}Ar^*$ ratio and the $^{40}Ar^*$ content is modeled by starting from an initial composition equal to that measured in sample MSB3. Most of our samples show elemental abundance ratios compatible with fractionation from a degassing melt (Fig. 4).

Atmospheric contamination of the samples occurred alongside melt degassing (e.i. vesiculation and vesicle loss). Indeed, when the inverse of the ^{36}Ar concentration is plotted against the $^4He/^{36}Ar$ ratio (Fig. 5a) our samples lie on two straight lines indicating mixing of an atmospheric component (having a large ^{36}Ar concentration, left corner of the diagram) with two sources poorer in ^{36}Ar but richer in ^4He and with two ^4He initial concentrations given by the slopes of the respective straight lines. These two components could be the mantle and the crust, but this interpretation is not straightforward because the $^4He/^{36}Ar$ ratio is also modified by the solubility partitioning during melt degassing. If the $^4He/^{36}Ar$ ratio is plotted against the $^4He/^{40}Ar^*$ ratio we can indeed observe a rather complicated history of degassing and air contamination (not necessarily air but an atmospheric component in the crust, i.e. crustal contamination; Fig. 5b). In Fig. 5b, we assume a theoretical initial upper mantle source with $^4He/^{36}Ar$ = 7000 (Hiyagon et al., 1992) and $^4He/^{40}Ar^*$ = 2.5 (Graham, 2002). Air contamination of the initial melt would affect primarily the $^4He/^{36}Ar$ by decreasing of the ratio to the pole of air (straight line labeled "1"; Fig. 5b). After, melt degassing occurs

which would affect the $^{4}He/^{40}Ar^{*}$ by increasing the ratio to the upper right corner of diagram (dashed line labeled "2"; Fig. 5b). Thus, all variation in $^{4}He/^{40}Ar^{*}$ and $^{4}He/^{36}Ar$ ratios for the Monteregian samples can be explain by these two successive processes excepted for the sample MSG3 that was affected differently (left side of Fig. 5b). This sample have high $^{4}He/^{40}Ar^{*}$ and low $^{4}He/^{36}Ar$ ratios. After that the degassing occurred (dashed line labeled "2", Fig.5b), the atmospheric ^{36}Ar intake was produced at depth (probably through assimilation of crustal rocks) (straight line labeled "3"; Fig. 5b). This produces the shift of values towards the left of the diagram.

Degassing could potentially affect the $\delta^{15}N$ values and the Ar isotopic ratios of mineral separates (Fischer et al., 2005). Indeed, during degassing, the residual gas phase in the melt is enriched in heavier isotopes while lighter ones diffuse out of the melt and they are lost during vesiculation. In this case a direct relationship should be observed between the $^{40}Ar/^{36}Ar$ and $^{38}Ar/^{36}Ar$ ratios and between the inverse of the ^{36}Ar concentration and the $^{38}Ar/^{36}Ar$ ratio (or the $^{40}Ar/^{36}Ar$ ratio). This seems indeed the case for our samples (Figs. 6a, b). This process can be modeled again using equation (1) where R is the $^{38}Ar/^{36}Ar$ or $^{40}Ar/^{36}Ar$ isotopic ratio in the residual gas phase after melt degassing, R_0 initial Ar isotopic ratio prior of degassing, F the fraction of remaining Ar in the residual gas phase and α is the fractionation factor that is equal to the square root of the ratio of the two masses of the isotopes (e.g., $\sqrt{36/38}$) (Matsumoto et al., 2004).

Results of the modeling show that the isotopic fractionation does not match with the observed isotopic pattern (Fig. 6a). Further, to obtain the fractionated values of $^{38}Ar/^{36}Ar$ and $^{40}Ar/^{36}Ar$ observed in the gas inclusions requires complete degassing of the melt ($F = 1 \times 10^{-6}$), while ^{36}Ar data suggest that "only" 86% of the gas has been lost (Fig. 6b). The $^{38}Ar/^{36}Ar$ and $^{40}Ar/^{36}Ar$ ratios observed in the clinopyroxenes and amphiboles of Monteregian Hills could thus indicate a mixing between an atmospheric component and a component richer in radiogenic $^{40}Ar^{*}$ and possibly nucleogenic $^{38}Ar^{*}$ produced by the reaction $^{35}Cl\ (\alpha,p)^{38}Ar$. It is difficult to assess if this excess was introduced by Cl-rich crustal fluid contaminants (crustal source) or produced in the melt phase (mantle source). In the mantle, this nuclear reaction is assumed to be a minor process because of the low U, Th and Cl content. Cubic diamonds from mantle xenoliths of Zaire showed $^{38}Ar/^{36}Ar$ ratios as high as 0.1967 (Wada and

Matsuda, 1998), but calculations indicated that U content of 100 ppm and 10^9 years were required to produce the observed $^{38}Ar^*$ excess (Wada and Matsuda, 1998).

Degassing of the melt could also have fractionated the $\delta^{15}N$ values but a lack of relationship between $\delta^{15}N$ and N_2 contents (Fig. 2) and between $^4He/^{40}Ar^*$ ratios and $\delta^{15}N$ (not reported here) dismiss this hypothesis. Thus we can regard the isotopic ratios of Ar and N as indicative of the volatile sources of the Monteregian Hills.

3.6.2. N and Ar isotopic signatures of the Monteregian Hills

Fig. 7 shows the variations of the $\delta^{15}N$ values as a function of $^{40}Ar/^{36}Ar$ ratios in the Monteregian Hills. Dashed and dotted areas indicate isotopic variations measured in mantle samples representing MORBs (Marty and Humbert, 1997; Marty and Zimmermann, 1999), OIBs (Marty and Dauphas, 2003; Fischer et al., 2005) and SCLM (Matsumoto et al., 2002) measured using the crushing method. We have not included N data obtained using the heating method because this method has been shown to release N from the mineral matrix that is heterogeneous in isotopic composition and likely modified by surface-derived N (Marty and Zimmermann, 1999). Boxes labeled respectively "air", "sediment", "upper Mantle" and "OIB?" indicate the isotopic values of atmosphere defined by $\delta^{15}N = 0‰$ and $^{40}Ar/^{36}Ar = 295.5$ (Ozima and Podosek, 1983), crust ($\delta^{15}N = +7‰$ and $^{40}Ar/^{36}Ar \geq 300$; Sano et al., 2001), upper mantle and lower mantle, respectively. The upper mantle $\delta^{15}N$ value should be -5±2‰ (Marty and Dauphas, 2003), though values as low as -10‰ has been observed in MORB-derived lavas and thermal springs of Iceland (Marty et al., 1991; Fischer et al., 2005). Here we assumed a MORB-like upper mantle with a range of $\delta^{15}N$ from -10 to -3‰ and a $^{40}Ar/^{36}Ar$ of 35,000 ± 5000 by taking into account the observed variability in MORBs and popping rocks (Moreira et al., 1998; Raquin et al., 2008). The N isotopic composition of the lower mantle is less constrained. Data obtained from carbonatites and OIBs suggest that the lower mantle should have a $\delta^{15}N = +3 \pm 2‰$ (Dauphas and Marty 1999; Marty and Dauphas 2003). Based on the oxygen isotopic composition of materials derived from the Earth's mantle, Javoy (1997) has suggested that the Earth formed with a dominant contribution from enstatite chondrite-like (EH) meteorites. If the lower mantle is the reservoir containing primordial volatiles, then the $\delta^{15}N$ value should be close to that found in EH-type meteorites,

which is -45‰ (Javoy, 1997). A $\delta^{15}N$ value of -25‰ measured in peridotitic diamonds support this hypothesis (Cartigny et al., 1997). Based on very negative values measured in OIBs, by the heating method, Mohapatra et al. (2009) suggested that the N isotopic signature of OIBs should be -25‰ (box labeled "OIB?"). The best estimate for the $^{40}Ar/^{36}Ar$ value in lower mantle is about 8000 (Trieloff et al., 2000) as measured in dunites from Loihi seamount.

Two samples of the Monteregian Hills intrusions (MS10 and MB15) fall close to the "crustal" source while all other samples fall within the field of the MORB (more precisely their values are close to that of E-MORB measured by Marty and Zimmermann, 1999). The N and Ar isotopic compositions of the Monteregian Hills are consistent with a mixing between an atmospheric component and the upper mantle reservoir (Fig. 7). The data are also consistent with the mixing between an OIB source and the atmosphere, but the resulting mixing hyperbola would be close to a straight line, which means that the curvature parameter $K_{mix}= [^{36}Ar/^{14}N]_{OIB}/[^{36}Ar/^{14}N]_{air}$ should be close to 1. However, this is not the case as the $[^{36}Ar/^{14}N]_{OIB} = 7.4 \times 10^5$ and the $[^{36}Ar/^{14}N]_{air}$ equal to 2.47×10^4 (Marty and Dauphas, 2003). Thus, a calculated mixing hyperbola between a hypothetical OIB source and the atmosphere, using the correct K_{mix} (dashed line; Fig. 7) cannot explain the N and Ar isotopic composition of the Monteregian Hills.

Figure 8 represents the variations of the $\delta^{15}N$ values as a function of $N_2/^{36}Ar$ molar ratios in the Monteregian Hills. Symbols are the same as in Fig. 7. The $N_2/^{36}Ar$ ratios of MORBs and the crust are from Sano et al. (1998). Again most of the samples from the Monteregian Hills show N and Ar isotopic and elemental ratios that can be explained by the mixing of an atmospheric source and an upper mantle source (Fig. 8). The data cannot be explained by a mixing between a hypothetical OIB source (Mohapatra et al., 2009) and the atmosphere (dashed line; Fig. 8), neither do they fall within the OIB field defined by data from Marty and Dauphas (2003).

3.6.3. Correlation between nitrogen lead isotopes and trace elements: an upper mantle signature

The isotopic fingerprints of volatiles preserved in mantle-derived samples (e.g. $^3He/^4He$) have often been compared to the isotopic signature of radiogenic elements such as

Sr-Nd-Pb (Kurz et al., 1982) in order to identify mantle sources, although the relationship remains unclear and there are no simple global constraints (Graham, 2002). More recently, Sarda et al. (1999) showed that there is a correlation between $^{206,207,208}Pb/^{204}Pb$ ratios and maximum $^{40}Ar/^{36}Ar$ values measured in the North Atlantic MORBs. The authors argued that this correlation is due to mixing between a degassed-depleted upper mantle (DMM; $^{40}Ar/^{36}Ar$, 40,000 and $^{206}Pb/^{204}Pb$ of 17.8) and a recycled component in the mantle (HIMU) that has non-radiogenic Ar as a consequence of recycling of atmospheric Ar ($^{40}Ar/^{36}Ar$ = 300).

Here we show for the first time that there is a broad correlation between the variations of $\delta^{15}N$ values measured in the Monteregian Hills intrusions and the radiogenic isotopes of lead (data from Roulleau and Stevenson, 2010), particularly $^{208}Pb/^{204}Pb$ (Fig. 9a) and $^{207}Pb/^{204}Pb$ (Fig. 9b). Rough correlations with trace element ratios Ba/Nb and La/Nb are also observed (Fig.10a, b).

Samples of Mts Royal, St Bruno, St Hilaire and St Gregoire have Pb isotopic compositions comparable to those measured in North-Atlantic MORBs ($^{208}Pb/^{204}Pb$ = 39.25-38.80; GEOROC database). A Mt Rougemont sample (MRG9) shows a low $^{207}Pb/^{204}Pb$ of 15.01 and a $^{208}Pb/^{204}Pb$ ratio of 37.6 close to that measured in an Iceland MORB at Theistareykir ($^{207}Pb/^{204}Pb$ = 15.32, $^{208}Pb/^{204}Pb$ = 37.6) and representing the depleted mantle (DMM; Fischer et al., 2005). Sample MY3 from Mt Yamaska has slightly higher $^{207}Pb/^{204}Pb$ (15.55) and $^{208}Pb/^{204}Pb$ (38.6) ratios. Both samples show the most depleted $\delta^{15}N$ values of all Monteregian Hills, -7.4 ± 1.4‰ and -7.6 ± 0.5‰, respectively (Table 1; Figs. 9a,b). However, even if we accept that sample MY3 represents the DMM source, then certainly the $^{207}Pb/^{204}Pb$ ratio for sample MRG9 is too low to be considered an upper mantle source. Low ratios such as these are more characteristic of Archean lower crust (Davis et al., 1996) and the Archean lithospheric mantle beneath North America ($^{207}Pb/^{204}Pb$ = 14.5-15.30 and $^{208}Pb/^{204}Pb$ (34.46-36.42; Schmidberger et al., 2007). Studies based on peridotite xenoliths as well as surface heat flow estimations also suggest a strongly depleted U–Th–K environment in the SCLM of the Canadian Shield (Rudnick and Nyblade, 1999), which could explain the non- radiogenic Pb isotopic signatures.

The light $\delta^{15}N$ value measured in the MRG9 sample excludes the possibility of the incorporation of Archean crust which is characterized by positive $\delta^{15}N$ values. Thus, the

involvement of an Archean, U-Th-depleted SCL mantle is more consistent with the negative $\delta^{15}N$ values observed for MRG9. Recently, Castro et al. (2009) have found He and Ne in brines from the Michigan Basin with a primordial, solar-like composition. Because there has been no plume-related magmatism in the Great Lakes region for 1 billion years, Castro et al. (2009) suggested that the primordial signature is accounted for by a shallow buoyant refractory reservoir in the Archean SCLM which was preserved from mantle convection and was thus able to record ancient, solar-like, primordial He and Ne. The $\delta^{15}N$ of the primordial mantle was likely more negative than the present day value, as suggested by values measured in Archean diamonds (-25‰; Cartigny et al., 1998). The increase in the N isotopic composition of the present day mantle reflects progressive enrichment of ^{15}N by recycling of continental crust (Pinti, 2002). Thus, the low $\delta^{15}N$ values measured in samples MY3 and MRG9, (*i.e.*; lower than those normally found in MORBs; -3±2‰; Marty and Zimmermann, 1999) could indicate an isolated Archean SCLM reservoir stacked beneath the Monteregian Hills. Interestingly, a solar-like He, Ne and Ar isotopic signature has been identified in brines of the St-Lawrence Lowlands, at a site only a hundred km away from the Monteregian Hills (Pinti et al., 2010).

Trace element ratios for the Monteregian Hills present a geochemical signature close to those typical of MORBs but with some noticeable difference (Figs. 10a, b). Indeed, the measured Ba/Nb and La/Nb ratios indicate a more enriched source in incompatible elements than those feeding MORBs. The range of the Ba/Nb (5-10) and La/Nb (0.2-1.5) ratios are characteristic of continental alkaline rocks (Furman, 2007; Melluso and Morra, 2000; Späth, 1996), consistent with the geochemical character of a continental lithospheric mantle (SCLM) feeding the Monteregian Hills. With the exception of sample MB15 in the Pb vs. $\delta^{15}N$ and Ba/Nb vs. $\delta^{15}N$ plots and sample MSH13 in the La/Nb vs. $\delta^{15}N$ plot, a series of best fit mixing hyperbola were obtained for the $^{208}Pb/^{204}Pb$ vs. $\delta^{15}N$, $^{207}Pb/^{204}Pb$ vs. $\delta^{15}N$, Ba/Nb vs. $\delta^{15}N$ and La/Nb vs. $\delta^{15}N$ data by applying a simple inverse method (Albarède, 1995; pages 267-295) The isotopic and trace element variability observed in the Monteregian Hills rocks (Figs. 9 and 10) can be explained by a first-order binary mixing between a MORB-like source contaminated by the crust. In all these plots, the lower mantle is represented by Loihi Seamount data from the literature (Sano et al., 2001) and seems to be excluded as melt source of the Monteregian Hills.

3.7. Conclusion

The N, Ar and He isotopic variations of mineral separates from the Monteregian Hills gabbros and essexites (Figs. 7-8) and their correlation with Pb isotopes and trace elements ratios (Figs. 9-10) suggests that this igneous province was formed by melting within the SCLM rather than the result of the passage of the Great Meteor hot-spot (Sleep, 1990). To obtain an unequivocal proof would require precise analyses of the He ($^{3}He/^{4}He$) and Ne ($^{20}Ne/^{22}Ne$) ratios in these minerals. However, correlations between He and Ar isotopes (Figs. 6a, b) indicate that these rocks were affected by complex processes of melt degassing and crustal/atmospheric depth/surface contamination, possibly by metasomatic fluids. We doubt that a pristine He mantle signature has been preserved. Indeed, Sasada et al. (1997) measured He and Xe isotopes in the carbonatites of Oka, but the He and Ne isotopic signatures were strongly altered by radiogenic/nuclegeonic production of ^{4}He, ^{20}Ne and $^{21}Ne^{*}$ possibly originating from U-Th-rich fluids. Sasada et al. (1997) also measured the $^{40}Ar/^{36}Ar$ ratios in the Oka carbonatites and obtained a range of values similar to the Monteregian Hills of this study (from 301 to 650). Orthomagmatic aqueous fluids liberated from the carbonatitic magmas were involved in the formation of hydrothermal rare element mineralization associated with carbonatites of Oka (Samson et al., 1995) and possibly these fluids participated in the production of radiogenic/nucleogenic noble gas isotopes in the system, diluting the pristine mantle isotopic signature, beyond recognition.

The results of our study suggest that the mantle sources of the Monteregian Hills were subcontinental mantle melts rather than deep asthenospheric melts related to the passage of the Great Meteor hot spot (Sleep 1990). It is possible that these melts ascended along what were originally Proterozoic faults of the Ottawa-Bonnechère rift to create the observed linear alignment of alkaline intrusions of the Monteregian Hills. These Proterozoic faults were reactivated by the opening of the North Atlantic Ocean which was concurrent with the formation of the Monteregian Hills.

Acknowledgements

DLP and RKS were supported by NSERC Discovery grant # XXX and XXX, respectively. This is GEOTOP contribution YYY.

References

Albarède, F., 1995. *Introduction to geochemical modeling.* Cambridge University Press.

Ballentine, C. J., Mazurek, M., and Gautschi, A., 1994. Thermal constraints on crustal rare gas release and migration: Evidence from Alpine fluid inclusions. Geochim. Cosmochim. Acta 58, 4333-4348.

Carroll, M. E., Stolper, E. M., 1993. Noble gas solubilities in silicate melts and glasses: New experimental results for argon and the relationship between solubility and ionic porosity. Geochim. Cosmochim. Acta 57, 5039-5051.

Cartigny, P., Boyd, S. R., Harris, J. W., Javoy, M., 1997. Nitrogen isotopes in peridotitic diamonds from Fuxian, China: the mantle signature. Terra Nova 9, 175-179.

Cartigny, P., Jendrzejewski, N., Pineau, F., Petit, E., Javoy, M., 2001. Volatile (C, N, Ar) variability in MORB and the respective roles of mantle source heterogeneity and degassing: the case of the Southwest Indian Ridge. Earth Planet. Sci. Lett. 194, 241-257.

Castro, M. C., Ma, L., Hall, C. M., 2009. A primordial, solar He-Ne signature in crustal fluids of a stable continental region. Earth Planet. Sci. Lett. 279, 174-184.

Dauphas, N., Marty, B., 1999. Heavy nitrogen in carbonatites of the Kola Peninsula: A possible signature of the deep mantle. Science 286, 2488-2490.

Davis, W. J., Garièpy, C., van Breemen, O., 1996. Pb isotopic composition of late Archaean granites and the extent of recycling early Archaean crust in the Slave Province, northwest Canada. Chem. Geol. 130, 255-269.

Eby, N., 1984. Monteregian Hills I. Petrography, major and trace element geochemistry and strontium isotopic chemistry of the western intrusions: Mont Royal, St. Bruno and Johnson. J. Petrol. 25, 421-452.

Eby, N., 1985. Monteregian Hills II. Petrography, major and trace element geochemistry and strontium isotopic chemistry of the western intrusions: Mont Royal, St. Bruno and Johnson. J. Petrol. 26, 418-448.

Eby, N., 1988. Geology and petrology of Mounts Johnson & St.-Hilaire, Monteregian Hills Petrographic Province. Annual Meeting (New York): Guidebook 29-43.

Faure, S., Tremblay, A., Angelier, J., 1996. State of intraplate stress and tectonism of northeastern America since Cretaceous times, with particular emphasis on the New

England-Quebec igneous province. Tectonophysics 255, 111-134.

Fischer, T., Takahata, N., Sano, Y., Sumino, H., Hilton, D., 2005. Nitrogen isotopes of the mantle: Insights from mineral separates. Geophys. Res. Lett. 32, L11305.

Fischer, T. P., Burnard, P., Marty, B., Hilton, D. R., Füri, E., Palhol, F., Sharp, Z. D., Mangasini, F., 2009. Upper-mantle volatile chemistry at Oldoinyo Lengai volcano and the origin of carbonatites. Nature 459, 77-80.

Fisher, C. M., 2006. An exotic southern and central Appalachian basement: Pb and Nd isotopic evidence. Graduate School of Vanderbilt University, Msc. Thesis.

Foland, K. A., Gilbbert, L. A., Sebring, C. A., Jiang-Feng, C., 1986. $^{40}Ar/^{39}Ar$ ages for plutons of the Monteregian Hills, Quebec: Evidence for a single episode of Cretaceous magmatism. Geol. Soc. Am. Bull. 97, 966-974.

Foland, K. A., Jiang-feng, C., Gilbbert, L. A., Hofmann, W. A., 1988. Nd and Sr isotopic signatures of Mesozoic plutons in northeastern North America. Geology 16, 684-687.

Furman, T., 2007. Geochemistry of East African Rift basalts: An overview. J. Afr. Earth Sci. 48, 147-160.

GEOROC, Geochemistry of Rocks of the Oceans and continents, 2006. Max Planck Institute für Chemie. http://georoc.mpch-mainz.gwdg.de/georoc/Entry.html.

Graham, D. W., 2002. Noble gas isotope geochemistry of mid-ocean ridge and ocean island basalts: Characterization of mantle source reservoirs. Rev. Mineral. Geochem. 47, 247-317.

Hiyagon, H., Ozima, M., Marty, B., Zashu, S., Sakai, H., 1992. Noble gases in submarine glasses from mid-oceanic ridges and Loihi seamount: Constraints on the early history of the Earth. Geochim. Cosmochim. Acta 56, 1301-1316.

Hofstetter, A., Bock, G., 2004. Shear-wave velocity structure of the Sinai subplate from receiver function analysis. Geophys. J. Int. 158, 67-84.

Javoy, M., 1997. The major volatile elements of the Earth: Their origin, behavior, and fate. Geophys. Res. Lett. 24, 177-180.

Kurz, M. D., Jenkins, W. J., Hart, S. R., 1982. Helium isotopic systematics of oceanic islands and mantle heterogeneity. Nature 297, 43-47.

Landoll, J. D., Foland, K. A., 1996. The formation of quartz syenite by crustal contamination: Mont Shefford and other Monteregian complexes, Quebec. Canadian Mineral. 34,

301-324.

Lustrino, M., Wilson, M., 2007. The circum-Mediterranean anorogenic Cenozoic igneous province. Earth-Science Rev. 81, 1-65.

Mariotti, A., 1984. Natural ^{15}N abundance measurements and atmospheric nitrogen standard calibration. Nature 311, 251-252.

Marty, B., Dauphas, N., 2003. The nitrogen record of crust-mantle interaction and mantle convection from Archean to Present. Earth Planet. Sci. Lett. 206, 397-410.

Marty, B., Gunnlaugsson, E., Jambon, A., Oskarsson, N., Ozima, M., Pineau, F., and Torssander, P., 1991. Gas Geochemistry of Geothermal Fluids, the Hengill Area, Southwest Rift-Zone of Iceland. Chem. Geol. 91, 207-225.

Marty, B., Humbert, F., 1997. Nitrogen and argon isotopes in oceanic basalts. Earth Planet. Sci. Lett. 152, 101-112.

Marty, B., Zimmermann, L., 1999. Volatiles (He, C, N, Ar) in mid-ocean ridge basalts: Assessment of shallow-level fractionation and characterization of source composition. Geochim. Cosmochim. Acta 63, 3619-3633.

Matsumoto, T., Honda, M., McDougall, I., Yatsevich, I., O'Reilly, S. Y., 2004. Isotope fractionation of neon during stepheating extraction? Terra Nova 16, 23-26.

Matsumoto, T., Orihashi, Y., Matsuda, J., Yamamoto, K., 2008. Argon isotope ratio of the plume-source deduced from high-resolution stepwise crushing extraction. Geochem. J. 42, 39-49.

Matsumoto, T., Pinti, D. L., Matsuda, J., Umino, S., 2002. Recycled noble gas and nitrogen in the subcontinental lithospheric mantle: Implications from N-He-Ar in fluid inclusions of SE Australian xenoliths. Geochem. J. 36, 209-217.

Melluso, L. and Morra, V., 2000. Petrogenesis of Late Cenozoic mafic alkaline rocks of the Nosy Be archipelago (northern Madagascar): relationships with the Comorean magmatism. J. Volcanol. Geotherm. Res. 96, 129-142.

Mohapatra, R. K., Harrison, D., Ott, U., Gilmour, J. D., Trieloff, M., 2009. Noble gas and nitrogen isotopic components in Oceanic Island Basalts. Chem. Geol. 266, 29-37.

Moreira, M., Kunz, J., Allegre, C., 1998. Rare gas systematics in Popping Rocks: Isotopic and elemental compositions in the upper mantle. Science 279, 1178-1180.

Moreira, M., Sarda, P., 2000. Noble gas constraints on degassing processes. Earth Planet. Sci.

Lett. 176, 375-386.

Ozima, M., Podosek, F. A., 1983. *Noble Gas Geochemistry*. Cambridge University Press, Cambridge.

Pinet, N., Tremblay, A., 1995. Tectonic evolution of the Quebec-Maine Appalachians; from oceanic spreading to obduction and collision in the Northern Appalachians American J. Sci. 295, 173-200.

Pinti, D. L., 2002. The isotopic record of Archean nitrogen and the evolution of the early earth. Trends in Geochemistry 2, 1-17.

Pinti, D. L., Béland-Otis, C., Tremblay, A., Castro, M. C., Hall, C. M., Marcil, J.-S., Lavoie, J.-P., Lapointe, R. (2010). Primordial He, Ne and Ar in brines of the St. Lawrence Lowlands, QC, Canada: thermal, tectonic and fluid evolution of a passive margin. Geochim. Cosmochim. Acta, submitted.

Raquin, A., Moreira, M. A., Guillon, F., 2008. He, Ne and Ar systematics in single vesicles: Mantle isotopic ratios and origin of the air component in basaltic glasses. Earth Planet. Sci. Lett. 274, 142-150.

Roulleau, E. R., Stevenson, R., 2010. Geochemical and isotopic (Nd-Sr-Hf-Pb) evidence for lithospheric mantle source in the formation of the alkaline Monteregian Province (Québec). Chap. 2, Ph.D. Thesis, UQAM, Montréal, 177pp.

Rudnick, R.L., Nyblade, A.A., 1999. The thickness and heat production of Archean lithosphere: constrains from xenolith thermobarometry and surface heat flow. In: Fei, Y., Bertka, C.M., Mysen, B.O. (Eds.), Mantle Petrology: Field Observations and High Pressure Experiments, Geochemical Society, pp. 3–12.

Samson, I. M., Liu, W., Williams-Jones, A. E., 1995. The nature of orthomagmatic hydrothermal fluids in the Oka carbonatite, Quebec, Canada: Evidence from fluid inclusions. Geochim. Cosmochim. Acta 59, 1963-1977.

Sano, Y., Nagao, K., Pillinger, C. T., 1994. Carbon and noble gases in Archean chert. Chem. Geol. 112, 327-342.

Sano, Y., Takahata, N., Nishio, Y., Fischer, T. P., Williams, S. N., 2001. Volcanic flux of nitrogen from the Earth. Chem. Geol. 171, 263-271.

Sano, Y., Takahata, N., Nishio, Y., Marty, B., 1998. Nitrogen recycling in subduction zones. Geophys. Res. Lett. 25, 2289-2292.

Sarda, P., Graham, D., 1990. Mid-ocean ridge popping rocks: implications for degassing at ridge crests. Earth Planet. Sci. Lett. 97, 268-289.

Sarda, P., Moreira, M., Staudacher, T., 1999. Argon-Lead Isotopic Correlation in Mid-Atlantic Ridge Basalts. Science 283, 666-668.

Sasada, T., Hiyagon, H., Bell, K., Ebihara, M., 1997. Mantle-derived noble gases in carbonatites. Geochim. Cosmochim. Acta 61, 4219-4228.

Schmidberger, S., Simonetti, A., Heaman, H., Creaser, A., Whiteford, S., 2007. Lu–Hf, in-situ Sr and Pb isotope and trace element systematics for mantle eclogites from the Diavik diamond mine: Evidence for Paleoproterozoic subduction beneath the Slave craton, Canada. Earth Planet. Sci. Lett. 254, 55-68.

Sleep, N., 1990. Monteregian hotspot track: a long-lived mantle plume. J. Geophys. Res. 95, 21983-21990.

Späth, A., leRoex, A.P., Duncan, R.A., 1996. The geochemistry of lavas from the Comores archipelago, western Indian ocean: petrogenesis and mantle source region characteristics. J. Petrol. 37, 961-991.

Takahata, N., Nishio, Y., Yoshida, N., Sano, Y., 1998. Precise isotopic measurements of nitrogen at the sub-nanomole level. Anal. Sci. 14, 485-491.

Trieloff, M., Kunz, J., Clague, D. A., Harrison, D., Allègre, C. J., 2000. The nature of pristine noble gases in mantle plumes. Science 288, 1036-1038.

Wada, N., Matsuda, J., 1998. A noble gas study of cubic diamonds from Zaire: constraints on their mantle source. Geochim. Cosmochim. Acta 62, 2335-2345.

Wearer, B. L., 1991. Trace element evidence for the origin of ocean-island basalts. Geology 19, 123-126.

Wen, J., Bell, K., Blenkinsop, J., 1987. Nd and Sr isotope systematics of the Oka complex, Quebec, and their bearing on the evolution of the sub-continental upper mantle. Contrib. Mineral. Petrol. 97, 433-437.

Xu, S., Nakai, S., Wakita, H., Wang, X., 1995. Mantle-derived noble gases in natural gases from Songliao Basin, China. Geochim. Cosmochim. Acta 59, 4675-4683.

Yokochi, R., Marty, B., Chazot, G., Burnard, P., 2009. Nitrogen in peridotite xenoliths: Lithophile behavior and magmatic isotope fractionation. Geochim. Cosmochim. Acta 73, 4843-4861.

Table 1: N, Ar, and He isotopic compositions of the Monteregian Hills

Locality	Samples	Mineral	Weight (g)	N_2 (10^{-10} mol/g)	$\delta^{15}N$ ‰ vs. Air	Weight (g)	^4He (10^{-12} mol/g)	^{40}Ar (10^{-12} mol/g)	$^{38}Ar/^{36}Ar$	$^{40}Ar/^{36}Ar$	$N_2/^{36}Ar$	$^4He/^{40}Ar^*$
Mount Royal	MR15	Amph	0.5906	2.71 ±0.14	-2.4 ±1.1	0.5147	5.26 ±0.24	5.46 ±0.43	0.2149 ±0.0240	531.4 ±58.6	26319 ±3410	2.2 ±0.2
St Bruno	MSB3	Cpx	0.5906	59.24 ±2.96	-3.6 ±0.6	0.3772	12.06 ±0.54	18.97 ±1.48	0.1986 ±0.0222	448.3 ±49.4	140047 ±11392	1.9 ±0.1
St Hilaire	MSH13	Cpx	0.6220	2.44 ±0.12	-5.8 ±1.7	0.3909	35.80 ±3.41	16.52 ±0.69	0.2111 ±0.0131	594.5 ±35.5	8768 ±621	4.3 ±0.5
St Gregoire	MSG3	Cpx	0.8555	7.34 ±0.37	-1.0 ±0.4	0.3983	8.99 ±0.86	7.91 ±0.33	0.1963 ±0.0121	331.7 ±19.8	30774 ±2709	10.4 ±0.1
Rougemont	MRG1	Cpx	0.7526	0.88 ±0.04	10.5 ±1.9	-	-	-	-	-	-	-
Rougemont	MRG9	Cpx	1.0068	18.38 ±0.92	-7.6 ±0.5	0.4828	11.46 ±1.09	10.13 ±0.42	0.2013 ±0.0125	408.4 ±24.4	74067 ±6017	4.1 ±0.2
Yamaska	MY3	Cpx	0.5709	2.19 ±0.11	-7.4 ±1.4	0.5505	6.55 ±0.62	2.38 ±0.10	0.2485 ±0.0154	631.6 ±37.7	58118 ±8215	5.2 ±0.7
Shefford	MS10	Amph	0.5146	3.77 ±0.19	7.0 ±0.8	0.4773	38.12 ±3.63	8.00 ±0.33	0.2219 ±0.0137	552.9 ±33.0	26054 ±2285	10.2 ±1.1
Brome	MB15	Amph	0.4855	3.01 ±0.15	8.1 ±1.2	0.5605	5.09 ±0.48	3.28 ±0.14	0.2414 ±0.0150	539.6 ±32.2	49449 ±6089	3.4 ±0.3
Air					0.0				0.1880	295.5	24804	5.60E-04

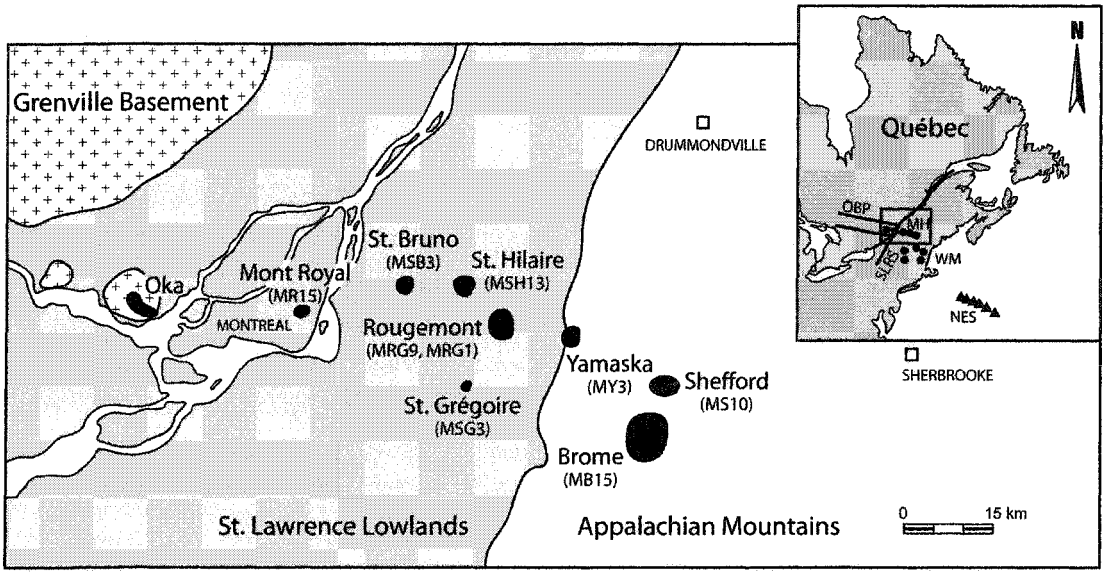

Figure 1. Location of the Monteregian Hills showing the distribution of Cretaceous magmatism. In the smaller figure, the position of the New England Seamounts (NSE) and the White Mountains (WM) which were supposedly formed by the Great Meteor hot spot are also reported. Other symbols: SLRS = St Lawrence Rift System; OBP: Ottawa-Bonnechere Paleo-rift, MH: Monteregian Hills.

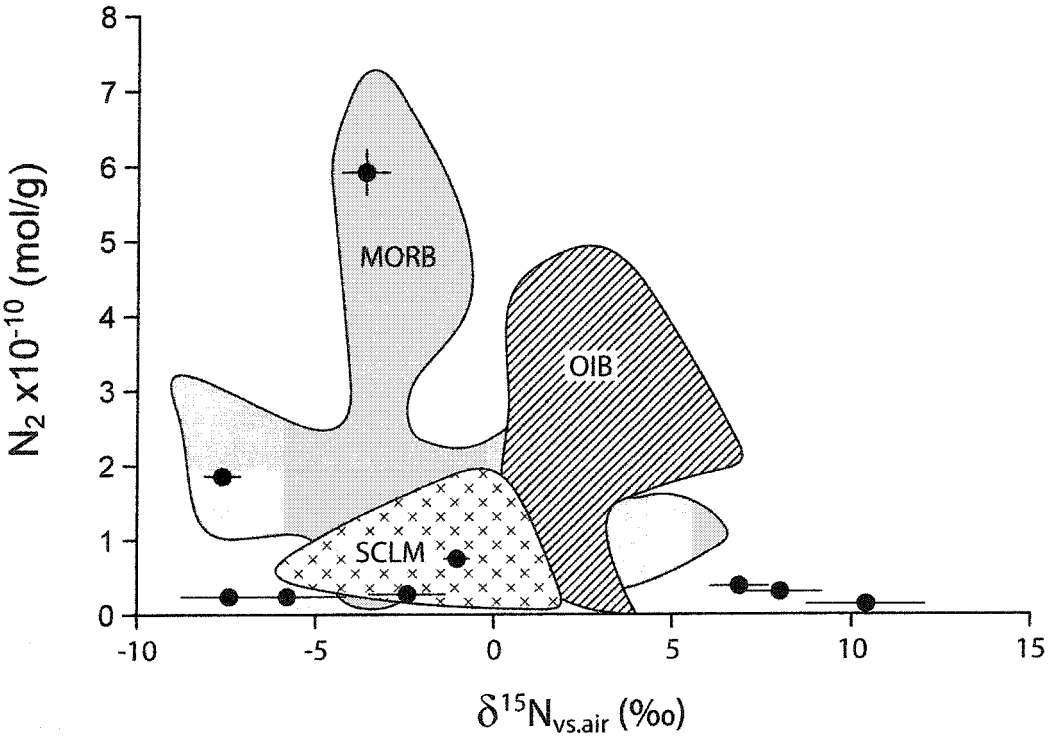

Figure 2. $\delta^{15}N$ values vs. N_2 content in the Monteregian Hills mineral separates. Dashed and dotted areas represent values obtained by crushing of mineral separates or whole rock of MORBs (Marty and Humbert, 1997; Marty and Zimmermann, 1999), OIBs (Fischer et al., 2005; Marty and Dauphas, 2003) and SCLM (Matsumoto et al., 2002).

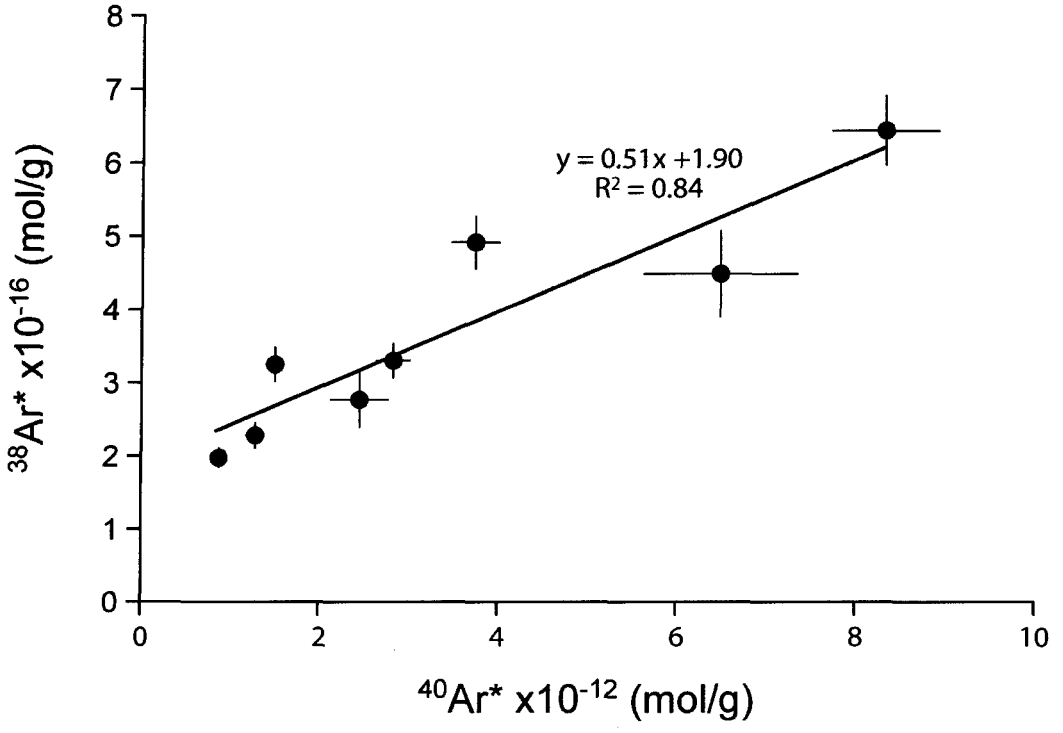

Figure 3. Plot of the excesses of nucleogenic/radiogenic $^{38}Ar^*$ and $^{40}Ar^*$.

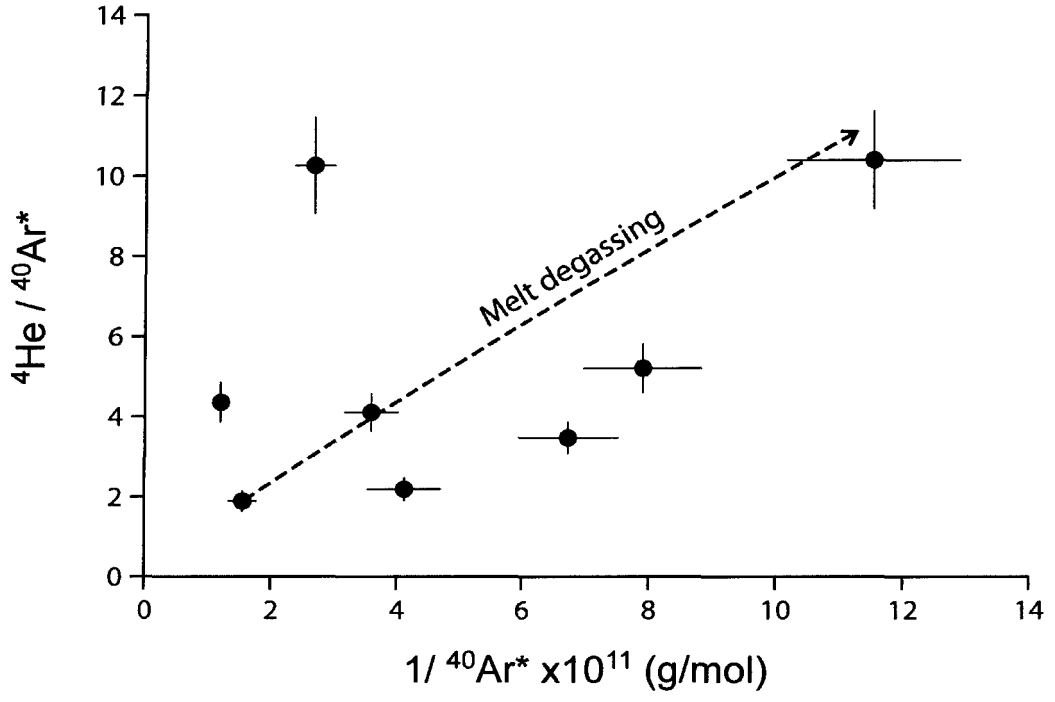

Figure 4. The $^4He/^{40}Ar^*$ ratio vs. $1/^{40}Ar^*$ content measured in the Monteregian Hills mineral separates, which suggests elemental fractionation caused by melt degassing. The dashed line illustrates the degassing path calculated by using a Rayleigh distillation (see text for explanation).

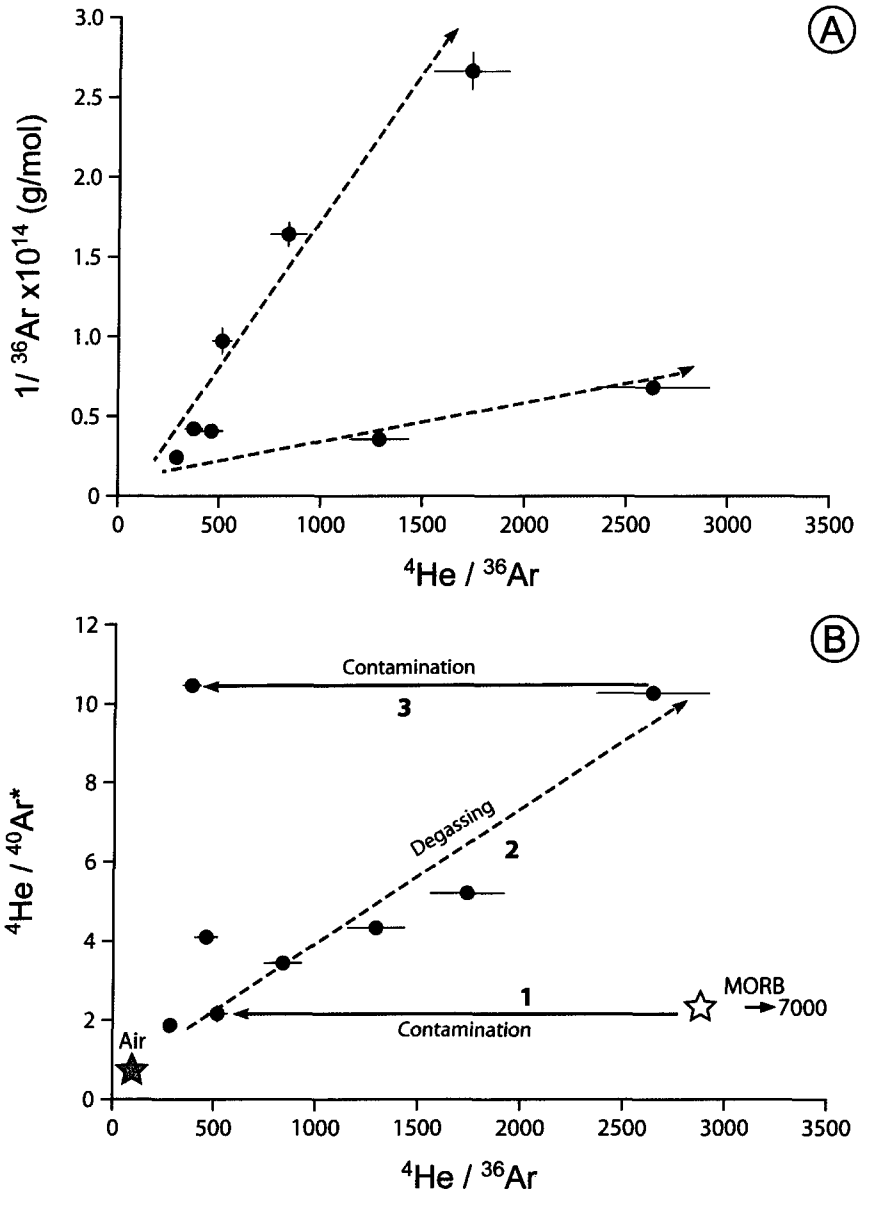

Figure 5. a) The $1/^{36}Ar$ abundance vs. the $^{4}He/^{36}Ar$ ratio showing the air/crustal contamination of two distinct sources characterized by different ^{4}He abundance. **b**) $^{4}He/^{40}Ar^{*}$ vs. $^{4}He/^{36}Ar$ ratios which suggests at least two episodes of air/crustal contamination and one melt degassing of the magmas of the Monteregian Hills

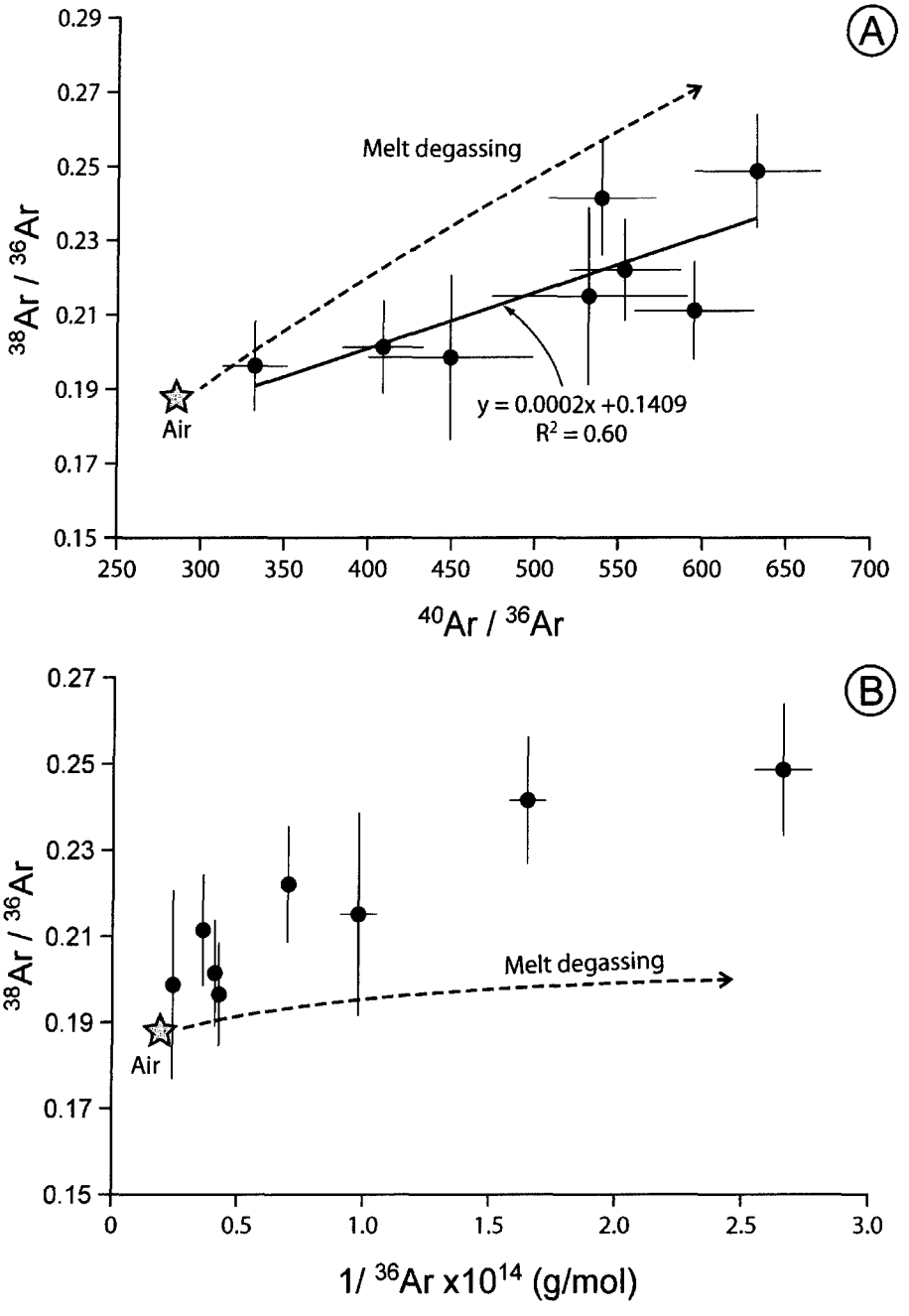

Figure 6. a) $^{38}Ar/^{36}Ar$ ratios vs. $^{40}Ar/^{36}Ar$ ratios and **b)** $^{38}Ar/^{36}Ar$ ratios vs. $1/^{36}Ar$ contents. The dashed line labeled "melt degassing" represents the isotopic variations during a "Rayleigh" distillation provoked by melt degassing. The isotopic variations of Ar cannot be explained by this process.

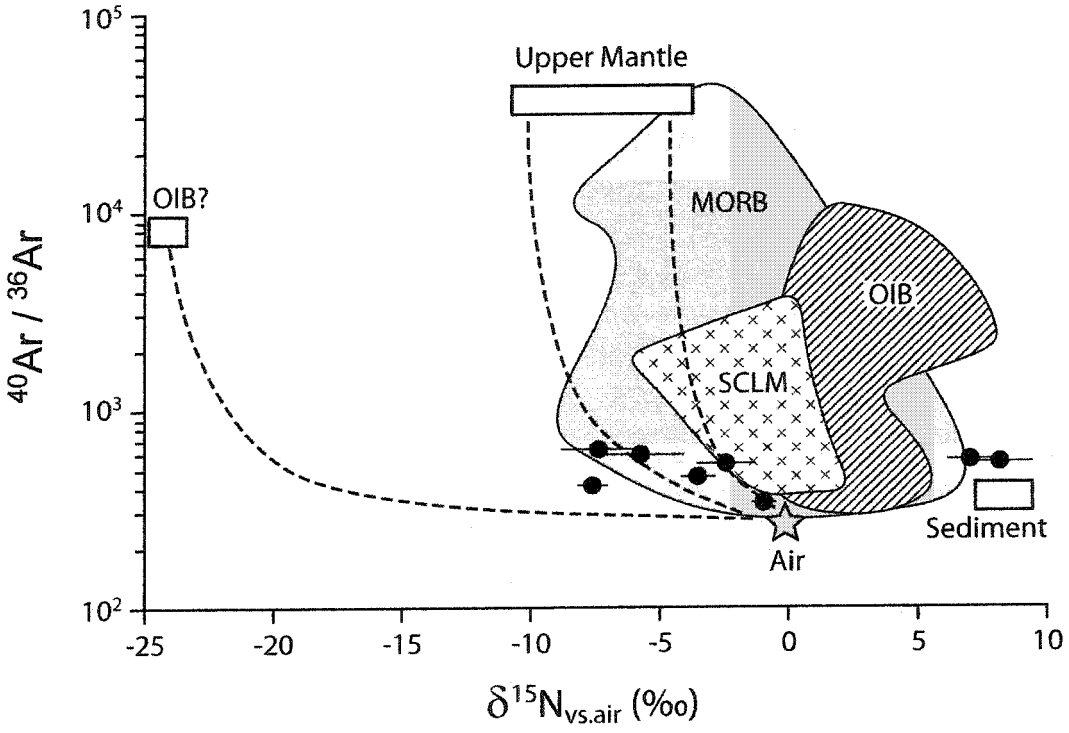

Figure 7. $\delta^{15}N_{vs.\ air}$ values vs. $^{40}Ar/^{36}Ar$ ratios measured in the Monteregian Hills mineral separates (black dots). Dashed and dotted areas represent N isotopic values measured by crushing in mineral separates and whole rocks in MORBs, OIBs and SCLM. References to literature data are reported in the text. The dashed lines represent mixing model between air and the upper (Sano et al., 1998) and lower mantle (OIB? following Mohapatra et al., 2009).

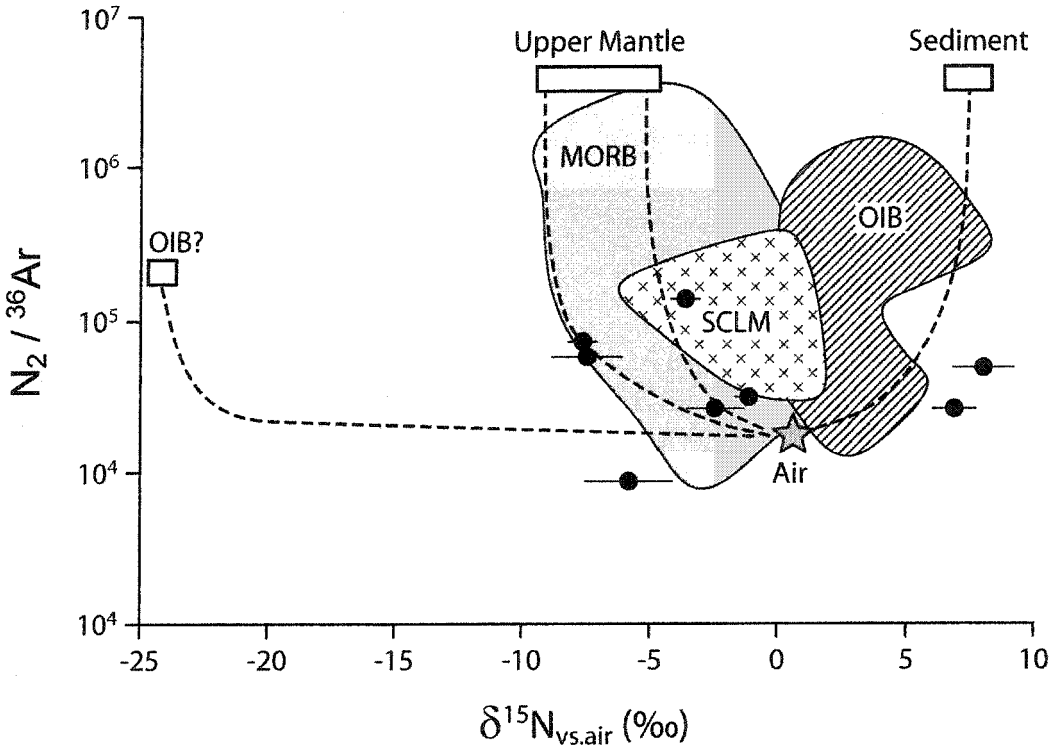

Figure 8. $\delta^{15}N$ values vs. the $N_2/^{36}Ar$ ratios measured in Monteregian Hills minerals separates. Meaning of the dashed and dotted areas, and boxes are the same as in the Fig. 7. The dashed lines represent mixing model between air and the upper (Sano et al., 1998) and lower mantle (OIB? following Mohapatra et al., 2009)

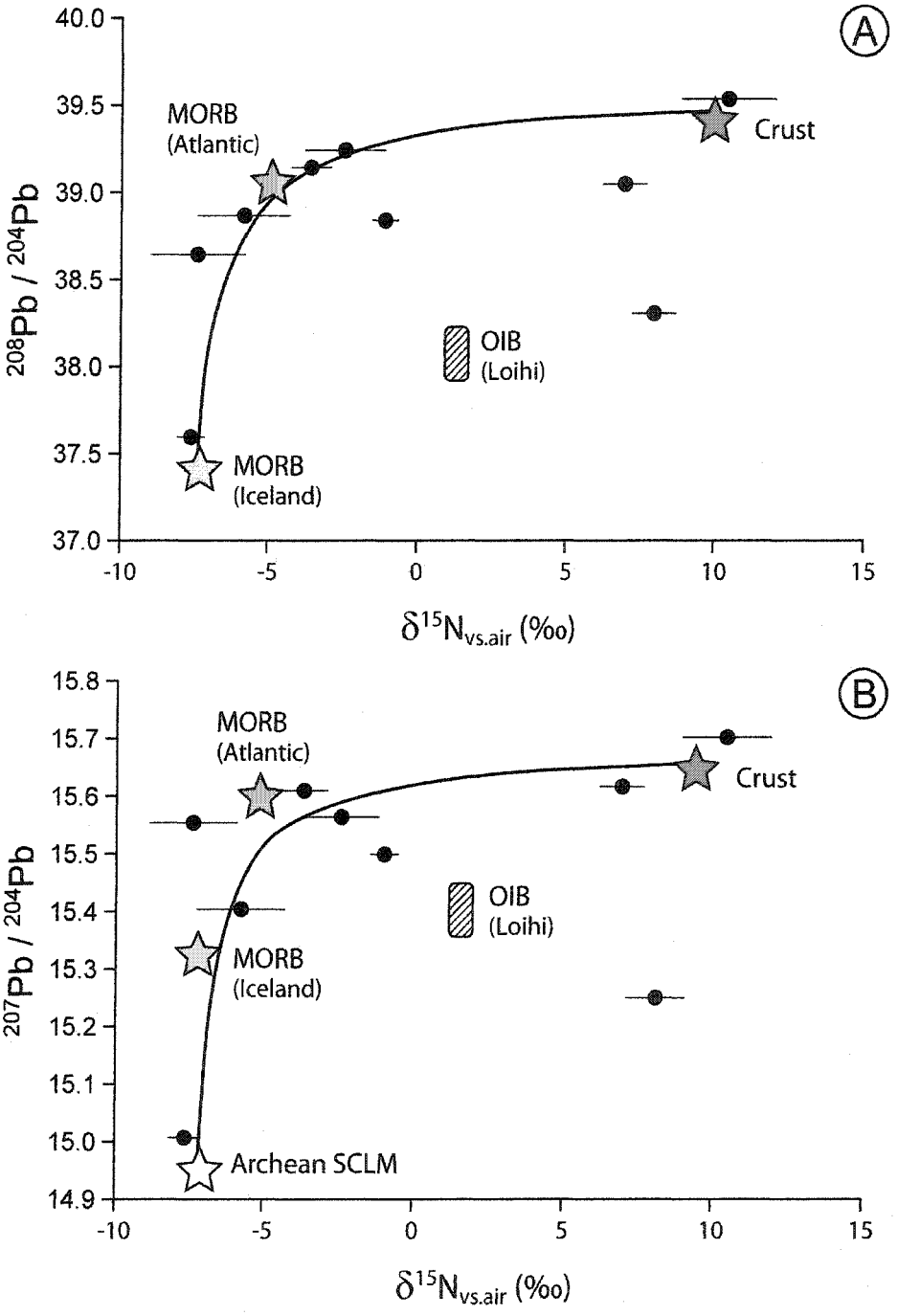
A
40.0
39.5
39.0
38.5
38.0
37.5
37.0
^{208}Pb / ^{204}Pb
MORB
(Atlantic)
Crust
OIB
(Loihi)
MORB
(Iceland)
-10
-5
0
5
10
15
$\delta^{15}N_{vs.air}$ (‰)
B
15.8
15.7
15.6
15.5
15.4
15.3
15.2
15.1
15.0
14.9
^{207}Pb / ^{204}Pb
MORB
(Atlantic)
Crust
OIB
(Loihi)
MORB
(Iceland)
Archean SCLM
-10
-5
0
5
10
15
$\delta^{15}N_{vs.air}$ (‰)

Figure 9. a) $^{208}Pb/^{204}Pb$ vs. $\delta^{15}N$ and **b)** $^{207}Pb/^{204}Pb$ vs. $\delta^{15}N$ measured in in Monteregian Hills minerals separates (black dots). Lead data are from Roulleau and Stevenson (2010) while N data are from this study. Stars indicate the Pb (GEOROC) and N isotopic composition of MORBs from Iceland (Fischer et al., 2005) and North Atlantic (Marty and Humbert, 1997; Marty and Zimmermann, 1999). Shaded area is the N and Pb isotopic composition of Loihi (Sano et al., 2001; GEOROC). Crustal values are from Fisher (2006) and Javoy (1997). Archean SCLM lead isotopes are from Schmidberger et al. (2007). Line indicates the best-fit hyperbola mixing between a mantle and a crustal source obtained by a data inversion technique from Albarède (1995).

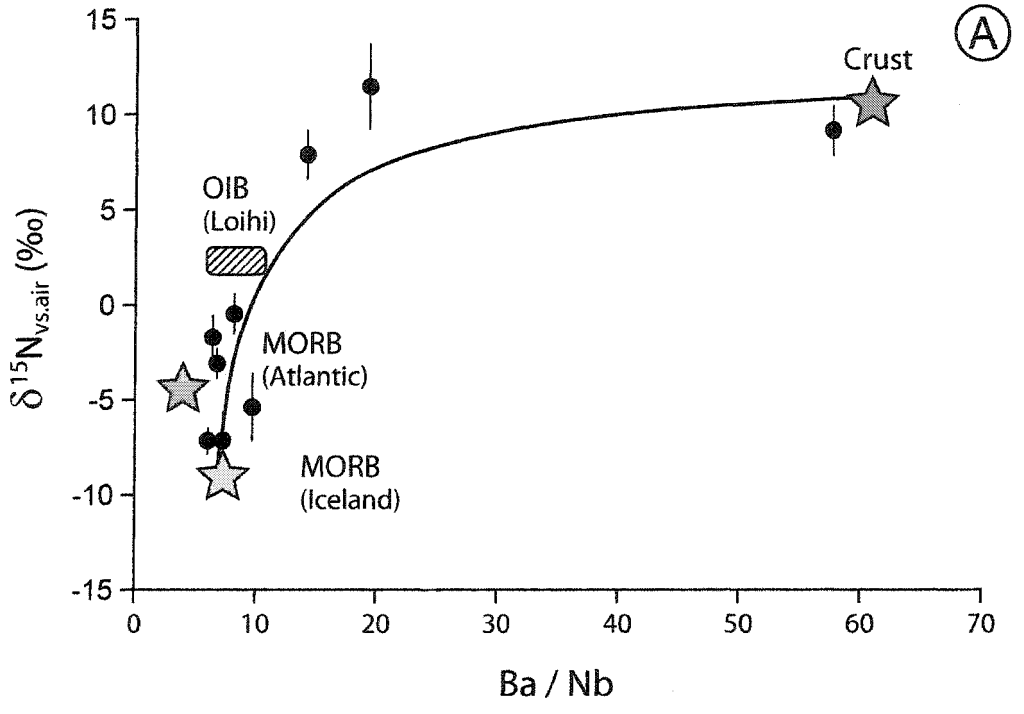
A
Crust
OIB
(Loihi)
MORB
(Atlantic)
MORB
(Iceland)
$\delta^{15}N_{vs.air}$ (‰)
15
10
5
0
-5
-10
-15
0
10
20
30
40
50
60
70
Ba / Nb

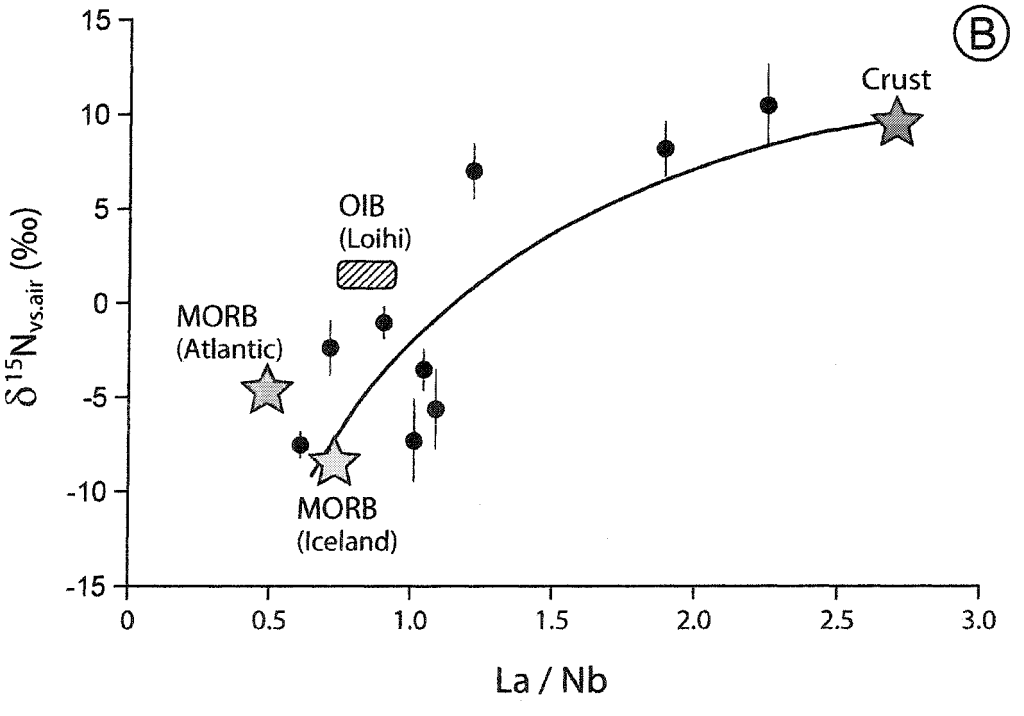
B
Crust
OIB
(Loihi)
MORB
(Atlantic)
MORB
(Iceland)
$\delta^{15}N_{vs.air}$ (‰)
15
10
5
0
-5
-10
-15
0
0.5
1.0
1.5
2.0
2.5
3.0
La / Nb

Figure 10. a) Ba/Nb vs. $\delta^{15}N$ and B) La/Nb vs. $\delta^{15}N$ measured in in Monteregian Hills minerals separates (black dots). Trace element data are from Roulleau and Stevenson (2010) while N data are from this study. Stars indicate the trace elements (GEOROC; Wearer, 1991) and N isotopic composition of MORBs from Iceland (Fischer et al., 2005) and North Atlantic (Marty and Humbert, 1997; Marty and Zimmermann, 1999). Shaded area is the N and Pb isotopic composition of Loihi (Sano et al., 2001). Crustal values are from Wearer, 1991 and Javoy, 1997. Line indicates the best-fit hyperbola mixing between a mantle and a crustal source obtained by a data inversion technique from Albarède (1995).

CONCLUSIONS

Cette thèse avait pour objectif d'identifier la contribution des sources mantelliques dans un contexte continental, en combinant plusieurs outils géochimiques (éléments majeurs et traces) et isotopiques (Nd-Sr, Hf, Pb, N, He, Ar), afin d'apporter de nouvelles données dans le cadre plus global de la compréhension de l'évolution géodynamique de la Terre. Cette thèse prétend montrer l'utilité de coupler différents systèmes isotopiques, en particulier les isotopes radiogéniques avec les isotopes de l'azote et des gaz rares, notamment dans des suites magmatiques continentales où les conditions de contamination crustale sont suffisamment importantes pour effacer une partie de la signature mantellique originelle.

Dans ce but, deux projets sur des roches magmatiques appartenant respectivement à une province magmatique continentale (les Collines Montérégiennes, Québec, Canada), et à des dépôts volcaniques distaux (téphras) retrouvés dans une séquence de varves carbonatées des Alpes italiennes (Formation de Piànico, Italie) ont été menés. La Province Magmatique des Montérégiennes est étudiée depuis plus de 100 ans (Adams, 1903) mais son origine est encore aujourd'hui débattue et deux hypothèses majeures s'opposent : (1) une origine mantellique profonde associée au passage sous la marge nord américaine du point chaud « Great Meteor » (Crough, 1981; Sleep, 1990) versus (2) une origine mantellique lithosphérique associée à l'ouverture de l'Atlantique Nord (Faure et al., 1996; Wen et al., 1987). La séquence carbonatée de Piànico représente la plus longue et la mieux préservée des séquences interglaciaires des Alpes occidentales (Moscariello et al., 2000). La découverte de deux téphras dans les séquences sédimentaires a représenté une opportunité déterminante dans l'estimation de la chronologie de ces terrains, et a ainsi permis d'obtenir des contraintes fortes en terme de changements paléoclimatiques. Cependant l'âge assigné à ces téphras, ou mesuré par la méthode K-Ar, reste encore très controversé. En effet, l'ambiguïté dans la détermination des sources magmatiques de ces dépôts distaux vient principalement de la distance entre le dépôt et la source magmatique ; les processus post-éruptifs qui auraient pu altérer la signature magmatique primaire ne représentent pas ici le problème principal.

D'un point de vue méthodologique, les chapitres 1 et 2 ont permis de mieux cerner les forces et les faiblesses des différents systèmes isotopiques utilisés. La double approche

isotopique Nd-Sr dans le chapitre 1 semble être plus sensible à la contamination crustale, et permet de mettre en évidence une augmentation de la contamination de l'Ouest vers l'Est de la région. Cette augmentation de la contamination est probablement liée aux volumes de sédiments impliqués. Les isotopes Lu-Hf semblent beaucoup moins sensibles à cette contamination et peuvent être préférentiellement utilisés pour tracer la source primaire magmatique. Cependant, comme on a pu l'observer dans les chapitres 1 et 2, les isotopes du Pb semblent être de bons traceurs des différents réservoirs mantelliques, puisqu'ils ont une demi-vie très courte et une grande sensibilité lors des processus de fusion partielle. Les isotopes de l'argon ($^{36-40}Ar$) et de l'azote ($^{15}N/^{14}N$) paraissent moins affectés que les isotopes du Nd et Sr par les effets de la contamination crustale. L'argon et l'azote étant des éléments incompatibles et peu solubles dans les magmas, ils représentent de bons indicateurs des processus de fusion partielle, permettant ainsi de mieux contraindre la source mantellique. Dans le chapitre 3, l'approche isotopique Nd-Sr couplée aux éléments traces semble être un moyen adapté au traçage univoque de la source volcanique des téphras de Piànico, contrairement aux précédentes approches basées sur les éléments majeurs (Brauer, 2007).

Concernant le meilleur traçage des sources mantelliques et la géologie régionale, cette étude permet de s'interroger sur l'interprétation des données géochimiques obtenues à partir de suites magmatiques complexes. Cette étude met en évidence le danger de la généralisation abusive quant à l'interprétation des signatures isotopiques versus l'observation physique de la source d'un magmatisme (cf. signature de type OIB et point chaud Great Meteor, dans le cas des Collines Montérégiennes). Cette étude n'est pas la première à le démontrer mais elle apporte de nouveaux outils permettant de mieux contraindre les sources magmatiques. L'étude des Collines Montérégiennes a permis de montrer l'existence d'un réservoir mantellique appauvri en éléments lithophiles, mais enrichi en éléments incompatibles par la circulation de fluides métasomatiques (chapitre 1) dans le manteau lithosphérique Protérozoique à l'aplomb de ces intrusions. De plus, la signature archéenne principalement observée avec les isotopes du Pb ($^{207}Pb/^{204}Pb$ et $^{208}Pb/^{204}Pb$) et de l'azote ($\delta^{15}N$) dans les magmas des Montérégiennes, témoigne de l'influence régionale du manteau lithosphérique archéen localisé sous le craton canadien. Ce manteau serait resté longtemps isolé du manteau convectif (DMM source des MORBs), permettant ainsi de garder une

signature isotopique primordiale ressemblant à celle observée dans les OIB, en créant ainsi l'ambiguïté de la présence d'un manteau source inférieur sous les Montérégiennes. Cette étude semble en accord avec de récentes études sur l'He, Ne et Ar des saumures localisées au Québec et dans le bassin du Michigan (Castro et al., 2009; Pinti et al., 2010). Ces études récentes montrent la présence d'He, Ne et Ar (au Québec) avec des signatures primordiales de type solaire, caractéristiques des gaz primordiaux piégés dans le manteau inférieur et observées normalement à Loihi, Hawaii (Trieloff et al., 2000). En réalité, Castro et al. (2009) ont montré que ces gaz primordiaux ne proviennent pas d'une contamination par un manteau profond asthénosphérique, mais d'un manteau archéen resté isolé et ayant préservé la signature primitive en gaz rares. Ainsi, la meilleure hypothèse actuellement pour expliquer le magmatisme des Montérégiennes provient de Faure et al., (1996) et serait le résultat de la réactivation du rift Ottawa-Bonnechère lors de l'ouverture de l'Océan Atlantique Nord vers 150 Ma. L'ouverture de l'Atlantique semble avoir produit de nombreuses provinces magmatiques à l'abord des côtes. Bien qu'une étude récente traite de ce sujet (Matton and Jébrak, 2009), il serait intéressant de poursuivre ces recherches afin d'établir ce lien entre les suites magmatiques et l'ouverture de l'Atlantique autant sur la marge américaine que sur la marge européenne.

D'un point de vue chronostratigraphique, la grande utilité des téphras comme marqueurs temporels et stratigraphiques n'est plus à démontrer, et vient principalement du fait de leur aptitude à être transportés sur plusieurs milliers de kilomètres. Il serait donc intéressant de comparer les téphras T21d et T32 à d'autres téphras non datés et également retrouvés dans des séquences sédimentaires. Une étude préliminaire est en cours sur un téphra retrouvé il y a plus de 10 ans en Hongrie (Le Bag Tephra; Pouclet et al., 1999). Ce téphra présente les mêmes caractéristiques géochimiques que l'un des deux téphras de Pianico (T32). Une étude isotopique en Sr et Nd est en cours pour confirmer si ce téphra a la même origine que le téphra T32.

Références

Adams, F.D., 1903. The Monteregian Hills : a Canadian petrographical province. Journal of Geology II, 239-282.

Brauer, A.W., S.; Mangili, C.; Moscariello, A., 2007. Tephrochronological dating of varved interglacial lake deposits from Pianico-Sellere (Southern Alps, Italy) to around 400 ka. Journal of Quaternary Science 22, 85-96.

Castro, M.C., Ma, L. and Hall, C.M., 2009. A primordial, solar He-Ne signature in crustal fluids of a stable continental region. Earth and Planetary Science Letters 279, 179-184.

Crough, S.T., 1981. Mesozoic hotspot epeirogeny in eastern North America. Geology Vol.9, p.342-343.

Faure, S., Tremblay, A. and Angelier, J., 1996. State of intraplate stress and tectonism of northeastern America since Cretaceous times, with particular emphasis on the New England-Quebec igneous province. Tectonophysics 255, 111-134.

Matton, G. and Jébrak, M., 2009. The Cretaceous Peri-Atlantic Alkaline Pulse (PAAP): Deep mantle plume origin or shallow lithospheric break-up? Tectonophysics 469 (1-4), 1-12.

Pinti, D.L. et al., 2010. Primordial He, Ne and Ar in brines of the St. Lawrence Lowlands, QC, Canada: thermal, tectonic and fluid evolution of a passive margin. Geochimica et Cosmochimica Acta submitted.

Pouclet, A., Horvath, E., Gabris, G. and Juvigné, E., 1999. The Bag tephra, a widespread tephrochronological marker in Middle Europe: chemical and mineralogical investigations. . Bulletin of Volcanology 60, 265-272.

Sleep, 1990. Monteregian hotspot track. Journal of geophysical research 95 (B13), 21 983-21 990.

Trieloff, M., Kunz, J., Clague, D., Harrison, D. and Allègre, C.J., 2000. The Nature of Pristine Noble Gases in Mantle Plumes Science 288 (5468), 1036 - 1038.

Wen, J., Bell, K. and Blenkinsop, J., 1987. Nd and Sr isotope systematics of the Oka complex, Quebec, and their bearing on the evolution of the sub-continental upper mantle. Contributions to Mineraloy and Petrology 97, 433-437.